
All ETDs from UAB

UAB Theses & Dissertations

2023

Spatial/Temporal Zonation, Diversification, and Evolutionary Conservation of Kidney Resident Macrophage Subpopulations in Mice and Humans After Kidney Injury

Elise Nicole Erman
University Of Alabama At Birmingham

Follow this and additional works at: <https://digitalcommons.library.uab.edu/etd-collection>



Part of the [Medical Sciences Commons](#)

Recommended Citation

Erman, Elise Nicole, "Spatial/Temporal Zonation, Diversification, and Evolutionary Conservation of Kidney Resident Macrophage Subpopulations in Mice and Humans After Kidney Injury" (2023). *All ETDs from UAB*. 429.

<https://digitalcommons.library.uab.edu/etd-collection/429>

This content has been accepted for inclusion by an authorized administrator of the UAB Digital Commons, and is provided as a free open access item. All inquiries regarding this item or the UAB Digital Commons should be directed to the [UAB Libraries Office of Scholarly Communication](#).

SPATIAL/TEMPORAL ZONATION, DIVERSIFICATION, AND EVOLUTIONARY
CONSERVATION OF KIDNEY RESIDENT MACROPHAGE SUBPOPULATIONS
IN MICE AND HUMANS AFTER KIDNEY INJURY

by

ELISE NICOLE ERMAN

CHRISTIAN FAUL, COMMITTEE CHAIR
ANUPAM AGARWAL
JAMES F. GEORGE
LOUIS B. JUSTEMENT
BRITTANY N. LASSEIGNE
JENNIFER S. POLLOCK

A DISSERTATION

Submitted to the graduate faculty of The University of Alabama at Birmingham,
in partial fulfillment of the requirements for the degree of
Doctor of Philosophy

BIRMINGHAM, ALABAMA

2023

Copyright by
Elise Nicole Erman
2023

SPATIAL/TEMPORAL ZONATION, DIVERSIFICATION, AND EVOLUTIONARY
CONSERVATION OF KIDNEY RESIDENT MACROPHAGE SUBPOPULATIONS
IN MICE AND HUMANS AFTER KIDNEY INJURY

ELISE NICOLE ERMAN

IMMUNOLOGY

ABSTRACT

In the United States, acute kidney injury (AKI) affects nearly 20% of all intensive care unit patients. Additionally, over a third of Americans aged 50 or older suffer from stage 3 chronic kidney disease (CKD) or higher. AKI and CKD are encompassing terms for many etiologies and pathological processes that affect different regions of the kidney but converge at tissue inflammation and fibrosis.

Macrophages perform vital homeostatic functions and can initiate or ameliorate inflammation and fibrosis. As the largest component of the kidney immune system, kidney resident macrophages (KRM) have been implicated in both disease propagation and mitigation, yet the specific functions of KRM remains unclear. I hypothesized the known heterogeneity of macrophage functions was representative of a more complex KRM population than has been previously considered.

To this end, this work identifies multiple KRM subpopulations that are transcriptionally and spatially distinct. Following AKI, subpopulations alter their location and transcriptional profile in differential responses to injury.

In human AKI samples this work identifies orthologous KRM subpopulations, along with a subpopulation unique to humans that expresses the transcriptional profile of activated microglia.

AKI and CKD result in the downregulation of major histocompatibility complex II (MHC II) by a subset of KRMs in mice and humans. The universal appearance following injury has led to the identification of this subpopulation as kidney injury associated (KIA) cells. In AKI, the absence of MHC II correlates with the expression of a wound healing profile by KIA cells in the location of greatest injury.

With the increased clarity on the location and function of KRM subpopulations provided in this work, they are an excellent potential therapeutic option. The spatial restriction of KRM subpopulations would allow for targeted therapies to specific regions of the kidney. Depending on the injury response, therapies should either enhance or ablate the subpopulation's function. KIA cells provide a unique AKI therapeutic target as they are restricted to the site of injury and may aid in recovery. The identification of orthologous populations across species will expedite the translation of murine research into clinical trials and help to focus future research efforts.

Keywords: kidney resident macrophage, sequencing, MHC II, acute kidney injury, chronic kidney disease

DEDICATION

This work is dedicated to my person, Tim Stanton, and my parents: Brad and Shannon.

ACKNOWLEDGMENTS

To Tim, your constant love and support made this work possible. Following your own dreams while supporting someone else's is never easy, but you make it look effortless. Thank you for the Dread River dinners, late-night doughnut drives, porch swing talks, IU basketball games, and the many, many, many hours spent traveling. Even when we were states apart, it is because of you that Alabama felt like home.

To Brad and Shannon, not everyone is lucky enough to be able to claim they had a wonderful childhood, but I am. Mom, you exemplify perseverance and determination, and it is only in my efforts to imitate you that any of this was possible. Dad, your unwavering support, and belief in me gave me the scaffold to believe in myself. Perhaps you both knew that all those nights crying over homework problems, or early mornings driving to University and Summit, would lead to this. Regardless, you two are the most instrumental people in who I am today, and I am proud to be your daughter and friend.

To Chelsea and Garrett, thank you for always providing me with a place to go and an errand to run. So many of my best memories were made at your house. Here's to many more to come.

To Kate, thank you for morning commute phone calls.

To Claudia, I cannot thank you enough for saying you liked country music, sports, and coffee shops on the first day of introductions.

To My Preschool Classes at Oak Mountain Presbyterian Church, thank you for allowing me to escape science for a few hours every week. I hope you all were able to learn as much from me as I did from you.

To Dr. Katherine Friedman, thank you for showing me that research could and should be fun. I would have become an economist if it was not for you.

To my mentors, Drs. James George, and Anupam Agarwal, thank you for letting me strong-arm my way into a rotation and ultimately a position in the lab. You provided me with a space to continue to explore my love of immunology. Thank you for letting me follow any wild idea I came up with, few questions asked. And thank you for the never-ending cheerleading.

TABLE OF CONTENTS

	<i>Page</i>
ABSTRACT.....	iii
DEDICATION.....	v
ACKNOWLEDGMENTS	vi
LIST OF TABLES.....	ix
LIST OF FIGURES	x
LIST OF ABBREVIATIONS.....	xii
INTRODUCTION	1
Acute Kidney Injury (AKI).....	2
<i>AKI Epidemiology and Etiology</i>	2
<i>Clinical Considerations and Emerging Therapeutics</i>	4
<i>Murine Models of AKI</i>	6
<i>General Pathophysiologic and Immunologic Mechanisms</i> <i>of Ischemic AKI</i>	7
Chronic Kidney Disease (CKD)	10
<i>CKD Epidemiology and Etiology</i>	10
<i>Clinical Considerations and Emerging Therapeutics</i>	11
<i>AKI to CKD Transition</i>	14
<i>Murine Models of CKD</i>	15
<i>General Pathophysiologic and Immunologic Mechanisms</i> <i>of AAN CKD</i>	17
Kidney Resident Macrophages and the Functions in AKI and CKD	18
<i>Mononuclear Phagocyte Lineage and Monocyte and</i> <i>Macrophage Differentiation</i>	18
<i>Characterization of the Kidney Resident Macrophage</i> <i>Population</i>	20
<i>Macrophages in AKI</i>	21
<i>Macrophages in CKD</i>	23
Statement of the Problem.....	25
Overall Hypothesis.....	26
Thesis	26
RESIDENT MACROPHAGE SUBPOPULATIONS OCCUPY DISTINCT MICROENVIRONMENTS IN THE KIDNEY	29

HUMAN AND MURINE KIDNEYS CONTAIN TRANSCRIPTIONALLY ORTHOLOGOUS RESIDENT MACROPHAGE SUBPOPULATIONS IN ACUTE KIDNEY INJURY	65
AN EVOLUTIONARILY CONSERVED KIDNEY RESIDENT MACROPHAGE PHENOTYPE WITH REDUCED MHC II EXPRESSION APPEARS AFTER KIDNEY INJURY.....	112
SUMMARY AND CONCLUSION	150
Overall Hypothesis.....	150
Summary	150
KRM Subpopulation Functions in Kidney Homeostasis and Injury Along the Nephron.....	152
<i>Cortical</i>	152
<i>Medullary</i>	154
Impact and Future Directions of Evolutionarily Conserved Subpopulations.....	156
Impact and Future Directions of Human Specific Subpopulations.....	157
Impact and Future Directions of MHC II Response Following Injury.....	159
Impact of KRM Research for Nephrology and Conclusions.....	160
REFERENCES	164
APPENDIX A.....	189
Supplementary Tables and Figures for Resident Macrophage Subpopulations Occupy Distinct Microenvironments in the Kidney	189
APPENDIX B.....	202
Supplementary Tables and Figures for Human and murine kidneys contain transcriptionally orthologous resident macrophage subpopulations in acute kidney injury	202
APPENDIX C	214
Supplementary Tables and Figures for An evolutionarily conserved kidney resident macrophage phenotype with reduced MHC II expression appears after kidney injury.....	214
APPENDIX D.....	224
Study Approvals.....	224

LIST OF TABLES

<i>Table</i>	<i>Page</i>
RESIDENT MACROPHAGE SUBPOPULATIONS OCCUPY DISTINCT MICROENVIRONMENTS IN THE KIDNEY	
1 Gene ontology analysis of KRM clusters in quiescence.....	56
HUMAN AND MURINE KIDNEYS CONTAIN TRANSCRIPTIONALLY ORTHOLOGOUS RESIDENT MACROPHAGE SUBPOPULATIONS IN ACUTE KIDNEY INJURY	
1 Summary of transcriptional profiles for each murine subpopulation at each timepoint	98
2 Identified Marker Genes	99
AN EVOLUTIONARILY CONSERVED KIDNEY RESIDENT MACROPHAGE PHENOTYPE WITH REDUCED MHC II EXPRESSION APPEARS AFTER KIDNEY INJURY	
1 List of genes used to delineate a transcriptional profile for MHC II and wound healing	140

LIST OF FIGURES

<i>Figure</i>		<i>Page</i>
INTRODUCTION		
1	Immunological mechanisms of ischemic AKI	28
2	Immunological mechanisms of aristolochic acid nephropathy CKD	28
RESIDENT MACROPHAGE SUBPOPULATIONS OCCUPY DISTINCT MICROENVIRONMENTS IN THE KIDNEY		
1	Model of acute kidney injury.....	60
2	Single-cell RNA Seq and spatial transcriptomics reveal distinct subpopulations of kidney-resident macrophages.....	61
3	Kidney-resident macrophages are found in distinct regions.....	62
4	Spatial validation of protein markers.....	63
5	Spatial and proportional changes to KRM subpopulations following injury	64
HUMAN AND MURINE KIDNEYS CONTAIN TRANSCRIPTIONALLY ORTHOLOGOUS RESIDENT MACROPHAGE SUBPOPULATIONS IN ACUTE KIDNEY INJURY		
1	The human kidney contains five transcriptionally distinct kidney resident macrophage (KRM) subpopulations.....	105
2	Kidney cell types present in the kidney sections based on histology and spatial transcriptomics.....	106
3	Human clusters 0 and 3 are orthologous to mouse cluster 4.....	107
4	The spatial location of human KRM 1 and 3 is orthologous to murine KRM 4	108
5	Human KRM 1 is orthologous to murine KRM 3	109
6	Human KRM 2 is orthologous to murine KRM 6	110

7	Human KRM 4 does not have a murine ortholog and expresses a microglia transcriptional profile	111
---	---	-----

AN EVOLUTIONARILY CONSERVED KIDNEY RESIDENT MACROPHAGE
PHENOTYPE WITH REDUCED MHC II EXPRESSION APPEARS AFTER KIDNEY
INJURY

1	The presence and persistence of KIA cells correlates with the type of injury	145
2	KIA cells in AKI express a wound healing profile and localize to the site of injury.....	146
3	KIA cells in CKD do not uniquely express a wound healing profile or localize to the site of injury	147
4	KIA cells are specific to the site of ischemic injury	148
5	Human AKI kidneys contain KIA cells that express a wound healing profile and localize with glomeruli	149

SUMMARY AND CONCLUSIONS

1	Summary of transcriptionally and spatially distinct orthologous KRM subpopulations and MHC II dynamics following kidney injury	163
---	--	-----

LIST OF ABBREVIATIONS

AAN	Aristolochic acid nephropathy
AKI	acute kidney injury
APCs	antigen presenting cells
BIRI	bilateral ischemia reperfusion injury
CKD	chronic kidney disease
DAMPs	damage associated molecular patterns
DEGs	differentially expressed genes
eGFR	estimated glomerular filtration rate
ESKD	end stage kidney disease
GFR	glomerular filtration rate
hKRM	human kidney resident macrophages
HSCs	hematopoietic stem cells
IL	interleukin
IRI	ischemia reperfusion injury
KDIGO	kidney disease improving outcomes
KIA	kidney injury associated
KRM	kidney resident macrophages
LPS	lipopolysaccharide
MDPs	macrophage-dendritic cell precursor
MHC II	major histocompatibility complex class II
mKRM	murine kidney resident macrophage
PRRs	pattern recognition receptors
S3PT	segment three proximal tubules

scRNAseq	single cell RNA sequencing
TGF- β	transforming growth factor-beta
TLRs	toll like receptors
TNF α	tumor necrosis factor-alpha
Treg	T regulatory cells
UMAP	uniform manifold approximation and projection
UUO	unilateral ureter obstruction

INTRODUCTION

Most humans contain two kidneys, one on either side of the spine, that filter blood and remove excess fluid to maintain homeostasis. The outermost region of the kidney is called the cortex, which becomes the cortico-medullary region, and then the medulla, as you progress deeper into the tissue. The functional unit of the kidney is called the nephron, and there are approximately 1 million in each human kidney. The nephron is a loop like structure that begins at the glomerulus in the cortex and proceeds to the tubule, which dips into the medulla before returning to the cortex. Initially, blood enters the glomerulus where certain materials are freely filtered using hydrostatic pressure. The filtrate continues along the tubule where additional substances are secreted by or reabsorbed into the blood vessel alongside the nephron before ultimately entering the collecting duct and moving to the bladder via the ureter. The kidney utilizes large amounts of energy to generate an osmotic gradient utilized in the filtration process and the secretion and reabsorption of ions, protons, and water. As a result, different regions of the kidney can vary drastically in a variety of physiologic characteristics which contributes to the fragility and complexity of the organ and the challenges in treating disorders (1).

Acute Kidney Injury (AKI)

AKI Epidemiology and Etiology

Acute kidney injury (AKI) is defined as the sudden and significant loss of kidney function lasting less than three months and leading to the accumulation of waste products such as blood urea nitrogen and imbalances in water, sodium, metabolites, and electrolytes (2-5). Diagnosis does not ascribe an origin of injury and exemplifies the variety and often unclear causes of acute kidney dysfunction (6). In the United States, 1% of hospitalized patients are diagnosed upon admission, with an incidence rate between 5 and 20% following admission, and above 50% upon admission to the intensive care unit (7, 8). Hospitalized patients are more likely to be older and Black (8). AKI diagnoses have been increasing in the United States and worldwide, both in absolute and relative terms, driven largely by increasing rates of diabetes, although the causes and risk factors for AKI are extensive (6, 9, 10). As a result of the lack of a single pathologic process resulting in kidney decline, AKI diagnosis relies on specified criteria, which vary slightly by source, to monitor changes in kidney function. Of these, the most widely used currently is Kidney Disease: Improving Global Outcomes (KDIGO). This set of standards is based on an increase in serum creatinine or decrease in urine volume over set time ranges and involves persistent monitoring of kidney function (11).

Kidney function is primarily monitored using serum creatinine to estimate glomerular filtration rate (GFR). GFR allows for an understanding of the functional capacity of the kidney nephrons. Ideally, a marker of kidney function would be freely filtered by the glomerulus, with no additional process along the rest of the nephron, so an

accurate GFR could be calculated from known serum and urine concentrations of the marker (12). Creatinine is a low molecular weight cation unbound to any plasma proteins, that begins as creatine synthesized in the liver and transported to the muscle where it becomes creatinine following nonenzymatic dehydration (13). It is freely filtered by the glomerulus, although there is an additional secretion by tubular cells further along the nephron. Secretion accounts for between 10-40% of creatinine clearance, and therefore GFR calculations reliant on creatinine are denoted as an estimated GFR (eGFR) (14). The sudden loss of kidney function typical of AKI may not initially be reflected in serum creatinine measurements and therefore delay diagnosis. Unfortunately, if a baseline value is unknown, a significant change in serum creatinine could require an approximately 50% reduction in GFR and an even more substantial decline in kidney function (6, 15, 16). Additionally, creatinine is variable by diet, activity level, muscle mass, and potentially race, making a baseline value that is applicable to all patients difficult to define. Clinical guidelines have struggled to account for these deviations in eGFR equations and to accurately diagnose AKI (17). Creatinine is the best and most facile marker nephrologists have found as an endogenous marker of kidney function, however, more accurate measurements are possible using exogenously provided molecules, such as inulin, iohexol, or iothalamate. These molecules do not suffer the issues of secretion like creatinine but are expensive and time-consuming to provide and measure (18). For these reasons, serum creatinine is still the most commonly used clinically relevant method of determining eGFR and kidney function.

AKI can be classified as prerenal, intrinsic renal, or postrenal and is staged 1 to 3 with increasing disease severity by KDIGO (4, 19). Prerenal AKI is caused by reduced

perfusion to the kidney, reducing the delivery of nutrients and oxygen. Loss of perfusion can be the result of hypotension, trauma, or circulatory dysfunction and inflammation resulting from sepsis, among others (20-22). Intrinsic AKI is generally the result of damage to cells that compose the nephron, either through nephrotoxic or mechanical damage or as the result of an autoimmune disorder (23-25). Postrenal AKI is predominantly caused by obstructions that impair urinary flow (26). Regardless of the pathologic process resulting in AKI, patients staged as 2 or 3 require immediate emergency department referral. Stage 1 patient referral depends on a variety of factors and is dependent on available healthcare (27). However, despite the wide array of causes and severity, treatment is primarily focused on supportive care and differs minimally.

Clinical Considerations and Emerging Therapeutics

Clinical management of AKI can be summarized as initial management, subsequent management, and follow-up. Following the removal of potential causes of insult, such as nephrotoxins or treatment of sepsis, initial care focuses on restoring fluid, electrolyte, and metabolic homeostasis as necessary (6, 28, 29). As creatinine values and GFR may not have changed immediately following the insult, the only initial evidence may be decreased urine output (5). Restoration of fluid homeostasis depends on whether the patient is suffering from hypovolemia or hypervolemia. For the treatment of hypovolemia, the determination of colloid versus crystalloid fluids and the amount is dependent on a variety of patient factors (27, 30). A lack of response to fluids likely means the patients are suffering from intrinsic AKI (27, 31). Diuretics can be used to treat hypervolemia, such as in the case of sepsis or previously hypovolemia patients who

have received too much fluid (32). Hyperkalemia and hyperphosphatemia that persist after restoring fluid homeostasis are treated with dietary restrictions and binder therapy to remove excess minerals (33, 34). Initial management can include kidney replacement therapy, especially in patients with hypervolemia that is non-responsive to diuretics, severe hyperkalemia, or if exposure to certain nephrotoxins has occurred (27, 35). Subsequent management primarily involves assessing the recurrence of uremia or fluid and electrolyte imbalances. Some patients may find benefits in more permanent nutrition management (33). All patients with moderate to severe AKI are encouraged to attend a follow-up appointment with a nephrologist to prevent recurrent AKI or progression to Chronic Kidney Disease (CKD) (6, 36).

AKI-associated mortality and increased risk for recurrence or progression to CKD necessitate continued research into novel therapeutics. According to DelveInsight, a leader in healthcare market research, as of 2022 more than 25 companies were involved in the development of novel AKI therapeutics (37). Unlike the majority of supportive care, emerging therapies are often specific to a particular cause of AKI. There is even debate as to whether greater attention should be given to fluid replacement, as studies suggest patients may have differential benefits and risks to crystalloid or colloid solutions depending on the cause of AKI (38). Many therapies have attempted to provide antioxidants to reduce free radicals and resulting cellular damage, as reactive oxygen species (ROS) are critical components in the propagation of kidney damage (39-41). In a similar direction, silencing RNA against p53 was developed to delay apoptosis and allow ROS-damaged DNA time to repair. Despite success in phase II clinical trials, phase III trials did not show any difference compared to controls (38, 42). Other therapies attempt

to dampen the inflammatory response, however like many immunotherapies, there are drawbacks to limiting an immune response to damaged tissue. Finally, antagonists to angiotensin II and adenosine receptors attempt to modulate the hemodynamics of the kidney to reduce localized microvascular issues and ischemia (43). Despite many successes in murine models, there is unfortunately no currently approved pharmacological therapy for any stage of AKI (38).

Murine Models of AKI

The complexity of modeling AKI and the variety of pathological processes requires equally diverse animal models. Rodent models of AKI are generally composed of those induced by sepsis, ischemia–reperfusion (IRI), drugs/toxins, and ureteral obstruction (UUO) (44-47). Post-renal AKI is commonly modeled using the UUO model. A single ureter is briefly tied off, either with a silk thread or a nontraumatic clamp, thereby preventing urine excretion and driving tubule dilation, oxidative stress, leukocyte migration, and ultimately fibrosis (48, 49). The resulting fibrosis makes UUO a potential AKI to CKD transition model as well. Intrinsic AKI models include drug and toxin models. These primarily include models where mice have been genetically rendered susceptible to toxins, such as diphtheria toxin, or treatment with known nephrotoxic agents, like cisplatin. Both models cause direct tubular injury and hemodynamic effects in the kidney (50). Prerenal models include sepsis and IRI. Sepsis can be induced either through treatment with lipopolysaccharide (LPS) sufficient to engender sepsis-like symptoms or cecal ligation and puncture to release normally sequestered sepsis-causing

bacteria (51). Damage associated with LPS is dependent on dosage and the resulting inhibition of nitric oxide and prostaglandins (50).

The hypoxic environment resulting from the prerenal IRI rodent models imitates ischemic AKI, accounting for approximately 50% of clinical presentations, particularly in the oldest and sickest patients (50). IRI occurs by a sudden lack of blood flow followed by re-establishment of perfusion to the nephron from a mechanical injury, often with the use of non-traumatic clamps to clamp the renal pedicle for a set amount of time. The ischemic phase interrupts both the arterial and venous blood flow. The model can target one kidney (unilateral) or both (bilateral) depending on the scientific question. Reperfusion is generally confirmed visually by the appearance of blood flow in the kidney (50). If the ischemic time is great enough, or if an adjuvant is given to increase inflammation, IRI models can result in significant fibrosis and progression to CKD (52-54).

General Pathophysiologic and Immunologic Mechanisms of Ischemic AKI

The kidneys have mitochondrial requirements on par with the heart and are therefore uniquely susceptible to ischemic injury (55, 56). The proximal tubule is divided into three main components, denoted the S1, S2, and S3 regions, differentiated by the concentration and type of receptors present on the surface of the proximal tubule cells (57-59). The S3 region of the proximal tubules (S3PT) is considered the most susceptible to ischemic injury in rat models, although the specific mechanisms are unknown (60). Glomerular filtration depends on hydrostatic pressure in the glomerulus and therefore does not require energy. Further down the nephron, however, proximal tubules participate

in the active transport of glucose, ions, and other nutrients against gradients (61). Damage to the kidney tissue begins with ischemia and the generation of a hypoxic environment. Cells quickly burn through their ATP reserves and suppress mitochondrial oxidative phosphorylation (62, 63). Sodium and calcium channels rely on free ATP and without it these ions begin to accumulate within the cells. Damage to mitochondria releases ROS, which initially contribute to oxidative stress and DNA damage (62, 64). Increasing calcium concentrations and cellular damage lead to the activation of apoptotic pathways (62). Reperfusion of the tissue washes ROS and cellular debris across it, promoting lipid peroxidation and tissue damage. Damaged cells release cytokines and chemokines, such as kidney injury molecule-1, interleukin (IL-) 6, and tumor necrosis factor-alpha (TNF α) (65). These along with increased expression of adhesion molecules facilitate the infiltration of the tissue by leukocytes. The resulting inflammation can restrict blood flow again and perpetuate the ischemia and reperfusion cycle (62, 66). The leukocyte infiltrate includes both lymphoid and myeloid cells, although the initial recruitment is largely by myeloid populations (67).

Myeloid cells are components of the innate immune system and encompass monocytes, macrophages, dendritic cells, and neutrophils, among others. Neutrophils are generally considered the first responders to areas of inflammation (68, 69). They adhere to adhesion molecules and release ROS, further inflaming the tissue. Neutrophil numbers peak within the first 24 hours following insult and may present in such numbers to impede renal blood flow, as mentioned above (70, 71). Myeloid populations present toll-like receptors (TLRs) and pattern recognition receptors (PRRs) that allow these cells to bind and recognize damage-associated molecular patterns (DAMPs) that have been

released by dying cells. DAMPs are normally sequestered inside cells and are biomarkers such as ATP, DNA, RNA, and heat-shock proteins. The binding of DAMPs by monocytes and macrophages promotes a pro-inflammatory profile and the phagocytosis of cellular debris (72-74).

Macrophages and dendritic cells are professional antigen-presenting cells (APCs) to T cells. However, IRI is considered a sterile injury without antigen. Therefore, the role of APCs in inflammation is most likely through the production of TNF α by damaged cells and biglycan released from the extracellular matrix and not the activation of the adaptive immune system (75). Yet, despite the lack of antigen present, mice lacking CD4⁺ T cells are protected from ischemia-induced AKI and demonstrate a deleterious role of the adaptive immune system (76). Although the exact mechanism has yet to be described, CD28, a coreceptor for the MHC II molecule found on dendritic cells and macrophages, is necessary for CD4⁺ T cell-mediated pathology (76). The role of B cells in AKI is similarly unknown. It is thought they have a deleterious function, as depletion studies show improvement in kidney function (77).

Macrophages and regulatory T (Treg) cells actively participate in the resolution of inflammation and AKI. It is thought Tregs dampen inflammation through the production of the anti-inflammatory cytokine, IL-10, and subsequent reduction in immune cell proliferation and inflammatory cytokine production (78, 79). At some point following insult, macrophages begin to take on an anti-inflammatory, pro-wound healing profile. Like Tregs, they release IL-10 and additionally transforming growth factor-beta (TGF- β) and extracellular matrix proteins (80-82). The mechanism allowing for the switch from a pro to an anti-inflammatory profile remains unknown. However, a dysregulation of the

anti-inflammatory profile can result in kidney fibrosis and ultimately progression to CKD (Figure 1)(83).

Chronic Kidney Disease (CKD)

CKD Epidemiology and Etiology

CKD is a broad classification for any deviation in kidney structure or function that persists for greater than 3 months and can be caused by a variety of diseases and factors (KDIGO). Initiating factors of the disease include age, genetics, nephrotoxin use, cardiovascular disease, and diabetes mellitus (84-89). Genetic diseases, such as polycystic kidney disease and Fabry's disease compose only a small proportion of diagnoses and often affect other tissues in the body (90, 91). Additionally, CKD can be caused by various inflammatory and autoimmune conditions, as is the case with CKD following AKI, infection, lupus nephritis, and IgA nephropathy (90, 92-94).

CKD is one of the few non-communicable diseases that have increased in incidence since 1990, driven largely by increasing rates of diabetes mellitus and an aging population. It is predicted to be the 5th most common cause of death by 2040 (95). The disease affects greater than 10% of the population worldwide, 14.2% of the United States population in 2016, and is slightly more prevalent in women than men (14.9% compared to 12.3%)(95, 96). CKD can progress to end-stage kidney disease (ESKD), and diabetes accounts for roughly half of ESKD diagnoses, whereas cardiovascular disease is the leading cause of CKD mortality (97). Fortunately, while rates of CKD have increased, associated mortality of ESKD in the United States has declined since 2001, suggesting improvements in disease awareness and management (98).

Initial diagnosis relies on changes in eGFR and albuminuria, protein that is inappropriately being passed by a damaged glomerulus, and associated numbers allow for staging of the disease state from 1 to 5 (99). Following an initial acknowledgment of kidney impairment, the KDIGO recommends first confirming the consistency of reduction to ensure the event is not AKI or AKI concurrent with CKD, to ensure appropriate treatment is given (99). Due to compensatory nephrons, early stages of CKD can be missed due to normal eGFR. However, GFR decline correlates linearly with continuous disease progression (97, 100, 101). Therefore, once CKD is confirmed, it is imperative to determine the cause so the appropriate course of treatment can be determined. Non-diabetic CKD may warrant a biopsy to determine the cause, the cellular location of nephritis, and inform management plans (102) (KDIGO). Biopsies may become more necessary should therapeutic options increase and be specific to a disease cause.

Clinical Considerations and Emerging Therapeutics

As in AKI, clinical considerations for CKD focus largely on disease management, although biopsies can confirm if specific treatment is needed. The KDIGO recommends that those diagnosed with CKD have their kidney function measured at least once a year and increase the frequency of measurement as the disease progresses. For most CKD diagnoses, the standard of care relies on blood pressure management by blocking the renin-angiotensin system with additional glycemic controls if necessary (103). Ultimately, treatment looks to restore hemodynamic homeostasis and reduce glomerular hyperfiltration. Angiotensin-converting enzyme inhibitor (ACEi) or angiotensin receptor

blockade (ARB) is the most prescribed (104). Patients should be treated singularly, however, as studies investigating the effects of dual treatment saw an increase in AKI and hyperkalemia without improvements in kidney function (97). However, dual treatment of sodium-glucose cotransporter-2 (SGLT2) inhibitors given in conjunction with either ACEi or ARB amplifies improvements to kidney function (105, 106).

Additional considerations may slow disease progression. Diet restrictions can reduce the workload of the kidney and the KDIGO recommends limits on both protein and salt intake (99, 107, 108). Patients with inflammation or auto-immune mediated CKD, as confirmed by biopsy, may benefit from immunosuppression, but increased risk for infection is a necessary consideration (109). Those who smoke should be advised that cessation has shown improvement in mortality, although the mechanism of protection remains debated (97, 99, 110, 111). Uric acid is increased in CKD patients, and some studies suggest lowering uric acid leads to an increase in eGFR and reduced cardiovascular events, and a long-term reduced risk of starting dialysis (112). Anemia and acidosis are common symptoms of CKD and should be treated should they occur (99, 113, 114).

Once kidneys have failed and the patient reaches ESKD kidney replacement therapy (KRT) will be required and potentially a kidney transplant (115). It is vital clinicians are aware of the physical and mental toll of KRT and work to slow disease progression following initial diagnosis (116). Kidney transplants are considered the most complete therapeutic option (117). Although, lifelong prescription of anti-rejection medication means it is not truly a cure and depending on the underlying cause of disease, function in the transplanted kidney can begin to similarly deteriorate (118, 119).

Additionally, kidney transplants suffer from severe organ shortage and clinicians should not assume this will be an option for most patients (120-122). Unfortunately, CKD therapeutic options remain limited and focus on slowing, not reversing, disease progression.

Emerging CKD therapeutics attempt to target the mechanisms of disease progression and range from small molecules to cellular therapy. Current research is primarily focused on reducing inflammation, fibrosis, and vascular repair (112). Vascular therapies generally attempt to restore the endothelial glycocalyx to repair the glomerular filtration barrier but have met with limited success (123). A promising study investigating the endothelin receptor agonist Avosentan was terminated early due to an increase in adverse outcomes in fluid overload (124). Therapies targeting fibrosis attempt to block fibroblast activation through TGF- β antagonists or microRNAs to prevent TGF- β transcription (125, 126). Anti-inflammatory therapies either target the complement system and could be beneficial in IgA nephropathy and multiple other nephropathies or aim to reduce inflammatory cell infiltrate into the tissue, either through TNF α or the chemokine receptor CCR2 inhibition (97, 127-129). Recently, basic research models have suggested that treatment with mesenchymal stem cells can lead to kidney repair in a variety of different disease models, although whether this will successfully translate into human trials remains to be seen (130, 131).

It is important to note the limitations of CKD therapeutic studies. The chronicity of the disease requires long time points, spanning years to decades, and slows the response of both positive and negative results. Additionally, all studies must be performed on patients already receiving the standard of care, including either ACEi or

ARB, which can complicate the planning of studies and interpretation of results. Finally, as with AKI, CKD encompasses a wide array of disease causes and treatments for one cause may be ineffective or detrimental to another (97).

AKI to CKD Transition

AKI and CKD have a bidirectional relationship where the diagnosis of one increases the risk of the other (132). Comorbidities that cause an increased risk for both AKI and CKD, such as diabetes mellitus, account for some of this correlation. However, studies show once an AKI event reaches a certain severity it progresses to CKD and increases the risk for ESKD. An AKI episode that requires dialysis, stage 2 or 3, is associated with a 28-fold increase in risk for CKD (36). Additionally, the magnitude of serum creatinine increase during an AKI episode is directly correlated to CKD progression (36). The KDIGO recommends that all patients with CKD be considered at an increased risk for AKI (99). There are multiple hypotheses as to the mechanisms of this relationship, and it is likely that more than one is occurring simultaneously.

Currently suggested mechanisms can be divided into failure to repair or maladaptive repair (133). Perhaps the simplest explanation is that nephrons that fail to repair during an AKI event or throughout the progression of CKD increase the workload on the remaining nephrons leading to glomerular hypertrophy, thereby increasing the risk of another kidney damage event (36, 134). However, tubulointerstitial fibrosis scores predict disease progression better than glomerular injury scores, so it is unlikely that glomerular hypertrophy fully explains the AKI to CKD relationship (36). Tubule damage is suggested to come from a failure of the vasculature to repair and maladaptive repair

functions of fibroblasts (135). Studies have shown that tubule repair often outpaces vascular repair and the resulting hypoxia can damage tubules and promote an inflammatory environment and increase fibrosis (136). Tubules may become cell cycle arrested and release TGF- β which continuously stimulates fibroblasts and prevents deactivation following AKI (137, 138). The result is increased fibrosis in the kidney, resulting in CKD progression and increased risk for future AKI events.

Murine Models of CKD

Murine models of CKD attempt to mimic fibrosis progression with a concurrent loss of kidney function over a reasonable timeline, and consist of mechanical, genetic, and toxic means of induction. Models that progress quickly do not accurately capture the advancement of human disease, whereas those that progress too slowly are logistically suboptimal for research studies. Mechanical models include UUO and 5% nephrectomy and are optimized for fibrosis development. UUO generates acute effects, as discussed previously, but if the ligature is allowed to remain fibrosis will quickly progress, although results differ by murine genetic backgrounds (126, 139). It is debated whether this model progresses too rapidly to CKD. Additionally, despite the recapitulation of CKD fibrosis, the remaining compensatory kidney and lack of urine flow from the UUO kidney limit the use of biomarkers for kidney function with this model (140). Removal of 2/3 of a kidney and complete removal of the unilateral kidney results in 5% nephrectomy, where the remaining nephrons suffer from hypertrophy and progress to CKD (141, 142). Mechanistically, this model is easier to perform in rats than in mice, however, in both species, the amount of kidney tissue remaining is small and limits downstream analyses.

Genetic models have been developed, or spontaneously appeared, to mimic a variety of human conditions, including polycystic kidney disease, diabetes mellitus, hereditary nephritis, and Pierson syndrome (143-145). Unfortunately, many mutations are lethal in early life or take many months to progress. Recently, there has been a movement to make genetic mutations specific to kidney cells in an effort to combat early lethality (140). Diabetic models may involve injections of streptozotocin to generate diabetic mice, but kidney fibrosis is often limited (146, 147). In an effort to circumvent this issue, genetic models can either spontaneously develop a diabetes-like profile, in the case of leptin-deficient mice, or injections can be layered over genetic models to increase kidney damage (147).

Toxic models involve the injection of kidney nephrotoxins or fibrotic agents. Perhaps the most well-known is the commonly given chemotherapeutic agent cisplatin. Cisplatin binds to DNA, forming cross-links between DNA strands, particularly mitochondria DNA, and causes cell cycle arrest and apoptosis (148, 149). Another option is folic acid injections. In high enough doses folic acid is filtered through the glomerulus and builds up in the tubules causing necrosis and fibrosis, although paradoxically it is also being investigated as a potential therapy to slow CKD progression in lower doses (52, 150-152). However, both protocols require continued injections throughout the duration of the study and can be time-consuming. Additionally, their application to human disease, where a nephrotoxic agent would be removed, is dubious.

Aristolochic acid provides a nephrotoxic alternative to continuous injection protocols, with a reasonable timeline and clear effects on kidney biomarkers. Progressive fibrosis and an elevated and sustained immune response are hallmarks of this model

(153). Aristolochic acid-induced nephropathy (AAN) requires an initial multiday protocol and has an acute phase but will naturally progress to CKD without the need for continuous injections (52). Injections consist of a mixture of nitrophenanthrene carboxylic acids isolated from the *Aristolochia* species of plants, native to the Balkans and parts of China (153). AAN has been suggested as the best chronic model to study mechanisms associated with IRI-induced CKD (151, 154). While murine models of severe IRI will eventually progress to CKD, the timeline is not always conducive to research (52). What would take many months following severe IRI can be accomplished within a few weeks in AAN.

General Pathophysiologic and Immunologic Mechanisms of AAN CKD

In the 1990s, *Aristolochia* plants were incorrectly substituted into diet pills which lead to a worldwide outbreak of AAN (155). Inadvertent ingestion of aristolochic acid I and/or II can rapidly develop into CKD and ultimately ESKD. Once ingested, aristolochic acid is absorbed from the gastrointestinal tract into the bloodstream before entering PTs through molecular organic anion transporters 1 and 3, where it forms covalent DNA adducts, cell cycle arrest, mutations, and apoptosis (156, 157). AAN was first identified in horses in the Balkans who consumed the *Aristolochia* plants growing in the fields in which they were kept and currently predominately affects those living in the Balkans and regions of China who rely on the local environment for sustenance or those taking unregulated herbal medications in which the plant continues to be used (158-160).

Initial symptoms of AAN include nausea, vomiting, rapidly progressing interstitial nephritis, reduced GFR, anemia, hypocellular infiltration, and ultimately

severe fibrosis and urothelial carcinomas (153, 158). Many symptoms appear to be the result of a massive infiltration by leukocytes, including macrophages, B and T cells present in medullary rays, and the outer medulla. These cells seemingly persist in the tissue, as they have been confirmed in terminal cases (161). As a result, there is significantly increased inflammasome activation and constant overexpression of TGF- β and therefore increased fibroblast activity (Figure 2)(162, 163). Patients suffering from AAN present with shrunken kidney cortexes and completely solidified glomeruli that present on a gradient towards to medulla (161).

Kidney Resident Macrophages and the functions in AKI and CKD

Mononuclear Phagocyte Lineage and Monocyte and Macrophage Differentiation

During homeostasis and injury, the kidney interacts with the immune system, both the peripheral and resident components (77, 164-166). As mentioned previously, the infiltration of the peripheral immune system in AKI can lead to inflammation and localized ischemia (70, 71). The immune system is composed of leukocytes that are subdivided into the innate and adaptive immune system. Lymphocytes of the adaptive immune system learns, responds to, and remembers the wide variety of pathogens seen over a lifetime. The primary components of the adaptive immune system are T and B cells. Myeloid cells of the innate immune system have a limited capacity to remember pathogens, but are primed against common characteristics of viruses, bacteria, fungi, and helminths, in order to initiate a rapid response to repeat offenders. Additionally, a primary function of the innate immune system is to phagocytose pathogens, and present processed components to initiate an adaptive immune response. This is done by members

of the mono-nuclear phagocyte system, consisting of macrophages, monocytes, and dendritic cells.

The origin of mononuclear phagocytes differs pre and post-birth (167). Following birth, mononuclear phagocytes derive from precursor hematopoietic stem cells (HSCs) in the bone marrow (168). Therefore, post birth, all peripheral MP populations are bone marrow derived. Anything arising before birth is considered of an embryonic lineage. Prior to birth, myelopoiesis begins at 3 to 4 weeks gestation in humans and on embryonic day 8 in mice and results in myeloid progenitor cells from the primitive ectoderm of the yolk sac (169, 170). Later in development, HSCs seed the fetal liver and expand and differentiate into monocyte/macrophage and dendritic cell progenitors (MDPs) (171-173). Regardless of location, it is thought that MDPs differentiate either into a dendritic cell precursor or a monocyte/macrophage precursor, however, it is debated whether there is an early linear restriction or a continuum of lineage development (174, 175). MDPs that differentiate into monocytes are defined as *Lyc6C* high or low in the mouse and *CD14* high or low in humans (176, 177). Previously, monocytes were considered immature forms of, or precursors to, macrophages, that patrol the body and would further differentiate upon entering tissue or encountering an inflammatory milieu. However, recent studies suggest that monocytes would be better considered a blood-resident population and that under homeostatic conditions, monocytes can enter tissues and remain monocytes (174, 178, 179).

These claims are bolstered by recent research into the lineage and maintenance of tissue-resident macrophage populations. Increasingly, macrophages have come to be defined as tissue-resident, making terms like tissue-resident macrophages debatably

redundant (180). However, as monocytes can differentiate into macrophages in inflamed tissue, resident macrophage is still used to denote macrophage populations present in the tissue during homeostasis (178). Many tissues in mice and humans are colonized by a population of macrophages. Embryonically derived resident macrophages are thought to colonize many tissues in the body and have lifespans that extend far beyond bone marrow-derived mononuclear phagocytes, which last between two weeks and a month (181, 182). These populations include microglia, Kupffer cells, Langerhans, and resident populations in the heart, lung, and peritoneal cavity (178, 183-186). Most resident macrophage populations are thought to self-maintain without peripheral monocyte differentiation and replacement, with exceptions in at least the intestine and skin, that are constantly being replaced (174, 187, 188). Others, such as in the lung and spleen, have monocyte-supplemented resident macrophage populations, where only a small proportion of the niche appears to receive monocyte-derived input (184).

Characterization of the Kidney Resident Macrophage Population

The kidney resident macrophage (KRM) was first described in 1981 as a mouse kidney mononuclear phagocyte population marked by high F4/80 expression in contrast to low F4/80 expression on peripheral macrophage populations (189, 190). In mice, KRMs are identifiable by high F4/80 and intermediate CD11b expression. However, neither F4/80 nor a known ortholog are present on human macrophages, and KRMs can instead be identified by the expression of C1q across species (191-193). The presence of dendritic cell markers, such as CD11c and MHC II, on the resident population, lead to their reclassification as dendritic cells for a time (194, 195). However, as the

understanding of resident macrophages increased, it was acknowledged that conventional markers and functions used to delineate dendritic cells and monocytes/inflammatory macrophages were not applicable to resident populations (196, 197). Increasingly, genomics assays, such as single cell RNA sequencing and spatial transcriptomics, have identified novel resident immune cell subpopulations and/or cell phases within tissues, that were previously undiscovered based on surface markers alone.

Much work has been accomplished in the last decade to elucidate KRM further. Parabiosis studies confirmed that adult murine KRMs are self-maintained and form a network throughout the entire tissue (198, 199) (200). Reporter mice were used to determine that the KRM niche is composed of both embryonic and bone-marrow-derived macrophages in the mouse, where upon birth peripheral macrophages differentiate and seed into the kidney and ultimately compose approximately half of the total KRM population (201). It still needs to be determined whether these early bone marrow-derived residents self-maintain, like their embryonically derived neighbors, or are continuously replaced as in the case of the skin and spleen. However, it is important to note the difference between mouse and human kidney development. The murine kidney continues to develop for one-month post-birth, the same period in which the bone marrow-derived KRMs appear, whereas human kidney development stops at birth and in theory could be composed of entirely embryonically derived KRMs (134, 202).

Macrophages in AKI

The role of macrophages in injury propagation and resolution is complex and dependent on the type of model used. The changing understanding and naming

convention of the mononuclear phagocyte population within the kidney further complicates the identification of specific roles for monocytes, dendritic cells, macrophages, and resident macrophages. Additionally, much of the previous research into macrophage functions relied on dichotomous phenotype assignments that are largely inconsistent with *in vivo* observations (203, 204). Activated macrophages are routinely portrayed as either M1 inflammatory macrophages, activated by LPS or IFN γ , or M2 anti-inflammatory macrophages, polarized by IL-10, IL-4, or IL-13 (205, 206). In practice, macrophages can readily shift between phenotypes and more accurately exist on a spectrum reliant on the available environmental signals (73, 181, 207, 208). In the transition from the highly inflammatory milieu of AKI to the pro-fibrotic nature of CKD, macrophages would experience and respond to a variety of environmental and immunological cues.

Immediately following reperfusion, monocytes, facilitated by CCR2 and CX3CR1 mediated chemotaxis, migrate into the tissue (209). Activation of toll-like receptors and stimulation by IFN γ promotes a proinflammatory phenotype and a possible differentiation into inflammatory macrophages (209-212). The responding cells begin secreting inflammatory cytokines which in turn upregulate selectins and integrins and therefore attract more immune infiltration (213, 214). Myeloid cells of the inflammatory infiltrate produce inducible nitric oxide synthase to add to already present ROS to further promote apoptosis and inflammation (213). Necrotic cells release damage-associated molecular patterns (DAMPs), such as ATP, heat shock proteins, hypomethylated DNA, and RNA. Mononuclear phagocytes begin to efferocytose dead and dying cells (72, 73). These internal signaling pathways converge in the inflammasome and interferon

pathways, which are central to inflammation and activation of the adaptive immune system. As injury resolves, macrophages dampen inflammation and transition towards an anti-inflammatory and possibly pro-fibrotic phenotype (73, 215).

Little is known about the specific function of KRM_s following ischemic AKI. Much of the knowledge of myeloid function following injury comes from various depletion models, none of which specifically target a single population. Clodronate liposome-based depletion methods target phagocytic cells and treatment prior to AKI has shown protective effects, suggesting a role in injury propagation by one or more subpopulations of the mononuclear phagocyte compartment (216). Diphtheria toxin receptor models selectively target cells genetically manipulated to be susceptible to diphtheria toxin. The most useful, to date, for studying KRM_s are those targeting CD11b⁺ and CD11c⁺ cells, as both markers are expressed intermediately on KRM_s (198-200). Unfortunately, these molecules are also expressed in varying degrees by monocytes and dendritic cells and fail to specifically target any one population. Regardless, unlike clodronate methods, diphtheria toxin-mediated depletion does not offer AKI protection (216). The contrast in the outcomes of the depletion models suggests that different mononuclear phagocytes in the kidney have divergent effects following AKI, however, the specific role of KRM_s, and whether it differs from infiltrating populations remains unknown.

Macrophages in CKD

The progressive nature of CKD and the variety of conditions possible within the damaged kidney, make it difficult to parse out the role of macrophages and monocytes.

Similar to AKI, the first immune cells are responding to damaged kidney cells and the release of DAMPs (217). Monocytes and macrophages that migrate into the tissue express TLRs that bind the DAMPs and respond to cytokines, such as $\text{IFN}\gamma$, secreted by other immune populations. Acting in concert, these signals produce a pro-inflammatory phenotype and secretion of inflammatory cytokines IL-6, $\text{TNF}\alpha$, IL-1 β , and ROS (217, 218). Expression of MHC II and co-receptors increases on dendritic cells, monocytes, and macrophages to allow for stimulation of the adaptive immune response (219, 220).

The second phase of CKD involves an increase in anti-inflammatory and perhaps pro-fibrotic macrophages. It is important to note the pro-inflammatory presence in the kidney remains, and regions of the tissue remain inflamed even as fibrosis progresses (221, 222). However, through an unknown mechanism, anti-inflammatory macrophages increase in number and secrete TGF- β , IL-10, and IL-13. The role of macrophages in CKD fibrosis is debated and can be attributed to pro and anti-inflammatory macrophages through different mechanisms. Macrophages and monocytes cluster around dead and dying tubules as apoptosis continues (161). Remaining pro-inflammatory macrophages are thought to increase fibrosis by increasing the production of matrix metalloproteinase 9 and facilitating the epithelial-mesenchymal transition (223). In contrast, anti-inflammatory macrophages secrete TGF- β , which when secreted by proximal tubules in the nephron has been shown to activate fibroblasts (224, 225). However, in a model of obstruction-mediated CKD, macrophage-specific loss of TGF- β did not show a significant effect on fibrosis and therefore complicates the hypothesis that anti-inflammatory macrophages mediate kidney fibrosis (226).

Generally, macrophages in AAN appear to respond as they would in any other CKD model. Following AAN, macrophages increase significantly in the kidney parenchyma, and a large and persistent immune infiltrate is a hallmark of this model and ischemic AKI (154). Studies that have investigated the macrophage compartment as one, both infiltrating and resident, find an increase in both pro- (IL-6 and TNF α) and anti- (TGF- β , IL-10, IL-13) inflammatory cytokines in comparison to vehicle-treated controls (151). A study that inhibited macrophage colony-stimulating factor showed that macrophage infiltration promotes oxidative stress and apoptosis in tubule cells, and inhibition of macrophage proliferation and activation reduced Nf-KB, TGF- β , and immune infiltrate (227). It is important to note that Nf-KB and TGF- β are thought to represent opposite ends of the inflammatory spectrum and emphasize the complex role of macrophages in the tissue. A transcriptional study identified KRMs based on the expression of *Clqa* and found this population expresses similar patterns in IL-1 β , TNF α , Arg-1, and TGF- β to infiltrating macrophages and monocytes (228). To date, there are no functional studies that identify features unique to KRMs in AAN.

Statement of the Problem

Patients suffering from AKI and CKD are afforded few therapeutic options with limited degrees of success in managing the disease. The immune system has been implicated in the propagation and amelioration of kidney injury, yet immune based therapies are nearly nonexistent and novel therapeutic options discovered in mouse models often fail upon progression to clinical trials. KRMs are found in mice and humans and are present and participatory for all phases of kidney injury and recovery or the lack

thereof, and therefore represent an excellent therapeutic target. However, most of the current understanding of macrophage responses to kidney injury fails to differentiate between resident and infiltrating populations, failing to identify KRM specific responses. Additionally, KRMs are dispersed throughout the tissue, and would inevitably be exposed to a variety of different microenvironments that would likely influence the homeostatic and injury specific functions within the KRM population. As a result, there is a need to further elucidate potential subpopulations within the human and murine KRM niche and the response of said subpopulations following AKI and CKD.

Overall hypothesis

The kidney resident macrophage niche is composed of transcriptionally and spatially distinct evolutionarily conserved subpopulations that modulate their MHC II expression at the injury location and for the duration of the injury

Thesis

As a result of investigating the above hypothesis, this dissertation elucidates the specific responses of KRM subpopulations to kidney injury and identifies transcriptionally and spatially conserved orthologs between mice and humans. Furthermore, this dissertation investigates the injury response of MHC II downregulation by a subset of KRMs. This work provides a necessary framework to identify KRM subpopulations across species and has begun the process of function identification.

Figure Legends

Figure 1. Immunologic mechanisms of ischemic AKI

(A) Macrophages recognize DAMPs, such as DNA, released by dead and dying cells. (B) The inflammatory milieu polarizes macrophages towards a pro-inflammatory phenotype and stimulates the release of pro-inflammatory cytokines, such as TNF α . (C) A potential interaction between CD4⁺ T cells at the site of sterile injury. (D) Neutrophil numbers peak within the first 24 hours, where they migrate into the tissue that has upregulated adhesion molecules, and release ROS.

Figure 2. Immunologic mechanisms of aristolochic acid nephropathy CKD

The hallmark of the immunological niche in Aristolochic Acid Nephropathy CKD is rapidly progressing fibrosis and massive immune infiltration. TGF-Beta released by damaged tissue stimulates the proliferation and maintenance of fibroblasts.

Figures

Figure 1.

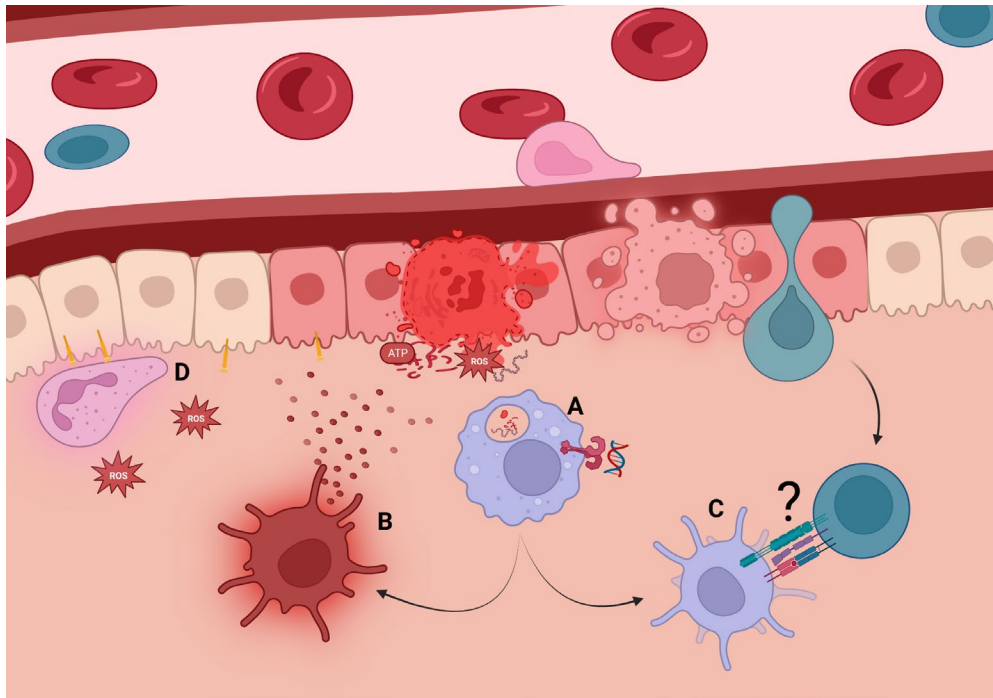
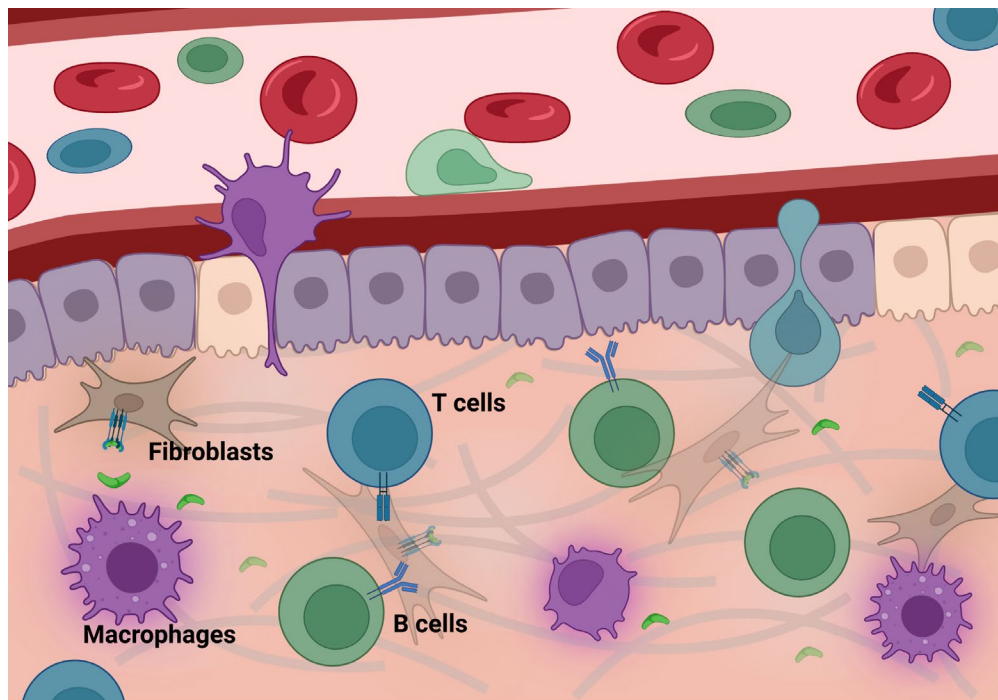


Figure 2.



RESIDENT MACROPHAGE SUBPOPULATIONS OCCUPY DISTINCT
MICROENVIRONMENTS IN THE KIDNEY

by

MATTHEW D. CHEUNG* and ELISE N. ERMAN*

*co-first authors

KYLE H MOORE, JEREMIE M.P. LEVER, ZHANG LI, JENNIFER R.
LAFONTAINE, GELARE GHAJAR-RAHIMI, SHANRUN LIU, ZHENGQIN YANG,
RAFAY KARIM, BRADLEY K. YODER, ANUPAM AGARWAL, JAMES F.
GEORGE

JCI Insight. 2022;7(20):e161078

Copyright

2022

by

Under the Creative Commons Attribution 4.0 International License

Used by permission

Format adapted for dissertation

Abstract

The kidney contains a population of resident macrophages from birth that expands as it grows and forms a contiguous network throughout the tissue. Kidney-resident macrophages (KRM) are important in homeostasis and the response to acute kidney injury. While the kidney contains many microenvironments, it is unknown whether KRMs are a heterogeneous population differentiated by function and location. We combined single-cell RNA-Seq (scRNA-Seq), spatial transcriptomics, flow cytometry, and immunofluorescence imaging to localize, characterize, and validate KRM populations during quiescence and following 19 minutes of bilateral ischemic kidney injury. scRNA-Seq and spatial transcriptomics revealed 7 distinct KRM subpopulations, which are organized into zones corresponding to regions of the nephron. Each subpopulation was identifiable by a unique transcriptomic signature, suggesting distinct functions. Specific protein markers were identified for 2 clusters, allowing analysis by flow cytometry or immunofluorescence imaging. Following injury, the original localization of each subpopulation was lost, either from changing locations or transcriptomic signatures. The original spatial distribution of KRMs was not fully restored for at least 28 days after injury. The change in KRM localization confirmed a long-hypothesized dysregulation of the local immune system following acute injury and may explain the increased risk for chronic kidney disease.

Introduction

Macrophages are ubiquitous in the kidney (1). They perform numerous functions within the kidney, including integration of signals related to tissue health, phagocytosis of debris and apoptotic cells, defense against infectious agents entering via the urinary tract, and response to physical injury or damage by pharmacologic agents. In a normal murine kidney, macrophages constitute approximately 50%–60% of CD45⁺ immune cells, and of those, the majority are tissue resident, having seeded into the kidney in embryonic and early life from the fetal yolk sac, fetal liver, and bone marrow (2). Kidney-resident macrophages (KRM) are defined as such because they are replenished primarily through self-renewal and receive no further input from the peripheral circulation (3, 4). The KRM population can be distinguished from infiltrating macrophages by their high expression of F4/80 (also known as Emr1 and Ly71) and intermediate expression of CD11b (integrin $\alpha_m\beta_2$, also known as Mac-1) (5). Infiltrating macrophages, which are exclusively bone marrow derived, turnover within 2 weeks (3) and express lower levels of the F4/80 antigen and higher levels of CD11b (F4/80^{int}, CD11b^{hi}). Parabiosis studies following an ischemic event show that these characteristics do not change after kidney injury (3).

Kidney macrophages are known to be important in acute kidney injury (AKI), but their conflicting roles in the pathogenesis of and recovery from injury are poorly understood. In models of AKI, such as kidney ischemia/reperfusion injury in mice, the extent and timing of macrophage depletion affect the outcome of injury (6, 7).

KRMs are distributed throughout the kidney, which contains distinct physiological microenvironments along the nephron. Macrophage location has been shown to affect function in other organs/tissues (8–12). Therefore, KRMs may have

specialized functions tailored to the local cellular environment and may possess transcriptional programs to respond distinctly to acute injury. We have previously shown in an ischemia/reperfusion injury model that there are changes in the expression of selected surface molecules, such as MHC II, and in transcriptional programming, as measured by bulk mRNA sequencing (3). It is not clear if the observed transcriptomic and phenotypic shifts reflect alterations in global macrophage programming or previously indistinguishable subpopulations.

We used single-cell RNA-Seq (scRNA-Seq) and spatial transcriptomics to demonstrate that KRMs consist of at least 7 major subpopulations localized to defined zones within the kidney. The distinct transcriptomic programs of each subpopulation suggest specialized functions, including type I IFN responses, heme/iron metabolism, inflammation, or antibacterial responses. Following acute ischemic injury, the transcriptomic programming is altered, and the delineation of the subpopulations within specific zones is lost and does not return to normal by 28 days after injury, possibly reflecting chronic immune dysregulation.

Results

Generation of a comprehensive single-cell KRM data set.

We performed scRNA-Seq on CD45⁺TCRb⁻CD19⁻NK1.1⁻Gr-1⁻ CD11b^{int}F4/80^{hi} KRMs identified and sorted by flow cytometry as described previously (Supplemental Figure 1; supplemental material available online with this article; <https://doi.org/10.1172/jci.insight.161078DS1>) (3). The KRMs were obtained from the kidneys of quiescent (uninjured) mice and those subjected to 19 minutes of

bilateral warm ischemia ($37^{\circ}\text{C} \pm 1^{\circ}\text{C}$ rectal temperature) under ketamine-xylazine anesthesia ([Figure 1A](#)). Histologic changes and serum creatinine confirmed the initial injury on day 1 after ischemia, with observed hypercellularity and an average increase of 0.21 mg/dL in serum creatinine and subsequent recovery of function from days 6 to 28 after injury ([Figure 1, B and C](#)). Samples from 3 quiescent mice and 3 mice each at 12 hours and days 1, 6, and 28 days after injury were sequenced using the 10X Genomics 3' Chromium platform. In total, 58,304 KRMs were sequenced and retained based on the expression of *Adgre1* (F4/80), *Itgam* (CD11b), and *C1qa* ([3](#), [13](#)). The data from all time points were integrated using Harmony to facilitate a direct comparison of the analyses at each time point by minimizing batch effects and nonbiologic variation. After quality control, 3000 variable genes were identified for all groups, and after normalization and scaling, the cells were clustered. Dimensional reduction using uniform manifold approximation and projection (UMAP) resolved 13 clusters ([Supplemental Figure 2A](#)). Elimination of contaminating kidney parenchymal cells and clusters constituting equal to or less than 1% of the total number of cells left 7 clusters, indicating that the KRM population is composed of at least 7 major distinct subpopulations with unique transcriptomic signatures ([Figure 2A](#) and [Supplemental Figure 2B](#)). KRMs were distinguished from parenchymal cells by expression of canonical markers such as of *C1qa* ([Figure 2B](#)) ([13](#)).

Delineation of transcriptionally distinct KRMs in quiescent mice.

We initially analyzed the quiescent samples to characterize the 7 major subpopulations in the uninjured state ([Figure 2A](#)). A heatmap of the top 5 significant

differentially expressed genes (DEGs) in each cluster illustrates distinct transcriptional profiles and provides potential markers for identification ([Figure 2C](#)). Very few transcripts were uniformly expressed at high levels in cluster 0, although *Ccr2* and *Ptpnc* (CD45) were among the DEGs that defined this cluster ([Figure 2C](#)). The top DEGs in the remaining 6 clusters indicated at least one specific function. Cluster 1 expressed heat shock protein transcripts and the *Fos* and *Btg2* transcription factor/cofactors, which are associated with the immediate early response ([Figure 2C](#)). These transcripts may be involved in homeostatic function or may indicate priming toward the immediate early response by this cluster, allowing for cluster 1 to preferentially upregulate the immediate early response during the dissociation protocol. Cluster 2 exhibited increased transcription of heme oxygenase-1 (*Hmox1*), which is the rate-limiting step in the degradation of heme into iron, biliverdin, and carbon monoxide. Notably, we also observed increased expression of ferroportin (*Slc40a1*), peroxiredoxin (*Prdx1*), ferritin heavy chain (*Fth*), and ferritin light chain (*Ftl*), which supports the supposition that heme/iron handling is an important function of cluster 2 ([Figure 2C](#) and [Supplemental Figure 3A](#)). Cluster 3 was enriched for genes associated with antimicrobial processes and inflammation, such as *Cxcl2*, macrophage inflammatory protein 1- α (*Ccl3*), and macrophage inflammatory protein 1- β (*Ccl4*), which are involved in the recruitment of inflammatory cells. *CD14*, which is engaged in Toll-like receptor signaling by LPS, was expressed by these cells at high levels ([Figure 2C](#) and [Supplemental Figure 3B](#)). Cluster 4 expressed transcripts involved in fibrosis, including *Pf4*, *CD206*, and *Stab1* ([Supplemental Figure 3C](#)) (14–18). Cluster 5 could be distinguished by the expression of *Vim*, *Ccl2*, *Tnfr3*, and *Ccr2* transcripts ([Figure](#)

[2C](#) and [Supplemental Figure 3D](#)). Cluster 6 was enriched in the expression of several genes associated with type I IFN responses, such as *Isg15*, *Ifit3*, and *Ifit2*, indicating a possible role in antiviral responses ([Figure 2C](#) and [Supplemental Figure 3E](#)). A full listing of the DEGs is provided in the Supplemental Excel File 1.

Gene ontology enrichment analysis (GO: biologic process) determines the extent to which genes associated with specific functions are represented in each cluster. As seen in [Table 1](#), enrichment of specific gene sets could be assigned with varying degrees of confidence to each cluster, with the exception of cluster 5, which contained too few cells in quiescence for a reliable estimation. The most significant terms in clusters 1, 3, and 6 were involved in antibacterial, antiviral, and antifungal responses. Cluster 2 contained terms related to responses to iron, phagocytosis, and wound healing, suggesting involvement in homeostatic functions. Clusters 0 and 4 mapped to few terms, but the analysis contained references to tumor necrosis factor and apoptosis. These disparate gene ontology mappings suggest that each cluster executes a distinct transcriptional program that could be a function of the location in which each cluster resides.

KRM subpopulations are localized to zones associated with specific nephron structures.

We identified KRM locations by integrating the scRNA-Seq data ([Figure 2A](#)) into spatial transcriptomic data sets generated from kidney sections of 3 individual mice. The spatial matrix was integrated with the scRNA-Seq data set using the anchor-based workflow built into the Seurat package, which allows the probabilistic mapping of scRNA-Seq- and/or single-nucleus RNA-sequencing (snRNA-Seq)-defined clusters onto a histological kidney image ([Supplemental Figure 4](#)) ([19–22](#)). We validated this approach using a single-nuclear data set from whole kidneys, in which the cell types identified by

snRNA-Seq mapped to expected histologic locations in the kidney ([Supplemental Figure 5](#)). The 7 transcriptionally defined KRM subpopulations were localized to distinct locations in the kidney ([Figure 3](#), right), corresponding to zones enriched for specific nephron structures ([Figure 3](#), left), which were designated zones I–V and confirmed using zone-specific transcripts (23) ([Figure 3](#), middle). The localization patterns suggest a zonal organization of KRMs from the cortex to the papilla. For example, cluster 0, appearing in zone II, was largely concentrated in the corticomedullary region and appeared to be associated with the S3 segment of the proximal tubule, as determined by marker transcripts for the S3 proximal tubule (*Slc7a13*, *Napsa*, *Nudt19*). Cluster 4 and cluster 6 are predominately located in zone III, and their spatial distributions were strikingly similar to the distributions of genes associated with the ascending loop of Henle. Within zones III and IV, we observed the localization of more than one KRM cluster. In both zones, each cluster was mapped similarly, but with slightly different distributions. The spatial organization of each KRM cluster was unique and associated with specific zones within the kidney ([Figure 3](#)).

Validation of select KRM markers.

To validate the general location of specific clusters shown by spatial transcriptomics, we used flow cytometry to visualize the expression of select proteins that were transcriptionally distinct within clusters. Because cluster 3 resided primarily in the medulla ([Figure 4A](#)), we performed flow cytometry to compare expression levels of CD14 protein among cells isolated separately from the medulla and the cortex. Analysis of the most significant DEGs for each KRM cluster by adjusted P value indicated that

transcripts for CD14, a pathogen-associated molecular pattern receptor involved in the recognition of LPS, were expressed in all KRMs but appeared to substantially increase in cluster 3 ([Figure 4A](#), dot plot). Flow cytometry of kidneys manually dissected into cortex and medulla allowed for the identification of increased CD14⁺⁺ cells among CD45⁺TCRb⁻CD19⁻NK1.1⁻Gr1⁻CD11b^{int}F4/80^{hi} KRMs in the medulla but not the cortex of the kidney ([Figure 4B](#)). This aligned with the plotting of cluster 3 using spatial transcriptomics, which appeared primarily in the medulla and papilla. In comparison, mannose receptor C-type 1 (Mrc1, also known as CD206) expression was increased in cluster 4. This cluster was spatially distributed in the inner medulla and, to a lesser extent, the outer cortex ([Figure 4C](#)). Immunofluorescence imaging revealed CD206/Mrc1⁺ KRMs in the outer cortex and inner medulla; however, they were largely absent from the inner cortex, which is consistent with the spatial transcriptomics data ([Figure 4, D and E](#)).

Ischemic injury alters the spatial and transcriptomic profiles of KRM subpopulations, and they remain altered 4 weeks after injury.

We next determined the effect of ischemic injury on transcriptomic programming and spatial distribution of KRMs as a function of time. [Figure 5A](#) shows UMAP plots for KRMs from quiescent kidneys and also those at 12 hours and days 1, 6, and 28 after injury. Relative to quiescent kidneys, proportional changes in the representation of each KRM cluster was observed within 12 hours following the ischemic insult. The proportions at day 28 appear similar to those at quiescence ([Figure 5B](#)). Most notable among these acute changes are increases in the proportions of cells in clusters 2 and 5. The GO terms following Days 1 and 6 post-injury are included in [Supplemental Tables 1 and 2](#).

Following injury, there was a change in cluster spatial locations ([Figure 5C](#)). This was observed in the early inflammatory phase (12 hours and day 1 after injury) as well as in the reparative phase (day 6 after injury). For reference, kidney cell markers at each time point are provided and appear similar to the quiescent profile ([Supplemental Figures 6–9](#)). At 12 hours, we identified clusters that appeared to be in intermediate locations between their initial sites and their positions on day 1 and day 6 after injury. This was exemplified by the medullary subpopulations, clusters 1 and 3. During quiescence, these populations were predominantly present in zones V (papilla) and IV (inner medulla), respectively. At 12 hours after injury, cluster 1 and cluster 3 mapped to the cortical/medullary region. By day 1 after insult, cluster 1 was concentrated at the corticomedullary junction but also appeared to be distributed throughout the cortex. Cluster 3, initially found in the papilla, was also found in the cortex ([Figure 5C](#)).

Spatial transcriptomics from day 28 shows that some KRM subpopulations did not map to their initial locations ([Figure 5C](#)). A comparison of KRM subpopulations at day 28 to their quiescent profile showed that while clusters 0, 1, and 2 mostly mapped to their quiescent location, clusters 3, 4, 5, and 6 appeared scattered throughout the tissue ([Figure 5C](#)). Notably, the day 28 kidneys appeared to lose spatially distinct medullary KRM subpopulations.

The GO terms for clusters 1, 3, and 6 at day 28 remained antiviral and antibacterial ([Supplemental Table 3](#)). Cluster 2 had reestablished terms involved in iron handling. While GO terms appeared for cluster 0, they had FDRs above the significance level ($FDR < 0.05$). Clusters 4 and 5 continued to be involved in chemotaxis.

Discussion

Using scRNA-Seq in conjunction with spatial transcriptomics, we identified, characterized, and localized 7 major subpopulations of KRMs in the mouse kidney before and after ischemic injury. We revealed that KRM subpopulations exist within microenvironmental niches associated with specific zones, roughly approximating layers from the cortex to the papilla. After the injury, the original compartmentalization of KRM subpopulations is lost and is still not fully regained 28 days after injury.

Recent work in the area of the kidney myeloid immune system has focused on increasing the understanding of the various subpopulations in quiescence and following injury ([15](#), [24](#)). Our work expands on these evolving definitions and characterizes protein expression markers for multiple transcriptionally distinct subpopulations. Current studies analyze the macrophage compartment as a whole, which provides important information on infiltrating monocytes but can cloud the understanding of the KRM population. By focusing solely on the KRMs, we have identified at least 7 transcriptionally distinct major subpopulations. Some of these, such as the type I IFN–responding cluster 6, share similarities with resident macrophage populations in other tissues ([25](#), [26](#)). Others, like cluster 5, which expands after ischemic injury, may be unique to the kidney.

In an attempt to generate a comprehensive understanding of kidney macrophages, we identified quiescent protein expression markers for subpopulations that had been identified across injury models previously by other groups. We identified cluster 3 as CD14⁺⁺ and cluster 4 cells as CD206⁺. In human kidneys, CD14⁺⁺ macrophages have been identified as a subpopulation primed against bacterial infection and responsive to salt gradients in models of urinary tract infections ([27](#)). Additionally, medullary

CD14⁺⁺ cluster 3 KRMs express transcripts involved in neutrophil chemotaxis and activation. Previous studies by Berry et al. demonstrated that medullary CD14⁺⁺ macrophages isolated from human medulla activate neutrophils (27). CD206⁺ macrophages have been identified by other groups in models of unilateral ureteral obstruction and polycystic kidney disease (15, 28). Like in those studies, our CD206⁺ cluster 4 KRMs expressed transcripts for *Stab1*, *Fcrls*, and *Igf1*, which are associated with tissue regeneration and fibrosis. In the liver, resident macrophages that express similar transcripts to cluster 4 are thought to be involved in the prevention of fibrosis following insult (29). Zimmerman et al. identified CD206⁺ KRMs surrounding cysts in polycystic kidney disease development, and inhibition of KRM proliferation decreased CD206⁺ KRM numbers and lessened cyst growth and numbers, suggesting that cluster 4 cells could be involved in cyst formation or fibrosis progression (28).

Stratification of KRMs into specific zones within the kidney was previously unknown. The spatial location of macrophages affects their function in other tissues, such as the lung, spleen, and liver, and response to an immunological challenge, in the case of tuberculosis or tumors (8–12). Although many disease states have known connections with KRMs (30–32) and targeting populations holds great therapeutic promise, successful design and implementation of such strategies are limited by our current understanding of KRM regulation and response to injury. As it relates to location, cluster 0 is initially at the site of the greatest insult during an ischemic event. The lack of oxygen in the tissue damages the mitochondria-heavy S3 proximal tubule cells in the corticomedullary junction (33, 34). Cluster 1 was the second-largest KRM population and was concentrated in the papilla. Its presence in zone V, which has aquaporin 2 gene

expression, suggests that cluster 1 cells are found near the collecting ducts. Prior studies have indicated a relationship between macrophages and the collecting duct in the context of IgA nephropathy, with one study suggesting a role in driving fibrosis in that region ([35](#), [36](#)). Cluster 2, which is distinguished by its iron-handling transcripts, was located in the cortex around proximal tubules, where iron is reabsorbed in healthy conditions and accumulates during iron disorders ([37](#)). Additionally, the subpopulation locations suggest a coordinated positioning to protect the kidney from infection. The transcriptome and location of clusters 1, 3, and 6 depict a strategic immune barrier from the ureter, the most common origin of kidney infections ([38](#)). Macrophage subpopulations in other tissues, such as the lung, gut, and skin, are known to perform this function ([39–42](#)). Our work highlights the diversity among the KRMs and the corresponding need to selectively target specific subpopulations with respect to the originating mechanism of insult.

It is similarly important to consider timing, as the KRMs alter their spatial location after injury. This apparent movement can be ascribed either (a) to a physical translocation of the KRMs following injury and/or (b) to KRM subpopulations in specific locations undergoing a transition from transcriptional profiles associated with one cluster to another. The former hypothesis is supported by data showing that 12 hours after injury, clusters 1 and 3 appear at intermediate locations between their quiescent and 24-hour locations. In addition, GO analysis from time points following injury identifies many terms involved in cell migration and motility. This further supports that the KRM subpopulations have location-specific responses to areas of damage within the kidney and may both relocate and alter their transcriptional profile in response to injury. While our

data support the possibility that KRMs are migrating, future experiments will need to confirm KRM locomotion.

Nevertheless, the transcriptomic atlas, with many KRM subpopulations no longer expressing their original profiles and existing within new locations, is persistently altered and future therapeutics will need to consider the location at the time of treatment to accurately gain the desired effect. During the course of our studies, the transcriptomic profile failed to return to quiescence, even after 28 days. Given the continued disruption in transcriptional and spatial distribution beyond acute injury, KRMs may influence the transition from AKI to chronic kidney disease (CKD). A single AKI event drastically increases the risk for the development of CKD ([43–46](#)), although the mechanisms that underlie the AKI-to-CKD transition remain unclear. Multiple cell types have been implicated, including damaged proximal tubules and vascular cells, in addition to leukocytes ([47](#)). KRMs are of particular interest given their capacity for inflammation and fibrosis and continued presence in the tissue beyond an acute injury ([48–52](#)). Future studies should consider the effect of the altered KRM subpopulations on long-term kidney function both from native kidneys and following transplant.

This work has characterized the subpopulations of KRMs and determined their location within healthy kidneys. Following insult, we tracked the subpopulations as they appear to relocate throughout the tissue, suggesting locomotion by these cells in response to injury, as a result of tubule cell death and/or transient ischemia to the various subpopulations. Finally, our data confirm a long-hypothesized dysregulation of the immune system following AKI and provide a foundational framework for the increased risk for CKD following an AKI event. The result is a KRM atlas of the murine kidney

that can provide a point of reference for future studies into the role of the resident macrophage system in the normal and injured kidney.

Methods

Animals.

Male C57BL/6J mice, 12–16 weeks of age, were obtained from The Jackson Laboratory. Mice were housed at the University of Alabama at Birmingham (UAB) animal facilities in compliance with the NIH guidelines regarding the care and use of live animals.

Bilateral ischemia/reperfusion injury.

Mice were subjected to bilateral ischemia/reperfusion injury, as previously described ([3](#), [4](#)). All surgeries were performed in the morning. Mice were anesthetized using ketamine and xylazine (i.p.). Under aseptic precautions, both kidneys were clamped at the renal pedicle using a microserrafine vascular clamp (Fine Science Tools, 18055-05). After 19 minutes, the clamps were removed to allow reperfusion. Reperfusion was visually confirmed within 1 minute. Body temperature, measured by a rectal thermometer, was carefully maintained at $37^{\circ}\text{C} \pm 1^{\circ}\text{C}$.

Flow cytometry/FACS.

KRMs represent approximately 1%–2% of total viable cells in a quiescent kidney. In order to obtain a minimum number of cells to draw meaningful conclusions about KRM subpopulations as determined by scRNA-Seq, we isolated KRMs using flow

cytometric sorting. Leukocytes were isolated as previously described (3, 4). Mice were anesthetized under isoflurane and perfused through the left ventricle with 10 mL cold PBS. Kidneys were removed, stripped of the capsule, minced with a razor blade on a glass slide, and placed into Liberase (MilliporeSigma) at 37°C for 30 minutes. The digestion was stopped by adding cold PBS containing 1% BSA, and tissue was further disaggregated through an 18-gauge syringe. Red blood cells were lysed using ACK lysis buffer for 2 minutes at room temperature, and the remaining leukocytes were then washed with ice-cold PBS. Cells were then stained with violet fixable viability dye (Invitrogen L34955) and treated with unlabeled anti-CD16/32 antibody to block Fc γ 3 receptors. Cells were subsequently stained using anti-Gr-1 Alexa Fluor 700 (Ly6G, clone 1A8, BioLegend), anti-CD11b super bright 600 (M1/70, Invitrogen), anti-F4/80 APC-eFluor-780 (BM8, Invitrogen), anti-NK1.1 PE-C7 (PK136, Invitrogen), anti-CD45.2 BV-650 (104, BioLegend), anti-MHC II (I-A/I-E) PerCP (M5/114.15.2, BD Biosciences), anti-CD19 super bright 702 (6D5, BioLegend), anti-TCR β Pe-Cy5 (H57-597, BD Biosciences), and anti-CD14 APC (Sa2-8, Invitrogen) ([Supplemental Figure 1](#)).

Nuclear isolation from whole kidney.

Nuclei were isolated using Nuclei Lysis Buffer containing Nuclei Isolation Kit: Nuclei EZ Prep Buffer (MilliporeSigma) supplemented with cOmplete ULTRA Tablets (MilliporeSigma) and SUPERase IN (Thermo Fisher Scientific) and Promega RNAsin Plus nuclease inhibitors. Kidneys were minced into less than 1 mm pieces in 2 mL Nuclei Lysis Buffer. Samples were transferred to a dounce homogenizer (Kimble) and homogenized. An additional 2 mL Nuclei Lysis Buffer was added to the sample and

incubated for 5 minutes on ice. Samples were passed through a 40 μm filter into a 50 mL conical tube. Samples were centrifuged at 500g for 5 minutes at 4°C. The supernatant was removed, and the pellet was washed with 4 mL Nuclei Lysis Buffer containing 1% bovine serum albumin for 5 minutes on ice. Samples were centrifuged at 500g for 5 minutes at 4°C. Samples were passed through a 5 μm filter into a 50 mL conical tube and then centrifuged again. Nuclei were resuspended in a solution containing PBS, 1% BSA, and 0.1% RNase inhibitor.

scRNA-Seq/single-nuclear RNA-Seq.

Purified cells or nuclei were transferred on ice to the UAB Flow Cytometry and Single Cell Core and immediately processed using the Chromium 3' Single Cell RNA sequencing kit (10 \times Genomics) according to the manufacturer's instructions. The cell suspension was counted and combined with a 10 \times Chromium reagent mixture and loaded into a microfluidic single-cell partitioning device in which lysis and reverse transcriptions occur in microdroplets. The resulting cDNA was amplified by a polymerase chain reaction and subsequently processed to yield bar-coded sequencing libraries. Paired-end sequencing was carried out on an Illumina NovaSeq6000 sequencing platform (Illumina). Reads were processed using the 10 \times Genomics Cell Ranger Single-Cell Software Suite (version 6.0) on the UAB Cheaha High-Performance Computing Cluster. BCL files were converted to FASTQ files using the CellRanger mkfastq function. CellRanger count was used to align the FASTQ files to the mouse genome (mm10). The gene table, barcode table, and transcriptional expression matrices were created for the analysis indicated below.

Spatial transcriptomics.

The Visium system relies on a 2-dimensional matrix of 5000 spots distributed on a microscope slide in a 6.5 by 6.5 mm square. Each spot, which contains a poly-dT oligonucleotide with a unique sequence (bar code), is 50 μm in diameter at a distance from the other spots of 100 μm from center to center. Kidneys were embedded in the Optimal Cutting Temperature matrix (Fisher Scientific) and stored at -80°C . Before sectioning, blocks were equilibrated to -10°C for 30 minutes. A 10 μm section was placed onto specialized Spatial Gene Expression slides (10 \times Genomics) and processed according to the manufacturer's protocols. Briefly, slides were stained with H&E, and bright-field images were acquired using a Keyence BZ-X700 microscope. Tissues were permeabilized for 18 minutes, and cDNA was generated and used to create second-strand DNA. The resulting cDNA was subject to downstream amplification and library processing for scRNA-Seq. Reads were processed using the 10 \times Genomics Cell Ranger Single-Cell Software Suite (version 6.0) on the UAB Cheaha High-Performance Computing Cluster. BCL files were converted to FASTQ files using the SpaceRanger mkfastq function. SpaceRanger count was used to align the FASTQ files to the mouse genome (mm10).

Sequencing analysis.

Both scRNA-Seq and spatial transcriptomics analyses were carried out using packages created for the R statistical analysis environment (version 4.06). Data were primarily analyzed using Seurat (version 3.2.3) and its associated dependencies ([19](#), [53](#)) as previously described ([54](#)). Data from each mouse were imported using the Read10X

function and then structured into a Seurat object using `CreateSeuratObject`. For quality control, cells with unique feature counts over 2500 or under 200 were excluded. Data were normalized and scaled using `SCTransform` (55). Objects from each time point were labeled with unique group IDs and then merged into a single object using the Seurat merge function. Data objects were integrated using the Harmony R package (56). Principal component analysis was performed based on 30 principal components, and then cells were clustered using `FindAllMarkers` set to a resolution of 0.4. The dimensional reduction was done using UMAP. `WebGestaltR` was used for gene ontology analysis to identify pathways using the Biologic Process and Kyoto Encyclopedia of Genes and Genomes databases (57).

Integration of scRNA-Seq and spatial transcriptomics to resolve cell location.

The spatial matrix was integrated with the scRNA-Seq data set using the anchor-based workflow built into the Seurat package. `FindTransferAnchors` was used on the data object containing all 7 KRM clusters. Using the generated anchor set, the `TransferData` function created predictions from the KRM reference clusters and applied that to the spatial data set. Using a predictions assay, each subpopulation could be visualized using `SpatialFeaturePlots`.

Immunofluorescence staining and imaging.

Kidneys from Cx3Cr1⁺ GFP mice (obtained in-house) were cryosectioned onto glass slides and then fixed in 4% paraformaldehyde for 10 minutes. Tissues were permeabilized using 0.2% Triton X-100 in PBS for 8 minutes, washed 3 times with PBS,

and then blocked in a solution containing PBS, 0.1% Triton X-100, 1% bovine serum albumin, and 1% donkey serum for 30 minutes at room temperature. Primary antibodies, including anti-CD206 (abcam, ab64693, 1:250) were diluted in a blocking solution and stained overnight at 4°C. Tissues were washed with PBS; stained with secondary antibodies, including anti-rabbit Alexa Fluor 595 (Invitrogen, A21207, 1:1000) and anti-rat Alexa Fluor 647 (Invitrogen, A21247, 1:1000), for 30 minutes at room temperature; and then washed again with PBS. A 1:1000 DAPI solution was added for 5 minutes at room temperature and then washed with PBS. Slides were mounted with IMMU-MOUNT (Thermo Fisher). All images were captured on a Nikon Spinning-disk confocal microscope with a Yokogawa X1 disk, using a Hamamatsu flash4 sCMOS camera with a ×40 oil immersion objective. Images were processed and analyzed in NIS Elements software (Nikon; version 5.0) and ImageJ (NIH). A blinded observer quantified the number of CD206⁺Cx3cr1⁺ cells of the total Cx3Cr1⁺ cells per high-power field.

Data availability. The scRNA-Seq and spatial transcriptomics data generated for this paper were deposited in the NCBI's Gene Expression Omnibus database (GEO GSE200115).

Statistics.

GraphPad Prism 8.0 was used for statistical analysis. The mean ± SEM was determined for each treatment group in the experiment. A 1-way ANOVA followed by post hoc analysis was used to determine the statistical significance between groups. *P* values of less than 0.05 were considered significant.

Study approval. All animal work performed was reviewed and approved by the Institutional Animal Care and Use Committee at UAB.

Author Contributions

MDC, ENE, JMPL, AA, and JFG designed the experiments. MDC, EE, JMPL, JRL, SL, ZY, and ZL performed the experiments. MDC, EE, KHM, GGR, RK, BKY, AA, and JFG performed data analysis and interpretation. MDC, EE, KHM, AA, and JFG wrote the manuscript. All authors reviewed and approved the manuscript prior to submission. The authorship order among co-first authors was agreed upon after discussion by the authors.

Acknowledgments

The authors would like to thank Chiao-Wang Sun, Sagar Hanumanthu, and Harish Pal for their assistance with collection and processing of samples. We acknowledge the UAB Flow Cytometry and Single Cell Core (NIH P30-AR-04831) and the UAB Heflin Genomics Core (NIH 5P30CA013148-48). The graphical abstract was created with BioRender.com. This work was supported by NIH grants P30 DK079337, R01 DK59600, and R01 DK118932 (to AA and JFG), UAB Medical Scientist Training Program grants T32-GM-008361 and T32 AI007051 (to MDC), American Heart Association grant 906401 (to MDC), and American Heart Association grant 827257 (to ENE).

References

1. Soos TJ, et al. CX3CR1+ interstitial dendritic cells form a contiguous network throughout the entire kidney. *Kidney Int.* 2006;70(3):591–596.

2. Liu F, et al. Distinct fate, dynamics and niches of renal macrophages of bone marrow or embryonic origins. *Nat Commun.* 2020;11(1):2280.
3. Lever JM, et al. Resident macrophages reprogram toward a developmental state after acute kidney injury. [published online January 24, 2019]. *JCI Insight.* <https://doi.org/10.1172/jci.insight.125503>.
4. Lever JM, et al. Parabiosis reveals leukocyte dynamics in the kidney. *Lab Invest.* 2018;98(3):391–402.
5. Hume D, Gordon S. Mononuclear phagocyte system of the mouse defined by immunohistochemical localization of antigen F4/80. Identification of resident macrophages in renal medullary and cortical interstitium and the juxtaglomerular complex. *J Exp Med.* 1983;157(5):1704–1709.
6. Ferenbach DA, et al. Macrophage/monocyte depletion by clodronate, but not diphtheria toxin, improves renal ischemia/reperfusion injury in mice. *Kidney Int.* 2012;82(8):928–933.
7. Zhang M-Z, et al. CSF-1 signaling mediates recovery from acute kidney injury. *J Clin Invest.* 2012;122(12):4519–4532.
8. Kopf M, et al. The development and function of lung-resident macrophages and dendritic cells. *Nat Immunol.* 2015;16(1):36–44.
9. Blériot C, Ginhoux F. Understanding the heterogeneity of resident liver macrophages. *Front Immunol.* 2019;10:2694.
10. A-Gonzalez N, Castrillo A. Origin and specialization of splenic macrophages. *Cell Immunol.* 2018;330:151–158.

11. Marakalala MJ, et al. Inflammatory signaling in human tuberculosis granulomas is spatially organized. *Nat Med.* 2016;22(5):531–538.
12. Huang Y-K, et al. Macrophage spatial heterogeneity in gastric cancer defined by multiplex immunohistochemistry. *Nat Commun.* 2019;10(1):3928.
13. Zimmerman KA, et al. Single-cell RNA sequencing identifies candidate renal resident macrophage gene expression signatures across species. *J Am Soc Nephrol.* 2019;30(5):767–781.
14. Affandi AJ, et al. CXCL4 drives fibrosis by promoting several key cellular and molecular processes. *Cell Rep.* 2022;38(1):110189.
15. Conway BR, et al. Kidney single-cell atlas reveals myeloid heterogeneity in progression and regression of kidney disease. *J Am Soc Nephrol.* 2020;31(12):2833–2854.
16. Schledzewski K, et al. Deficiency of liver sinusoidal scavenger receptors stabilin-1 and -2 in mice causes glomerulofibrotic nephropathy via impaired hepatic clearance of noxious blood factors. *J Clin Invest.* 2011;121(2):703–714.
17. Rantakari P, et al. Stabilin-1 expression defines a subset of macrophages that mediate tissue homeostasis and prevent fibrosis in chronic liver injury. *Proc Natl Acad Sci U S A.* 2016;113(33):9298–9303.
18. Silva-Cardoso SC, et al. CXCL4 links inflammation and fibrosis by reprogramming monocyte-derived dendritic cells in vitro. *Front Immunol.* 2020;11:2149.
19. Butler A, et al. Integrating single-cell transcriptomic data across different conditions, technologies, and species. *Nat Biotechnol.* 2018;36(5):411–420.

20. Ferreira RM, et al. Integration of spatial and single-cell transcriptomics localizes epithelial cell–immune cross-talk in kidney injury. *JCI Insight*. 2021;6(12):147703.
21. Janosevic D, et al. The orchestrated cellular and molecular responses of the kidney to endotoxin define a precise sepsis timeline. *Elife*. 2021;10:e62270.
22. Dixon EE, et al. Spatially resolved transcriptomic analysis of acute kidney injury in a female murine model. *J Am Soc Nephrol*. 2022;33(2):279–289.
23. Wu H, et al. Advantages of single-nucleus over single-cell RNA sequencing of adult kidney: rare cell types and novel cell states revealed in fibrosis. *J Am Soc Nephrol*. 2019;30(1):23–32.
24. Salei N, et al. The kidney contains ontogenetically distinct dendritic cell and macrophage subtypes throughout development that differ in their inflammatory properties. *J Am Soc Nephrol*. 2020;31(2):257–278.
25. Zaman R, et al. Selective loss of resident macrophage-derived insulin-like growth factor-1 abolishes adaptive cardiac growth to stress. *Immunity*. 2021;54(9):2057–2071.
26. Schaupp L, et al. Microbiota-induced type I interferons instruct a poised basal state of dendritic cells. *Cell*. 2020;181(5):1080–1096.
27. Berry MR, et al. Renal sodium gradient orchestrates a dynamic antibacterial defense zone. *Cell*. 2017;170(5):860–874.
28. Zimmerman KA, et al. Tissue-resident macrophages promote renal cystic disease. *J Am Soc Nephrol*. 2019;30(10):1841–1856.

29. Tan-Garcia A, et al. Liver fibrosis and CD206⁺ macrophage accumulation are suppressed by anti-GM-CSF therapy. *JHEP Rep.* 2020;2(1):100062.
30. Kishore BK, et al. CD39-adenosinergic axis in renal pathophysiology and therapeutics. *Purinergic Signal.* 2018;14(2):109–120.
31. Weisheit CK, et al. Dendritic cells and macrophages: sentinels in the kidney. *Clin J Am Soc Nephrol.* 2015;10(10):1841–1851.
32. Chen T, et al. M2 macrophages in kidney disease: biology, therapies, and perspectives. *Kidney Int.* 2019;95(4):760–773.
33. Venkatachalam MA, et al. Ischemic damage and repair in the rat proximal tubule: differences among the S1, S2, and S3 segments. *Kidney Int.* 1978;14(1):31–49.
34. Shanley PF, et al. Topography of focal proximal tubular necrosis after ischemia with reflow in the rat kidney. *Am J Pathol.* 1986;122(3):462–468.
35. Pawluczyk IZA, et al. Macrophage interactions with collecting duct epithelial cells are capable of driving tubulointerstitial inflammation and fibrosis in immunoglobulin A nephropathy. *Nephrol Dial Transplant.* 2020;35(11):1865–1877.
36. Zheng Y, et al. Single-cell transcriptomics reveal immune mechanisms of the onset and progression of IgA nephropathy. *Cell Rep.* 2020;33(12):108525.
37. Van Raaij S, et al. Tubular iron deposition and iron handling proteins in human healthy kidney and chronic kidney disease. *Sci Rep.* 2018;8(1):9353.
38. Munoz JA, et al. Innate bacteriostatic mechanisms defend the urinary tract. *Annu Rev Physiol.* 2022;84(1):533–558.

39. Feuerstein R, et al. Dynamic interactions between dermal macrophages and *Staphylococcus aureus*. *J Leukoc Biol*. 2017;101(1):99–106.
40. Mowat AM, et al. Barrier-tissue macrophages: functional adaptation to environmental challenges. *Nat Med*. 2017;23(11):1258–1270.
41. Lipscomb MF, et al. The regulation of pulmonary immunity. *Adv Immunol*. 1995;59:369–455.
42. Arques JL, et al. Salmonella induces flagellin- and MyD88-dependent migration of bacteria-capturing dendritic cells into the gut lumen. *Gastroenterology*. 2009;137(2):579–587.
43. Goldberg R, Dennen P. Long-term outcomes of acute kidney injury. *Adv Chronic Kidney Dis*. 2008;15(3):297–307.
44. Basile DP, et al. Renal ischemic injury results in permanent damage to peritubular capillaries and influences long-term function. *Am J Physiol Renal Physiol*. 2001;281(5):F887–F899.
45. Ponte B, et al. Long-term functional evolution after an acute kidney injury: a 10-year study. *Nephrol Dial Transplant*. 2008;23(12):3859–3866.
46. Chawla LS, et al. Acute kidney injury and chronic kidney disease as interconnected syndromes. *N Engl J Med*. 2014;371(1):58–66.
47. Sato Y, Yanagita M. Immune cells and inflammation in AKI to CKD progression. *Am J Physiol Renal Physiol*. 2018;315(6):F1501–F1512.
48. Sears SM, et al. F4/80^{hi} resident macrophages contribute to cisplatin-induced renal fibrosis. *Kidney360*. 2022;3(5):818–833.

49. Maria NI, Davidson A. Renal macrophages and dendritic cells in SLE nephritis. *Curr Rheumatol Rep.* 2017;19(12):81.
50. Lill JK, et al. Tissue-resident macrophages mediate neutrophil recruitment and kidney injury in shiga toxin-induced hemolytic uremic syndrome. *Kidney Int.* 2021;100(2):349–363.
51. Duffield JS, et al. Conditional ablation of macrophages halts progression of crescentic glomerulonephritis. *Am J Pathol.* 2005;167(5):1207–1219.
52. Kanayama M, et al. Autophagy enhances NFκB activity in specific tissue macrophages by sequestering A20 to boost antifungal immunity. *Nat Commun.* 2015;6(1):5779.
53. Stuart T, et al. Comprehensive integration of single-cell data. *Cell.* 2019;177(7):1888–1902.
54. Cheung MD, et al. Single-cell RNA sequencing of urinary cells reveals distinct cellular diversity in COVID-19–associated AKI. *Kidney360.* 2022;3(1):28–36.
55. Hafemeister C, Satija R. Normalization and variance stabilization of single-cell RNA-seq data using regularized negative binomial regression. *Genome Biol.* 2019;20(1):296.
56. Korsunsky I, et al. Fast, sensitive and accurate integration of single-cell data with Harmony. *Nat Methods.* 2019;16(12):1289–1296.
57. Wang J, et al. WebGestalt 2017: a more comprehensive, powerful, flexible and interactive gene set enrichment analysis toolkit. *Nucleic Acids Res.* 2017;45(w1):W130–W137.

Tables

Table 1. Gene ontology analysis of KRM clusters in quiescence

Cluster	Gene set	Description	Enrichment		
			ratio	P value	FDR
0	GO:0046631	α - β T cell activation	15.9	1.13×10^{-4}	0.0470
0	GO:0032640	Tumor necrosis factor production	15.6	1.19×10^{-4}	0.0470
0	GO:1903555	Regulation of tumor necrosis factor superfamily cytokine production	15.6	1.19×10^{-4}	0.0470
1	GO:0072593	Reactive oxygen species metabolic process	9.6	1.70×10^{-6}	0.0026
1	GO:0034405	Response to fluid shear stress	33.3	9.85×10^{-5}	0.0120
1	GO:2001057	Reactive nitrogen species metabolic process	16.5	1.01×10^{-4}	0.0120
1	GO:0072538	T helper 17-type immune response	30.1	1.33×10^{-4}	0.0140
1	GO:0042110	T cell activation	4.9	5.26×10^{-4}	0.0298
1	GO:0009611	Response to wounding	4.6	7.66×10^{-4}	0.0361
1	GO:0002294	CD4 ⁺ α - β T cell differentiation	15.3	9.93×10^{-4}	0.0424
2	GO:0042060	Wound healing	7.2	3.96×10^{-6}	0.0012
2	GO:0006909	Phagocytosis	10.7	2.09×10^{-5}	0.0038
2	GO:0010039	Response to iron ion	26.2	2.03×10^{-4}	0.0178
2	GO:0006956	Complement activation	19.8	4.69×10^{-4}	0.0328
2	GO:0002448	Mast cell-mediated immunity	18.9	5.34×10^{-4}	0.0342
2	GO:0031663	LPS-mediated signaling pathway	17.8	6.41×10^{-4}	0.0387
3	GO:0071222	Cellular response to LPS	8.8	6.14×10^{-13}	0.0000
3	GO:0030099	Myeloid cell differentiation	6.3	2.30×10^{-12}	0.0000
3	GO:0032640	Tumor necrosis factor production	8.8	2.91×10^{-9}	0.0000
3	GO:0035710	CD4 ⁺ α - β T cell activation	11.0	2.55×10^{-8}	0.0000
3	GO:0032611	IL-1 β production	13.0	2.83×10^{-8}	0.0000
4	GO:0034349	Glial cell apoptotic process	102.0	3.17×10^{-6}	0.0099
4	GO:0071825	Protein-lipid complex subunit organization	49.6	2.95×10^{-5}	0.0460
6	GO:0051607	Defense response to virus	16.4	0	0.0000
6	GO:0034341	Response to IFN- γ	15.3	0	0.0000
6	GO:0034340	Response to type I IFN	15.3	3.06×10^{-7}	0.0000
6	GO:0032606	Type I IFN production	9.7	3.54×10^{-7}	0.0000
6	GO:0032496	Response to LPS	4.3	5.44×10^{-7}	0.0000

*No statistically significant results were found for cluster 5. Gene ontology analysis of terms with an FDR < 0.05.

Figure Legends

Figure 1. Model of acute kidney injury

(A) Schematic depicting work flow for scRNA-Seq and spatial transcriptomics. Mice were subjected to bilateral ischemia/reperfusion injury for 19 minutes. Kidneys were harvested at day 0, 12 hours, and days 1, 6, and 28 after injury. Kidneys were either utilized for spatial transcriptomics or digested and flow sorted for KRMs and subjected to scRNA-Seq. There were 3 biological replicates per time point. (B) Serum creatinine levels (mg/dL) at quiescence (day 0) and days 1, 6, and 28 after injury from at least 2 independent experiments. Data are reported as mean \pm SEM. A 1-way ANOVA was used

to determine the statistical significance between groups. * $P < 0.05$. (C) H&E-stained kidney sections at quiescence and days 1, 6, and 28 after injury. Scale bar: 2000 μm (top row); 100 μm (bottom row).

Figure 2. Single-cell RNA-Seq and spatial transcriptomics reveal distinct subpopulations of kidney-resident macrophages.

(A) Uniform manifold approximation and projection (UMAP) plot of sequenced kidney-resident macrophages (KRM) demonstrating 13 clusters. Contaminating kidney cells and clusters representing less than 1% were removed to leave 7 unique clusters in quiescence. (B) *Clqa* expression in all KRM clusters during quiescence. (C) Heatmap of top 5 differentially expressed genes among each subpopulation in quiescence ordered by adjusted P value.

Figure 3. Kidney-resident macrophages are found in distinct regions.

An integrated analysis of the single-cell RNA-Seq (scRNA-Seq) and spatial transcriptomics data was performed to localize the kidney-resident macrophage (KRM) clusters on a kidney section. A diagram of a nephron is color coded to delineate different nephron segments (see **nephron zones; left**). Gray shading and numbering (I–V) describes nephron zones that would be enriched in areas of a kidney cross-section. The spatial location of the nephron segments is shown by mapping segment-specific transcripts onto the histological image (see zone-specific transcripts; middle). Transcript markers are listed in the bottom right-hand corner of each section. Specific nephron segments are listed above each image. Colored bars correspond to the location of the

segments from the nephron shown on the left. Row number (**I–V**) indicates the nephron zone. The integration of the KRM scRNA-Seq data onto the spatial section plots the location of KRM subpopulations within the quiescent kidney (right). The clusters are aligned with the kidney nephron segments that are found in the same zone to highlight the colocalization between KRMs and kidney cells. CNT, connecting tubule; DCT, distal convoluted tubule; PT, proximal tubule.

Figure 4. Spatial validation of protein markers.

(A) Spatial location of cluster 3 overlaid on the histological image and a dot plot of *CD14* transcript expression for each cluster. **(B)** Kidneys were harvested and dissected to separate the cortex from the medulla to confirm the location of cluster 3 $CD14^{++}$ cells in the medulla. Flow cytometry analysis of *CD14* expression in KRMs of the whole kidney (left) and dissected cortex compared with medulla (right) along with the fluorescence minus one (FMO) control. **(C)** Spatial location of cluster 4 overlaid on histological image and a dot plot of *Mrc1* transcript expression show that cluster 4 is localized in the outer cortex and inner medulla but not the inner cortex. **(D)** Representative images from immunofluorescence of kidney sections of *Cx3Cr1* $GFP^{+/-}$ mice stained with *CD206* and the nuclear stain DAPI to validate cluster 4 KRMs by confocal microscopy (original magnification, $\times 40$). Results were averaged from 4 separate fields within each area with 4 mice in total over 2 independent experiments. Scale bar: 20 μm . **(E)** Quantitation from a blinded observer of $CD206^{+}$ KRMs in the outer cortex, inner cortex, and medulla, expressed as a proportion of $Cx3Cr1^{+}$ cells.

**** $P < 0.0001$ by 1-way ANOVA followed by Tukey's test. Data are shown as mean \pm SEM.

Figure 5. Spatial and proportional changes to KRM subpopulations following injury.

(A) Uniform manifold approximation and projection (UMAP) plot of KRM clusters at quiescence and 12 hours, day 1, day 6, and day 28 after injury to assess changes after injury. **(B)** Changes in proportions of each cluster over time. **(C)** scRNA-Seq data from each time point integrated with their respective spatial transcriptomic kidney sections to resolve cluster locations. Each row represents a KRM cluster, whereas each column depicts a time point from quiescence to day 28 (left to right). Images were taken with $\times 4$ objective then stitched together so they appear as $\times 2$.

Figure 1.

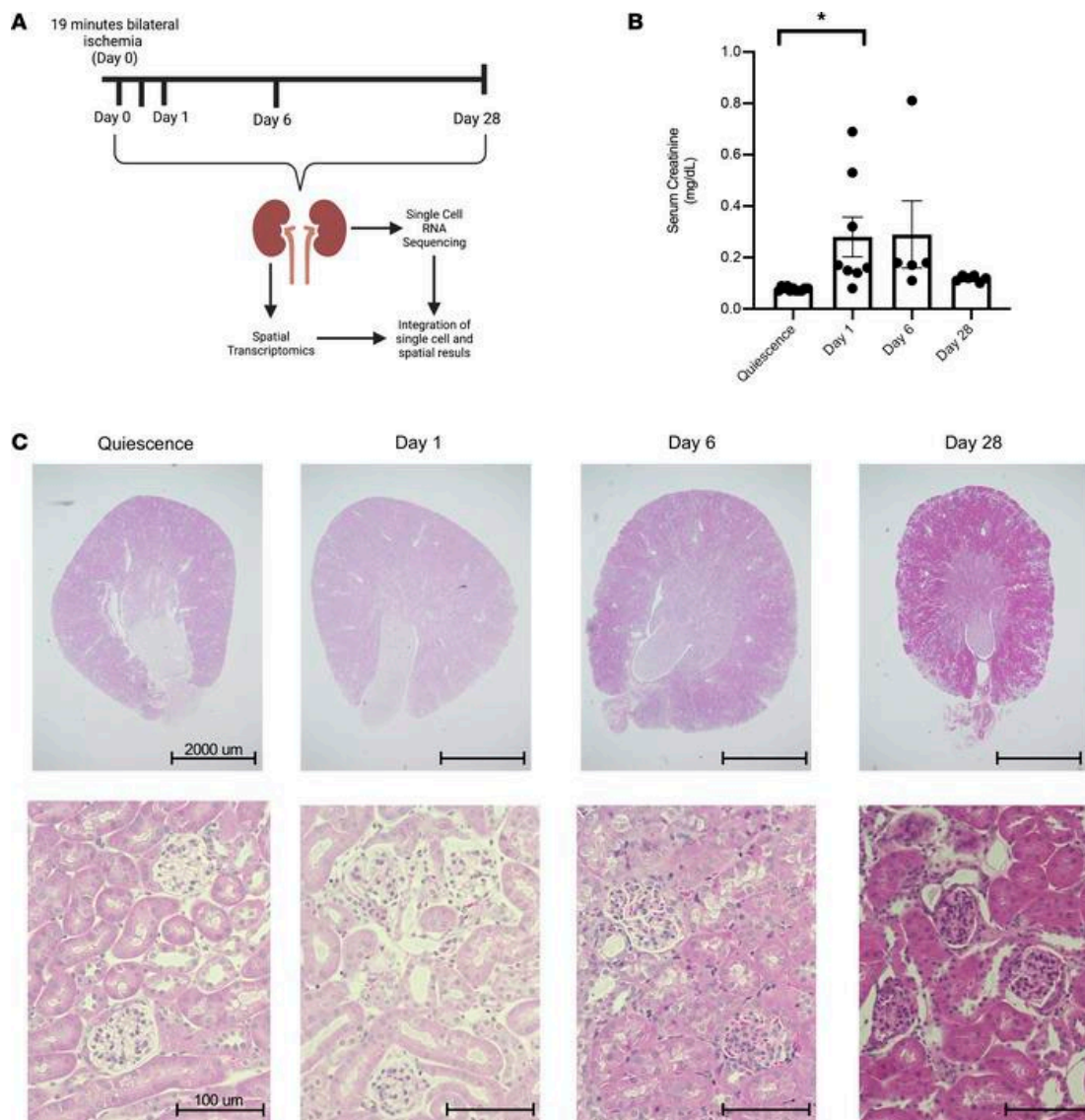


Figure 2.

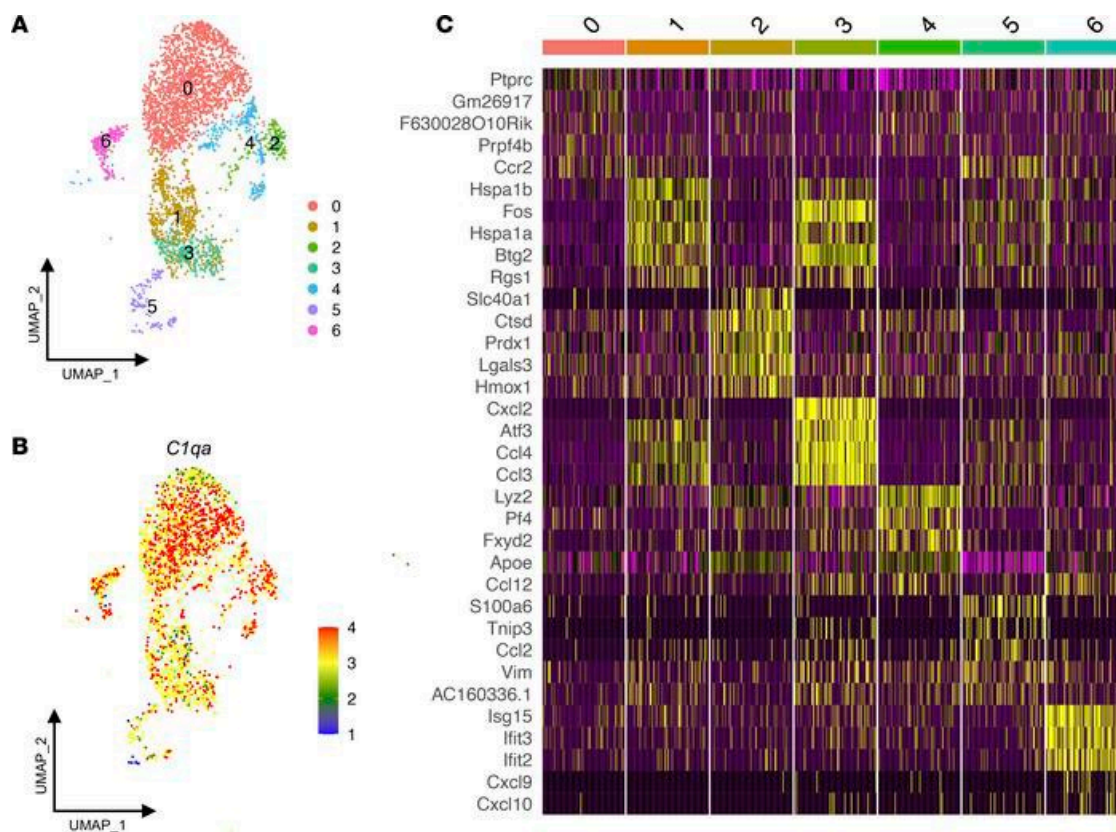


Figure 3.

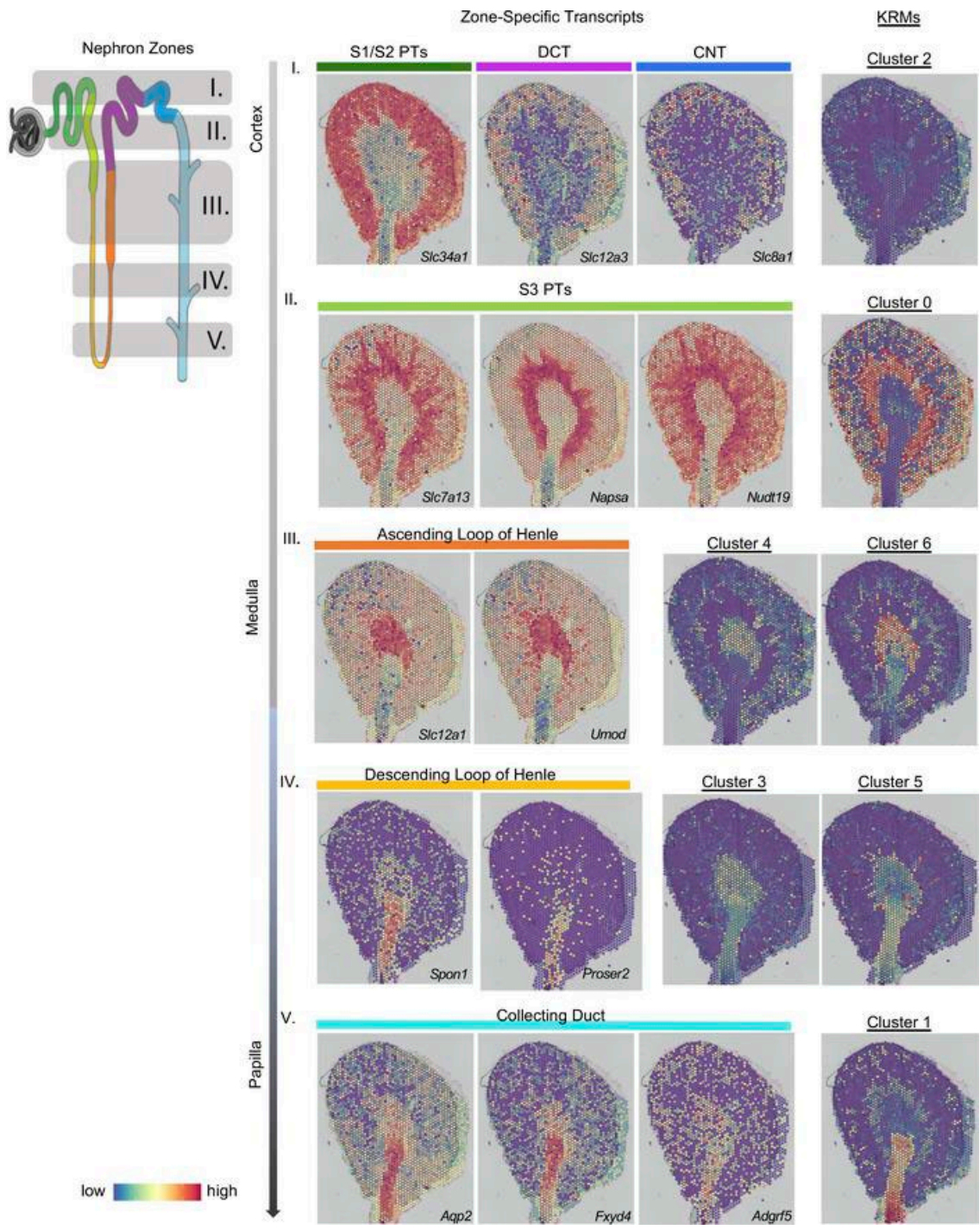


Figure 4.

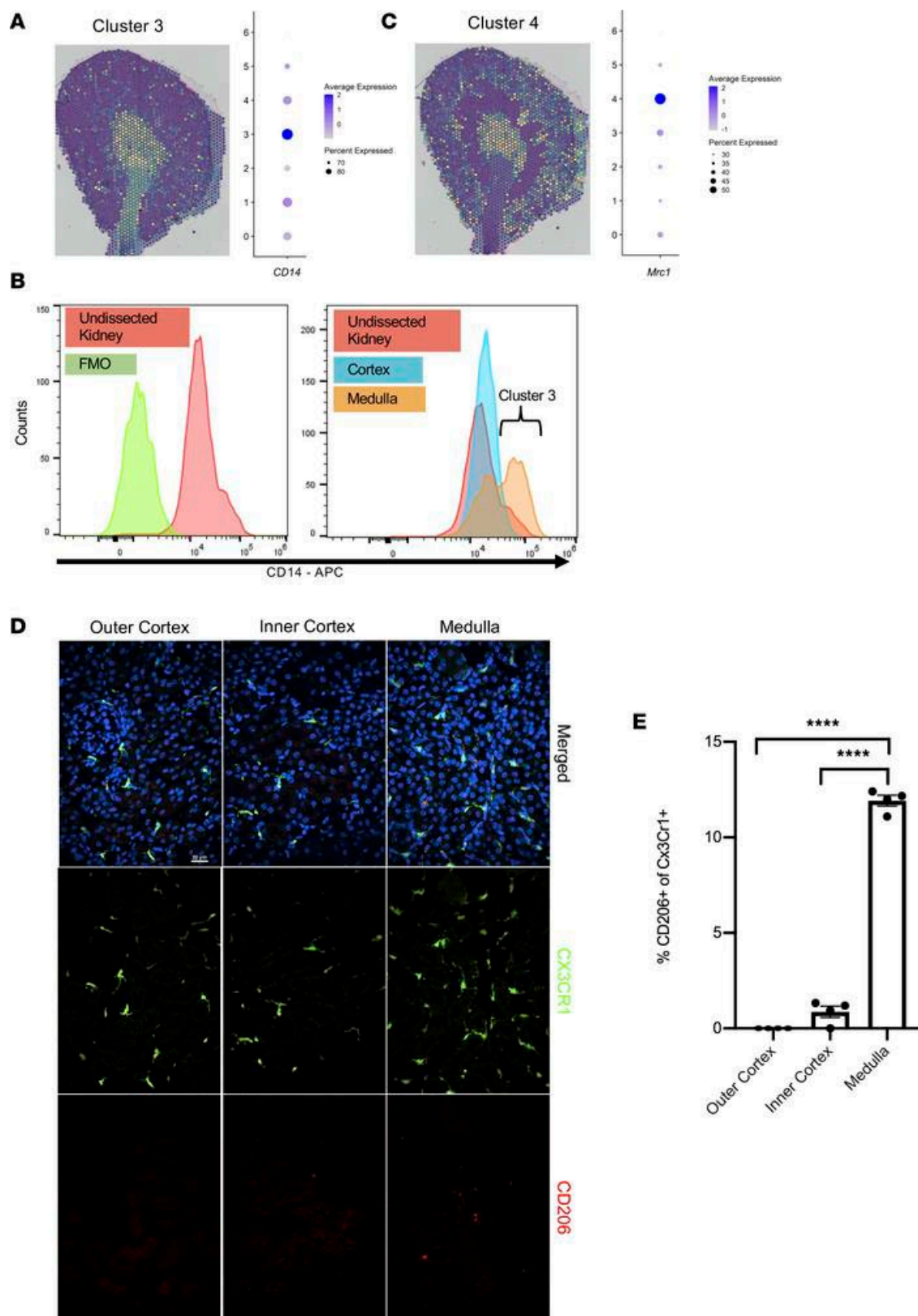
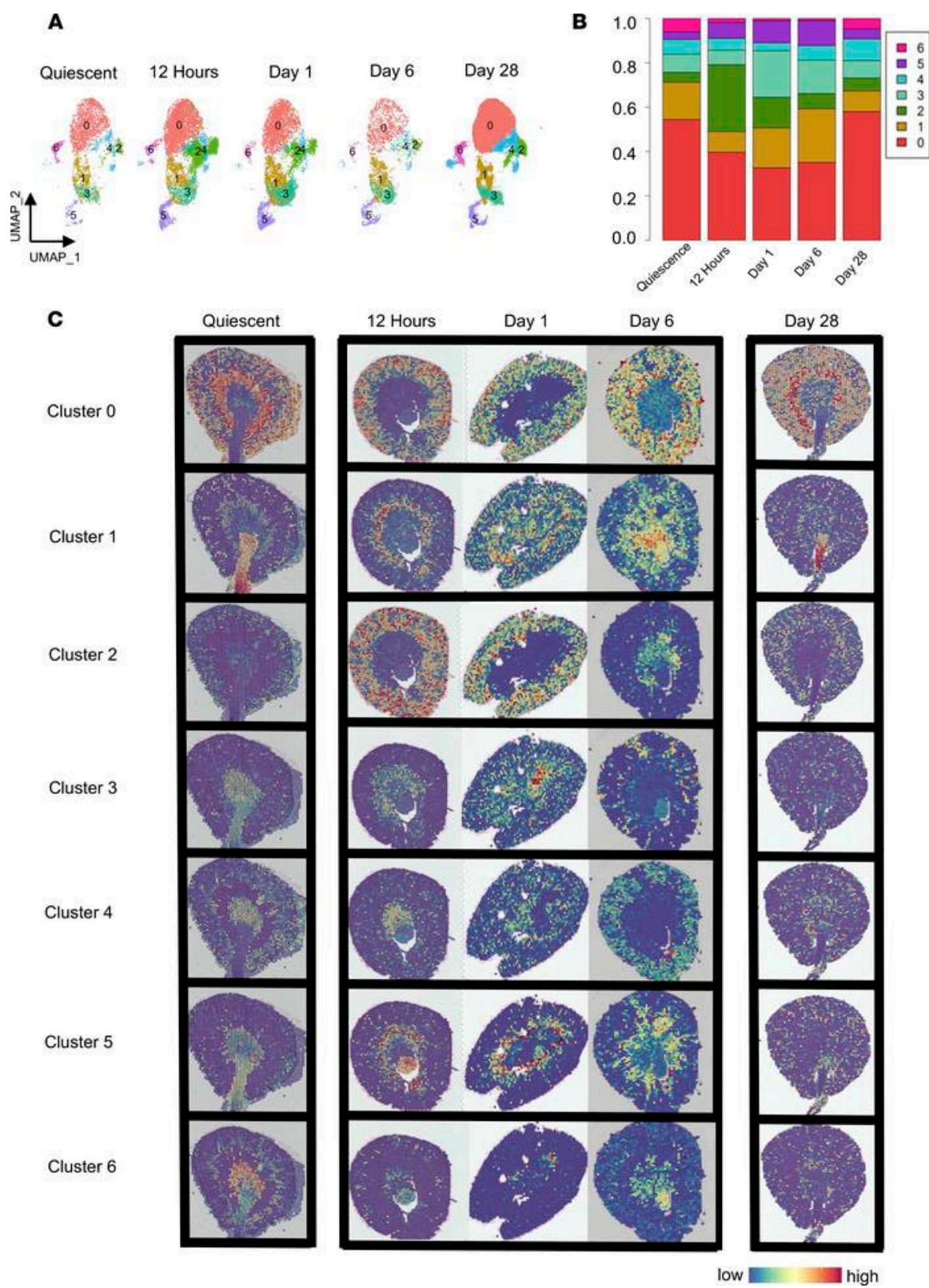


Figure 5.



HUMAN AND MURINE KIDNEYS CONTAIN TRANSCRIPTIONALLY
ORTHOLOGOUS RESIDENT MACROPHAGE SUBPOPULATIONS IN ACUTE
KIDNEY INJURY

by

ELISE N. ERMAN

KYLE H. MOORE, REHAM H. SOLIMAN, MATTHEW D. CHEUNG, ANUPAM
AGARWAL, JAMES F. GEORGE

Submitted to *Journal of the American Society of Nephrology*

Format adapted for dissertation

Significance Statement

Using mouse AKI samples and samples from two donors diagnosed with mild to moderate acute kidney injury, this work identified evolutionarily conserved resident macrophage populations in humans, and an additional subpopulation not found in mice. This increases the understanding of the human kidney resident macrophage niche and provides potential homeostatic and immune functions within the tissue that may be exploited for future therapies. These findings provide a framework to identify orthologous populations within other datasets and increase the translatability of murine research.

Abstract

Background

A challenge in the interpretation of studies of acute kidney injury, a major health burden in the United States, is the difference between the human and mouse immune systems. The translation of experimental results in the mouse to humans is complicated by different nomenclatures and marker systems as well as considerable uncertainty about whether cell populations have similar functions. In the mouse, kidney resident macrophages (KRM), contain multiple subpopulations that are involved in homeostasis and the response to injury. Each subpopulation is functionally distinct with a unique transcriptional profile and spatial distribution.

Methods

Using single cell RNA sequencing and spatial transcriptomics, we compared transcriptional profiles of mouse and human KRM subsets. AddModuleScore was used to provide statistical weight to conclusions.

Results

Four human KRM subpopulations with transcriptionally orthologous murine KRM subpopulations that occupy the same cellular compartments post-AKI were identified. Marker genes were identified for each orthologous subpopulation to allow for simple identification in future studies. Human kidneys contained a unique KRM subpopulation with a transcriptional profile that includes genes expressed by activated microglia.

Conclusions

Therefore, KRM subtypes, their transcriptional profiles, and their spatial locations are largely evolutionarily conserved.

Introduction

Mouse models have long been used to study human physiology and disease and are used extensively in the study of acute kidney injury (AKI), a major health burden in the United States, with in hospital mortality rates between 30 and 50%.^{1,2} Mice make an excellent experimental model due to the availability of wide genetic variety of strains and the relative ease of husbandry. However, success in murine models translates into clinical

trials only about a third of the time, and the success rate for those that do take place is even lower.^{3,4} This lack of correspondence fuels a growing concern over the utility of using murine models to inform human research.⁵ Yet, using human models exclusively is not a viable solution. Therefore, there is a need for increasing the translatability of mouse models.

It is only in the last decade that many immune populations well known in mice were described in humans.⁶⁻⁹ Identification of orthologous immune populations between mice and humans is limited by the difficulty of obtaining healthy human tissue and the disparate markers and classification schemes implemented in mice and humans, in conjunction with the continuing adaptations of an individual's immune system.¹⁰⁻¹² The majority of work in humans has been done in peripheral immune populations, based on the comparative ease of access. Therefore, information regarding orthologous tissue resident immune populations is lacking.^{13,14} The lack of identification of orthologous resident immune populations between mice and humans severely limits the translatability of data from murine models to humans.

Macrophages are key mediators of AKI in mice, and are known to alter their transcriptional profiles to be pro and anti-inflammatory as well as pro-fibrotic.¹⁵⁻²² In humans, the study of macrophage responses to AKI have been restricted to biopsy samples and the characterization of macrophages has been limited to the M1/M2 classification.²²⁻²⁴ Biopsies limit the study of macrophages to the cortex and the biopsy process tends to distort the local architecture.

Murine kidneys contain multiple subpopulations of resident macrophages (KRM) that have distinct transcriptomic profiles.^{15,25,26} The subpopulations occupy distinct

microenvironments that are shaped by the physiologic actions of the cell types associated with the nephrons, the main functional units in the kidney. The transcriptional profile of these murine KRM subpopulations suggests functional differences in processes such as iron handling, immune signaling, and antigen presentation.¹⁵

In the study described here, we analyzed human KRM subpopulations from donors with mild to moderate AKI by scRNAseq and spatial transcriptomics using the 10X Genomics Visium platform. We compared the results to murine KRMs pre- and 24 hours post-bilateral ischemia-reperfusion injury, a murine model of AKI. We have identified human KRM subpopulations in AKI which are transcriptionally and spatially orthologous to murine KRMs within the kidney tissue. We found several KRM subpopulations are evolutionarily conserved between mice and humans with similar transcriptional profiles. The corresponding subpopulations are located within the same spatial cellular compartments. One human specific subpopulation with a transcriptional profile similar to that seen in activated microglia was also found.

Methods

Animals.

Male C57BL/6J mice, 10–16 weeks of age, were obtained from The Jackson Laboratory.

Human Samples.

Human kidney samples were obtained from kidneys deemed unsuitable for transplantation. Kidney A was from a 68-year-old White man with a serum creatinine of

1.8 mg/dL, resulting in the diagnosis of mild AKI. Kidney B was from a 57-year-old white man, 5 days post brain death with a serum creatinine of 2.5 mg/dL, resulting in the diagnosis of mild-moderate AKI

Bilateral ischemia/reperfusion injury.

Mice were subjected to bilateral ischemia/reperfusion injury, as previously described^{26,27}. Surgeries were performed in the morning. Mice were anesthetized using ketamine and xylazine (i.p.). Under aseptic precautions, both kidneys were clamped at the renal pedicle using a microserrafine vascular clamp (Fine Science Tools, 18055-05). After 19 minutes, the clamps were removed to allow reperfusion. Reperfusion was visually confirmed within 1 minute. Body temperature, measured by a rectal thermometer, was carefully maintained at $37^{\circ}\text{C} \pm 1^{\circ}\text{C}$. Resulting effects on kidney function in these mice were described in Cheung et al.¹⁵

Flow cytometry/FACS.

Murine KRMs were obtained as previously described.¹⁵ Leukocytes were isolated as previously described.^{26,27} Mice were anesthetized under isoflurane and perfused through the left ventricle with 10 mL cold PBS. Kidneys were removed, stripped of the capsule, minced with a razor blade on a glass slide, and placed into Liberase (MilliporeSigma) at 37°C for 30 minutes. The digestion was stopped by adding cold PBS containing 1% BSA, and tissue was further disaggregated through an 18-gauge syringe. Red blood cells were lysed using ACK lysis buffer for 2 minutes at room temperature, and the remaining leukocytes were then washed with ice-cold PBS. Cells

were then stained with violet fixable viability dye (Invitrogen L34955) and treated with unlabeled anti-CD16/32 antibody to block Fc γ 3 receptors. Cells were subsequently stained using anti-Gr-1 Alexa Fluor 700 (Ly6G, clone 1A8, BioLegend), anti-CD11b super bright 600 (M1/70, Invitrogen), anti-F4/80 APC-eFluor-780 (BM8, Invitrogen), anti-NK1.1 PE-C7 (PK136, Invitrogen), anti-CD45.2 BV-650 (104, BioLegend), anti-MHC II (I-A/I-E) PerCP (M5/114.15.2, BD Biosciences), anti-CD19 super bright 702 (6D5, BioLegend), anti-TCR β Pe-Cy5 (H57-597, BD Biosciences). Murine flow cytometric data were previously described in Cheung et al.¹⁵

Human kidney samples were minced with a razor blade and placed into Liberase (MilliporeSigma) at 37°C for 30 minutes. The digestion was stopped by adding cold PBS containing 1% BSA, and tissue was further disaggregated through an 18-gauge syringe. Red blood cells were lysed using ACK lysis buffer for 2 minutes at room temperature, and the remaining leukocytes were then washed with ice-cold PBS. Cells were then stained with violet fixable viability dye (Invitrogen L34955) and treated with unlabeled anti-CD16/32 antibody to block Fc γ 3 receptors. Cells were subsequently stained using anti-CD45 FITC (YTH24.5, BioRad). Human macrophages do not express an ortholog of F4/80 and therefore require a different FACS sorting protocol than that used in the previously generated Cheung et al. dataset. Staining for C1q, a conserved marker for KRMs, requires fixation, and is therefore incompatible for single cell RNA sequencing and single nuclear RNA sequencing is poorly suited for immune cells. Transcription of *C1qa/C1QA* was found to identify KRMs in mice and humans.²⁸ For these reasons, we elected to identify human KRMs at the transcriptional level from CD45⁺ sorted cells.

scRNA-Seq.

Purified cells were transferred on ice to the UAB Flow Cytometry and Single Cell Core and immediately processed using the Chromium 3' Single Cell RNA sequencing kit (10× Genomics) according to the manufacturer's instructions. The cell suspension was counted and combined with a 10× Chromium reagent mixture and loaded into a microfluidic single-cell partitioning device in which lysis and reverse transcriptions occur in microdroplets. The resulting cDNA was amplified by a polymerase chain reaction and subsequently processed to yield bar-coded sequencing libraries. Paired-end sequencing was carried out on an Illumina NovaSeq6000 sequencing platform (Illumina). Reads were processed using the 10× Genomics Cell Ranger Single-Cell Software Suite (version 6.0) on the UAB Cheaha High-Performance Computing Cluster. BCL files were converted to FASTQ files using the CellRanger mkfastq function. CellRanger count was used to align the FASTQ files to the mouse genome (mm10) or human GRCh38 (GCA_000001405.28). The gene table, barcode table, and transcriptional expression matrices were created for the analysis indicated below.

Spatial transcriptomics.

The Visium system relies on a 2-dimensional matrix of 5000 spots distributed on a microscope slide in a 6.5 by 6.5 mm square. Each spot, which contains a poly-dT oligonucleotide with a unique sequence (bar code), is 50 μm in diameter at a distance from the other spots of 100 μm from center to center. Kidneys were embedded in the Optimal Cutting Temperature matrix (Fisher Scientific) and stored at -80°C. Before

sectioning, blocks were equilibrated to -10°C for 30 minutes. A $10\ \mu\text{m}$ section was placed onto specialized Spatial Gene Expression slides (10 \times Genomics) and processed according to the manufacturer's protocols. Briefly, slides were stained with H&E, and bright-field images were acquired using a Keyence BZ-X700 microscope. Tissues were permeabilized for 12 minutes and cDNA was generated and used to create second-strand DNA. The resulting cDNA was subject to downstream amplification and library processing for scRNA-Seq. Reads were processed using the 10 \times Genomics Space Ranger Single-Cell Software Suite (version 6.0) on the UAB Cheaha High-Performance Computing Cluster. BCL files were converted to FASTQ files using the SpaceRanger mkfastq function. SpaceRanger count was used to align the FASTQ files to the mouse genome (mm10).

Sequencing Data Analysis.

Both scRNA-Seq and spatial transcriptomics analyses were carried out using packages created for the R statistical analysis environment (version 4.2.1). Data were primarily analyzed using Seurat (version 4.3.0) and its associated dependencies.^{29,30} Data from each sample were imported using the Read10X function and then structured into a Seurat object using CreateSeuratObject. For quality control, cells with unique feature counts over 2500 or under 200 were excluded. Data were normalized and scaled using SCTransform or NormalizeData/ScaleData.³¹ Objects from each time point were labeled with unique group IDs and then merged into a single object using the Seurat merge function. Data objects were integrated using the Harmony R package³². Principal component analysis was performed based on 30 principal components,

and then cells were clustered using FindAllMarkers. The dimensional reduction was done using UMAP. As the human dataset contains all CD45+ cells, KRMs were identified using transcription of *CIQA*, which has been identified as a conserved marker of KRMs across species (Fig S1A).²⁸ *CIQA* expressing clusters from both samples were combined resulting in 613 identified KRMs. As described in Cheung et al., murine KRMs were identified by *Clqa* expression. Therefore, all comparisons were made between samples gated for *Clqa/CIQA* expression. The limited number of resulting human KRMs means that the subpopulations described here may not be exhaustive and rarer populations may have fallen below the threshold of detection. Clusters identified as cycling cells (Cluster 5) or derived from a single sample (smallest cluster in human sample A) were removed.

Integration of scRNA-Seq and spatial transcriptomics to resolve cell location.

The spatial matrix was integrated with the scRNA-Seq data set using the anchor-based workflow built into the Seurat package. FindTransferAnchors was used. Using the generated anchor set, the TransferData function created predictions from the KRM reference clusters and applied that to the spatial data sets. Using the predictions, each subpopulation could be visualized using SpatialFeaturePlots.

Data availability.

The scRNA-Seq and spatial transcriptomics data used or generated for this paper were deposited in the NCBI's Gene Expression Omnibus database (GEO GSE200115)

and (GEO GSE226533). Visium data from GEO GSE200115 has been used for other publications within the laboratory.

AddModuleScore.

The AddModuleScore function in Seurat was used to determine the expression of provided gene lists (Tables 1 and 2) and control genes were set to 500.³³ The resulting meta data of the Seurat object was moved to a dataframe for statistical analysis. AddModuleScore is commonly used to identify a cell type or functional phenotype with statistical significance based on a known transcriptional profile.³⁴⁻³⁹ Transcriptional profiles for this publication were based on the differentially expressed genes (DEGs) identified in the analysis of Cheung et al. for day 0 and day 1 post AKI.¹⁵

To adjust for the differences in naming conventions, lack of orthologous genes, and genes with different functions across species. Human orthologs to the murine genes at days 0 and 1 were manually identified and provided in Table 1. All removed genes are identified and the reason for removal provided (Table 1). As the goal of this publication is to identify transcriptionally similar subpopulations, and the statistical power of DEGs varies by subpopulation and at each timepoint, profiles were limited to the top 20 orthologous DEGs and the p-value of the least significant DEG used is provided (Table 1).

AddModuleScore accounts for the expression of every included gene and therefore provides a comprehensive expression value of the transcriptional profile that allows for statistical analysis. Module scores compare the expression level of a given

gene set (ie. transcriptional profile or marker genes) across the clusters to the expression of randomly selected control genes from the bins where a provided gene was identified (n= 500). If there is no increased expression of the provided gene list, the output, when subtracting the expression of the control gene set, would be 0.³³

Statistics.

Statistics were performed in R and plotted using ggplot. Boxplots report the median and standard deviation of a dataset. The Kruskal Wallis test was used to determine a difference within a dataset and the Pairwise Wilcoxon test for nonparametric data was used to compare individual groups to each other. All p-values for data shown are reported in Supplemental Tables 1- 4.

Study Approval.

Mice were housed at the University of Alabama at Birmingham (UAB) animal facilities in compliance with the NIH guidelines regarding the care and use of live animals. All animal work performed was reviewed and approved by the Institutional Animal Care and Use Committee at UAB (IACUAC)(APN 21531). Human samples were taken for single-cell RNA sequencing and spatial transcriptomics in accordance with IRB-300004648 from the UAB Institutional Review Board for Human Use (IRB). Written consent was received for all human samples.

Results

The human kidney contains transcriptionally distinct resident macrophage subpopulations

We isolated live CD45⁺ cells by flow cytometric sorting for single-cell RNA sequencing (scRNAseq) from samples of two AKI kidneys. Human KRMs in the CD45⁺ dataset expressed the highest levels of KRM defining *CIQA* transcripts²⁸. Identification of the KRM clusters was confirmed by high co-expression of *CD74* and *CD81* (Fig S1A-B).²⁸ Furthermore, the KRMs expressed canonical macrophage markers (*CD68* and *CD14*), not found on dendritic cells (Fig S1A-B).^{28,40} We subset and then re-clustered the *CIQA* high clusters from both kidney samples. All the resulting subpopulations contained cells originating from both donors, except Cluster 6, which was therefore removed from following analyses (Fig S1C). Cluster 5 expressed *MKI67*, a marker of proliferation, and was also removed (Fig S1D). The result was five transcriptionally distinct hKRM subpopulations (Fig 1A-B). Human KRM subpopulation (hKRM) 0 expresses multiple genes involved in efferocytosis, such as *MERTK* and *STAB1*.⁴¹ Human KRM 1 expresses genes involved in calcium handling such as the *S100* genes and *CD52*, along with activation genes *NFKN1A*, *FOS*, and *ILR2*.⁴² Human KRM 2 expresses a DEG associated with interferon signaling: d *IFITM3*.⁴³ Although they are transcriptionally distinct, hKRMs 0 and 3 are the most similar, as shown by expression of many of hKRM 0 DEGs by hHRM 3 and vice versa. Human KRM 3 differs from hKRM 0 primarily by the lack of canonical activation genes, represented here by *JUN*, *JUNB*, and *NFKB1A* (Fig 1C-E). Human KRM 4 has the highest transcription of *HLA* genes, suggesting an increased role in antigen presentation (Fig 1B).^{44,45}

To ensure we had appropriately clustered the subpopulations and to increase the applicability of our conclusions, we investigated the expression of known human KRM subpopulation markers in our data (Fig 1F). At least four separate laboratories have identified various human kidney macrophage subpopulations and included marker genes. We were able to identify the subpopulations defined by Yao et al. (*S100A8/S100A9*), Subramanian et al. (*TREM2*), Dick et al. (*HLA-DQA1* for subpopulation 1) and (*LYVE1/FOLR2/MRC1* for subpopulation 2), and Li et al. (*MRC1*) in our dataset as distinct subpopulations.⁴⁶⁻⁴⁹ All subpopulations were associated with at least one previously identified subpopulation, and we did not find any unidentified subpopulations. Therefore, the definition of the human data set is consistent with prior studies, so the analyses of the data should be applicable to other human experimental systems.

Human kidney spatial transcriptomics identifies nephron structures and areas of healthy and damaged tissue.

We performed spatial transcriptomics on sections of the kidney samples used for scRNAseq. The protocol timing restricts micrographs to 4X resolution; however, we were still able to identify distinct kidney nephron structures and pathology (Fig 2A). Kidney section A shows signs of interstitial fibrosis and inflammation, primarily in the cortex (Fig S2)(Fig 2A). Spatial transcriptomics and histology identified the location of tubules (*GPX3*, *PTH1R*), loop of Henle (*UMOD*, *SLC12A1*), and collecting duct (*AQP2*, *AQP3*) in kidney section A (Fig 2B-D)(Fig S2).⁵⁰⁻⁵⁵ Kidney section B shows sign of tubulointerstitial nephritis in the cortex and fibrotic regions in the medulla, however tubular structures are clearer than in kidney section A (Fig 2F)(Fig S3). Spatial transcriptomics and histology identified the location of proximal tubules (*GPX3*, *PTH1R*,

SLC5A12), loop of Henle (*UMOD*, *SLC12A1*), and vasculature in an area of fibroblasts (Fig 2F-G)(Fig S3).^{50-52,55,56} Both sections contain cell types primarily localized to either the cortex or medulla. Therefore, we divided the sections based on the demarcation between the cortex and medulla (Fig 2A and E).

Murine KRM transcripts can be used to identify orthologous populations.

A transcriptional profile for each murine KRM subpopulation (mKRM) from before bilateral ischemia-reperfusion induced AKI and 1 day after injury was generated to identify possible orthologous hKRM. ¹⁵ The transcriptional profiles consist of approximately the top 20 differentially expressed genes (DEGs) ranked by adjusted p-value for each murine cluster and from each time point (Table 1). Some murine genes do not have well-defined human orthologs and were thus excluded, causing the number of genes used as a transcriptional profile to differ slightly from 20 for some analyses. The Seurat function `AddModuleScore` was used to quantify the expression of the mouse transcriptional profiles among the human KRM subpopulations. ³³ Key marker genes were selected from each transcriptional profile based on expected functional relevance and expression level and compared to the human KRMs and the murine KRMs at both time points to allow for identification of orthologous subpopulations (Fig 3A). All transcriptional profiles and marker genes are provided in Tables 1 and 2.

Human KRMs 0 and 3 have statistically significant ($p < 0.0001$) expression of the transcriptional profiles for mKRM 4 in quiescence and 1 day-post AKI (Fig 3B-C), which indicates these are highly likely to be orthologous subpopulations. Marker genes *LYZ*, *PF4*, *F13A1*, *STAB1*, and *SLC40A1* were identified, and show statistically significant

increased expression in hKRM 0 and 3, and mKRM 4 pre and post-AKI, identifying them as a marker gene set across species ($p < 0.0001$, Fig 3D-F). *LYZ* is the gene for lysozyme. *PF4* and *FI3A1* are most commonly involved in platelet function.⁵⁷ *STAB1* is a large transmembrane protein involved in cell adhesion and endocytosis.⁴¹ *SLC40A1* is the gene for the iron exporter, ferroportin.

KRM subpopulations identified as orthologous occupy the same anatomical regions of human and mouse kidneys.

We integrated the single-cell sequencing data with the spatial transcriptomics data to identify the location of the human KRMs within the kidney and compared their locations to the spatial location of the mKRMs (Fig 1A)(Fig 2A and G).¹⁵ The spatial location of all hKRM subpopulations is provided (Fig S4). For both sections A and B, hKRM 0 and 3 are primarily colocalized with tubules. Human KRM 0 is more specific to the cortex. Human KRM 3 is found throughout the section but has a stronger presence in the cortex (Fig 4A-B). The transcriptionally orthologous murine KRM 4 is located in the medullary region prior to insult, but adopts a cortical location within 24 hours post-AKI, and therefore is located within the same region as hKRM 0 and 3 (Fig 4C). Of note, mKRM 2 is the only entirely cortical murine subpopulation prior to injury (Fig 4D). The transcriptional profile for mKRM 2 did not show statistical significance for any human subpopulation (data not shown). However, mKRM 2 is transcriptionally very similar to mKRM 4, expands following AKI, and also expresses high levels of the same transcripts.¹⁵ Therefore, it is relevant to note, that while mKRM 4 is the orthologous population, it is possible that hKRM 0 and 3 share features with mKRM 2, particularly prior to insult, despite the lack of statistical significance.

Human KRM 1 is orthologous to murine KRM 3

Human KRM 1 has a similar transcriptional expression profile to mKRM 3 before and 1 day post-AKI ($p < 0.05$)(Fig 5A-B). Marker genes of *CXCL2*, *EGRI*, *FOS*, and *IL1B*, were identified, and show statistically significant higher expression in hKRM 1 and mKRM 3 at both timepoints ($p < 0.001$) (Fig 5C-E). All genes are involved in macrophage activation and inflammation.

For both human kidneys A and B, hKRM 1 is primarily localized in the medulla. In Section A, where collecting duct cells are present, hKRM1 shows predominate colocalization with the collecting duct (Fig 5F). Section B, where there are few collecting duct cells, hKRM1 shows colocalization with the loop of Henle (Fig 5G). These indicate that, in injured human kidneys, hKRM cluster 1 cells are primarily confined to the medulla among the collecting ducts and loop of Henle. In mice, we find that the KRM cluster 3 also localizes to the medullary region in normal tissue and also following injury, although after injury there also appears to be some presence in the inner cortex (Fig 5H).

Human KRM 2 is orthologous to murine KRM 6.

Human KRM 2 has a similar transcriptional expression profile as mKRM 6 before AKI ($p < 0.0001$) (Fig 6A). Following AKI in the mouse, there is no longer a significant difference between hKRM 2 and 4, caused by an increase in immune signaling genes following the injury (Table 1). Marker genes of *ISG15*, *IRF77*, *IFITM3*, and *IFITM2*, were identified, and show statistically significant higher expression in hKRM 2, and mKRM 6 at both timepoints ($p < 0.01$) (Fig 6C-E).

For both human sections A and B, hKRM 2 is localized almost exclusively to the medulla, with the least cortical presence of any other hKRM subpopulation. In both sections, hKRM2 colocalizes with vasculature present in a fibrotic background within the medulla. Murine KRM 6 is also localized to the medulla, with no cortical presence in injured mice. In normal kidneys, there appears to be some localization at the cortico-medullary region.

Human KRM 4 does not have a mouse ortholog and expresses genes associated with activated microglia

The methodology of generating a Module Score to determine orthologous human and murine KRM subpopulations did not return an orthologous population for hKRM 4. The DEGs for hKRM 4 were largely associated with antigen presentation and complement signaling (Fig 1E). Additionally, hKRM 4 differentially expresses *TREM2*, *APOE*, *CD9*, *CLEC7A* and *CX3CR1* (Fig 7A).⁵⁸⁻⁶¹ These genes are known to be expressed by activated microglia, the resident macrophage population in the brain.^{25,62} Activated microglia are essential in the pruning of synapses using a complement-mediated pathway, specifically *C3* and *CIQ* transcripts.⁶³⁻⁶⁵ Further investigation into microglia markers revealed that many are exclusively transcribed by hKRM 4 (Fig 7A). In contrast, these same markers are not unique to any single murine subpopulation, either during quiescence or following acute kidney injury; *Clec7a* was not found in the dataset (Fig 7B-C). This relationship holds for day 1 identified mKRMs that have not been integrated with other timepoints to confirm that this is not an injury specific response by a single subpopulation in mice (Fig S5). Calculating module scores using marker genes associated for microglia returns a significantly higher score for hKRM 4 relative to other

human KRM clusters. (Fig 7D)(Table 2). We then expanded the analysis to include other genes known to be involved in microglia pruning, and again generated a significant module score for hKRM 4 (Fig 7E)(Table 1). Human KRM 4 is strictly cortical and colocalizes with proximal tubules (Fig 7 F-G).

Discussion

Using scRNAseq and spatial transcriptomics, we identified transcriptional profiles and the location of five previously undescribed subpopulations of human KRMs in injured human kidneys. These findings mirror recent findings in mice, and current bioinformatics approaches allowed us to compare the murine KRM subpopulations to the human KRM subpopulations and discover orthologs, in addition to a resident macrophage subpopulation that appears to be specific to humans.¹⁵

Macrophages are first and foremost immune cells that are present in even the most primitive organisms. Resident macrophages in the lungs and skin have been known to form part of the first line of defense against pathogenic invaders.^{66,67} The kidney medulla is relatively exposed to pathogens that can enter the body through the urinary tract. It has been suggested by Berry *et al.* that the macrophage populations present in the medulla provide barrier protection, similar to that seen in the skin or lungs.⁶⁸ Indeed, our previous work in murine models described three immune-responding mKRM subpopulations (mKRM 1, 3, and 6) localized to the medulla during homeostasis.¹⁵ With this work, we have identified human orthologs to mKRM 3 and 6, which are also localized to the medulla in the human kidney. Human KRM 1 is orthologous to mKRM 3 and hKRM 2 is orthologous to mKRM 6.

Human KRM 2 expresses a transcriptional profile and marker genes associated with type I interferon (IFN) signaling. In the spatial transcriptomic sections, this population appears colocalized with areas of kidney damage. Type I IFN is well known to play a role in lupus nephritis, and multiple clinical trials are currently ongoing to target this pathway.^{69,70} The murine type I IFN ortholog is known to exist in homeostasis, but tissue damage increases the signaling of type I IFN, possibly creating a positive feedback loop and amplifying the signal.⁷¹ Given the presence of the cells at the site of injury in kidneys from patients without lupus nephritis, perhaps therapeutics targeting the type I IFN pathway would benefit patients suffering from a variety of kidney disorders.

Macrophages, more than most immune cell populations have known homeostatic functions, including apoptotic cell clearance and tissue development.^{72,73} However, recent work in microglia has found that resident macrophages perform other homeostatic functions, showing that C1q, which is expressed prominently by KRMs and other resident macrophage populations, is involved in labeling synapses in need of removal or pruning in the brain.^{28,63,64,74,75} Human KRM 4 does not have a murine ortholog, but expresses genes similar to activated microglia and therefore is of potential functional relevance. Human KRM 4 is specific to the cortex and could therefore be involved in pruning proximal tubule cells, in a function reminiscent of microglia. Microglia are shown to upregulate this profile and specifically expression of *Trem2* and *ApoE* following damage.^{58,60} Given that both human kidneys had experienced mild to moderate AKI, it is possible that hKRM 4 is a damage response, therefore the colocalization of hKRM 4 with the proximal tubules and the expression of an activated microglia-like transcriptional profile warrants further investigation.

Human KRMs 0 and 3 are transcriptionally and spatially similar. The primary difference is a lack of activation markers in subpopulation 3, and the combined subpopulations were identified as a single subpopulation by Dick et al.⁴⁶ As all cells were isolated from kidneys with mild to moderate AKI and histological evidence of damage, perhaps hKRM3 is an example of an exhausted or tolerized version of hKRM 0.⁷⁶ Both subpopulations are orthologous to mKRM 4 and appear colocalized with proximal tubules. The marker genes of *PF4*, *F13A1*, *STAB1*, and *SLC40A1*, suggest some function involved in wound healing and/or iron handling.

A limitation of this work is the directionality of the analysis. Applying the transcriptional profile of the mKRMs to the hKRMs biases the conclusions towards the identified mouse clustering. However, laboratory mice are known to have more similar immune phenotypes to newborns than to adult humans, based on the limited immune challenges faced under laboratory conditions.^{10,77} For this reason, we chose to apply the more limited immune profile (murine) to the more expansive immune profile (human) to try and describe the most basic orthologous similarities.

A second limitation is the size and extent of injury of the hKRMs. Due to the severe organ shortage, healthy human kidneys are almost always needed for transplantation. Therefore, we chose to limit our samples to available AKI donor specimens. As a consequence, our sample size was limited and restricted our ability to increase the number of hKRMs identified. For this reason, it is possible that the human kidney contains more KRM subpopulations than defined here or previously identified. The subpopulations described here are by no means exhaustive, as rarer hKRM

subpopulations likely exist or those herein defined may vary transcriptionally in uninjured kidneys.

Scientific research relies on simpler model systems to understand the human system. Of course, model systems differ from humans in a variety of known and unknown factors, obscuring the translatability of any non-human findings into clinically relevant data. The kidneys are a particularly fragile organ system, given the complexity of their physiology, and high metabolic needs.^{78,79} This complexity has inhibited kidney research, and modern therapeutics remain extremely limited.⁸⁰⁻⁸³ Resident macrophages are found throughout the body and are thought to perform homeostatic and immune functions, making them an excellent target in the search for novel therapies for kidney diseases.

In this work, we enhanced the translatability of kidney macrophage research by identifying orthologous KRM subpopulations between the common model organism, C57Bl/6J mice, and humans and confirming our hKRM subpopulations with those previously described. Single-cell RNA sequencing, spatial transcriptomics, and bioinformatics approaches allowed us to identify transcriptionally significant and spatially similar KRM orthologs. Like murine KRMs, there are multiple subpopulations of human KRMs with distinct spatial locations within kidney anatomical regions. The results of this study can be applied to previous research and leveraged as a framework for future research.

Disclosures

Anupam Agarwal serves as a consultant for Dynamed and is on the advisory boards of Alpha Young and Creegh Pharmaceuticals for work outside the scope of this manuscript.

Funding

This work was supported by NIH grants P30 DK079337, R01 DK59600, and R01 DK118932 (to AA and JFG), and American Heart Association grant 827257 (to ENE).

Authors Contributions

Conception & Design: ENE

Data Collection and Management: ENE, KHM, RS, MDC, JFG, AA

Data Analysis: ENE, KHM, RS

Manuscript Writing: ENE

Manuscript Editing: ENE, KHM, RS, MDC, JFG, AA

Acknowledgments

The authors would like to thank Dr. Paige Porrett, Dr. Jayme Locke, Gavin Baker, and Jackson Baker for their assistance in this project. We acknowledge the UAB Flow Cytometry and Single Cell Core (NIH P30-AR-04831) and the UAB O'Brien Preclinical Studies of AKI Core. Some figures were generated with BioRender.com. This work was supported by NIH grants P30 DK079337, R01 DK59600, and R01 DK118932 (to AA and JFG), and American Heart Association grant 827257 (to ENE)

Data availability

The scRNA-Seq and spatial transcriptomics data generated for this paper were deposited in the NCBI's Gene Expression Omnibus database (GEO GSE200115) and (GEO GSE226533).

References

1. Goyal, A, Daneshpajouhnejad, P, Hashmi, MF, et al.: Acute Kidney Injury. In: *StatPearls*. Treasure Island (FL), StatPearls Publishing
Copyright © 2022, StatPearls Publishing LLC., 2022.
2. Black, LM, Lever, JM, Agarwal, A: Renal Inflammation and Fibrosis: A Double-edged Sword. *J Histochem Cytochem*, 67: 663-681, 2019.
3. Hackam, DG, Redelmeier, DA: Translation of research evidence from animals to humans. *Jama*, 296: 1731-1732, 2006.
4. Mak, IW, Evaniew, N, Ghert, M: Lost in translation: animal models and clinical trials in cancer treatment. *Am J Transl Res*, 6: 114-118, 2014.
5. Seok, J, Warren, HS, Cuenca, AG, et al.: Genomic responses in mouse models poorly mimic human inflammatory diseases. *Proc Natl Acad Sci U S A*, 110: 3507-3512, 2013.
6. Farber, DL, Yudanin, NA, Restifo, NP: Human memory T cells: generation, compartmentalization and homeostasis. *Nat Rev Immunol*, 14: 24-35, 2014.
7. Park, CO, Kupper, TS: The emerging role of resident memory T cells in protective immunity and inflammatory disease. *Nat Med*, 21: 688-697, 2015.

8. Simoni, Y, Fehlings, M, Kløverpris, HN, et al.: Human Innate Lymphoid Cell Subsets Possess Tissue-Type Based Heterogeneity in Phenotype and Frequency. *Immunity*, 46: 148-161, 2017.
9. Zilionis, R, Engblom, C, Pfirschke, C, et al.: Single-Cell Transcriptomics of Human and Mouse Lung Cancers Reveals Conserved Myeloid Populations across Individuals and Species. *Immunity*, 50: 1317-1334.e1310, 2019.
10. Shay, T, Jojic, V, Zuk, O, et al.: Conservation and divergence in the transcriptional programs of the human and mouse immune systems. *Proc Natl Acad Sci U S A*, 110: 2946-2951, 2013.
11. Röhrli, J, Yang, D, Oppenheim, JJ, et al.: Human beta-defensin 2 and 3 and their mouse orthologs induce chemotaxis through interaction with CCR2. *J Immunol*, 184: 6688-6694, 2010.
12. Conrad, ML, Davis, WC, Koop, BF: TCR and CD3 antibody cross-reactivity in 44 species. *Cytometry A*, 71: 925-933, 2007.
13. Nkongolo, S, Mahamed, D, Kuiper, A, et al.: Longitudinal liver sampling in patients with chronic hepatitis B starting antiviral therapy reveals hepatotoxic CD8+ T cells. *J Clin Invest*, 133, 2023.
14. Krämer, B, Nalin, AP, Ma, F, et al.: Single-cell RNA sequencing identifies a population of human liver-type ILC1s. *Cell Rep*, 42: 111937, 2023.
15. Cheung, MD, Erman, EN, Moore, KH, et al.: Resident macrophage subpopulations occupy distinct microenvironments in the kidney. *JCI Insight*, 7, 2022.

16. Arai, S, Kitada, K, Yamazaki, T, et al.: Apoptosis inhibitor of macrophage protein enhances intraluminal debris clearance and ameliorates acute kidney injury in mice. *Nat Med*, 22: 183-193, 2016.
17. Baek, JH: The Impact of Versatile Macrophage Functions on Acute Kidney Injury and Its Outcomes. *Front Physiol*, 10: 1016, 2019.
18. Cao, Q, Harris, DC, Wang, Y: Macrophages in kidney injury, inflammation, and fibrosis. *Physiology (Bethesda)*, 30: 183-194, 2015.
19. Chung, S, Overstreet, JM, Li, Y, et al.: TGF- β promotes fibrosis after severe acute kidney injury by enhancing renal macrophage infiltration. *JCI Insight*, 3, 2018.
20. Cramer, T, Yamanishi, Y, Clausen, BE, et al.: HIF-1alpha is essential for myeloid cell-mediated inflammation. *Cell*, 112: 645-657, 2003.
21. Huen, SC, Cantley, LG: Macrophage-mediated injury and repair after ischemic kidney injury. *Pediatr Nephrol*, 30: 199-209, 2015.
22. Huen, SC, Cantley, LG: Macrophages in Renal Injury and Repair. *Annu Rev Physiol*, 79: 449-469, 2017.
23. Han, HI, Skvarca, LB, Espiritu, EB, et al.: The role of macrophages during acute kidney injury: destruction and repair. *Pediatr Nephrol*, 34: 561-569, 2019.
24. Palmer, MB, Vichot, AA, Cantley, LG, et al.: Quantification and localization of M2 macrophages in human kidneys with acute tubular injury. *Int J Nephrol Renovasc Dis*, 7: 415-419, 2014.
25. Gomez Perdiguero, E, Klapproth, K, Schulz, C, et al.: Tissue-resident macrophages originate from yolk-sac-derived erythro-myeloid progenitors. *Nature*, 518: 547-551, 2015.

26. Lever, JM, Yang, Z, Boddu, R, et al.: Parabiosis reveals leukocyte dynamics in the kidney. *Lab Invest*, 98: 391-402, 2018.
27. Lever, JM, Hull, TD, Boddu, R, et al.: Resident macrophages reprogram toward a developmental state after acute kidney injury. *JCI Insight*, 4, 2019.
28. Zimmerman, KA, Bentley, MR, Lever, JM, et al.: Single-Cell RNA Sequencing Identifies Candidate Renal Resident Macrophage Gene Expression Signatures across Species. *J Am Soc Nephrol*, 30: 767-781, 2019.
29. Butler, A, Hoffman, P, Smibert, P, et al.: Integrating single-cell transcriptomic data across different conditions, technologies, and species. *Nat Biotechnol*, 36: 411-420, 2018.
30. Stuart, T, Butler, A, Hoffman, P, et al.: Comprehensive Integration of Single-Cell Data. *Cell*, 177: 1888-1902.e1821, 2019.
31. Hafemeister, C, Satija, R: Normalization and variance stabilization of single-cell RNA-seq data using regularized negative binomial regression. *Genome Biol*, 20: 296, 2019.
32. Korsunsky, I, Millard, N, Fan, J, et al.: Fast, sensitive and accurate integration of single-cell data with Harmony. *Nat Methods*, 16: 1289-1296, 2019.
33. Tirosh, I, Izar, B, Prakadan, SM, et al.: Dissecting the multicellular ecosystem of metastatic melanoma by single-cell RNA-seq. *Science*, 352: 189-196, 2016.
34. Wang, XM, Zhang, JY, Xing, X, et al.: Global transcriptomic characterization of T cells in individuals with chronic HIV-1 infection. *Cell Discov*, 8: 29, 2022.

35. Qi, J, Sun, H, Zhang, Y, et al.: Single-cell and spatial analysis reveal interaction of FAP(+) fibroblasts and SPP1(+) macrophages in colorectal cancer. *Nat Commun*, 13: 1742, 2022.
36. Li, C, Hua, K: Dissecting the Single-Cell Transcriptome Network of Immune Environment Underlying Cervical Premalignant Lesion, Cervical Cancer and Metastatic Lymph Nodes. *Front Immunol*, 13: 897366, 2022.
37. Kiner, E, Willie, E, Vijaykumar, B, et al.: Gut CD4(+) T cell phenotypes are a continuum molded by microbes, not by T(H) archetypes. *Nat Immunol*, 22: 216-228, 2021.
38. Khatun, A, Kasmani, MY, Zander, R, et al.: Single-cell lineage mapping of a diverse virus-specific naive CD4 T cell repertoire. *J Exp Med*, 218, 2021.
39. Lin, W, Noel, P, Borazanci, EH, et al.: Single-cell transcriptome analysis of tumor and stromal compartments of pancreatic ductal adenocarcinoma primary tumors and metastatic lesions. *Genome Med*, 12: 80, 2020.
40. Serbina, NV, Pamer, EG: Monocyte emigration from bone marrow during bacterial infection requires signals mediated by chemokine receptor CCR2. *Nat Immunol*, 7: 311-317, 2006.
41. Elliott, MR, Koster, KM, Murphy, PS: Efferocytosis Signaling in the Regulation of Macrophage Inflammatory Responses. *J Immunol*, 198: 1387-1394, 2017.
42. Scheibenbogen, C, Keilholz, U, Richter, M, et al.: The interleukin-2 receptor in human monocytes and macrophages: regulation of expression and release of the alpha and beta chains (p55 and p75). *Res Immunol*, 143: 33-37, 1992.

43. Zhao, X, Li, J, Winkler, CA, et al.: IFITM Genes, Variants, and Their Roles in the Control and Pathogenesis of Viral Infections. *Front Microbiol*, 9: 3228, 2018.
44. Bach, FH: Histocompatibility genes in man. *Proc Can Cancer Conf*, 8: 362-380, 1969.
45. Snell, GD, Higgins, GF: Alleles at the histocompatibility-2 locus in the mouse as determined by tumor transplantation. *Genetics*, 36: 306-310, 1951.
46. Dick, SA, Wong, A, Hamidzada, H, et al.: Three tissue resident macrophage subsets coexist across organs with conserved origins and life cycles. *Sci Immunol*, 7: eabf7777, 2022.
47. Subramanian, A, Vernon, K, Zhou, Y, et al.: Obesity-instructed TREM2^{high} macrophages identified by comparative analysis of diabetic mouse and human kidney at single cell resolution. *bioRxiv*, 2021.
48. Yao, W, Chen, Y, Li, Z, et al.: Single Cell RNA Sequencing Identifies a Unique Inflammatory Macrophage Subset as a Druggable Target for Alleviating Acute Kidney Injury. *Adv Sci (Weinh)*, 9: e2103675, 2022.
49. Li, Z, Zimmerman, KA, Cherakara, S, et al.: A kidney resident macrophage subset is a candidate biomarker for renal cystic disease in preclinical models. *Dis Model Mech*, 16, 2023.
50. Avissar, N, Ornt, DB, Yagil, Y, et al.: Human kidney proximal tubules are the main source of plasma glutathione peroxidase. *Am J Physiol*, 266: C367-375, 1994.
51. Guo, J, Song, L, Liu, M, et al.: Fluorescent ligand-directed co-localization of the parathyroid hormone 1 receptor with the brush-border scaffold complex of the

- proximal tubule reveals hormone-dependent changes in ezrin immunoreactivity consistent with inactivation. *Biochim Biophys Acta*, 1823: 2243-2253, 2012.
52. Mao, S, Zhang, A, Huang, S: The signaling pathway of uromodulin and its role in kidney diseases. *J Recept Signal Transduct Res*, 34: 440-444, 2014.
53. Kwon, TH, Nielsen, J, Masilamani, S, et al.: Regulation of collecting duct AQP3 expression: response to mineralocorticoid. *Am J Physiol Renal Physiol*, 283: F1403-1421, 2002.
54. Chen, L, Lee, JW, Chou, CL, et al.: Transcriptomes of major renal collecting duct cell types in mouse identified by single-cell RNA-seq. *Proc Natl Acad Sci U S A*, 114: E9989-e9998, 2017.
55. Markadieu, N, Delpire, E: Physiology and pathophysiology of SLC12A1/2 transporters. *Pflugers Arch*, 466: 91-105, 2014.
56. Gopal, E, Umopathy, NS, Martin, PM, et al.: Cloning and functional characterization of human SMCT2 (SLC5A12) and expression pattern of the transporter in kidney. *Biochim Biophys Acta*, 1768: 2690-2697, 2007.
57. Supernat, A, Popęda, M, Pastuszak, K, et al.: Transcriptomic landscape of blood platelets in healthy donors. *Sci Rep*, 11: 15679, 2021.
58. Pimenova, AA, Marcora, E, Goate, AM: A Tale of Two Genes: Microglial Apoe and Trem2. *Immunity*, 47: 398-400, 2017.
59. Kleinberger, G, Yamanishi, Y, Suárez-Calvet, M, et al.: TREM2 mutations implicated in neurodegeneration impair cell surface transport and phagocytosis. *Sci Transl Med*, 6: 243ra286, 2014.

60. Filipello, F, Morini, R, Corradini, I, et al.: The Microglial Innate Immune Receptor TREM2 Is Required for Synapse Elimination and Normal Brain Connectivity. *Immunity*, 48: 979-991.e978, 2018.
61. Favuzzi, E, Huang, S, Saldi, GA, et al.: GABA-receptive microglia selectively sculpt developing inhibitory circuits. *Cell*, 184: 4048-4063.e4032, 2021.
62. Schulz, C, Gomez Perdiguero, E, Chorro, L, et al.: A lineage of myeloid cells independent of Myb and hematopoietic stem cells. *Science*, 336: 86-90, 2012.
63. Fu, H, Liu, B, Frost, JL, et al.: Complement component C3 and complement receptor type 3 contribute to the phagocytosis and clearance of fibrillar A β by microglia. *Glia*, 60: 993-1003, 2012.
64. Hong, S, Beja-Glasser, VF, Nfonoyim, BM, et al.: Complement and microglia mediate early synapse loss in Alzheimer mouse models. *Science*, 352: 712-716, 2016.
65. Peterson, SL, Li, Y, Sun, CJ, et al.: Retinal Ganglion Cell Axon Regeneration Requires Complement and Myeloid Cell Activity within the Optic Nerve. *J Neurosci*, 41: 8508-8531, 2021.
66. Kopf, M, Schneider, C, Nobs, SP: The development and function of lung-resident macrophages and dendritic cells. *Nat Immunol*, 16: 36-44, 2015.
67. Tay, SS, Roediger, B, Tong, PL, et al.: The Skin-Resident Immune Network. *Curr Dermatol Rep*, 3: 13-22, 2014.
68. Berry, MR, Mathews, RJ, Ferdinand, JR, et al.: Renal Sodium Gradient Orchestrates a Dynamic Antibacterial Defense Zone. *Cell*, 170: 860-874.e819, 2017.

69. Banchereau, J, Pascual, V: Type I interferon in systemic lupus erythematosus and other autoimmune diseases. *Immunity*, 25: 383-392, 2006.
70. Paredes, JL, Niewold, TB: Type I interferon antagonists in clinical development for lupus. *Expert Opin Investig Drugs*, 29: 1025-1041, 2020.
71. Deng, B, Lin, Y, Chen, Y, et al.: Plasmacytoid dendritic cells promote acute kidney injury by producing interferon- α . *Cell Mol Immunol*, 2020.
72. Wu, Y, Hirschi, KK: Tissue-Resident Macrophage Development and Function. *Front Cell Dev Biol*, 8: 617879, 2020.
73. Roberts, AW, Lee, BL, Deguine, J, et al.: Tissue-Resident Macrophages Are Locally Programmed for Silent Clearance of Apoptotic Cells. *Immunity*, 47: 913-927.e916, 2017.
74. Casanova-Acebes, M, Dalla, E, Leader, AM, et al.: Tissue-resident macrophages provide a pro-tumorigenic niche to early NSCLC cells. *Nature*, 595: 578-584, 2021.
75. Pinto, AR, Paolicelli, R, Salimova, E, et al.: An abundant tissue macrophage population in the adult murine heart with a distinct alternatively-activated macrophage profile. *PLoS One*, 7: e36814, 2012.
76. Pradhan, K, Yi, Z, Geng, S, et al.: Development of Exhausted Memory Monocytes and Underlying Mechanisms. *Front Immunol*, 12: 778830, 2021.
77. Beura, LK, Hamilton, SE, Bi, K, et al.: Normalizing the environment recapitulates adult human immune traits in laboratory mice. *Nature*, 532: 512-516, 2016.
78. Bhargava, P, Schnellmann, RG: Mitochondrial energetics in the kidney. *Nat Rev Nephrol*, 13: 629-646, 2017.

79. Barnett, LMA, Cummings, BS: Nephrotoxicity and Renal Pathophysiology: A Contemporary Perspective. *Toxicol Sci*, 164: 379-390, 2018.
80. King-Wing Ma, T, Kam-Tao Li, P: Depression in dialysis patients. *Nephrology (Carlton)*, 21: 639-646, 2016.
81. Breyer, MD, Susztak, K: The next generation of therapeutics for chronic kidney disease. *Nat Rev Drug Discov*, 15: 568-588, 2016.
82. Wong, CY: Current advances of stem cell-based therapy for kidney diseases. *World J Stem Cells*, 13: 914-933, 2021.
83. Xu, J, Buchwald, JE, Martins, PN: Review of Current Machine Perfusion Therapeutics for Organ Preservation. *Transplantation*, 104: 1792-1803, 2020.

Tables

Table 1. Summary of transcriptional profiles for each murine subpopulation at each timepoint.

Murine KRM Subpopulation	Transcriptional Profile Genes Used	Not used genes	Caveat
Day 0 Subpopulation 0	Ptprc, P2ry6, Ogt, Tgfb1, Cfl1, Atrx, Arhgap45, Prpf4b, Tpt1, Pnlsr, Ttc14, Arl10, Abca9, Csf2ra, Dock10, Adcy7, Eef1a1, Itch	Gm26740(%)	
Day 1 Subpopulation 0	C1qa, Cd81, Cd74, Fyb, HLA-Dqb2, Ctss, P2ry6, Itm2b, Hexb, tmem176b, Cx3cr1, Tgfb1, Serinc3, B2m, Tmem176a, Ptprc, Mbnl1	H2-Eb1 (*), H2-Aa (*), Gm26917(%)	
Day 0 Subpopulation 1	Hspa1b, Klf4, Ppp1r15a, Klf2, Tnf, Gadd45b, Nabp1, Nfkbiz, Hexim1, Hsp90aa1, Ppp1r10, Tob1, Sertad1, Atf4, Tob2, Nfkbid, Ubb, Cdkn1a	Gstp3(*), Gm6377(%)	
Day 1 Subpopulation 1	Hspa1a, Btg2, Hspa1b, Fos, Ubc, Atf3, Junb, Zfp36, Junb, Ccl3, Hsp90aa1, Ier5, Il1b, Dusp1, Egr1, Gadd45b, Ccl4, Rgs1, Nfkbiz, Nfkia		
Day 0 Subpopulation 2	Slc40a1, Ctsb, Ctsc, Ms4a7, Lgals3, Prdx1, Cts, Cd63, Lgmn, Hmox1, Apoe, Pmp22, Cd84, Lamp1, Ftl, Cstb, Cd68, Igf1, Hexa, Trem2		
Day 1 Subpopulation 2	Hmox1, Slc40a1, Ftl, Prdx1, Ctsc, Psap, Cd63, Lgals3, Apoe, Lgmn, Vcam1, Fth1, Blvrb, Creg1, Cd84, Ms4a7, Pla2g7, Lipa, Ctsz, Taldo1, Oxa1l	Mpeg1(*)	
Day 0 Subpopulation 3	Cxcl2, Egr1, Fos, Atf3, Junb, Ccl4, Ccl3, Dusp1, Zfp36, Ier2, Fosb, Btg2, Nfkbiz, Nfkbia, Ppp1r15a, Gadd45b, Socs3, Ier5, Ier3	Gm26532(%)	
Day 1 Subpopulation 3	Cxcl2, Il1b, Ccl3, Nfkbia, Fos, Egr1, Cd14, Cxcl1, Junb, Ier3, Socs3, Nfkbiz, Gadd45b, Zfp36, Cdkn1a, Cd83, Tnf, Tnfaip3, Tnfsf9, Nlrp3		
Day 0 Subpopulation 4	Lyz, Pf4, F13a1, Gas6, Trem2, Pltp, Igf1, Sult1a1, Tf, Clec10a, Stab1, Selenop, C5ar1, Bank1, Ltc45, Gas7, Lgals1, Itm2b, Mrc1		
Day 1 Subpopulation 4	Pf4, Cd163, Nxpe5, Cd63, Ccl7, Ftl, Lgals1, Actb, F13a1, Cd68, Ctsb, Ctsc, Ppp1r15a, Ms4a6d, Trem2, Calr, Mrc1, Prdx1	Nxpe5 (*), Ccl9 (*), Ms4a6d(*), Ccl6(*)	
Day 0 Subpopulation 5	S100a4, S100a6, Cd209, Gpr141, Olm1, Il17ra, Nfkbid, S100a10, Itgb7, Clec12a, Napsa, Emb, Adgre5, Trem14, Vim, Pbxip1, Coq10b, Cd44, Slc38a1	Adgre4(%), Gm6377(%), Skint3(%)	
Day 1 Subpopulation 5	S100a6, S100a4, Fn1, Vim, Thbs1, Ecm1, S100a10, Arg1, Ccr2, Tmsb10, Capg, Anxa2, Ahnak, Gda, Vcan, Cfp, Lt4r, Hp, Dok2, Adgre5	Sirpb1(*), Ms4a4a (*)	
Day 0 Subpopulation 6	Ifit3, Isg15, Ifit2, Irf7, Ifit1, Ifit3b, Ifi211, Zbp1, Usp18, Rsad2, Stat1, Sifn5, Mx1, Cmpk2, Rtp4, Oasl	Ifi47(*), Ifi206(*), Oasl2(%), Ifi204(*)	
Day 1 Subpopulation 6	Ifit3, Ifit2, Ifit1, Ifng, Cxcl10, Rsad2, Cmpk2, Mx1, Usp18, Isg15, Gbp2, Irf7, Cxcl9, Isg20	Ifit3b(*), Ifi205 (*), Ifi208(*), Ifi47(*), Ifi206(*)	Does not discriminate between hKRM 2 and hKRM 4
Microglia Transcriptional Profile	Trem2, Apoe, Cx3cr1, Cd9, Clec7a, Tyrobp, Syk, Spp1, Itgb2, Itgam, C3		Transcripts associated with C1q were excluded, despite their involvement in microglia pruning, as C1qa was used to identify KRMs

* - no singular clear human ortholog
% - no human ortholog

Table 2. Identified Marker Genes

Human KRM Subpopulation	Murine KRM Subpopulation	Marker Genes
0	4	<i>Lyz, Pf4, F13a1, Stab1, Slc40a1</i>
1	3	<i>Cxcl2, Egr1, Fos, Il1b</i>
2	6	<i>Isg15, Irf7, Ifitm3, Ifitm2</i>
3	4	<i>Lyz, Pf4, F13a1, Stab1, Slc40a1</i>
4	/	<i>TREM2, APOE, CX3CR1, CD9, CLEC7A</i>

Figure Legends

Figure 1. The human kidney contains five transcriptionally distinct kidney resident macrophage (KRM) subpopulations

(A) UMAP of five KRM subpopulations isolated from human kidneys A and B. KRMs were identified using *CIQA* expression and confirmed using *CD81* and *CD74*. (B) Heatmap of the top ten differentially expressed genes for each human KRM subpopulation. (C) Violin plot of *JUN* expression. (D) Violin plot of *JUNB* expression. (E) Violin plot of *NFKBIA* expression. (F) DotPlot of expression of marker genes associated with previously identified human KRM subpopulations. Black bars represent markers identified within the same publication.

Figure 2. Kidney cell types present in the kidney sections based on histology and spatial transcriptomics

(A) 4X image of kidney section A. The black line denotes medulla and cortex. The section shows signs interstitial fibrosis and inflammation, primarily in the cortex. (B) The location of the tubules spatial cluster. Identified using *GPX3*, *PTH1R*. (C) The location of the loop of Henle spatial cluster. Identified using *UMOD*, *SLC12A1*. (D) The location of the collecting duct spatial cluster. Identified using *AQP2*, *AQP3*. (E) 4X image of kidney section B. The black line denotes the cortex and medulla. This section shows sign of tubulointerstitial nephritis in the cortex and fibrotic regions in the medulla. (F) The location of the proximal tubules spatial cluster. Identified using *GPX3*, *SLC5A12*, *PTH1R*. (G) The location of the loop of Henle spatial cluster. Identified using *UMOD*, *SLC12A1*. (H) The location of the spatial cluster containing endothelial cells and fibroblasts, representing vasculature in fibrotic background. Identified using endothelial cell and fibroblast markers: *PECAMI1*, *CD34*, *COL1A1*, *COL1A2*.

Figure 3. Human clusters 0 and 3 are orthologous to mouse cluster 4

(A) Transcriptional profiles (~ 20 genes) and Top Marker Genes were identified from mouse KRMs pre and 1-day post-acute kidney injury. The resulting genes were used to generate Module Scores for human KRMs isolated from acute kidney injury. The results were compared by the non-parametric Pairwise Wilcox Test. All p-values are available in Supplemental Tables 1 - 4. Generated using BioRender. (B) Violin Plot of Human KRM expression of a transcriptional profile of mouse KRM cluster 4 prior to acute kidney injury (Day 0). Boxplot represents the median and one standard deviation. All values are

significant compared to the colored subpopulations. # $p < 0.0001$. (C) Violin Plot of Human KRM expression of a transcriptional profile of mouse KRM cluster 4 following acute kidney injury (Day 1). Boxplot represents the median and one standard deviation. All values are significant compared to the colored subpopulations. # $p < 0.0001$. (D) Violin plot of human KRM expression of marker genes (*LYZ*, *PF4*, *F13A1*, *STAB1*, *SLC40A1*). Boxplot represents the median and one standard deviation. All values are significant compared to the colored subpopulations. # $p < 0.0001$. (E) Violin plot of mouse KRMs at day 0 expression of marker genes (*Lyz*, *Pf4*, *F13a1*, *Stab1*, *Slc40a1*). Boxplot represents the median and one standard deviation. All values are significant compared to the colored subpopulations. # $p < 0.0001$. (F) Violin plot of mouse KRMs at day 1 expression of marker genes (*Lyz*, *Pf4*, *F13a1*, *Stab1*, *Slc40a1*). Boxplot represents the median and one standard deviation. All values are significant compared to the colored subpopulations. # $p < 0.0001$.

Figure 4. The spatial location of human KRM 1 and 3 is orthologous to murine KRM 4

(A) The location of the tubule cells cluster and Human KRM 0 and 3 on kidney section A. (B) The location of proximal tubule cells cluster and Human KRM 0 and 3 on kidney section B. (C) The location of murine KRM 4 pre and 1-day post-acute kidney injury. (D) The location of murine KRM 2 pre and 1-day post-acute kidney injury.

Figure 5. Human KRM 1 is orthologous to murine KRM 3

(A) Violin Plot of Human KRM expression of a transcriptional profile of mouse KRM cluster 4 prior to acute kidney injury (Day 0). Boxplot represents the median and one

standard deviation. All values are significant compared to the colored subpopulation. * = $p < 0.05$ ** = $p < 0.01$ † = $p < 0.001$ # = $p < 0.0001$. **(B)** Violin Plot of Human KRM expression of a transcriptional profile of mouse KRM cluster 4 following acute kidney injury (Day 1). Boxplot represents the median and one standard deviation. All values are significant compared to the colored subpopulation. * = $p < 0.05$ ** = $p < 0.01$ † = $p < 0.001$ # = $p < 0.0001$. **(C)** Violin plot of human KRM expression of marker genes (*CXCL2*, *EGR1*, *FOS*, *IL1B*). Boxplot represents the median and one standard deviation. All values are significant compared to the colored subpopulation. * = $p < 0.05$ ** = $p < 0.01$ † = $p < 0.001$ # = $p < 0.0001$. **(D)** Violin plot of mouse KRMs at day 0 expression of marker genes (*Cxcl2*, *Egr1*, *Fos*, *Il1b*). Boxplot represents the median and one standard deviation. All values are significant compared to the colored subpopulation. # $p < 0.0001$. **(E)** Violin plot of mouse KRMs at day 1 expression of marker genes (*Cxcl2*, *Egr1*, *Fos*, *Il1b*). Boxplot represents the median and one standard deviation. All values are significant compared to the colored subpopulation. # $p < 0.0001$. **(F)** The location of collecting duct cells and Human KRM 1 on kidney section A. **(G)** The location of loop of Henle cells and Human KRM 1 on kidney section B. **(H)** The location of murine KRM 3 pre and 1-day post-acute kidney injury.

Figure 6. Human KRM 2 is orthologous to murine KRM 6

(A) Violin Plot of Human KRM expression of a transcriptional profile of mouse KRM cluster 4 prior to acute kidney injury (Day 0). Boxplot represents the median and one standard deviation. All values are significant compared to the colored subpopulation. * = $p < 0.05$ ** = $p < 0.01$ † = $p < 0.001$ # = $p < 0.0001$. **(B)** Violin Plot of Human KRM

expression of a transcriptional profile of mouse KRM cluster 4 following acute kidney injury (Day 1). Boxplot represents the median and one standard deviation. All values are significant compared to the colored subpopulation. * = $p < 0.05$ ** = $p < 0.01$ † = $p < 0.001$ # = $p < 0.0001$. All p-values are available in Supplemental Table 3. (C) Violin plot of human KRM expression of marker genes (*ISG15*, *IRF7*, *IFITM3*, *IFITM2*). Boxplot represents the median and one standard deviation. All values are significant compared to the colored subpopulation. * = $p < 0.05$ ** = $p < 0.01$ † = $p < 0.001$ # = $p < 0.0001$. (D) Violin plot of mouse KRMs at day 0 expression of marker genes (*Isg15*, *Irf7*, *Ifitm3*, *Ifitm2*). Boxplot represents the median and one standard deviation. All values are significant compared to the colored subpopulation. # $p < 0.0001$. (E) Violin plot of mouse KRMs at day 1 expression of marker genes (*Isg15*, *Irf7*, *Ifitm3*, *Ifitm2*). Boxplot represents the median and one standard deviation. All values are significant compared to the colored subpopulation. # $p < 0.0001$. (F) The location of collecting duct cells and Human KRM 2 on kidney section A. (G) The location of vasculature on a fibrotic background cells and Human KRM 2 on kidney section B. (H) The location of murine KRM 6 pre and 1-day post-acute kidney injury.

Figure 7: Human KRM 4 does not have a murine ortholog and expresses a microglia transcriptional profile

(A) DotPlot of activated microglia markers showing predominate expression by human KRM 4. (B) DotPlot of activated microglia markers showing similar expression amongst all murine KRM subpopulations prior to AKI. (C) DotPlot of activated microglia markers showing similar expression amongst all murine KRM subpopulations post-AKI. (D) Violin plot of human KRM expression of marker genes (*TREM2*, *APOE*, *CX3CR1*, *CD9*,

CLEC7A). Boxplot represents the median and one standard deviation. All values are significant compared to the colored subpopulation. * = $p < 0.05$ ** = $p < 0.01$ † = $p < 0.001$ # = $p < 0.0001$. (E) Violin Plot of Human KRM expression of a transcriptional profile of a transcriptional profile associated with pruning microglia (Table 1). Boxplot represents the median and one standard deviation. All values are significant compared to the colored subpopulation. * = $p < 0.05$ ** = $p < 0.01$ † = $p < 0.001$ # = $p < 0.0001$. (F) The location of proximal tubule cells and Human KRM 4 on kidney section A. (G) The location of proximal tubule cells and Human KRM 4 on kidney section B.

Figures

Figure 1.

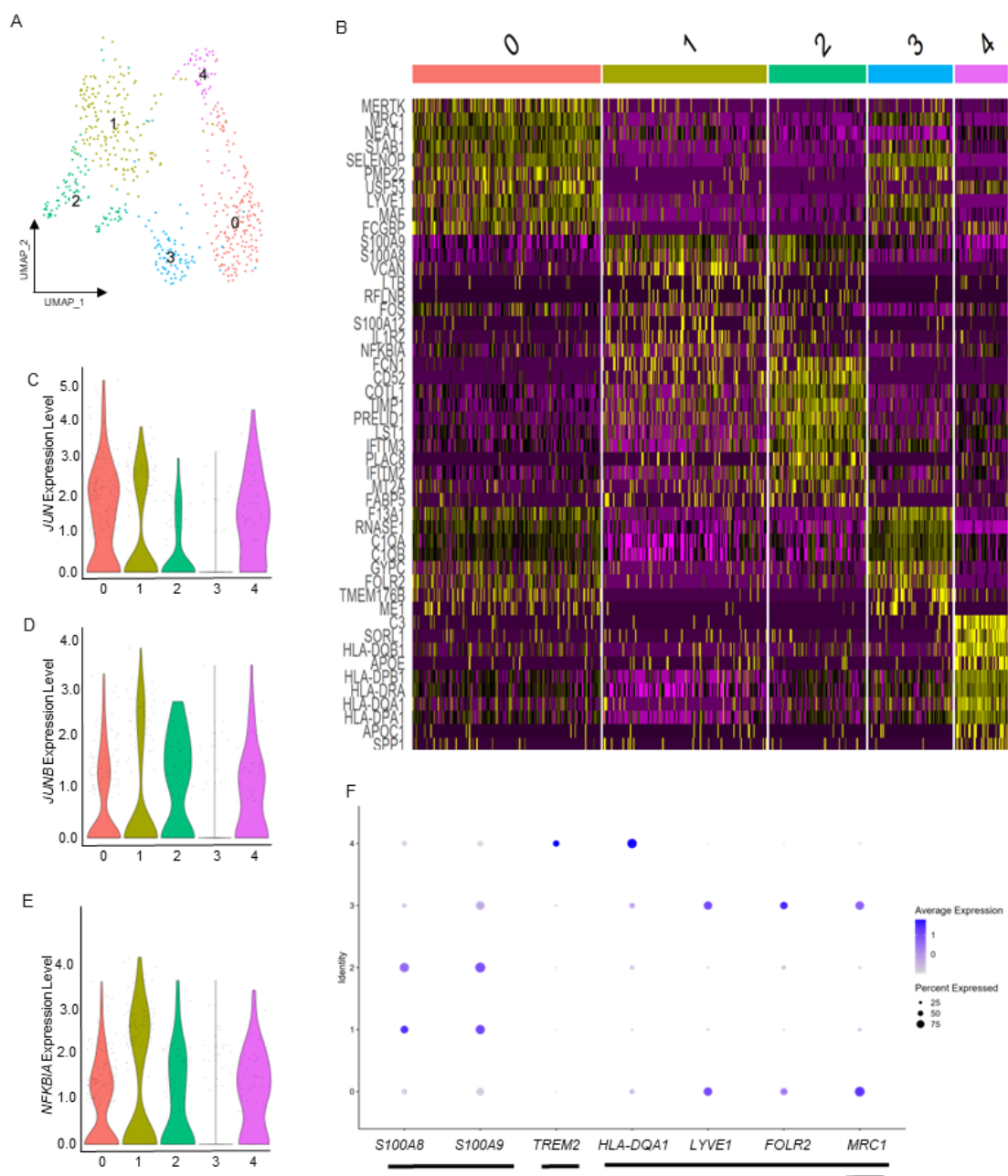


Figure 2.

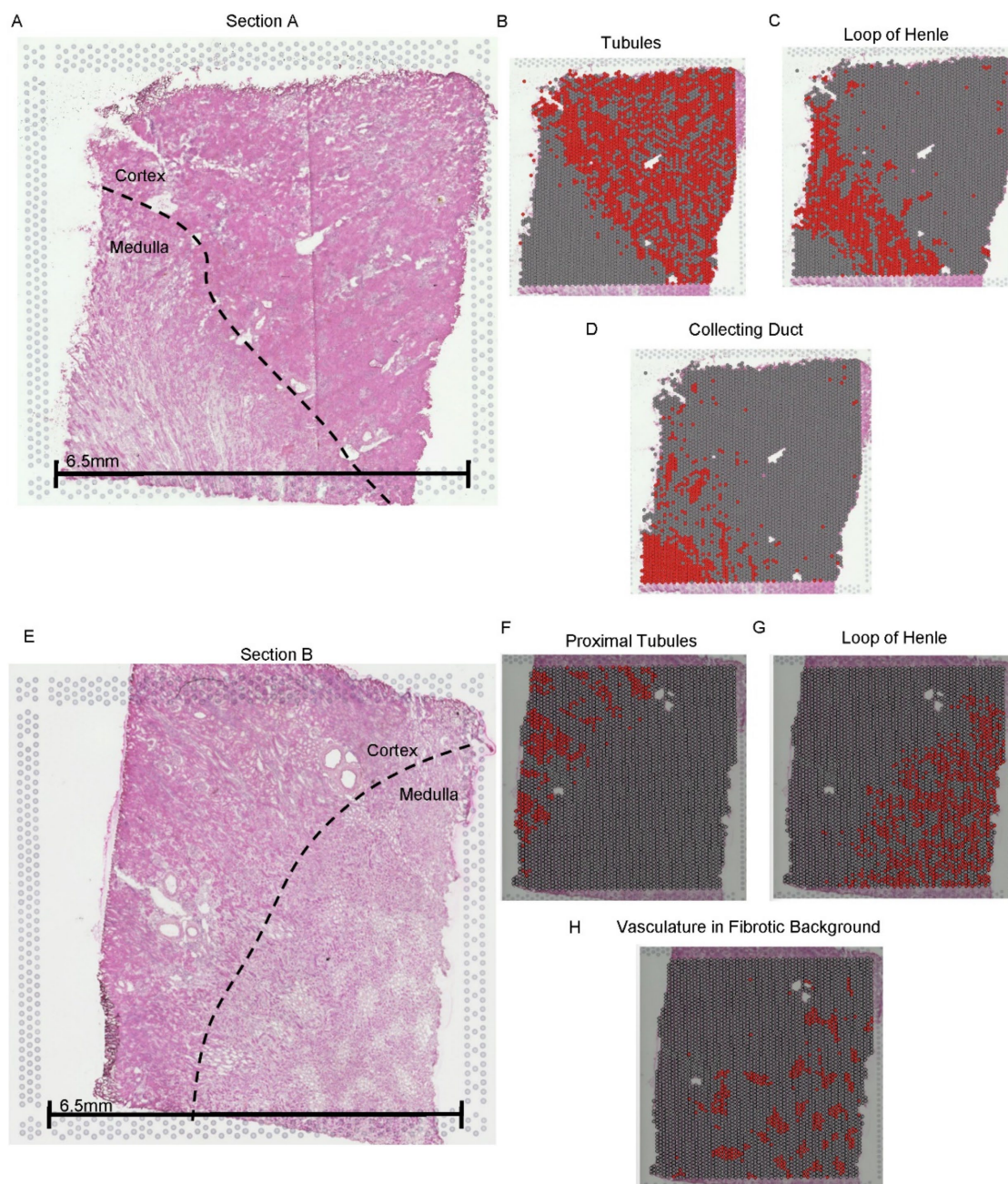


Figure 3.

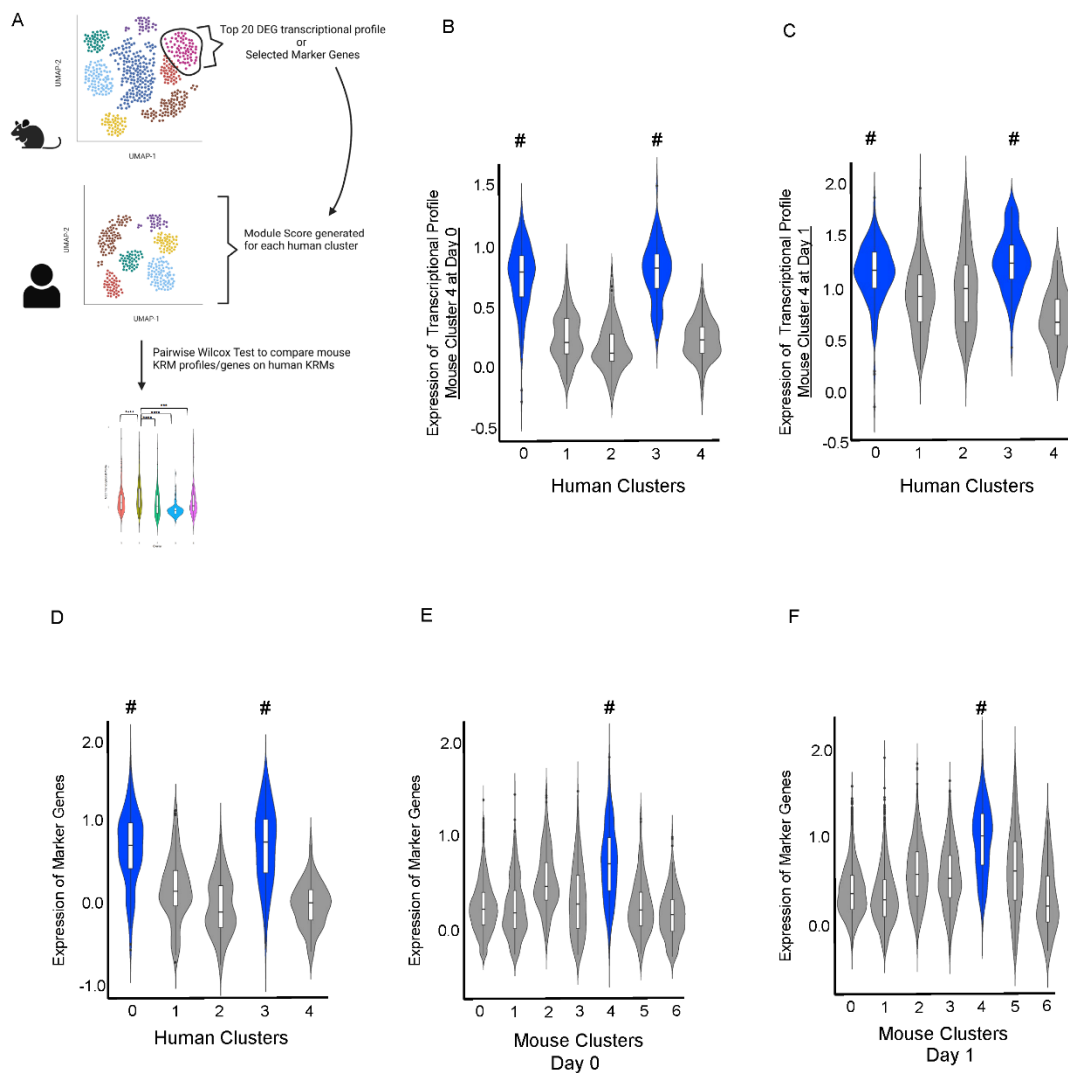


Figure 4.

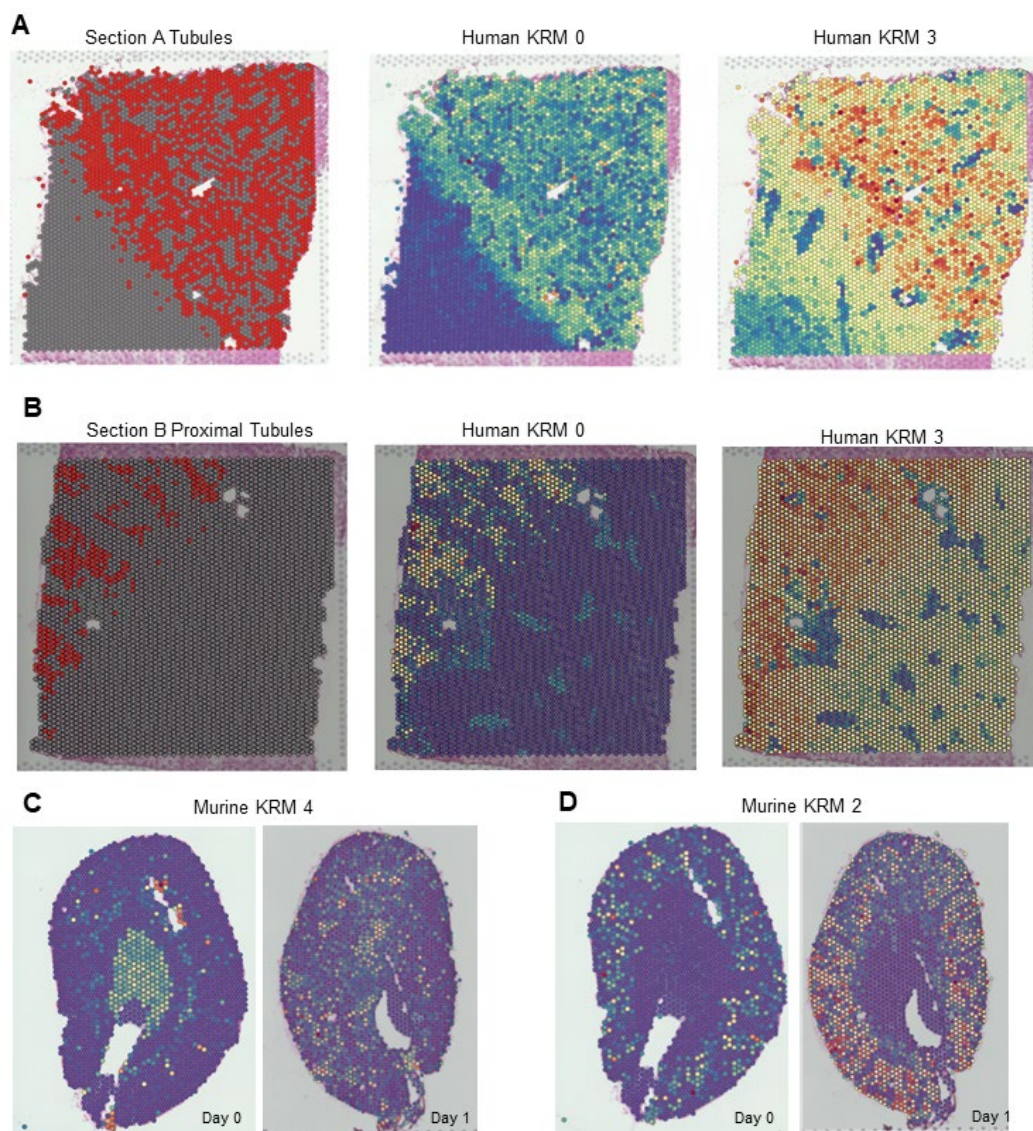


Figure 5.

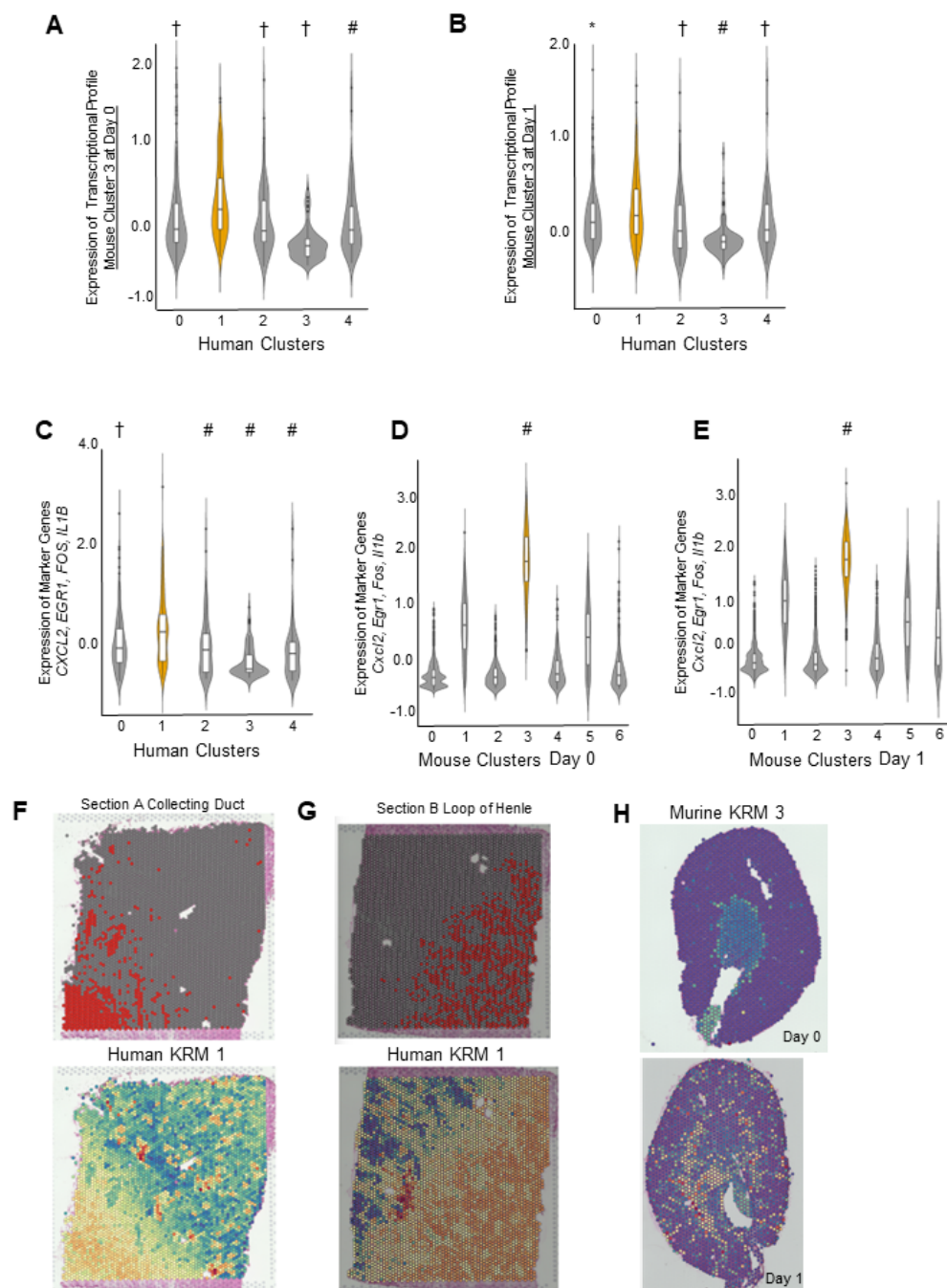


Figure 6.

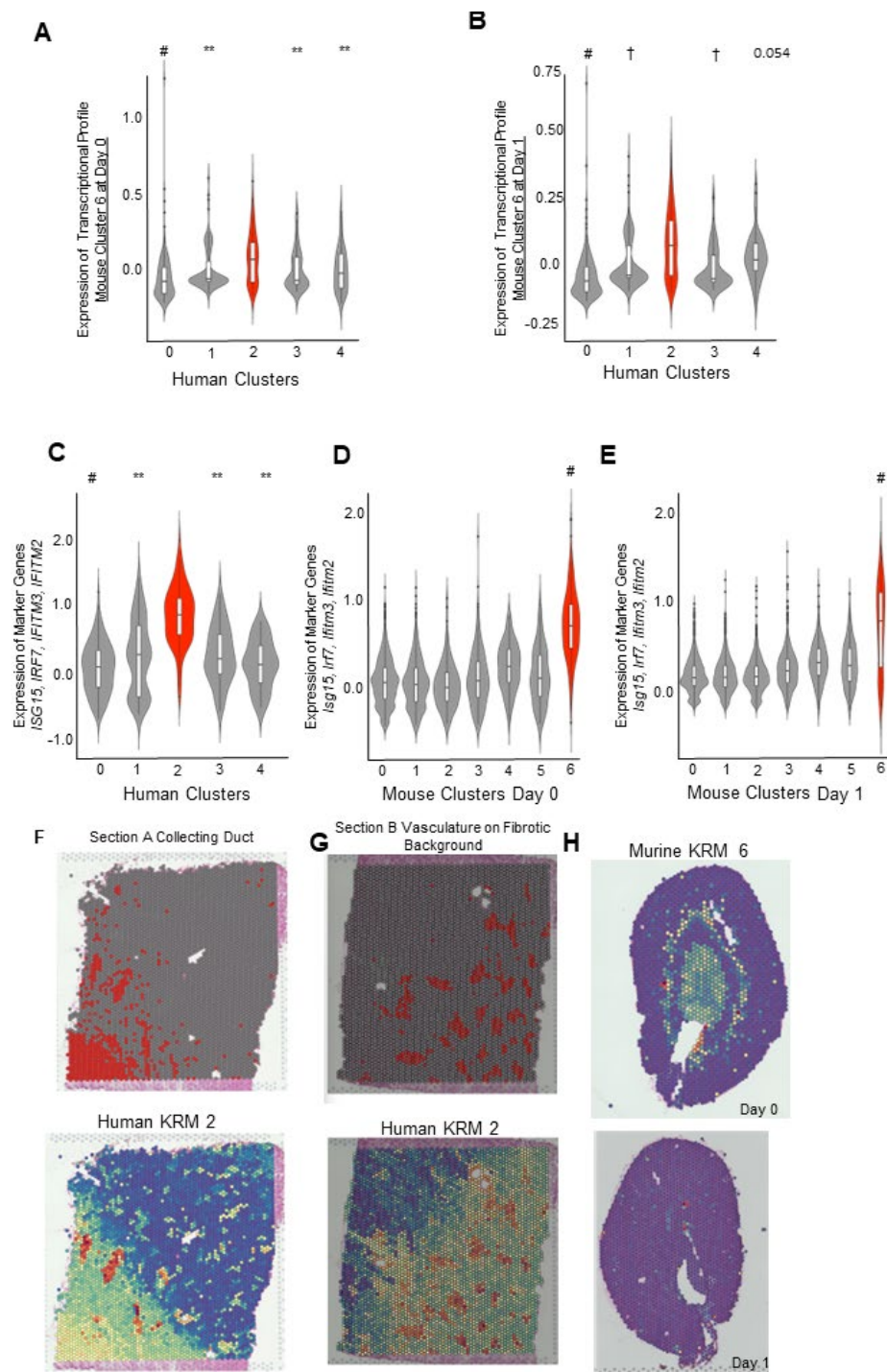
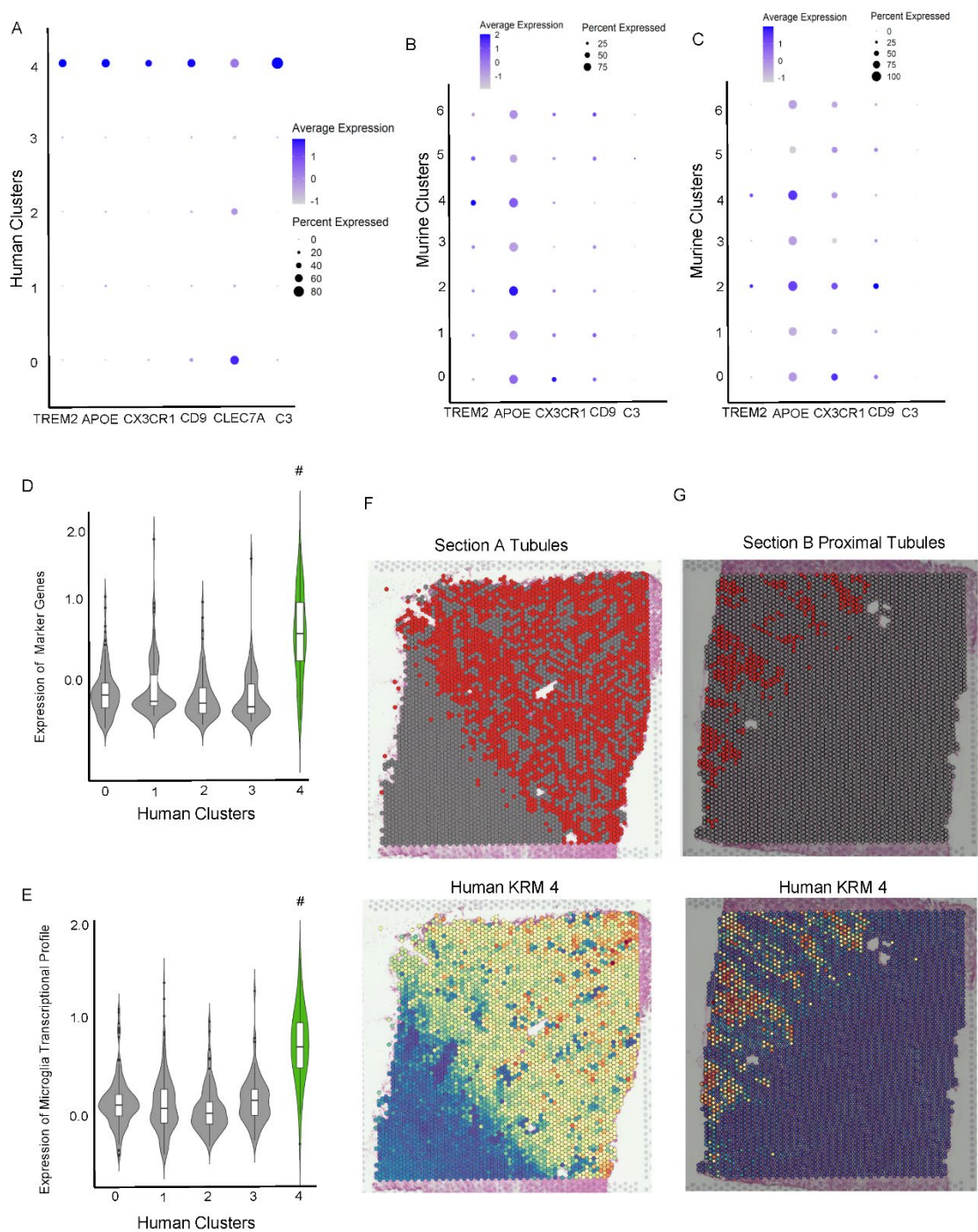


Figure 7.



AN EVOLUTIONARILY CONSERVED KIDNEY RESIDENT MACROPHAGE
PHENOTYPE WITH REDUCED MHC II EXPRESSION APPEARS AFTER KIDNEY
INJURY

by

ELISE N. ERMAN

KYLE H. MOORE, MATTHEW D. CHEUNG, JENNIFER LA FONTAINE,
ZHENGQIN YANG, REHAM H. SOLIMAN, ANUPAM AGARWAL, JAMES F.
GEORGE

Submitted to *Journal of the American Society of Nephrology*

Format adapted for dissertation

Significance Statement

Unlike peripheral populations, kidney resident macrophages (KRM) represent the first and persistent responders to kidney damage given their residency in the tissue. Little is known about the specific response of KRM following injury. This work identifies a subset of KRM that downregulate MHC II following multiple models of acute and chronic injury. This kidney injury associated (KIA) phenotype is evolutionarily conserved between mice and humans and presents concurrently with a wound healing transcriptional profile at the site of damage in acute injury. Therefore, KIA cells are an excellent potential therapeutic target, and their function could be amplified in AKI to facilitate recovery.

Abstract

Background

Kidney resident macrophages (KRM) are involved in amelioration and propagation of acute kidney injury and chronic kidney disease. They express high levels of surface MHC II during homeostasis. Here, we describe downregulation of MHC II by a subset of KRM, termed kidney injury-associated (KIA) cells, that appear across injury models and are conserved between mice and humans.

Methods

KIA cells were identified in mice following AKI and CKD using flow cytometry. AKI and CKD were confirmed using GFR and serum creatinine. Single cell RNA sequencing and spatial transcriptomics were performed on kidney from mouse and human AKI and mouse CKD samples to investigate the location and transcriptional profile of KIA cells. A 2/3 ligation model was used to confirm the localization of KIA cells to damaged tissue. Human samples came from donors with mild to moderate AKI.

Results

KIA cells were identified in every model of injury tested, although KIA cells appear among different KRM subsets depending on the injury model. KIA cells resolve in AKI and persist in CKD. Human and mouse AKI-generated KIA cells localize to the site of damage and present a wound-healing transcriptional profile.

Conclusions

The presentation of MHC II negative KIA cells is evolutionarily conserved following AKI and CKD. AKI-generated KIA cells localize to the site of injury and may be involved in wound response or repair.

Introduction

The incidence of acute kidney injury (AKI) and chronic kidney disease (CKD) rates continue to increase globally and specifically in the United States.^{1,2} Numerous epidemiological studies show that AKI is a risk factor for subsequent development of

CKD and patients with CKD are more susceptible to developing AKI.³⁻⁷ While the immune system has been implicated, the mechanisms within AKI and CKD remain relatively undefined.⁸

Macrophages are an important component of the pathogenesis of AKI and the subsequent recovery response. Depletion of mononuclear phagocytes protects against injury or prevents recovery depending on the time and completeness of depletion.⁹ Macrophages have been implicated in kidney disease propagation and mitigation; however, most studies did not delineate between peripheral and resident macrophage populations and therefore their role in injury responses has been difficult to discern.¹⁰⁻¹³ Thus, there is a need to understand the specific roles of resident macrophages in kidney injury and in the normal uninjured state. Recently, we discovered that there is significant underlying complexity in kidney resident macrophages (KRM) populations, with a number of functionally distinct subpopulations that reside within specific zones in the kidney.¹⁴

In homeostasis, KRM subpopulations express high levels of major histocompatibility complex class II (MHC II).^{15,16} Macrophages are canonically thought to exist as expressing low MHC II in homeostasis and increase expression following activation, however resident macrophage populations are known to express the molecule, though expression patterns differ by tissue.¹⁷⁻¹⁹ Antigen endocytosed from the extracellular environment is processed and presented on MHC II molecules to CD4+ T cells to coordinate T cell activation and B cell differentiation.²⁰

Here, we show that KRMs down regulate MHC II in multiple models of kidney injury in a subpopulation specific manner that varies as a function of the injury model.

We further show that the appearance of this phenotype is evolutionarily conserved in mice and humans. We have termed these MHC II negative KRM kidney injury associated (KIA) cells. In AKI, these cells maintain a wound healing profile and may be integral to tissue repair.

Methods

Animals.

Male C57BL/6J mice, 8–16 weeks of age, were obtained from The Jackson Laboratory. For supplemental figures the additional mouse strains, on a C57BL/6J background, were obtained from The Jackson Laboratory: IL-6 KO (B6.129S2-IL6^{tm1korf}/J, TLR2 KO (B6.129-Tlr2^{tm1kir}/J, IL-10 receptor KO (B6.129S2-IL10rb^{tm1Agt}/J). PKD^{Rc/Rc} mice were generously provided by collaborator Dr. Michal Mrug. Mice were housed at the University of Alabama at Birmingham (UAB) animal facilities in compliance with the NIH guidelines regarding the care and use of live animals. All animal work performed was reviewed and approved by the Institutional Animal Care and Use Committee at UAB (IACUC).

Human Samples

Human kidney samples were obtained from kidneys deemed unsuitable for transplantation. Donor A was a 68-year-old White man, as determined from health records. The serum creatinine of the donor of sample A was 1.8 mg/dL two days prior to tissue acquisition at which time the serum creatinine had dropped to 0.6 mg/dL. The histological section shows extensive tubular atrophy and extensive fibrosis. The

glomeruli appear atrophied with damaged glomerular capillaries (Fig S4). Donor B was a 57-year-old White man, 5 days post brain death, as determined from health records. The serum creatinine of the donor of sample B at the time of acquisition was 2.5 mg/dL and presented with mild to moderate AKI. The histological section also presents with tubular atrophy but less severe glomeruli damage (Fig S4). Samples were taken for single-cell RNA sequencing and spatial transcriptomics in accordance with IRB-300004648.

Bilateral ischemia/reperfusion injury (BIRI AKI).

Mice were subjected to bilateral ischemia/reperfusion injury, as previously described.^{21,22} Surgeries were performed in the morning. Mice were anesthetized using ketamine and xylazine (i.p.). Under aseptic precautions, both kidneys were clamped at the renal pedicle using a microserrafine vascular clamp (Fine Science Tools, 18055-05). After 19 minutes, the clamps were removed to allow reperfusion. Reperfusion was visually confirmed within 1 minute. Body temperature, measured by a rectal thermometer, was carefully maintained at $37^{\circ}\text{C} \pm 1^{\circ}\text{C}$.

Aristolochic Acid Nephropathy (AAN CKD).

10-week-old mice (Jackson Laboratory) were randomly assigned to either the AA group or the control group and were subjected to 5 consecutive days of AA (A9451, Sigma-Aldrich) i.p. 3 mg/kg body weight to induce CKD or equal volume of saline vehicle as a control. Mice were sacrificed two and six weeks, as well as six months, after their first injection for evaluation of kidney injury and downstream analysis.

2/3 Kidney Ligation.

10-week-old mice C57BL/6J mice (Jackson Laboratory) were subjected to unilateral ligation of both poles of a single kidney. Surgeries were performed in the morning. Mice were anesthetized using ketamine and xylazine (i.p.). Body temperature, measured by a rectal thermometer, was carefully maintained at $37^{\circ}\text{C} \pm 1^{\circ}\text{C}$ throughout the surgery. Ligatures were applied to prevent slicing the kidney tissue but reduce blood flow to both renal poles. Kidneys were harvested 24 hours post injury. The contralateral kidney served as a control. At the time of harvest, the ligated kidney was separated into the upper pole, center, and lower pole, and the resulting sections were processed in conjunction with the control contralateral kidney.

LPS.

10-week-old mice (Jackson Laboratory) were randomly assigned to either the LPS group or the control group and were subjected to a single injection of lipopolysaccharide (Millipore Core, LPS25 Lot. 3795228) i.p. 2 mg/kg body weight or equal volume of saline vehicle as a control. Mice were sacrificed at 24 hours for evaluation of kidney injury and downstream analysis.

Flow cytometry/FACS.

Murine KRMs were obtained as previously described.¹⁴ Briefly, we isolated KRMs using flow cytometric sorting. Leukocytes were isolated as previously described.^{21,22} Mice were anesthetized under isoflurane and perfused through the left ventricle with 10 mL cold PBS. Kidneys were removed, stripped of the capsule, minced with a razor

blade on a glass slide, and placed into Liberase (MilliporeSigma) at 37°C for 30 minutes. The digestion was stopped by adding cold PBS containing 1% BSA, and tissue was further disaggregated through an 18-gauge syringe. Red blood cells were lysed using ACK lysis buffer for 2 minutes at room temperature, and the remaining leukocytes were then washed with ice-cold PBS. Cells were then stained with violet fixable viability dye (Invitrogen L34955) and treated with unlabeled anti-CD16/32 antibody to block Fc γ 3 receptors. Cells were subsequently stained using anti-Gr-1 Alexa Fluor 700 (Ly6G, clone 1A8, BioLegend), anti-CD11b super bright 600 (M1/70, Invitrogen), anti-F4/80 APC-eFluor-780 (BM8, Invitrogen), anti-NK1.1 PE-C7 (PK136, Invitrogen), anti-CD45.2 BV-650 (104, BioLegend), anti-MHC II (I-A/I-E) PerCP (M5/114.15.2, BD Biosciences), anti-CD19 super bright 702 (6D5, BioLegend), anti-TCR β Pe-Cy5 (H57-597, BD Biosciences).

Murine and human single cell suspensions were generated identically. Briefly, human kidney cross sections were cut and minced with a razor blade and placed into Liberase (MilliporeSigma) at 37°C for 30 minutes. The digestion was stopped by adding cold PBS containing 1% BSA, and tissue was further disaggregated through an 18-gauge syringe. Red blood cells were lysed using ACK lysis buffer for 2 minutes at room temperature, and the remaining leukocytes were then washed with ice-cold PBS. Cells were then stained with violet fixable viability dye (Invitrogen L34955) and treated with unlabeled anti-CD16/32 antibody to block Fc γ 3 receptors. Cells were subsequently stained using anti-CD45 FITC (YTH24.5, BioRad). Human macrophages do not express an ortholog of F4/80 and therefore require a different FACS sorting protocol. Staining for C1q, a conserved marker for KRM, requires fixation, and is therefore incompatible for

single cell RNA sequencing. Transcription of *Clqa/CIQA* was found to accurately identify KRMs in mice and humans. For these reasons, we elected to identify human KRMs at the transcriptional level from CD45+ sorted cells.

scRNA-Seq.

Purified cells were transferred on ice to the UAB Flow Cytometry and Single Cell Core and immediately processed using the Chromium 3' Single Cell RNA sequencing kit (10× Genomics) according to the manufacturer's instructions. The cell suspension was counted and combined with a 10× Chromium reagent mixture and loaded into a microfluidic single-cell partitioning device in which lysis and reverse transcriptions occur in microdroplets. The resulting cDNA was amplified by polymerase chain reaction and subsequently processed to yield bar-coded sequencing libraries. Paired-end sequencing was carried out on an Illumina NovaSeq6000 sequencing platform (Illumina). Reads were processed using the 10× Genomics Cell Ranger Single-Cell Software Suite (version 6.0) on the UAB Cheaha High-Performance Computing Cluster. BCL files were converted to FASTQ files using the CellRanger mkfastq function. CellRanger count was used to align the FASTQ files to the mouse genome (mm10) or human GRCh38 (GCA_000001405.28). The gene table, barcode table, and transcriptional expression matrices were created for the analysis indicated below.

Spatial transcriptomics.

The Visium system relies on a 2-dimensional matrix of 5000 spots distributed on a microscope slide in a 6.5 by 6.5 mm square. Each spot, which contains a poly-dT oligonucleotide with a unique sequence (bar code), is 50 μm in diameter at a distance from the other spots of 100 μm from center to center. Kidneys were embedded in the Optimal Cutting Temperature matrix (Fisher Scientific) and stored at -80°C . Before sectioning, blocks were equilibrated to -10°C for 30 minutes. A 10 μm section was placed onto specialized Spatial Gene Expression slides (10 \times Genomics) and processed according to the manufacturer's protocols. Briefly, slides were stained with H&E, and bright-field images were acquired using a Keyence BZ-X700 microscope. Tissues were permeabilized for 12 minutes (human) or 18 minutes (mouse) and cDNA was generated and used to create second-strand DNA. The resulting cDNA was subject to downstream amplification and library processing for scRNA-Seq. Reads were processed using the 10 \times Genomics Space Ranger Single-Cell Software Suite (version 1.2) on the UAB Cheaha High-Performance Computing Cluster. BCL files were converted to FASTQ files using the SpaceRanger mkfastq function. SpaceRanger count was used to align the FASTQ files to the mouse genome (mm10).

Sequencing Data Analysis.

Both scRNA-Seq and spatial transcriptomics analyses were carried out using packages created for the R statistical analysis environment (version 4.2.1). Data were primarily analyzed using Seurat (version 4.3.0) and its associated dependencies.^{23,24} Data from each sample were imported using the Read10X function and then structured into a

Seurat object using `CreateSeuratObject`. For quality control, cells with unique feature counts over 2500 or under 200 were excluded. Data were normalized and scaled using either log normalization or `SCTransform`.²⁵ Objects from each time point were labeled with unique group IDs and then merged into a single object using the Seurat merge function. Data objects were integrated using the Harmony R package.²⁶ Principal component analysis was performed based on 30 principal components, and then cells were clustered using `FindAllMarkers`. The dimensional reduction was done using UMAP.

Integration of scRNA-Seq and spatial transcriptomics to resolve cell location.

The spatial matrix was integrated with the scRNA-Seq data set using the anchor-based workflow built into the Seurat package. `FindTransferAnchors` was used. Using the generated anchor set, the `TransferData` function created predictions from the KRM reference clusters and applied that to the spatial data sets. Using the predictions, each subpopulation could be visualized using `SpatialFeaturePlots`.

AddModuleScore.

The `AddModuleScore` function in Seurat was used to determine the expression of provided gene lists (Tables 1 and 2) and control genes were set to 500. The resulting meta data of the Seurat object was moved to a dataframe for statistical analysis.

Statistics.

For Figures 1 and 4, statistics were calculated using Prism version 8. One-way ANOVAs with multiple comparisons were used to determine significance. For Figures 2,3, and 5, statistics were performed in R and plotted using ggplot. Boxplots report the median and standard deviation of a dataset. Kruskal Wallis test was used to determine a difference within a dataset and the Pairwise Wilcox test for nonparametric data was used to compare individual groups to each other.

Results

The presence and persistence of KIA cells correlates with the type of injury.

We investigated the dynamics of MHC II expression by KRMs in mouse models of BIRI AKI and AAN CKD (Fig 1A). KRMs are identifiable within the tissue by their high expression of F4/80 and intermediate expression of CD11b and transcriptionally by *Clqa*.^{22,27,28} The downregulation of MHC II was initially identified using flow cytometry and the appearance of an MHC II-negative population following injury (Fig 1B). KRMs lacking MHC II following injury were termed kidney injury associated (KIA) cells.

Kidney function following AKI was determined using glomerular filtration rate (GFR). A significant decrease in GFR was observed on day 1 following injury compared to quiescence (131.1 ± 12.72 vs 210.4 ± 13.87 mL/min; $p=0.025$) (Fig 1C). Following injury, approximately 28.23% of KRMs become KIA cells by downregulating MHC II in comparison to approximately 1.69% of KRMs in the controls (28.23 ± 2.34 vs 1.69 ± 0.20 %; $p<0.0001$)(Fig 1D). There was a significant reduction in the percentage of KIA cells from day 1 post injury to day 6 (14.98 ± 5.08 %KIA of KRMs; $p=0.02$) correlating with the restoration of kidney function (Fig 1C and D). The percentage of KIA cells

returned to quiescent levels two weeks following injury ($2.952 \pm 1.55\%$; $p=0.98$ compared to controls). To confirm that the appearance of KIA cells was a result of the induction of AKI, we performed sham surgeries and confirmed that there was no increase in KIA cells in sham mice at day 1 ($2.50 \pm 0.16\%$; $p<0.0001$) or day 6 (0.39 ± 0.05 ; $p=0.004$)(Fig 1E).

There was a significant reduction in GFR of aristolochic acid treated (CKD) mice at 2 weeks compared to quiescent mice (23.47 ± 3.47 vs 224.8 ± 22.13 mL/min; $p<0.0001$)(Fig 1F). While GFR appeared to remain reduced at six-week time points, the sample size was limited because of injection site stress and reduced health of CKD mice. Therefore, kidney injury was confirmed by serum creatinine measurements from the CKD mice, which identified significant increases in serum creatinine at 2 weeks (0.084 ± 0.004 in control mice vs 0.588 ± 0.0819 mg/dL; $p=0.0104$) and 6 weeks (0.076 ± 0.0114 vs 0.4683 ± 0.0482 mg/dL; $p=0.0013$), compared to vehicle treated controls. Serum creatinine showed a trend towards elevation 6 months after CKD induction (0.1133 ± 0.01202 vs 0.3050 ± 0.05362 ; $p=0.0995$) (Fig 1G). KIA cells were significantly increased 2 weeks post-CKD induction compared to vehicle controls ($0.9733 \pm 0.1561\%$ vs $22.02 \pm 5.757\%$; $p=0.0433$) (Fig 1 H). There was no significant difference between vehicle treated mice and CKD mice at 6 weeks, but significance had returned at 6 months (1.783 ± 0.200 vs 3.277 ± 0.923 ; $p=0.0032$) (Fig 1H).

KIA cells were also identified in LPS-induced sepsis and a genetic model of PKD (Fig S1). Interleukin (IL-) 6, IL-10, and TLR2 have all been shown to be involved in MHC II downregulation on other macrophage populations.^{19,29,30} However, we repeated small cohort studies utilizing global knockout mice and our CKD model outlined in

Figure 1 which suggested that IL-10, IL-6 or TLR2 are not necessary for the downregulation of MHC II by KRMs (Fig S2).

KIA cells in AKI express a wound healing profile and localize to the site of injury.

We performed single cell RNA sequencing on kidneys isolated from mice at quiescence, 12 hours, and 1-day post AKI. In uninjured mice, the majority of KRMs have moderate to high expression of MHC II gene *H2-Aa* (Fig 2A). A small proportion of KRMs lack MHC II prior to injury, as identified in Figure 1D and are likely represented by cluster 5, which is rare in quiescence with low *H2-Aa* expression (Figure 2A). However, by day 1 cluster 5 expanded and upregulated MHC II expression compared to quiescence, whereas cluster 3 significantly and uniquely downregulated MHC II expression, identifying it as KIA cells (Fig 2B). To confirm that this is not an artifact of using a single gene (*H2-Aa*), we used the *AddModuleScore* feature to determine the expression level of an MHC II transcriptional profile (Table 1).³¹ Although cluster 5 has the lowest expression of an MHC II transcriptional profile at quiescence, it displays a clear upregulation following injury (Table S1) (Fig 2C). In contrast, KIA cells (cluster 3), delineated in orange, show a significant downregulation of MHC II transcriptional at Day 1 compared to all other KRM subpopulations (Table S1)(Fig 2C).

We used gene ontology terms and *AddModuleScore* to determine a potential function for KIA cells. Prior to insult, cluster 5 cells show significant upregulated expression of gene ontology set Wound Healing (GO:009303)(Table 1)(Table S2)(Fig 2D).³² Following AKI, cluster 5, in conjunction with an increase in MHC II expression, downregulates the wound healing profile in a possible inverse relationship. In contrast,

KIA cells have the highest expression of the wound healing profile day 1 post AKI in conjunction with the lowest MHC II transcriptional profile (Fig 2D)(Table S2).

Next, we used spatial transcriptomics to localize KIA cells in the kidney tissue. At quiescence prior to the appearance of the KIA phenotype, pre-KIA cells (MHC II expressing) are localized throughout the kidney, but are spatially distinct from the expression of *Napsa*, a marker gene for S3 proximal tubules in the cortico-medullary region (Fig 2E).¹⁴ Twelve hours and 1-day post injury, the KIA cells are localized to the cortico-medullary region, the area most sensitive to injury in ischemic AKI (Fig 2E).³³

KIA cells do not uniquely express a wound healing profile or localize to the site of injury in CKD

As with AKI, we performed scRNAseq on mice at quiescence and two weeks post CKD. We were unable to integrate the KRMs identified prior to injury with those identified post-injury indicating highly disparate transcriptomic profiles (Fig S3). For this reason, we were not able to identify changes in KIA cells over time in CKD. However, KIA cells were identified in the 2-week CKD dataset, both by low expression of the single gene *H2-Aa* and the entire MHC II transcriptional profile (Fig 3A-B)(Table 1)(Table S3). In CKD, there was no difference in expression of a wound healing profile by KIA cells (Fig 3C)(Table S4). Figure 3D shows that KIA cells are found throughout the tissue, but preferentially localize from the cortico-medullary region (*Napsa*) to the inner medulla (*Umod*, loop of Henle).^{14,34}

KIA cells are specific to the site of ischemic injury.

We utilized a model of $\frac{2}{3}$ kidney ligation without contralateral nephrectomy to generate localized ischemia in the kidney poles while leaving the center of the kidney relatively unharmed in order to determine if KIA cells are specific to the region of injury in ischemic injury (Fig 4A). The percentage of KIA cells was significantly increased in the ischemic poles compared to both the center (33.56 ± 4.105 vs $10.12 \pm 1.347\%$; $p=0.0001$) and uninjured unilateral kidney ($2.887 \pm 0.4435\%$; $p<0.0001$). There was no significant difference between the center and the uninjured contralateral kidney (Fig 4B). To further confirm that KIA cells localize to the site of injury, we expressed the difference in percent of KRMs that were KIA cells between 1) the poles compared to the uninjured unilateral kidney, 2) the poles compared to the center, and 3) the center to the uninjured contralateral kidney. This revealed no statistical significance in the difference in KIA cells within injured poles when comparing them to uninjured contralateral kidney vs center. There is a statistical difference comparing the poles to the center when both are normalized to the uninjured unilateral kidney (30.59 ± 4.124 vs $7.728 \pm 1.450\%$; $p=0.0009$)(Fig 4C). The difference in %KIA cells were significantly increased in the poles-minus-uninjured contralateral kidney (30.59 ± 4.124) vs the center compared to uninjured unilateral kidney (7.728 ± 1.450 ; $p=0.0009$).

Next, we used the top ten differentially expressed genes (DEGs) from AKI and CKD KIA cells to compare the transcriptional profile of KIA cells across models. The resulting heatmaps showed that the transcriptome of KIA cells differs across models (Fig 4D and E). When generating a heatmap with the DEGs of CKD KIA cells onto the AKI dataset, AKI cluster 6 appears to have a uniquely high pattern of expression. When

generating a heatmap with the DEGs of the AKI KIA cells onto the CKD dataset, cluster 2 has the higher pattern of expression. It appears that while comparative subpopulations exist across both injury models, different subpopulations downregulate MHC II expression in AKI compared to CKD.

Human AKI kidneys contain KIA cells that express a wound healing profile and localize with glomeruli.

Non-cancerous human kidneys that did not meet the criteria for transplantation were used for scRNAseq of CD45+ cells and spatial transcriptomics. As in mice, we identified human KIA cells by a lack of *HLA-DRA* transcripts, a human MHC II gene (Fig 5A). We confirmed a reduced expression of the MHC II transcriptional profile by KIA cells with appropriate correction for human orthologous genes (Table 1)(Fig 5B)(Table S5). We observed significantly increased expression of the wound healing transcriptional profile in human KIA cells in comparison to all other clusters except cluster 2 (Fig 5B)(Table S6)(Table 1).

To identify the location of the cells within the tissue, we performed spatial transcriptomics on samples proximal to those used for scRNAseq. Glomeruli are identifiable on section A (mild AKI) both by histology and the localization of podocytes, confirmed by expression of the gene for podocin. identified on the spatial section (Fig S4)(Fig 5C). A region of the tissue is marked with a black box to aid in the identification of colocalized cell types. KIA cells are identified in the same section and are most predominate in the glomeruli and around the thickened blood vessels and atrophic tubules (Fig 5D)(Fig S4). CD4+ T cells appeared throughout the section (Fig 5E). Section B has glomeruli throughout the tissue (Fig S4)(Fig 5F). In moderate AKI, KIA cells were

distinctly co-localized in glomeruli (Figure 5G). Additionally, KIA cells were spatially distinct from CD4+ T cells, which were present in the section but did not appear around or within glomeruli.

Discussion

Macrophages amplify initial inflammation following AKI via expression of TNF α and are involved in recruitment of additional leukocytes.³⁵⁻³⁷ The shift to an anti-inflammatory profile is not thought to occur until multiple days post-injury.³⁸ MHC II is considered a marker of pro-inflammatory macrophages, and its downregulation was unexpected in AKI and CKD.³⁹ KIA cells specifically downregulate MHC II after injury and do so in both acute and chronic injury models. They are found at the site of injury and their induction appears to be a conserved and universal response following injury. AKI and CKD encompass many etiologies and pathological processes, yet we identified KIA cells in mice bearing a PKD mutation and following ischemic, nephrotoxic, and septic injury.⁴⁰⁻⁴⁴ KIA cells are conserved across species as they are observed in both mice and humans.

In AKI, the appearance of a KIA phenotype appears to be biased towards the region of injury. The S3 portion of the proximal tubule is most sensitive to ischemic injury.³³ In the mouse, the corticomedullary region is highly enriched for the S3 segment, which can be visualized on a spatial transcriptomic section with the S3 proximal tubule gene *Napsa*.^{14,33} We found that within 12 hours, murine KIA cells localize to the corticomedullary region. To confirm that KIA cells localize to injured tissue, we used a ligation injury model to selectively injure the poles of the kidney and found that KIA cells were

subsequently found there. In the human donor samples, the kidney sections presented with colocalization of KIA cells and glomeruli, a component of the nephron. that is susceptible to damage as the result of a variety of AKI pathologies.⁴⁵⁻⁴⁹

In AAN CKD, the site of injury is primarily cortical, yet the KIA cells were predominately localized in the cortico-medullary region and medulla two weeks post injury.^{50,51} Whether the KIA cells were initially in the cortex is unknown and will require additional studies. Additionally, the model of CKD utilized here is known for rapid fibrosis of the cortex.^{12,52} We speculate that KIA cells preferentially localize with kidney cells and not within fibrotic tissue, which would restrict them to the medulla away from greatest damage. Another possibility is that different subpopulations downregulate MHC II depending on the type of injury. DEGs from AKI and CKD KIA cells differ significantly. DEGs associated with AKI KIA cells do not identify CKD KIA cells, but instead an MHC II expressing subpopulation. The same is true for CKD KIA cells, where the DEGs again match an MHC II expressing subpopulation and not the AKI KIA cells. Therefore, it is possible that in AKI the subpopulation that becomes KIA cells may be restricted to the cortico-medullary region, whereas in CKD a different subpopulation becomes KIA cells and is restricted to the medulla. Finally, KIA cells may initially colocalize with the site of greatest injury in our model of CKD but could alter location as the disease progresses.

In both the mice and human AKI samples KIA cells were identified as the KRM subpopulation with the highest expression of a wound healing profile, but not in CKD. Again, this could be because fibrosis has progressed in CKD and that this altered the transcriptional profile of all KRM subpopulations similarly. This is supported by the

smaller number of subpopulations identified in CKD compared to AKI (4 vs 9) and the inability to integrate an uninjured dataset with the two-week CKD timepoint, which suggests vast transcriptional changes compared to quiescence. Another possibility is that because KIA cells in CKD are not in the areas of greatest damage, they are not receiving the signal that is present in AKI which leads to the expression of a wound healing profile. Future research into the location of KIA cells across kidney injury models and any changes that occur therein will provide further insight into their function.

KRMs that lack MHC II were initially described in Lever *et al.* and posited that this was a recapitulation of a developmental phenotype, as murine KRMs lack MHC II during kidney development.²¹ Wound healing compared to tissue growth and remodeling during development may require similar functions, so it remains possible that the upregulation of a wound healing profile in concert with a downregulation of MHC II is indeed a recapitulation of the MHC II negative developmental phenotype observed in mice. It is possible that the mechanisms of MHC II downregulation in KIA cells could be unique, as common inducers of MHCII downregulation (IL-10, IL-6, and TLR2) did not appear to be necessary for the presence of KIA cells.^{19,29,30}

A distinct or related function may be to dampen an adaptive immune response at the site of sterile injury. The MHC II molecule binds with CD4 to increase TCR stimulation on CD4⁺ T cells. The coreceptor CD28 binds to CD80/86 on MHC II⁺ cells to further strengthen this interaction. CD4⁺ T cells have been implicated in the pathogenesis of sterile kidney injury in a CD28 dependent manner.⁵³ Therefore, it is possible that the downregulation of MHC II by KIA cells and the lack of interaction with CD4⁺ T cells in areas occupied by KIA cells may be a mechanism to prevent CD4⁺ T

cell activation and further damage. This concept is supported by the distinct lack of CD4⁺ T cells in the section of kidney from the human donor B. While we did not identify any spatial distinction in murine AKI between KIA cells and CD4⁺ T cells (data not shown), this could be because spatial transcriptomics on mouse kidney sections is currently unable to resolve glomeruli due to the reduced size of the structures and the limited resolution of the Visium spatial transcriptomics system.

Ideal cellular therapeutic targets should be at the site of injury to effectively target pathological processes, reduce off-target effects, span multiple etiologies and be translatable from model organisms to human clinical trials. We have demonstrated that KIA cells are present in both AKI and CKD in mice and in AKI in humans. In AKI, KIA cells are specific to the region of the kidney where the greatest injury occurs and resolve when the injury resolves. In both murine and human AKI, KIA cells express a wound healing profile, being the only population to do so in mice and one of two in humans. For these reasons, KIA cells make an excellent potential therapeutic target, and their function should likely be amplified in AKI to facilitate recovery.

Future work will be necessary to determine the role of MHC II, the function of KIA cells at the site of injury, and to further expand the recognition of KIA cells in a variety of human kidney diseases.

Disclosures

Anupam Agarwal serves as a consultant for Dynamed and is on the advisory boards of Alpha Young and Creegh Pharmaceuticals for work outside the scope of this manuscript.

Funding

This work was supported by NIH grants P30 DK079337, R01 DK59600, and R01 DK118932 (to AA and JFG), and American Heart Association grant 827257 (to ENE).

Acknowledgments

We acknowledge the UAB Flow Cytometry and Single Cell Core (NIH P30-AR-04831) and the UAB O'Brien Preclinical Studies of AKI Core. Some figures were generated with BioRender.com.

Data availability

The scRNA-Seq and spatial transcriptomics data generated for this paper were deposited in the NCBI's Gene Expression Omnibus database (GSE228516, GSE228169, GSE226533, and GSE200115). Visium data from GEO GSE200115 has been used for other publications within the laboratory.

References

1. Pavkov, ME, Harding, JL, Burrows, NR: Trends in Hospitalizations for Acute Kidney Injury - United States, 2000 - 2014 *Morbidity and Mortality Weekly Report (MMWR)*. CDC, 2018.
2. Foreman, KJ, Marquez, N, Dolgert, A, et al.: Forecasting life expectancy, years of life lost, and all-cause and cause-specific mortality for 250 causes of death: reference and alternative scenarios for 2016-40 for 195 countries and territories. *Lancet*, 392: 2052-2090, 2018.

3. Mehta, RL, Pascual, MT, Soroko, S, et al.: Spectrum of acute renal failure in the intensive care unit: the PICARD experience. *Kidney Int*, 66: 1613-1621, 2004.
4. Chawla, LS, Kimmel, PL: Acute kidney injury and chronic kidney disease: an integrated clinical syndrome. *Kidney Int*, 82: 516-524, 2012.
5. Waikar, SS, Liu, KD, Chertow, GM: The incidence and prognostic significance of acute kidney injury. *Curr Opin Nephrol Hypertens*, 16: 227-236, 2007.
6. Metnitz, PG, Krenn, CG, Steltzer, H, et al.: Effect of acute renal failure requiring renal replacement therapy on outcome in critically ill patients. *Crit Care Med*, 30: 2051-2058, 2002.
7. Mehta, RL, Pascual, MT, Soroko, S, et al.: Diuretics, mortality, and nonrecovery of renal function in acute renal failure. *Jama*, 288: 2547-2553, 2002.
8. Coca, SG, Singanamala, S, Parikh, CR: Chronic kidney disease after acute kidney injury: a systematic review and meta-analysis. *Kidney Int*, 81: 442-448, 2012.
9. Ferenbach, DA, Sheldrake, TA, Dhaliwal, K, et al.: Macrophage/monocyte depletion by clodronate, but not diphtheria toxin, improves renal ischemia/reperfusion injury in mice. *Kidney Int*, 82: 928-933, 2012.
10. Berry, MR, Mathews, RJ, Ferdinand, JR, et al.: Renal Sodium Gradient Orchestrates a Dynamic Antibacterial Defense Zone. *Cell*, 170: 860-874.e819, 2017.
11. Stamatiades, EG, Tremblay, ME, Bohm, M, et al.: Immune Monitoring of Trans-endothelial Transport by Kidney-Resident Macrophages. *Cell*, 166: 991-1003, 2016.

12. Baudoux, T, Jadot, I, Declèves, AE, et al.: Experimental Aristolochic Acid Nephropathy: A Relevant Model to Study AKI-to-CKD Transition. *Front Med (Lausanne)*, 9: 822870, 2022.
13. Huen, SC, Cantley, LG: Macrophage-mediated injury and repair after ischemic kidney injury. *Pediatr Nephrol*, 30: 199-209, 2015.
14. Cheung, MD, Erman, EN, Moore, KH, et al.: Resident macrophage subpopulations occupy distinct microenvironments in the kidney. *JCI Insight*, 7, 2022.
15. Lever, JM, Hull, TD, Boddu, R, et al.: Resident macrophages reprogram toward a developmental state after acute kidney injury. *JCI Insight*, 4: 125503, 2019.
16. Cheung, MD, Erman, EN, Moore, KH, et al.: Resident macrophage subpopulations occupy distinct microenvironments in the kidney. *JCI Insight*, 7, 2022.
17. Dick, SA, Wong, A, Hamidzada, H, et al.: Three tissue resident macrophage subsets coexist across organs with conserved origins and life cycles. *Sci Immunol*, 7: eabf7777, 2022.
18. Deng, T, Lyon, CJ, Minze, LJ, et al.: Class II major histocompatibility complex plays an essential role in obesity-induced adipose inflammation. *Cell Metab*, 17: 411-422, 2013.
19. Qian, J, Luo, F, Yang, J, et al.: TLR2 Promotes Glioma Immune Evasion by Downregulating MHC Class II Molecules in Microglia. *Cancer Immunol Res*, 6: 1220-1233, 2018.
20. Shevach, EM, Paul, WE, Green, I: Histocompatibility-linked immune response gene function in guinea pigs. Specific inhibition of antigen-induced lymphocyte proliferation by alloantisera. *J Exp Med*, 136: 1207-1221, 1972.

21. Lever, JM, Hull, TD, Boddu, R, et al.: Resident macrophages reprogram toward a developmental state after acute kidney injury. *JCI Insight*, 4, 2019.
22. Lever, JM, Yang, Z, Boddu, R, et al.: Parabiosis reveals leukocyte dynamics in the kidney. *Lab Invest*, 98: 391-402, 2018.
23. Butler, A, Hoffman, P, Smibert, P, et al.: Integrating single-cell transcriptomic data across different conditions, technologies, and species. *Nat Biotechnol*, 36: 411-420, 2018.
24. Stuart, T, Butler, A, Hoffman, P, et al.: Comprehensive Integration of Single-Cell Data. *Cell*, 177: 1888-1902.e1821, 2019.
25. Hafemeister, C, Satija, R: Normalization and variance stabilization of single-cell RNA-seq data using regularized negative binomial regression. *Genome Biol*, 20: 296, 2019.
26. Korsunsky, I, Millard, N, Fan, J, et al.: Fast, sensitive and accurate integration of single-cell data with Harmony. *Nat Methods*, 16: 1289-1296, 2019.
27. Soos, TJ, Sims, TN, Barisoni, L, et al.: CX3CR1⁺ interstitial dendritic cells form a contiguous network throughout the entire kidney. *Kidney Int*, 70: 591-596, 2006.
28. Zimmerman, KA, Bentley, MR, Lever, JM, et al.: Single-Cell RNA Sequencing Identifies Candidate Renal Resident Macrophage Gene Expression Signatures across Species. *J Am Soc Nephrol*, 30: 767-781, 2019.
29. Redpath, S, Angulo, A, Gascoigne, NR, et al.: Murine cytomegalovirus infection down-regulates MHC class II expression on macrophages by induction of IL-10. *J Immunol*, 162: 6701-6707, 1999.

30. Velásquez, LN, Milillo, MA, Delpino, MV, et al.: Brucella abortus down-regulates MHC class II by the IL-6-dependent inhibition of CIITA through the downmodulation of IFN regulatory factor-1 (IRF-1). *J Leukoc Biol*, 101: 759-773, 2017.
31. Tirosh, I, Izar, B, Prakadan, SM, et al.: Dissecting the multicellular ecosystem of metastatic melanoma by single-cell RNA-seq. *Science*, 352: 189-196, 2016.
32. Ashburner, M, Ball, CA, Blake, JA, et al.: Gene ontology: tool for the unification of biology. The Gene Ontology Consortium. *Nat Genet*, 25: 25-29, 2000.
33. Venkatachalam, MA, Bernard, DB, Donohoe, JF, et al.: Ischemic damage and repair in the rat proximal tubule: differences among the S1, S2, and S3 segments. *Kidney Int*, 14: 31-49, 1978.
34. Mao, S, Zhang, A, Huang, S: The signaling pathway of uromodulin and its role in kidney diseases. *J Recept Signal Transduct Res*, 34: 440-444, 2014.
35. Alikhan, MA, Ricardo, SD: Mononuclear phagocyte system in kidney disease and repair. *Nephrology (Carlton)*, 18: 81-91, 2013.
36. Duffield, JS: Macrophages and immunologic inflammation of the kidney. *Semin Nephrol*, 30: 234-254, 2010.
37. Jo, SK, Sung, SA, Cho, WY, et al.: Macrophages contribute to the initiation of ischaemic acute renal failure in rats. *Nephrol Dial Transplant*, 21: 1231-1239, 2006.
38. Wen, Y, Crowley, SD: The varying roles of macrophages in kidney injury and repair. *Curr Opin Nephrol Hypertens*, 29: 286-292, 2020.

39. Stables, MJ, Shah, S, Camon, EB, et al.: Transcriptomic analyses of murine resolution-phase macrophages. *Blood*, 118: e192-208, 2011.
40. Ronco, C, Bellomo, R, Kellum, JA: Acute kidney injury. *Lancet*, 394: 1949-1964, 2019.
41. Leaf, DE, Christov, M: Dysregulated Mineral Metabolism in AKI. *Semin Nephrol*, 39: 41-56, 2019.
42. Rahman, M, Shad, F, Smith, MC: Acute kidney injury: a guide to diagnosis and management. *Am Fam Physician*, 86: 631-639, 2012.
43. Afkarian, M, Katz, R, Bansal, N, et al.: Diabetes, Kidney Disease, and Cardiovascular Outcomes in the Jackson Heart Study. *Clin J Am Soc Nephrol*, 2016.
44. Matsushita, K, Ballew, SH, Wang, AY, et al.: Epidemiology and risk of cardiovascular disease in populations with chronic kidney disease. *Nat Rev Nephrol*, 18: 696-707, 2022.
45. Barnett, LMA, Cummings, BS: Nephrotoxicity and Renal Pathophysiology: A Contemporary Perspective. *Toxicol Sci*, 164: 379-390, 2018.
46. Grgic, I, Campanholle, G, Bijol, V, et al.: Targeted proximal tubule injury triggers interstitial fibrosis and glomerulosclerosis. *Kidney Int*, 82: 172-183, 2012.
47. Patschan, D, Muller, GA: Acute Kidney Injury in Diabetes Mellitus. *Int J Nephrol*, 2016: 6232909, 2016.
48. Helal, I, Fick-Brosnahan, GM, Reed-Gitomer, B, et al.: Glomerular hyperfiltration: definitions, mechanisms and clinical implications. *Nat Rev Nephrol*, 8: 293-300, 2012.

49. Remuzzi, G, Zoja, C, Bertani, T: Glomerulonephritis. *Curr Opin Nephrol Hypertens*, 2: 465-474, 1993.
50. Pozdzik, AA, Berton, A, Schmeiser, HH, et al.: Aristolochic acid nephropathy revisited: a place for innate and adaptive immunity? *Histopathology*, 56: 449-463, 2010.
51. Jadot, I, Declèves, AE, Nortier, J, et al.: An Integrated View of Aristolochic Acid Nephropathy: Update of the Literature. *Int J Mol Sci*, 18, 2017.
52. Fu, Y, Tang, C, Cai, J, et al.: Rodent models of AKI-CKD transition. *Am J Physiol Renal Physiol*, 315: F1098-f1106, 2018.
53. Burne, MJ, Daniels, F, El Ghandour, A, et al.: Identification of the CD4(+) T cell as a major pathogenic factor in ischemic acute renal failure. *J Clin Invest*, 108: 1283-1290, 2001.

Tables

Table 1. List of genes used to delineate a transcriptional profile for MHC II and wound healing.

Mouse MHC II Transcriptional Profile Genes	Human MHC II Transcriptional Profile Genes	Mouse Wound Healing Transcriptional Profile Genes	Human Wound Healing Transcriptional Profile Genes
H2-Aa, Cd74, H2-Ab1, Cd81, H2-DMa, H2-Eb1, H2-Eb2, Ciita, Tap1, Tap2, Psmb9, Psmb8	HLA-DQA1, CD74, HLA-DQB1, CD81, HLA-DMA, HLA-DRB1, CIITA, B2M, TAP1, TAP2, PSMB9, PSMB8	Actg1, Adra2a, Ano6, Anxa1, Arfgef1, Ccl2, Ccn4, Cd36, Cldn1, Cldn3, Cldn4, Cxcr4, Ddr2, Dmtn, Emilin2, Enpp4, F2r, F3, F7, Fermt1, Fermt2, Hbegf, Hmgb1, Hpse, Hras, Itgb1, Kank1, Mtor, Mylk, Nfe2l2, Plat, Plau, Prdx2, Prkce, Ptger4, Ptk2, Rreb1, S100a9, Serpine1, Serpinf2, Smoc2, St3gal4, Tbx2r, Thbs1, Vegfb, Xbp1	ACTG1, ADRA2A, ANO6, ANXA1, APOH, ARFGEF1, CCL2, CCN4, CD36, CLDN1, CLDN3, CLDN4, CLDN13, CPB2, CXCR4, DDR2, DMTN, DUOX1, DUOX2, EMILIN2, ENPP4, F2, F2R, F3, F7, F12, FERMT1, FERMT2, FOXC2, HBEGF, HMGB1, HPSE, HRAS, HRG, INS13' TGB1, KANK1, KLRH1, MTOR, MYLK, NFE2L2, PLAT, PLAU, PLG, PRDX2, PRKCE, PTGER4, PTK2, REG3A, REG3G, RREB1, S100A9, SERPINE1, SERPINF2, SMOC2, ST3GAL4, TBXA2R, THBS1, VEGFB, XBP1

Figure Legends

Figure 1. The presence and persistence of KIA cells correlates with the type of injury.

(A) Schematic showing the timepoints for injury induction and flow cytometry and single cell RNA sequencing studies for bilateral ischemia reperfusion injury (BIRI) induced AKI and aristolochic acid nephropathy (AAN) induced CKD.

(B) Gating strategy for flow cytometry. Moving from left to right, the plots show the gating of single cells, live CD45⁺ cells, removal of Ly6G⁺ neutrophils, and the identification of F4/80⁺/CD11b intermediate KRM. Expression of MHC II in a control mouse (blue) is shown in comparison to a mouse 2 weeks after administration of aristolochic acid (red). **(C)** Glomerular filtration rate (GFR) of B6 mice pre (black) and

post (red) AKI. Day 1 is the only significant reduction in GFR (131.1 +/- 12.72 vs 210.4 +/- 13.87; p=0.025) **(D)** KIA cells as a percentage of KRMs pre and post AKI. KIA cells significantly increase within one day of injury (28.23 +/- 2.34 vs 1.69 +/- 0.20; p<0.0001) and have returned to quiescent levels by day 14 (2.952 +/- 1.55; p=0.98).

(E) KIA cells are significantly increased in AKI mice (red) compared to sham injured (blue) at both day 1 and day 6 post injury (2.50 +/- 0.16; p<0.0001)(0.39 +/- 0.05;

p=0.004) **(F)** GFR 2 and 6 weeks post first injection for CKD. GFR is significantly reduced 2 weeks post CKD induction and remains visually reduced at 6 weeks (23.47 +/-

3.47 vs 224.8 +/- 22.13; p<0.0001) **(G)** Serum creatinine of vehicle (blue) and AA (red) treated mice. There is a significant increase in serum creatinine at 2 and 6 weeks (0.084 +/- 0.004 vs 0.588 +/- 0.0819; p=0.0104)(0.076 +/- 0.0114 vs 0.4683 +/- 0.0482;

p=0.0013) and is visually elevated at 6 months. **(H)** KIA cells as a percentage of KRMS at 2 and 6 weeks and 6 months post CKD induction. The percentage of KIA cells is significantly increased at 2 weeks and 6 months (1.783 +/- 0.200 vs 3.277 +/- 0.923; p=0.0032)

Figure 2. KIA cells in AKI express a wound healing profile and localize to the site of greatest injury.

(A) Featureplot of *H2-Aa* expression at quiescence and day 1 from Single cell RNA sequencing of mice 0, 12 hours, and 1 day post bilateral ischemia reperfusion AKI.

Uninjured mice have high expression of H2-Aa in all subpopulations other than Cluster 5, which is rare prior to injury. Cluster 3 will become KIA cells and are identified with a

black box. **(B)** Featureplot of H2-Aa at day-1 post AKI. Cluster 3 has the lowest expression of H2-Aa and are KIA cells (black box). **(C)** Expression of an MHC II

transcriptional profile provided in Table 1 for the identified subpopulations in uninjured and 1 day post injury mice. Prior to injury, cluster 5 has uniquely low expression.

Following injury, cluster 5 has upregulated MHC II profile and KIA cells (orange) are statistically significant for the downregulation of the MHC II profile ($p < 0.0001$). All p values are presented in Supplemental Table 1. **(D)** Expression of a wound healing

transcriptional profile provided in Table 1 for the identified subpopulations in uninjured and 1 day post injury mice. Prior to injury, cluster 5 has uniquely high expression.

Following injury, KIA cells (orange) are statistically significant for increased expression of a wound healing profile ($p < 0.001$). All p values are presented in Supplemental Table 2. * = $p < 0.05$ ** = $p < 0.01$ † = $p < 0.001$ # = $p < 0.0001$. **(E)** The location of KIA cells at day 0, 12 hours, and day 1 post injury. KIA cells localize to the cortico-medullary region of the kidney following injury, as identified by *Napsa* transcripts.

Figure 3. KIA cells do not uniquely express a wound healing profile or localize to the site of injury in CKD.

(A) Featureplot of *H2-Aa* at 2 weeks post Aristolochic acid induced CKD. Cluster 0 has the lowest expression of *H2-Aa* and are KIA cells (black box). **(B)** Expression of an MHC II transcriptional profile provided in Table 1. KIA cells (orange) are statistically significant for the downregulation of the MHC II profile ($p < 0.0001$) All p values are presented in Supplemental Table 3. **(C)** Expression of a wound healing transcriptional profile provided in Table 1 for the identified subpopulations in CKD. There is no statistical difference for KIA cells compared to the other subpopulations. All p values are presented in Supplemental Table 4. **(D)** The location of KIA cells at the 2 week

timepoint. KIA cells localize to the cortico-medullary and medullary region of the kidney following injury, as identified by *Napsa* and *Umod* expression.

Figure 4. KIA cells are specific to the site of ischemic injury.

(A) Schematic of 2/3 ligation model with example images of uninjured unilateral kidney and ligated kidney. **(B)** KIA cells as a percentage of KRMs in the manually isolated ischemic poles, center of ligated kidney, and uninjured unilateral kidney. KIA cells are significantly increased in the poles compared to both the center (33.56 ± 4.105 vs 10.12 ± 1.347 ; $p=0.0001$) and unilateral kidney (2.887 ± 0.4435 ; $p<0.0001$). **(C)** Percentage of KIA cells in the poles and center normalized to either the uninjured kidney or center. There is no statistical difference in the percentage of KIA cells in the pole when normalized to either the center or unilateral kidney. There is a statistical difference comparing the poles to the center when both are normalized to the uninjured unilateral kidney (30.59 ± 4.124 vs 7.728 ± 1.450 ; $p=0.0009$) **(D)** A heatmap from the AKI dataset of DEGs from AKI KIA cells and CKD KIA cells. AKI KIA cell DEGs represent the first 10 listed genes, followed by the CKD KIA cell DEGs. KIA cells as identified in Figure 2 are cluster 3. **(E)** A heatmap from the CKD dataset of DEGs from AKI KIA cells and CKD KIA cells. AKI KIA cell DEGs represent the first 10 listed genes, followed by the CKD KIA cell DEGs. KIA cells as identified in Figure 3 are cluster 0.

Figure 5. Human AKI kidneys contain KIA cells that express a wound healing profile and localize with glomeruli.

(A) Featureplot of *HLA-DRA* on human KRMs, cluster 1 has the lowest expression and are therefore KIA cells (back box). **(B)** KIA cells (orange) have significantly reduced

expression of the MHC II transcriptional profile compared to other KRM subpopulations and significantly express the wound healing transcriptional profile compared to KRM subpopulations 0, 3, and 4. All p values are presented in Supplemental Table 5 and 6. * = $p < 0.05$ ** = $p < 0.01$ † = $p < 0.001$ # = $p < 0.0001$ (C) The location of glomeruli on a kidney section from kidney section A. (D) The location of KIA cells on a kidney section from kidney section A. (E) The location of CD4⁺ T cells on a kidney section from kidney section A (F) The location of glomeruli on a kidney section from kidney section B G. The location of KIA cells on a kidney section from kidney section B. (H) The location of CD4⁺ T cells on a kidney section from kidney section B

Figures

Figure 1.

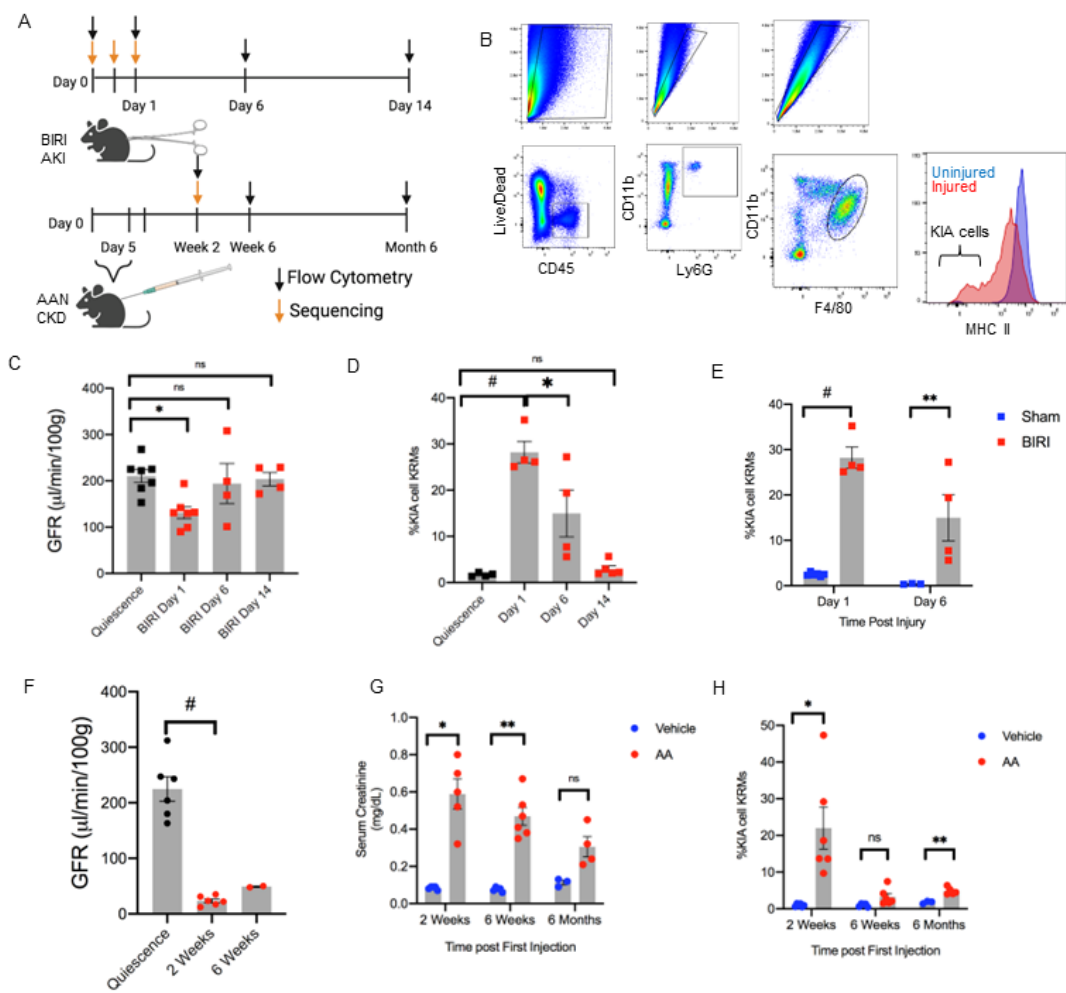


Figure 2.

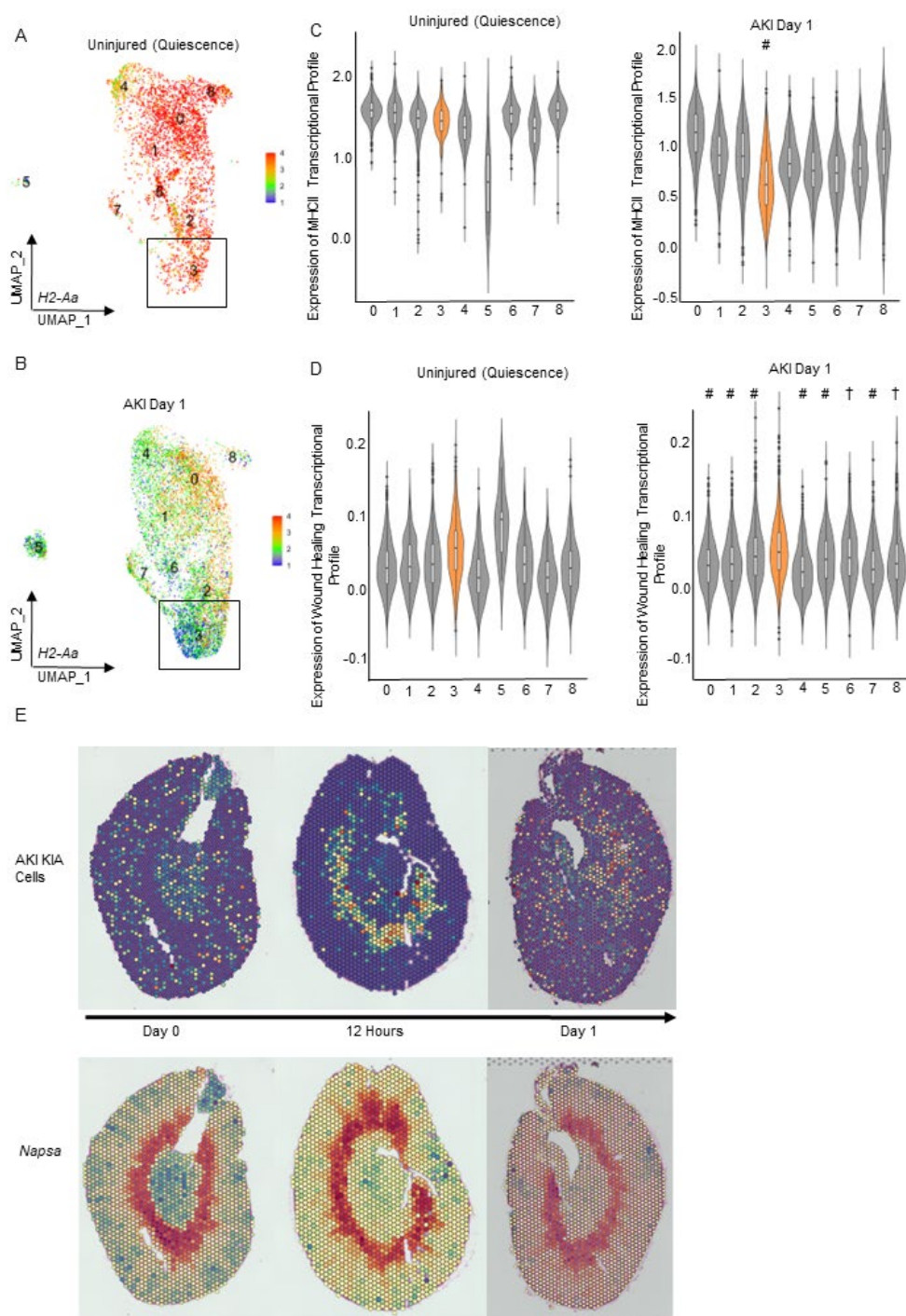


Figure 3.

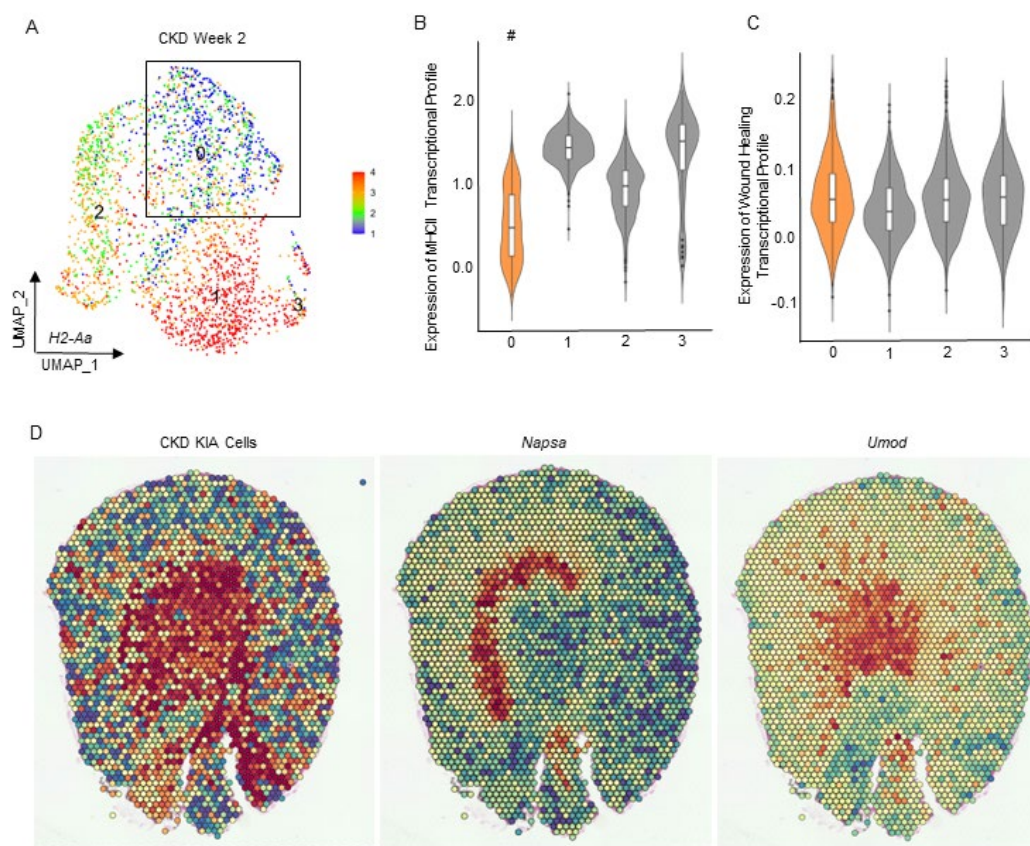


Figure 4.

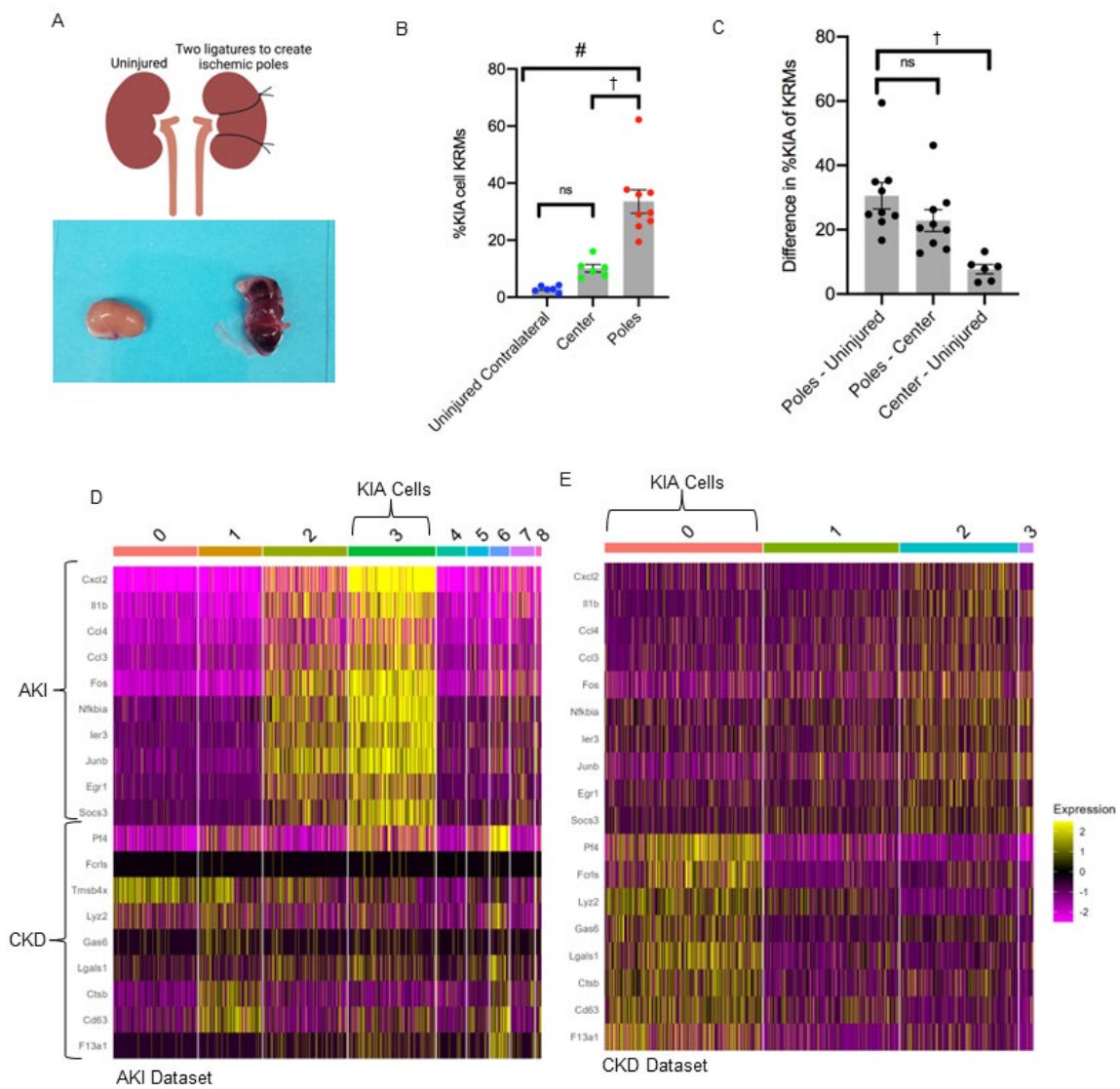
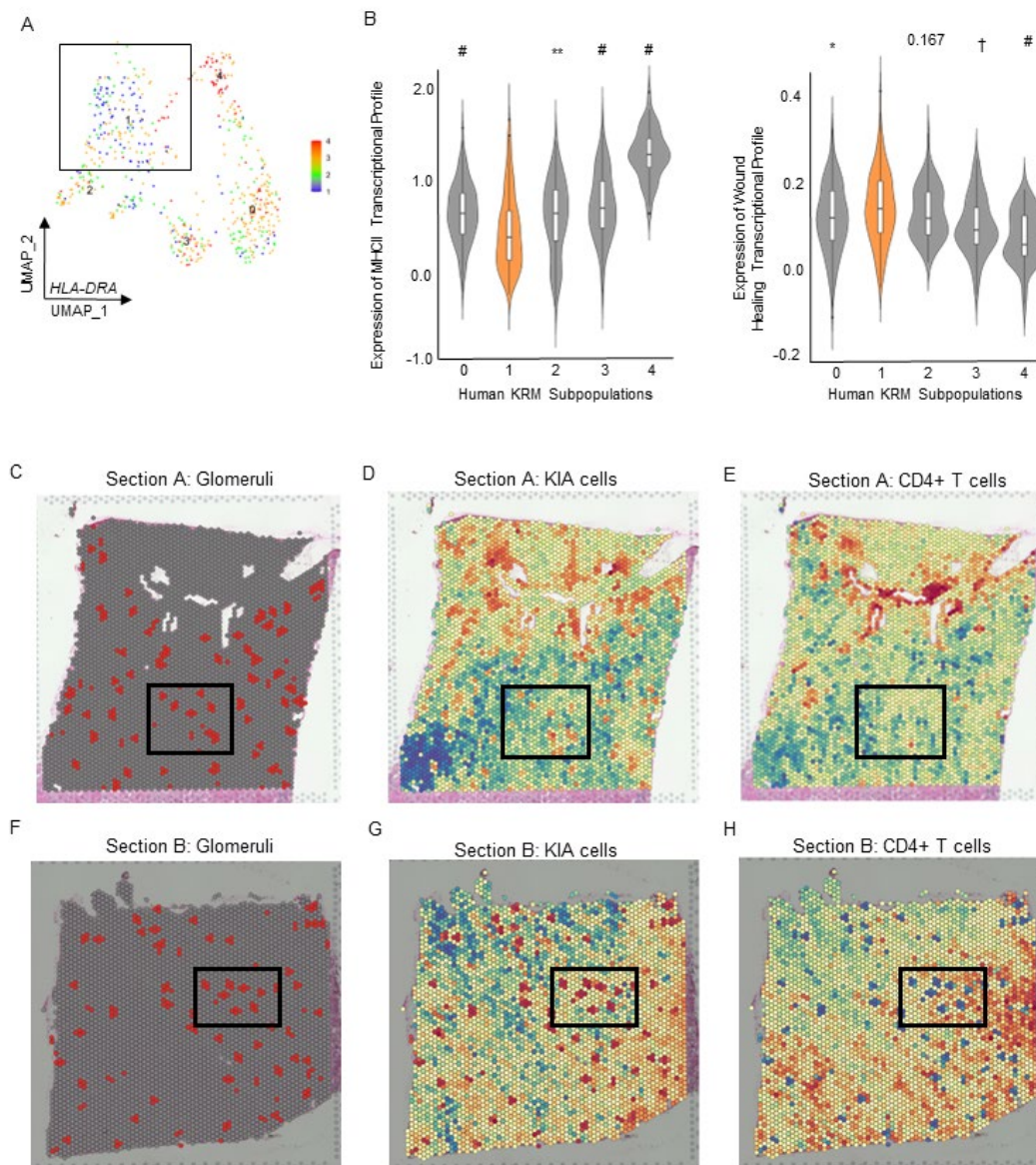


Figure 5.



SUMMARY AND CONCLUSIONS

Overall hypothesis

The kidney resident macrophage niche is composed of transcriptionally and spatially distinct evolutionarily conserved subpopulations that modulate their MHC II expression at the injury location and for the duration of the injury.

As a result of testing the above hypothesis, I have reached the following conclusions:

Summary

KRMs are a heterogeneous population with transcriptionally and spatially distinct subpopulations. Until recently, the identity of the resident mononuclear phagocytes was contested as they present canonical markers of both dendritic cells and macrophages. The perceived uniformity of surface protein expression has obscured the recognition of subpopulations. Advancements in DNA and RNA sequencing have greatly increased the ability to investigate differences between cells. Using the techniques of single-cell RNA sequencing and spatial transcriptomics, the transcriptional differences within the KRMs became clear and allowed for the identification of protein markers of subpopulations, such as CD14 and CD206. The kidney itself is a heterogeneous tissue with areas of strong ion, proton, and oxygen gradients (229). Likely as a result, KRM subpopulations are distinct to particular regions of the kidney. Spatially, KRMs can be broadly divided into

medullary and cortical subpopulations. Medullary populations include the innermost portion of the kidney and the papilla. Cortical includes everything from the cortico-medullary region outwards. Each location contains multiple transcriptionally distinct subpopulations.

KRM subpopulations are not limited to mice and are identifiable in human samples (191). Within the human samples, five KRM subpopulations were identified in comparison to the seven in mice. Of the five human subpopulations, four have murine counterparts, although two are orthologous to the same mouse subpopulation. The remaining human KRM subpopulation was not orthologous to any known murine populations but does express a transcriptional profile similar to activated microglia, the resident macrophage population in the brain (230-232) (Figure 1).

Following an injury in both mice and humans, a subset of the KRM population downregulates MHC II and presents with a kidney injury-associated (KIA) phenotype, both at the protein and transcriptional levels (Figure 1). KIA cells occur within 24 hours following AKI and are still significantly present in the tissue six months post the induction of CKD. Additionally, KIA cells are preferentially located at the site of injury in AKI, as identified across species. It appears that various KRM subpopulations have the capability to adopt a KIA phenotype which may be simply a consequence of the location of kidney damage, as the KIA presenting subpopulation is different between AKI and CKD. However, it is also possible that over the extended time period required for CKD, KIA cells have altered their transcriptional profile so as to appear as a different subpopulation when compared to quiescent profiles. Post AKI, KIA cells adopt a wound healing profile, however, this either does not occur in CKD or is no longer occurring at

the extended time points. Following human AKI, KIA cells are spatially distinct from CD4⁺ T cells, which have been implicated in the pathogenesis of AKI.

KRM Subpopulation Functions in Kidney Homeostasis and Injury Along the Nephron *Cortical*

Beginning from the outermost layer of the kidney, mKRM 2 is the most cortical population and is primarily localized to the outer cortex. This population is relatively rare in quiescence and expands following AKI. Murine KRM 2 appears to increase in number following injury and express genes associated with iron handling. Macrophages participate in the homeostatic recycling of iron in the reticuloendothelial system through the phagocytosis and degradation of erythrocytes and different regions of the kidney nephron participate in iron reabsorption (233-235). Additionally, macrophages are known to sequester iron in an anti-bacterial response and to regulate adipocyte metabolism (236, 237). The presence of iron has been shown to increase the expression of ferroportin mRNA level, an iron exporter, by macrophages *in vitro* (238). Following BIRI, there is an increase in urinary free iron and treatment with iron chelators protects against injury (239, 240). In the skin, resident macrophages utilize ferroportin to export iron to damaged epithelial cells to promote cell replication and wound healing without a concurrent increase in inflammation (241). Therefore, mKRM 2 is potentially increasing ferroportin gene expression in response to an increase in extra-cellular iron to facilitate a wound healing response as seen in skin resident macrophages.

A human ortholog subpopulation was not discovered for this subpopulation, questioning the essentiality of its function. However, the transcriptionally similar mKRM

4 does have human orthologs that expresses the gene for ferroportin. Although mKRM 4 is transcriptionally orthologous, it is only spatially orthologous following AKI. The human orthologs to mKRM 4 are localized to the cortex, at least in AKI, and appear spatially more similar to mKRM 2, suggesting any iron handling function may be cortex specific.

The largest murine KRM subpopulation, mKRM 0, localizes deeper into the cortex within the cortico-medullary region. Given their location and increased expression of *Cx3cr1*, mKRM 0 may be the identified CX3CR1⁺ cortical immune sentinel population (198). If so, then it is possible that the seemingly undifferentiated nature of this population allows them to sample the environment without instigating a broader immune response unless necessary. Alternatively, should this subpopulation be sampling the microenvironment, the relatively clean conditions in which laboratory mice are raised and maintained might have prevented this subpopulation from pathogen interactions necessary to cause differentiation (242). Altering the housing of laboratory mice has shown to better recapitulate human immune populations (243). This could account for the lack of a human orthologous population.

A mKRM 0 ortholog was not found in any of the human subpopulations and may be considered less valuable as a therapeutic target. Murine KRM 0 is the least transcriptionally distinct murine KRM subpopulation and the gene expression provides little evidence of a potential function. Therefore, it is possible this subpopulation is not essential to human kidney function or protection and as a result was not conserved between mice and humans. However, should mKRM 0 be an immune sentinel population that is undifferentiated in the mice due to a lack of pathogenic stimulation, in human

samples, this population would have interacted with a great number of pathogens and therefore be unrecognizable compared to the murine counterpart (198, 243). Studies have shown that increasing the pathogen exposure of laboratory mice better recapitulates human immune cell phenotypes (243). Future investigations into mice that have had repeated and diverse pathogen exposure should investigate the effects on the KRM niche. Any resulting changes would provide increased insight into the function of pathogen exposure in resident immune populations and tissue homeostasis.

Medullary

Murine KRM 4 localizes to the medulla as identified using spatial transcriptomics and protein expression of CD206. Murine KRM 4 expresses genes associated with extracellular matrix handling and scavenging receptors. Both *Stab1* and CD206 are considered markers of anti-inflammatory macrophages but have disparate associations identified in the development of fibrosis (244, 245). *Stab1* is generally considered a scavenger receptor for calcium and mediator of monocyte recruitment, it has also known to uptake LPS in a TLR4-independent manner (244, 246). *Stab1* expressing macrophages reduce fibrosis following ischemia in the liver (245). However, CD206⁺ macrophages in the kidney are involved in the pathogenesis of acute tubular necrosis and acute interstitial nephritis (247). In polycystic kidney disease, CD206⁺ macrophages are found surrounding cysts and are believed to be involved in disease pathogenesis (248). Importantly, cysts can occur anywhere along the nephron, so it is unknown whether CD206⁺ macrophages migrate to the regions of damage or local cells upregulate CD206 expression in response to cyst formation.

The human orthologs to mKRM 4 are hKRM 0 and 3, which are nearly identical except for a unique lack of any activation markers by hKRM 3. Additionally, unlike all other identified orthologs, which are spatially similar in both quiescence and AKI, mKRM 4 is only spatially orthologous to the cortical hKRM 0 and 3 following AKI. As both human samples come from donors with AKI, there is a potential function in the migration of this subpopulation to the cortex following injury. As it expresses both scavenger and fibrotic markers, perhaps the damage in the cortex induces a migration of this population to the region for repair. In the context of AKI and the transition to CKD, the function of mKRM 4, hKRM 0, and 3, and their role in either the propagation or amelioration of fibrosis requires further investigation.

Murine KRM 1,3, and 6 compose the rest of the medullary subpopulations and are primed for an immune response based on their differential expression of anti-bacterial, anti-viral, and chemokine genes. These subpopulations localize to the hypoxic medulla prior to insult. Resident macrophages are known to exist in areas completely lacking blood vessels, such as the epidermis and cornea, where they are both the first line of defense and required for the homeostasis (249-251). Besides lacking oxygen, the medulla contains a high salt concentration, and macrophages have been shown to migrate towards increasing salt gradients (252). The work of Berry et al. discovered that CD14⁺ macrophages in the kidney, not specified as infiltrating or resident, utilize this gradient to form an immunologic barrier to pathogens invading the medulla from the ureter (253, 254). Of the resident populations, mKRM 3 and hKRM 1 have the highest expression of *CD14* and express genes associated with an anti-bacterial response and inflammatory immune signaling, as if primed against uropathogenic bacteria. Further research will be

needed to determine how subpopulations respond to bacterial and viral infections in the kidney. As the kidney is uniquely susceptible to sepsis, it is possible that modulation of these subpopulations could translate into better patient outcomes (255). In instances where inflammation in the kidney has resulted in massive immune infiltration, it is likely that these subpopulations are providing the chemokines, and specifically targeting them may reduce inflammation and improved recovery.

The unique expression of type I IFN genes by mKRM 6 and hKRM 3, in both homeostasis and AKI suggests a specific function for these conserved subpopulations. While type I IFN producing resident macrophages have been identified in other tissues, a tissue maintenance function in the kidney has not yet been identified (256, 257). However, should this population be functioning as an immunological barrier to viruses, a high expression of type I IFNs in the medulla would be expected (258). In disorders characterized by increased type I IFN production, such as in lupus nephritis, a potential local source is these KRM subpopulations (259, 260). As type I IFN production is a positive feedback loop, and this subpopulation is identifiable in both mice and humans, KRMs represent a potential therapeutic target for the disease progression of lupus nephritis (261).

Impact and Future Directions of Evolutionarily Conserved Subpopulations

Orthologous populations will increase translatability and help focus research efforts in the future. Kidneys from two human patients with mild to moderate AKI were used to identify transcriptionally and spatially orthologous hKRM subpopulations to those described in the mouse. This represents a valuable increment in our understanding

of the human kidney and is a necessity for future therapeutic research using murine models. Future sequencing-based research, that will have the capability to identify the described subpopulations, should do its best to add to and amend the current knowledge base of KRMs as defined here. The provided framework will allow for shared knowledge and results across laboratories and should increase the pace at which our understanding of the human kidney can progress.

The newly elucidated KRM subpopulations likely selectively participate in the instigation or propagation of kidney diseases. Macrophages have long been identified for their ability to promote tissue damage first through inflammation and second through fibrosis (69, 207, 262). The inflammatory response to glomerulonephritis compared to acute tubular necrosis or uropathogenic bacteria in the papilla is likely propagated by the different KRM subpopulations located in the damaged section. Additionally, other nephropathies have known immunologic causes or explanations, such as the case of C1q nephropathy or lupus nephritis (263-265). Continued work to identify protein markers of each subpopulation will serve to increase the accessibility of KRM research. Future steps should be taken to test the potential functions of KRMs specifically, and the identification of orthologous populations should aid in the translation of results from murine models to human samples and patients.

Impact and Future Directions of Human-Specific Subpopulations

A murine ortholog for hKRM 4 could not be identified and this population appears uniquely like activated microglia. As mentioned previously, C1q is increasingly being considered a marker of resident macrophage populations (191, 266-268). However,

it is primarily in microglia research where the increased gene expression of C1q has been described as performing a specific function (269). Activated microglia produce and secrete the complement protein C1q to persistently monitor synapses. Healthy synapses are able to deactivate membrane-bound C1q produced by microglia and prevent the activation of apoptotic pathways. Damaged or overactive synapses are thought to lose this ability and are therefore efferocytosed by microglia (232, 270-272). Beyond identifying a similar transcriptional profile, this function has yet to be identified in the human kidney. It is important to note that murine KRM s do express the genes associated with the transcriptional profile, however, they are not specific to any one population.

Human KRM 4 is localized to the cortex in the two human samples analyzed here. If this location is the homeostatic location, perhaps the same mechanism is occurring in the kidneys as in the brain, and hKRM 4 is monitoring tubule cells and clearing out those that are damaged or dying. However, since both samples came from patients diagnosed with mild to moderate AKI, perhaps this is a response to injury and the resident macrophages have changed their transcriptional profile in response to damaged tissue. It is additionally possible that the transcriptional similarities are only a coincidence and future research will need to mimic the studies done with microglia to confirm or deny this potential function. Should it be confirmed, this subpopulation could be targeted for therapies to either enhance or limit the ability of this population to clear damaged and dying tubules depending on the pathology of the specific disease.

Impact and Future Directions of MHC II Response Following Injury

The appearance of KIA cells appears to occur universally following injury and be a conserved response. Following AKI, they significantly increase the transcriptional profile associated with wound healing. Generally, it is assumed that in cases of inflammation, macrophages will first increase MHC II expression and adopt a pro-inflammatory phenotype (273, 274). This upregulation of MHC II expression has been documented in other tissue-resident macrophage populations in response to a variety of conditions (219, 275, 276). Indeed, very few instances where tissue macrophages will decrease MHC II expression in response to a stimulus are known (277-279). Therefore, the KIA cell response may be unique to the kidney, and its conservation from mice to humans implies a necessary function following injury.

One potential function is the prevention of an autoimmune response. MHC II molecules present exogenously acquired antigens to T cell receptors to coordinate the recognition of invading pathogens and stimulate an adaptive immune response (220). Following injury, normal sequestered molecules and proteins will be released into the microenvironment by necrotizing cells where they may be endocytosed by macrophages and other phagocytes. Should these molecules be presented on MHC II, there is the possibility that should a T cell express a receptor that incorrectly recognizes self-antigen will propagate an autoimmune response (280).

A second, but related possibility is that the downregulation of MHC II prevents the colocalization of CD4⁺ T cells to the site of damage (76). MHC II specifically interacts with CD4⁺ T cells, which have a known pathology in sterile ischemic reperfusion kidney injury. Mice that lack T cells are protected from IRI. The

reintroduction of CD4⁺ T cells, but not CD8⁺ T cells restores a control injury phenotype. To be precise, the CD4⁺ T cells must express CD28, a co-receptor for the CD4/MHC II interaction (76). The reduction of CD4⁺ T cells in areas of damage may be solely the result of downregulated MHC II by KIA cells or in concert with additional mechanisms still undescribed.

Still, a remaining possibility is that the downregulation of MHC II is simply an artifact of macrophages responding to stress and is not the result of any specific functional response to damage. This is relatively unconvincing given the upregulation of a wound healing profile by KIA cells in AKI. Regardless, KIA cells are still the KRM subpopulation present as the site of damage in AKI in mice and humans and are therefore worth further investigation as a valuable therapeutic option. Therapies that can utilize receptors present on KIA cells may be able to selectively target regions of damage. Additionally, therapies that can further enhance a wound healing response may be able to facilitate faster or more complete tissue recovery.

Impact of KRM Research for Nephrology and Conclusions

Prior to the work outlined here, most studies investigating the immune system's role in kidney injury failed to acknowledge the complexity of the resident immune niche and its use for future therapeutics. This in conjunction with confusion as to the identity of the resident F4/80⁺ population has stunted much-needed research into the role of the kidney resident macrophage population in homeostasis and injury. Resident macrophages perform vital homeostatic and immune functions in tissues throughout the body, and it is likely that functions identified in one tissue will apply to others (185, 281, 282). For

example, C1q, first identified as a marker of resident macrophage populations in the kidney and the brain, is now being used to delineate resident populations in many tissues (191, 266-268).

AKI and CKD are increasing problems both in the United States and worldwide (10, 95). Kidney diseases have limited therapeutic options. Both active and passive immune-driven mechanisms play a pathogenic role in kidney disease. Leukocytes are increasingly targets of both pharmacological and cellular therapy given their plasticity and ability to reach and infiltrate areas of damage or stress and are therefore an important consideration in the future of kidney therapeutic options.

Resident macrophage populations have increasingly identified homeostatic and immune functions, that are both tissue and subpopulation specific. Within the kidney, macrophages have known positive and deleterious roles following AKI and CKD, and the contrasting roles have caused confusion as to their therapeutic potential (73, 83, 133, 283). Resident macrophages have extended lifespans compared to peripheral mononuclear phagocyte counterparts (201). As a result, they are more susceptible to long-term effects as a result of injury or immune-modulating therapeutics. This could both increase the effectiveness of therapies by increasing the effects or lead to long-term side effects. It is possible to have long-term effects on the adaptive immune system in tissue by targeting the resident innate immune system, which could reduce off-target effects of targeting peripheral APCs. As a resident population, KRMs would by default be the first responders to any trauma and potential instigators of various diseases. Additionally, the known plasticity of macrophages and their acknowledged role in both

propagating and ameliorating inflammation increases the interest in targeting the resident population for therapeutic studies.

The work presented here identifies transcriptionally and spatially distinct subpopulations within the murine and human kidney and suggests the macrophage niche is far more complex than previously considered. Much of the confusion as to the roles of macrophages in kidney injury can likely be attributed to functional and spatially distinct subpopulations. Although further research will be needed to identify additional unique subpopulations and their specific functions, this work provides a necessary framework to identify KRM subpopulations across species and has begun the process of function identification.

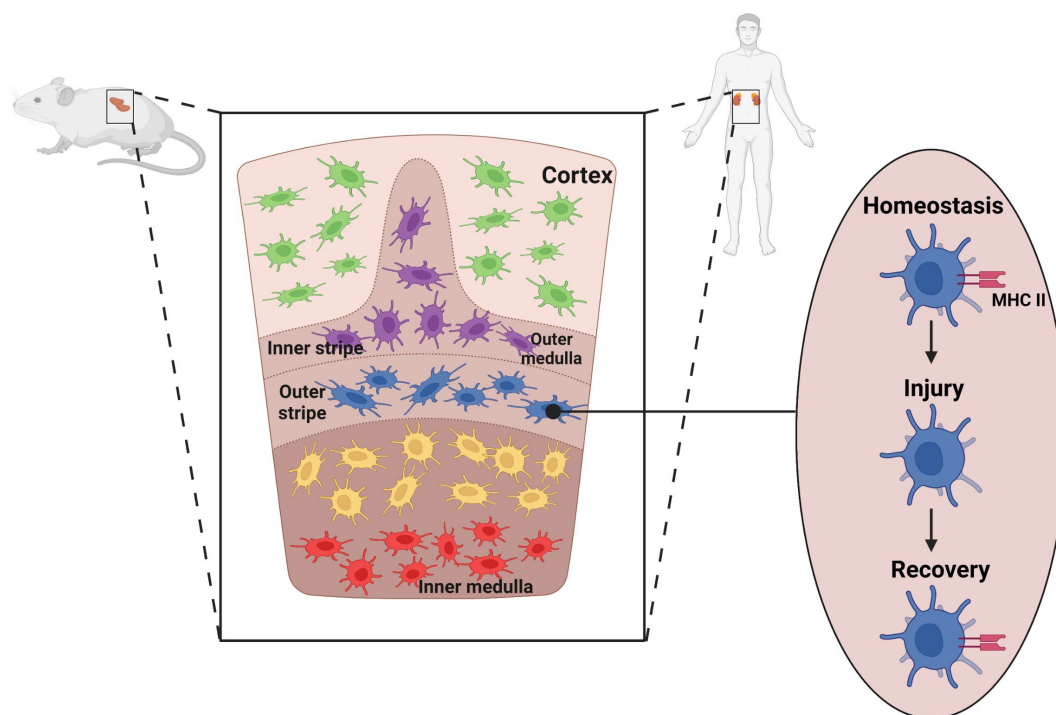
Figure Legend

Figure 1. Summary of transcriptionally and spatially distinct orthologous KRM subpopulations and MHC II dynamics following kidney injury

Mice and humans contain transcriptionally and spatially distinct KRM subpopulations that are evolutionarily conserved. Subpopulations have distinct locations within zones in the kidney. Following injury, a subset of KRMs downregulate MHC II expression. Following recovery, MHC II expression is restored.

Figures

Figure 1.



REFERENCES

1. Morgan T. Renal physiology. *Med J Aust.* 1976;2(10):386-9.
2. Ronco C, et al. Acute kidney injury. *Lancet.* 2019;394(10212):1949-64.
3. Leaf DE, and Christov M. Dysregulated Mineral Metabolism in AKI. *Semin Nephrol.* 2019;39(1):41-56.
4. Rahman M, et al. Acute kidney injury: a guide to diagnosis and management. *Am Fam Physician.* 2012;86(7):631-9.
5. Goyal A, et al. *StatPearls.* Treasure Island (FL): StatPearls Publishing

Copyright © 2022, StatPearls Publishing LLC.; 2022.
6. Murugan R, and Kellum JA. Acute kidney injury: what's the prognosis? *Nat Rev Nephrol.* 2011;7(4):209-17.
7. Hoste EA, et al. Epidemiology of acute kidney injury in critically ill patients: the multinational AKI-EPI study. *Intensive Care Med.* 2015;41(8):1411-23.
8. Wang HE, et al. Acute kidney injury and mortality in hospitalized patients. *Am J Nephrol.* 2012;35(4):349-55.
9. Ali T, et al. Incidence and outcomes in acute kidney injury: a comprehensive population-based study. *J Am Soc Nephrol.* 2007;18(4):1292-8.
10. Pavkov ME, et al. *Morbidity and Mortality Weekly Report (MMWR).* CDC; 2018.

11. Pan HC, et al. Acute Kidney Injury Classification for Critically Ill Cirrhotic Patients: A Comparison of the KDIGO, AKIN, and RIFLE Classifications. *Sci Rep*. 2016;6:23022.
12. Soveri I, et al. Measuring GFR: a systematic review. *Am J Kidney Dis*. 2014;64(3):411-24.
13. Levey AS, et al. Serum creatinine and renal function. *Annu Rev Med*. 1988;39:465-90.
14. Inker LA, and Titan S. Measurement and Estimation of GFR for Use in Clinical Practice: Core Curriculum 2021. *Am J Kidney Dis*. 2021;78(5):736-49.
15. Han WK, et al. Urinary biomarkers in the early diagnosis of acute kidney injury. *Kidney Int*. 2008;73(7):863-9.
16. Swan SK. The search continues--an ideal marker of GFR. *Clin Chem*. 1997;43(6 Pt 1):913-4.
17. Luis-Lima S, and Porrini E. An Overview of Errors and Flaws of Estimated GFR versus True GFR in Patients with Diabetes Mellitus. *Nephron*. 2017;136(4):287-91.
18. Amin R, et al. *Biochemical and Molecular Basis of Pediatric Disease*. Academic Press 2021:167-228.
19. KDIGO. Official Journal of the International Society of Nephrology; 2012.
20. Kuwabara S, et al. The Pathophysiology of Sepsis-Associated AKI. *Clin J Am Soc Nephrol*. 2022;17(7):1050-69.
21. Lankadeva YR, et al. Role of perioperative hypotension in postoperative acute kidney injury: a narrative review. *Br J Anaesth*. 2022;128(6):931-48.
22. Don Bosco D, et al. Acute Kidney Injury in Severe Trauma Patients; a Record-Based Retrospective Study. *Adv J Emerg Med*. 2019;3(3):e22.
23. Hanif MO, et al. *StatPearls*. Treasure Island (FL): StatPearls Publishing

Copyright © 2022, StatPearls Publishing LLC.; 2022.

24. Zhang L, et al. Clinicopathological features and risk factors analysis of IgA nephropathy associated with acute kidney injury. *Ren Fail.* 2016;38(5):799-805.
25. Mata-Miranda MM, et al. Nephroprotective Effect of Embryonic Stem Cells Reducing Lipid Peroxidation in Kidney Injury Induced by Cisplatin. *Oxid Med Cell Longev.* 2019;2019:5420624.
26. Manzoor H, and Bhatt H. *StatPearls*. Treasure Island (FL): StatPearls Publishing

Copyright © 2022, StatPearls Publishing LLC.; 2022.

27. Okusa MD, and Rosner MH. In: Palevsky PM, and Taylor EN eds. *UpToDate*. UpToDate; 2022.
28. Bellomo R, et al. Acute kidney injury in sepsis. *Intensive Care Med.* 2017;43(6):816-28.
29. Shaikhouni S, and Yessayan L. Management of Acute Kidney Injury/Renal Replacement Therapy in the Intensive Care Unit. *Surg Clin North Am.* 2022;102(1):181-98.
30. Ostermann M, et al. Fluid Management in Acute Kidney Injury. *Chest.* 2019;156(3):594-603.
31. Argaziz ER, et al. Fluid management in acute kidney injury: from evaluating fluid responsiveness towards assessment of fluid tolerance. *Eur Heart J Acute Cardiovasc Care.* 2022;11(10):786-93.
32. Novak JE, and Ellison DH. Diuretics in States of Volume Overload: Core Curriculum 2022. *Am J Kidney Dis.* 2022;80(2):264-76.
33. MacLaughlin HL, et al. Nutrition in Kidney Disease: Core Curriculum 2022. *Am J Kidney Dis.* 2022;79(3):437-49.
34. Palmer BF, et al. Renal Tubular Acidosis and Management Strategies: A Narrative Review. *Adv Ther.* 2021;38(2):949-68.

35. Ostermann M. Acute kidney injury on admission to the intensive care unit: where to go from here? *Crit Care*. 2008;12(6):189.
36. Chawla LS, and Kimmel PL. Acute kidney injury and chronic kidney disease: an integrated clinical syndrome. *Kidney Int*. 2012;82(5):516-24.
37. LLP DBR. 2022.
38. Pickkers P, et al. New drugs for acute kidney injury. *Intensive Care Med*. 2022;48(12):1796-8.
39. Zhang H, et al. The Nephroprotective Effect of MS-275 on Lipopolysaccharide (LPS)-Induced Acute Kidney Injury by Inhibiting Reactive Oxygen Species (ROS)-Oxidative Stress and Endoplasmic Reticulum Stress. *Med Sci Monit*. 2018;24:2620-30.
40. Badri S, et al. Effect of N-acetylcysteine against Vancomycin-Induced Nephrotoxicity: A Randomized Controlled Clinical Trial. *Arch Iran Med*. 2020;23(6):397-402.
41. Chen L, and Gong X. Efficacy and Safety of Chuan Huang Fang Combining Reduced Glutathione in Treating Acute Kidney Injury (Grades 1-2) on Chronic Kidney Disease (Stages 2-4): Study Protocol for a Multicenter Randomized Controlled Clinical Trial. *Evid Based Complement Alternat Med*. 2022;2022:1099642.
42. Thielmann M, et al. Teprasiran, a Small Interfering RNA, for the Prevention of Acute Kidney Injury in High-Risk Patients Undergoing Cardiac Surgery: A Randomized Clinical Study. *Circulation*. 2021;144(14):1133-44.
43. Chen H, and Busse LW. Novel Therapies for Acute Kidney Injury. *Kidney Int Rep*. 2017;2(5):785-99.
44. Wei Q, and Dong Z. Mouse model of ischemic acute kidney injury: technical notes and tricks. *Am J Physiol Renal Physiol*. 2012;303(11):F1487-94.
45. Aomatsu A, et al. MicroRNA expression profiling in acute kidney injury. *Transl Res*. 2022;244:1-31.

46. Narváez Barros A, et al. Reversal Unilateral Ureteral Obstruction: A Mice Experimental Model. *Nephron*. 2019;142(2):125-34.
47. Perše M, and Večerić-Haler Ž. Cisplatin-Induced Rodent Model of Kidney Injury: Characteristics and Challenges. *Biomed Res Int*. 2018;2018:1462802.
48. Martínez-Klimova E, et al. Unilateral Ureteral Obstruction as a Model to Investigate Fibrosis-Attenuating Treatments. *Biomolecules*. 2019;9(4).
49. Bao YW, et al. Kidney disease models: tools to identify mechanisms and potential therapeutic targets. *Zool Res*. 2018;39(2):72-86.
50. Heyman SN, et al. Animal models of renal dysfunction: acute kidney injury. *Expert Opin Drug Discov*. 2009;4(6):629-41.
51. Sunahara S, et al. Influence of autophagy on acute kidney injury in a murine cecal ligation and puncture sepsis model. *Sci Rep*. 2018;8(1):1050.
52. Fu Y, et al. Rodent models of AKI-CKD transition. *Am J Physiol Renal Physiol*. 2018;315(4):F1098-f106.
53. Black LM, et al. Divergent effects of AKI to CKD models on inflammation and fibrosis. *Am J Physiol Renal Physiol*. 2018;315(4):F1107-f18.
54. Liu J, et al. Molecular characterization of the transition from acute to chronic kidney injury following ischemia/reperfusion. *JCI Insight*. 2017;2(18).
55. Wang Z, et al. Specific metabolic rates of major organs and tissues across adulthood: evaluation by mechanistic model of resting energy expenditure. *Am J Clin Nutr*. 2010;92(6):1369-77.
56. Bhargava P, and Schnellmann RG. Mitochondrial energetics in the kidney. *Nat Rev Nephrol*. 2017;13(10):629-46.
57. Parks LD, and Barfuss DW. Transepithelial transport and metabolism of glycine in S1, S2, and S3 cell types of the rabbit proximal tubule. *Am J Physiol Renal Physiol*. 2002;283(6):F1208-15.

58. Mather A, and Pollock C. Glucose handling by the kidney. *Kidney Int Suppl.* 2011(120):S1-6.
59. Dominguez JH, et al. Glucose transporters of rat proximal tubule: differential expression and subcellular distribution. *Am J Physiol.* 1992;262(5 Pt 2):F807-12.
60. Venkatachalam MA, et al. Ischemic damage and repair in the rat proximal tubule: differences among the S1, S2, and S3 segments. *Kidney Int.* 1978;14(1):31-49.
61. Brezis M, and Rosen S. Hypoxia of the renal medulla--its implications for disease. *N Engl J Med.* 1995;332(10):647-55.
62. Malek M, and Nematbakhsh M. Renal ischemia/reperfusion injury; from pathophysiology to treatment. *J Renal Inj Prev.* 2015;4(2):20-7.
63. Yamamoto S, et al. Spatiotemporal ATP Dynamics during AKI Predict Renal Prognosis. *J Am Soc Nephrol.* 2020;31(12):2855-69.
64. Zhao M, et al. Mitochondrial ROS promote mitochondrial dysfunction and inflammation in ischemic acute kidney injury by disrupting TFAM-mediated mtDNA maintenance. *Theranostics.* 2021;11(4):1845-63.
65. Bonventre JV. Kidney injury molecule-1: a translational journey. *Trans Am Clin Climatol Assoc.* 2014;125:293-9; discussion 9.
66. Jang HR, and Rabb H. Immune cells in experimental acute kidney injury. *Nat Rev Nephrol.* 2015;11(2):88-101.
67. Kinsey GR, et al. Inflammation in acute kidney injury. *Nephron Exp Nephrol.* 2008;109(4):e102-7.
68. Jones HR, et al. The role of neutrophils in inflammation resolution. *Semin Immunol.* 2016;28(2):137-45.
69. Akcay A, et al. Mediators of inflammation in acute kidney injury. *Mediators Inflamm.* 2009;2009:137072.

70. Awad AS, et al. Compartmentalization of neutrophils in the kidney and lung following acute ischemic kidney injury. *Kidney Int.* 2009;75(7):689-98.
71. Friedewald JJ, and Rabb H. Inflammatory cells in ischemic acute renal failure. *Kidney Int.* 2004;66(2):486-91.
72. Barton GM. A calculated response: control of inflammation by the innate immune system. *J Clin Invest.* 2008;118(2):413-20.
73. Baek JH. The Impact of Versatile Macrophage Functions on Acute Kidney Injury and Its Outcomes. *Front Physiol.* 2019;10:1016.
74. Zindel J, and Kubes P. DAMPs, PAMPs, and LAMPs in Immunity and Sterile Inflammation. *Annu Rev Pathol.* 2020;15:493-518.
75. Poluzzi C, et al. Biglycan evokes autophagy in macrophages via a novel CD44/Toll-like receptor 4 signaling axis in ischemia/reperfusion injury. *Kidney Int.* 2019;95(3):540-62.
76. Burne MJ, et al. Identification of the CD4(+) T cell as a major pathogenic factor in ischemic acute renal failure. *J Clin Invest.* 2001;108(9):1283-90.
77. Jang HR, et al. B cells limit repair after ischemic acute kidney injury. *J Am Soc Nephrol.* 2010;21(4):654-65.
78. McGeachy MJ, et al. Natural recovery and protection from autoimmune encephalomyelitis: contribution of CD4+CD25+ regulatory cells within the central nervous system. *J Immunol.* 2005;175(5):3025-32.
79. Ouyang W, et al. Regulation and functions of the IL-10 family of cytokines in inflammation and disease. *Annu Rev Immunol.* 2011;29:71-109.
80. Xie X, et al. Trib1 Contributes to Recovery From Ischemia/Reperfusion-Induced Acute Kidney Injury by Regulating the Polarization of Renal Macrophages. *Front Immunol.* 2020;11:473.
81. Shapouri-Moghaddam A, et al. Macrophage plasticity, polarization, and function in health and disease. *J Cell Physiol.* 2018;233(9):6425-40.

82. DiPietro LA. Wound healing: the role of the macrophage and other immune cells. *Shock*. 1995;4(4):233-40.
83. Kim MG, et al. The Role of M2 Macrophages in the Progression of Chronic Kidney Disease following Acute Kidney Injury. *PLoS One*. 2015;10(12):e0143961.
84. Anders HJ, et al. CKD in diabetes: diabetic kidney disease versus nondiabetic kidney disease. *Nat Rev Nephrol*. 2018;14(6):361-77.
85. Jankowski J, et al. Cardiovascular Disease in Chronic Kidney Disease: Pathophysiological Insights and Therapeutic Options. *Circulation*. 2021;143(11):1157-72.
86. Yang B, et al. Nephrotoxicity and Chinese Herbal Medicine. *Clin J Am Soc Nephrol*. 2018;13(10):1605-11.
87. Lee M, et al. Chronic Kidney Disease in Cancer Survivors. *Adv Chronic Kidney Dis*. 2021;28(5):469-76.e1.
88. Carrero JJ, et al. Prolactin levels, endothelial dysfunction, and the risk of cardiovascular events and mortality in patients with CKD. *Clin J Am Soc Nephrol*. 2012;7(2):207-15.
89. Orr SE, and Bridges CC. Chronic Kidney Disease and Exposure to Nephrotoxic Metals. *Int J Mol Sci*. 2017;18(5).
90. Almaani S, et al. Update on Lupus Nephritis. *Clin J Am Soc Nephrol*. 2017;12(5):825-35.
91. Harris PC, and Torres VE. Polycystic kidney disease. *Annu Rev Med*. 2009;60:321-37.
92. Rajasekaran A, et al. IgA Nephropathy: An Interesting Autoimmune Kidney Disease. *Am J Med Sci*. 2021;361(2):176-94.
93. Venkatachalam MA, et al. Failed Tubule Recovery, AKI-CKD Transition, and Kidney Disease Progression. *J Am Soc Nephrol*. 2015;26(8):1765-76.

94. Henson JB, and Sise ME. The association of hepatitis C infection with the onset of CKD and progression into ESRD. *Semin Dial*. 2019;32(2):108-18.
95. Foreman KJ, et al. Forecasting life expectancy, years of life lost, and all-cause and cause-specific mortality for 250 causes of death: reference and alternative scenarios for 2016-40 for 195 countries and territories. *Lancet*. 2018;392(10159):2052-90.
96. Kovesdy CP. Epidemiology of chronic kidney disease: an update 2022. *Kidney international supplements*. 2022;12(1):7-11.
97. Breyer MD, and Susztak K. The next generation of therapeutics for chronic kidney disease. *Nat Rev Drug Discov*. 2016;15(8):568-88.
98. Foley RN, and Collins AJ. End-stage renal disease in the United States: an update from the United States Renal Data System. *J Am Soc Nephrol*. 2007;18(10):2644-8.
99. KDIGO. Official Journal of the International Society of Nephrology; 2013.
100. Szabo AJ, et al. Nephron number determines susceptibility to renal mass reduction-induced CKD in Lewis and Fisher 344 rats: implications for development of experimentally induced chronic allograft nephropathy. *Nephrol Dial Transplant*. 2008;23(8):2492-5.
101. Schnaper HW. Remnant nephron physiology and the progression of chronic kidney disease. *Pediatr Nephrol*. 2014;29(2):193-202.
102. Hull KL, et al. Indications and considerations for kidney biopsy: an overview of clinical considerations for the non-specialist. *Clin Med (Lond)*. 2022;22(1):34-40.
103. Turner JM, et al. Treatment of chronic kidney disease. *Kidney International*. 2012;81(4).
104. Molnar MZ, et al. Angiotensin-converting enzyme inhibitor, angiotensin receptor blocker use, and mortality in patients with chronic kidney disease. *J Am Coll Cardiol*. 2014;63(7):650-8.

105. Vart P, et al. Estimated Lifetime Benefit of Combined RAAS and SGLT2 Inhibitor Therapy in Patients with Albuminuric CKD without Diabetes. *Clin J Am Soc Nephrol.* 2022;17(12):1754-62.
106. Dharia A, et al. SGLT2 Inhibitors: The Sweet Success for Kidneys. *Annu Rev Med.* 2023;74:369-84.
107. Rysz J, et al. The Effect of Diet on the Survival of Patients with Chronic Kidney Disease. *Nutrients.* 2017;9(5).
108. Banerjee T, et al. Dietary Patterns and CKD Progression. *Blood Purif.* 2016;41(1-3):117-22.
109. Dalrymple LS, and Go AS. Epidemiology of acute infections among patients with chronic kidney disease. *Clin J Am Soc Nephrol.* 2008;3(5):1487-93.
110. Staplin N, et al. Smoking and Adverse Outcomes in Patients With CKD: The Study of Heart and Renal Protection (SHARP). *Am J Kidney Dis.* 2016;68(3):371-80.
111. Lee S, et al. Smoking, Smoking Cessation, and Progression of Chronic Kidney Disease: Results From KNOW-CKD Study. *Nicotine Tob Res.* 2021;23(1):92-8.
112. Drawz P, et al. *Chronic Renal Disease (Second Edition)*. Academic Press; 2020.
113. Babitt JL, and Lin HY. Mechanisms of anemia in CKD. *J Am Soc Nephrol.* 2012;23(10):1631-4.
114. Kraut JA, and Madias NE. Metabolic Acidosis of CKD: An Update. *Am J Kidney Dis.* 2016;67(2):307-17.
115. Pannu N, et al. Renal replacement therapy in patients with acute renal failure: a systematic review. *Jama.* 2008;299(7):793-805.
116. King-Wing Ma T, and Kam-Tao Li P. Depression in dialysis patients. *Nephrology (Carlton).* 2016;21(8):639-46.

117. Scandling JD. Kidney transplant candidate evaluation. *Semin Dial.* 2005;18(6):487-94.
118. Williams AF, et al. Medicine non-adherence in kidney transplantation. *J Ren Care.* 2014;40(2):107-16.
119. Carminatti M, et al. Chronic kidney disease progression in kidney transplant recipients: A focus on traditional risk factors. *Nephrology (Carlton).* 2019;24(2):141-7.
120. Lewis A, et al. Organ donation in the US and Europe: The supply vs demand imbalance. *Transplant Rev (Orlando).* 2021;35(2):100585.
121. Yeung MY, et al. Kidney Organ Allocation System: How to Be Fair. *Semin Nephrol.* 2022;42(4):151274.
122. Thuret R, et al. [Chronic kidney disease and kidney transplantation]. *Prog Urol.* 2016;26(15):882-908.
123. Regier M, et al. A Dietary Supplement Containing Fucoidan Preserves Endothelial Glycocalyx through ERK/MAPK Signaling and Protects against Damage Induced by CKD Serum. *Int J Mol Sci.* 2022;23(24).
124. Mann JF, et al. Avosentan for overt diabetic nephropathy. *J Am Soc Nephrol.* 2010;21(3):527-35.
125. Xu Y, et al. Extended-release of therapeutic microRNA via a host-guest supramolecular hydrogel to locally alleviate renal interstitial fibrosis. *Biomaterials.* 2021;275:120902.
126. Tasanarong A, et al. Vitamin E ameliorates renal fibrosis by inhibition of TGF-beta/Smad2/3 signaling pathway in UUO mice. *J Med Assoc Thai.* 2011;94 Suppl 7:S1-9.
127. Ring T, et al. Use of eculizumab in crescentic IgA nephropathy: proof of principle and conundrum? *Clin Kidney J.* 2015;8(5):489-91.

128. Sayyed SG, et al. An orally active chemokine receptor CCR2 antagonist prevents glomerulosclerosis and renal failure in type 2 diabetes. *Kidney Int.* 2011;80(1):68-78.
129. Noh H, et al. Beta 2-adrenergic receptor agonists are novel regulators of macrophage activation in diabetic renal and cardiovascular complications. *Kidney Int.* 2017;92(1):101-13.
130. Chen YT, et al. Adipose-derived mesenchymal stem cell protects kidneys against ischemia-reperfusion injury through suppressing oxidative stress and inflammatory reaction. *J Transl Med.* 2011;9:51.
131. Zhu F, et al. Adipose-derived mesenchymal stem cells employed exosomes to attenuate AKI-CKD transition through tubular epithelial cell dependent Sox9 activation. *Oncotarget.* 2017;8(41):70707-26.
132. Coca SG, et al. Chronic kidney disease after acute kidney injury: a systematic review and meta-analysis. *Kidney Int.* 2012;81(5):442-8.
133. Guzzi F, et al. Molecular Mechanisms of the Acute Kidney Injury to Chronic Kidney Disease Transition: An Updated View. *Int J Mol Sci.* 2019;20(19).
134. Good PI, et al. Low nephron endowment increases susceptibility to renal stress and chronic kidney disease. *JCI Insight.* 2023;8(3).
135. Xu L, et al. Immune-mediated tubule atrophy promotes acute kidney injury to chronic kidney disease transition. *Nat Commun.* 2022;13(1):4892.
136. Tanaka S, et al. Hypoxia and Dysregulated Angiogenesis in Kidney Disease. *Kidney Dis (Basel).* 2015;1(1):80-9.
137. Yang L, et al. Epithelial cell cycle arrest in G2/M mediates kidney fibrosis after injury. *Nat Med.* 2010;16(5):535-43, 1p following 143.
138. Gewin LS. Transforming Growth Factor- β in the Acute Kidney Injury to Chronic Kidney Disease Transition. *Nephron.* 2019;143(3):154-7.

139. Puri TS, et al. Chronic kidney disease induced in mice by reversible unilateral ureteral obstruction is dependent on genetic background. *Am J Physiol Renal Physiol*. 2010;298(4):F1024-32.
140. Eddy AA, et al. Investigating mechanisms of chronic kidney disease in mouse models. *Pediatric nephrology*. 2012;27(8):1233-47.
141. Tan RZ, et al. An optimized 5/6 nephrectomy mouse model based on unilateral kidney ligation and its application in renal fibrosis research. *Ren Fail*. 2019;41(1):555-66.
142. Romen W, and Heine WD. [Renal parenchymal changes induced by 5-6 nephrectomy in rats]. *Virchows Arch A Pathol Pathol Anat*. 1972;356(1):42-57.
143. Takahashi H, et al. A new mouse model of genetically transmitted polycystic kidney disease. *J Urol*. 1986;135(6):1280-3.
144. Tomino Y. IgA nephropathy: lessons from an animal model, the ddY mouse. *J Nephrol*. 2008;21(4):463-7.
145. Korstanje R, and DiPetrillo K. Unraveling the genetics of chronic kidney disease using animal models. *Am J Physiol Renal Physiol*. 2004;287(3):F347-52.
146. Furman BL. Streptozotocin-Induced Diabetic Models in Mice and Rats. *Curr Protoc*. 2021;1(4):e78.
147. Becker GJ, and Hewitson TD. Animal models of chronic kidney disease: useful but not perfect. *Nephrol Dial Transplant*. 2013;28(10):2432-8.
148. Fu Y, et al. Chronic effects of repeated low-dose cisplatin treatment in mouse kidneys and renal tubular cells. *American journal of physiology Renal physiology*. 2019;317(6):F1582-f92.
149. Yu JB, et al. Repeated Administration of Cisplatin Transforms Kidney Fibroblasts through G2/M Arrest and Cellular Senescence. *Cells*. 2022;11(21).
150. Lim BJ, et al. Animal models of regression/progression of kidney disease. *Drug Discov Today Dis Models*. 2014;11:45-51.

151. Honarpisheh M, et al. Aristolochic acid I determine the phenotype and activation of macrophages in acute and chronic kidney disease. *Sci Rep.* 2018;8(1):12169.
152. Xu X, et al. Efficacy of Folic Acid Therapy on the Progression of Chronic Kidney Disease: The Renal Substudy of the China Stroke Primary Prevention Trial. *JAMA Intern Med.* 2016;176(10):1443-50.
153. Luciano RL, and Perazella MA. Aristolochic acid nephropathy: epidemiology, clinical presentation, and treatment. *Drug Saf.* 2015;38(1):55-64.
154. Baudoux T, et al. Experimental Aristolochic Acid Nephropathy: A Relevant Model to Study AKI-to-CKD Transition. *Front Med (Lausanne).* 2022;9:822870.
155. Vanherweghem JL, et al. Rapidly progressive interstitial renal fibrosis in young women: association with slimming regimen including Chinese herbs. *Lancet.* 1993;341(8842):387-91.
156. Dickman KG, et al. Physiological and molecular characterization of aristolochic acid transport by the kidney. *J Pharmacol Exp Ther.* 2011;338(2):588-97.
157. Schmeiser HH, et al. Exceptionally long-term persistence of DNA adducts formed by carcinogenic aristolochic acid I in renal tissue from patients with aristolochic acid nephropathy. *Int J Cancer.* 2014;135(2):502-7.
158. Ban TH, et al. Update of aristolochic acid nephropathy in Korea. *Korean J Intern Med.* 2018;33(5):961-9.
159. Jelaković B, et al. Balkan Endemic Nephropathy and the Causative Role of Aristolochic Acid. *Semin Nephrol.* 2019;39(3):284-96.
160. Martincic M. Toxic effects of *Aristolochia clematitis* on horses' kidneys. *Veterinerinarski Arhiv* 1957;37:51-9.
161. Pozdzik AA, et al. Aristolochic acid nephropathy revisited: a place for innate and adaptive immunity? *Histopathology.* 2010;56(4):449-63.

162. Wang S, et al. Interleukin-22 Attenuated Renal Tubular Injury in Aristolochic Acid Nephropathy via Suppressing Activation of NLRP3 Inflammasome. *Front Immunol.* 2019;10:2277.
163. Li W, et al. Isogenic mesenchymal stem cells transplantation improves a rat model of chronic aristolochic acid nephropathy via upregulation of hepatic growth factor and downregulation of transforming growth factor β 1. *Mol Cell Biochem.* 2012;368(1-2):137-45.
164. Jang HR, and Rabb H. The innate immune response in ischemic acute kidney injury. *Clin Immunol.* 2009;130(1):41-50.
165. Stewart BJ, et al. Spatiotemporal immune zonation of the human kidney. *Science.* 2019;365(6460):1461-6.
166. Hopfer H, et al. Characterization of the renal CD4+ T-cell response in experimental autoimmune glomerulonephritis. *Kidney Int.* 2012;82(1):60-71.
167. Lichanska AM, and Hume DA. Origins and functions of phagocytes in the embryo. *Exp Hematol.* 2000;28(6):601-11.
168. Keller R, et al. Mononuclear phagocytes from human bone marrow progenitor cells; morphology, surface phenotype, and functional properties of resting and activated cells. *Clin Exp Immunol.* 1993;91(1):176-82.
169. Tavian M, et al. The human embryo, but not its yolk sac, generates lymphomyeloid stem cells: mapping multipotent hematopoietic cell fate in intraembryonic mesoderm. *Immunity.* 2001;15(3):487-95.
170. Naito M, et al. Development, differentiation, and maturation of fetal mouse yolk sac macrophages in cultures. *J Leukoc Biol.* 1989;46(1):1-10.
171. Vanuytsel K, et al. Multi-modal profiling of human fetal liver hematopoietic stem cells reveals the molecular signature of engraftment. *Nature communications.* 2022;13(1):1103.
172. Popescu DM, et al. Decoding human fetal liver haematopoiesis. *Nature.* 2019;574(7778):365-71.

173. Kumaravelu P, et al. Quantitative developmental anatomy of definitive haematopoietic stem cells/long-term repopulating units (HSC/RUs): role of the aorta-gonad-mesonephros (AGM) region and the yolk sac in colonisation of the mouse embryonic liver. *Development*. 2002;129(21):4891-9.
174. Ginhoux F, and Jung S. Monocytes and macrophages: developmental pathways and tissue homeostasis. *Nature reviews Immunology*. 2014;14(6):392-404.
175. Watowich SS, and Liu YJ. Mechanisms regulating dendritic cell specification and development. *Immunol Rev*. 2010;238(1):76-92.
176. Antal-Szalmas P, et al. Quantitation of surface CD14 on human monocytes and neutrophils. *J Leukoc Biol*. 1997;61(6):721-8.
177. Mildner A, et al. Murine Monocytes: Origins, Subsets, Fates, and Functions. *Microbiol Spectr*. 2016;4(5).
178. Yona S, et al. Fate mapping reveals origins and dynamics of monocytes and tissue macrophages under homeostasis. *Immunity*. 2013;38(1):79-91.
179. Varol C, et al. Monocytes give rise to mucosal, but not splenic, conventional dendritic cells. *J Exp Med*. 2007;204(1):171-80.
180. Geissmann F, et al. Development of monocytes, macrophages, and dendritic cells. *Science (New York, NY)*. 2010;327(5966):656-61.
181. Jenkins SJ, and Allen JE. The expanding world of tissue-resident macrophages. *Eur J Immunol*. 2021;51(8):1882-96.
182. Gomez Perdiguero E, et al. Tissue-resident macrophages originate from yolk-sac-derived erythro-myeloid progenitors. *Nature*. 2015;518(7540):547-51.
183. Lahmar Q, et al. Tissue-resident versus monocyte-derived macrophages in the tumor microenvironment. *Biochim Biophys Acta*. 2016;1865(1):23-34.
184. Gorgani NN, et al. Gene signatures reflect the marked heterogeneity of tissue-resident macrophages. *Immunol Cell Biol*. 2008;86(3):246-54.

185. Alvarez-Argote S, and O'Meara CC. The Evolving Roles of Cardiac Macrophages in Homeostasis, Regeneration, and Repair. *Int J Mol Sci.* 2021;22(15).
186. Dick SA, et al. Three tissue resident macrophage subsets coexist across organs with conserved origins and life cycles. *Sci Immunol.* 2022;7(67):eabf7777.
187. Hashimoto D, et al. Tissue-resident macrophages self-maintain locally throughout adult life with minimal contribution from circulating monocytes. *Immunity.* 2013;38(4):792-804.
188. Zimmerman KA, et al. Kidney resident macrophages in the rat have minimal turnover and replacement by blood monocytes. *Am J Physiol Renal Physiol.* 2021;321(2):F162-f9.
189. Hume DA, and Gordon S. Mononuclear phagocyte system of the mouse defined by immunohistochemical localization of antigen F4/80. Identification of resident macrophages in renal medullary and cortical interstitium and the juxtaglomerular complex. *J Exp Med.* 1983;157(5):1704-9.
190. Hume DA, et al. The mononuclear phagocyte system of the mouse defined by immunohistochemical localization of antigen F4/80: macrophages of endocrine organs. *Proc Natl Acad Sci U S A.* 1984;81(13):4174-7.
191. Zimmerman KA, et al. Single-Cell RNA Sequencing Identifies Candidate Renal Resident Macrophage Gene Expression Signatures across Species. *J Am Soc Nephrol.* 2019;30(5):767-81.
192. Austyn JM, and Gordon S. F4/80, a monoclonal antibody directed specifically against the mouse macrophage. *Eur J Immunol.* 1981;11(10):805-15.
193. Hamann J, et al. EMR1, the human homolog of F4/80, is an eosinophil-specific receptor. *Eur J Immunol.* 2007;37(10):2797-802.
194. Dong X, et al. Resident dendritic cells are the predominant TNF-secreting cell in early renal ischemia-reperfusion injury. *Kidney Int.* 2007;71(7):619-28.
195. Qi F, et al. Depletion of cells of monocyte lineage prevents loss of renal microvasculature in murine kidney transplantation. *Transplantation.* 2008;86(9):1267-74.

196. Hashimoto D, et al. Dendritic cell and macrophage heterogeneity in vivo. *Immunity*. 2011;35(3):323-35.
197. Satpathy AT, et al. Re(de)fining the dendritic cell lineage. *Nat Immunol*. 2012;13(12):1145-54.
198. Stamatiades EG, et al. Immune Monitoring of Trans-endothelial Transport by Kidney-Resident Macrophages. *Cell*. 2016;166(4):991-1003.
199. Lever JM, et al. Parabiosis reveals leukocyte dynamics in the kidney. *Lab Invest*. 2018;98(3):391-402.
200. Soos TJ, et al. CX3CR1+ interstitial dendritic cells form a contiguous network throughout the entire kidney. *Kidney Int*. 2006;70(3):591-6.
201. Liu F, et al. Distinct fate, dynamics and niches of renal macrophages of bone marrow or embryonic origins. *Nat Commun*. 2020;11(1):2280.
202. Bonvalet JP, et al. Number of glomeruli in normal and hypertrophied kidneys of mice and guinea-pigs. *J Physiol*. 1977;269(3):627-41.
203. Huang X, et al. Polarizing Macrophages In Vitro. *Methods Mol Biol*. 2018;1784:119-26.
204. Martinez FO, and Gordon S. The M1 and M2 paradigm of macrophage activation: time for reassessment. *F1000Prime Rep*. 2014;6:13.
205. Zhang MZ, et al. CSF-1 signaling mediates recovery from acute kidney injury. *J Clin Invest*. 2012;122(12):4519-32.
206. Kumar S. Cellular and molecular pathways of renal repair after acute kidney injury. *Kidney Int*. 2018;93(1):27-40.
207. Braga TT, et al. Macrophages During the Fibrotic Process: M2 as Friend and Foe. *Front Immunol*. 2015;6:602.
208. Lever JM, et al. Resident macrophages reprogram toward a developmental state after acute kidney injury. *JCI Insight*. 2019;4(2).

209. Li L, et al. The chemokine receptors CCR2 and CX3CR1 mediate monocyte/macrophage trafficking in kidney ischemia-reperfusion injury. *Kidney Int.* 2008;74(12):1526-37.
210. Bonventre JV, and Yang L. Cellular pathophysiology of ischemic acute kidney injury. *J Clin Invest.* 2011;121(11):4210-21.
211. Huen SC, et al. GM-CSF Promotes Macrophage Alternative Activation after Renal Ischemia/Reperfusion Injury. *J Am Soc Nephrol.* 2015;26(6):1334-45.
212. Kemmner S, et al. STAT1 regulates macrophage number and phenotype and prevents renal fibrosis after ischemia-reperfusion injury. *Am J Physiol Renal Physiol.* 2019;316(2):F277-f91.
213. Han HI, et al. The role of macrophages during acute kidney injury: destruction and repair. *Pediatr Nephrol.* 2019;34(4):561-9.
214. Alikhan MA, and Ricardo SD. Mononuclear phagocyte system in kidney disease and repair. *Nephrology (Carlton).* 2013;18(2):81-91.
215. Yang Q, et al. Bone marrow-derived Ly6C(-) macrophages promote ischemia-induced chronic kidney disease. *Cell Death Dis.* 2019;10(4):291.
216. Ferenbach DA, et al. Macrophage/monocyte depletion by clodronate, but not diphtheria toxin, improves renal ischemia/reperfusion injury in mice. *Kidney Int.* 2012;82(8):928-33.
217. Komada T, et al. Macrophage Uptake of Necrotic Cell DNA Activates the AIM2 Inflammasome to Regulate a Proinflammatory Phenotype in CKD. *J Am Soc Nephrol.* 2018;29(4):1165-81.
218. Lee H, et al. Macrophage polarization in innate immune responses contributing to pathogenesis of chronic kidney disease. *BMC Nephrol.* 2020;21(1):270.
219. Torihashi S, et al. Resident macrophages activated by lipopolysaccharide suppress muscle tension and initiate inflammatory response in the gastrointestinal muscle layer. *Histochem Cell Biol.* 2000;113(2):73-80.

220. Watts C. Capture and processing of exogenous antigens for presentation on MHC molecules. *Annu Rev Immunol.* 1997;15:821-50.
221. Dai L, et al. End-Stage Renal Disease, Inflammation and Cardiovascular Outcomes. *Contrib Nephrol.* 2017;191:32-43.
222. Wu J, et al. Coexistence of micro-inflammatory and macrophage phenotype abnormalities in chronic kidney disease. *Int J Clin Exp Pathol.* 2020;13(2):317-23.
223. Zhao H, et al. Matrix metalloproteinases contribute to kidney fibrosis in chronic kidney diseases. *World J Nephrol.* 2013;2(3):84-9.
224. Johnson DW, et al. Paracrine stimulation of human renal fibroblasts by proximal tubule cells. *Kidney Int.* 1998;54(3):747-57.
225. Wang S, et al. Imatinib mesylate blocks a non-Smad TGF-beta pathway and reduces renal fibrogenesis in vivo. *Faseb j.* 2005;19(1):1-11.
226. Guiteras R, et al. Macrophage in chronic kidney disease. *Clin Kidney J.* 2016;9(6):765-71.
227. Dai XY, et al. Targeting c-fms kinase attenuates chronic aristolochic acid nephropathy in mice. *Oncotarget.* 2016;7(10):10841-56.
228. Chen J, et al. Integrated single-cell transcriptomics and proteomics reveal cellular-specific responses and microenvironment remodeling in aristolochic acid nephropathy. *JCI insight.* 2022;7(16).
229. Kurbel S, et al. The osmotic gradient in kidney medulla: a retold story. *Adv Physiol Educ.* 2002;26(1-4):278-81.
230. Favuzzi E, et al. GABA-receptive microglia selectively sculpt developing inhibitory circuits. *Cell.* 2021;184(15):4048-63.e32.
231. Peterson SL, et al. Retinal Ganglion Cell Axon Regeneration Requires Complement and Myeloid Cell Activity within the Optic Nerve. *J Neurosci.* 2021;41(41):8508-31.

232. Pimenova AA, et al. A Tale of Two Genes: Microglial Apoe and Trem2. *Immunity*. 2017;47(3):398-400.
233. van Swelm RPL, et al. The multifaceted role of iron in renal health and disease. *Nat Rev Nephrol*. 2020;16(2):77-98.
234. Smith CP, and Thévenod F. Iron transport and the kidney. *Biochim Biophys Acta*. 2009;1790(7):724-30.
235. Nairz M, et al. "Pumping iron"-how macrophages handle iron at the systemic, microenvironmental, and cellular levels. *Pflugers Arch*. 2017;469(3-4):397-418.
236. Joffin N, et al. Adipose tissue macrophages exert systemic metabolic control by manipulating local iron concentrations. *Nat Metab*. 2022;4(11):1474-94.
237. Kuang H, et al. Humoral regulation of iron metabolism by extracellular vesicles drives antibacterial response. *Nat Metab*. 2023;5(1):111-28.
238. Aydemir F, et al. Iron loading increases ferroportin heterogeneous nuclear RNA and mRNA levels in murine J774 macrophages. *J Nutr*. 2009;139(3):434-8.
239. Paller MS, and Hedlund BE. Role of iron in postischemic renal injury in the rat. *Kidney Int*. 1988;34(4):474-80.
240. Scindia Ph DY, et al. Iron Homeostasis in Healthy Kidney and its Role in Acute Kidney Injury. *Semin Nephrol*. 2019;39(1):76-84.
241. Recalcati S, et al. Macrophage ferroportin is essential for stromal cell proliferation in wound healing. *Haematologica*. 2019;104(1):47-58.
242. Willyard C. Squeaky clean mice could be ruining research. *Nature*. 2018;556(7699):16-8.
243. Beura LK, et al. Normalizing the environment recapitulates adult human immune traits in laboratory mice. *Nature*. 2016;532(7600):512-6.

244. Carai P, et al. Stabilin-1 mediates beneficial monocyte recruitment and tolerogenic macrophage programming during CVB3-induced viral myocarditis. *J Mol Cell Cardiol.* 2022;165:31-9.
245. Rantakari P, et al. Stabilin-1 expression defines a subset of macrophages that mediate tissue homeostasis and prevent fibrosis in chronic liver injury. *Proc Natl Acad Sci U S A.* 2016;113(33):9298-303.
246. Cabral F, et al. Stabilin receptors clear LPS and control systemic inflammation. *iScience.* 2021;24(11):103337.
247. Li J, et al. Clinicopathological significance of CD206-positive macrophages in patients with acute tubulointerstitial disease. *Int J Clin Exp Pathol.* 2015;8(9):11386-92.
248. Li Z, et al. A kidney resident macrophage subset is a candidate biomarker for renal cystic disease in preclinical models. *Dis Model Mech.* 2023;16(1).
249. Liu J, et al. CCR2(-) and CCR2(+) corneal macrophages exhibit distinct characteristics and balance inflammatory responses after epithelial abrasion. *Mucosal Immunol.* 2017;10(5):1145-59.
250. Bauer D, et al. Conjunctival macrophage-mediated influence of the local and systemic immune response after corneal herpes simplex virus-1 infection. *Immunology.* 2002;107(1):118-28.
251. Wang ECE, et al. A Subset of TREM2(+) Dermal Macrophages Secretes Oncostatin M to Maintain Hair Follicle Stem Cell Quiescence and Inhibit Hair Growth. *Cell Stem Cell.* 2019;24(4):654-69.e6.
252. Müller S, et al. Salt-dependent chemotaxis of macrophages. *PLoS One.* 2013;8(9):e73439.
253. Berry MR, et al. Renal Sodium Gradient Orchestrates a Dynamic Antibacterial Defense Zone. *Cell.* 2017;170(5):860-74.e19.
254. Groop L, et al. Renal papillary necrosis in patients with IDDM. *Diabetes Care.* 1989;12(3):198-202.

255. Peerapornratana S, et al. Acute kidney injury from sepsis: current concepts, epidemiology, pathophysiology, prevention and treatment. *Kidney Int.* 2019;96(5):1083-99.
256. Divangahi M, et al. Alveolar macrophages and type I IFN in airway homeostasis and immunity. *Trends Immunol.* 2015;36(5):307-14.
257. Wang J, et al. Resident bone marrow macrophages produce type I interferons that can selectively inhibit interleukin-7-driven growth of B lineage cells. *Immunity.* 1995;3(4):475-84.
258. Basler CF, and García-Sastre A. Viruses and the type I interferon antiviral system: induction and evasion. *Int Rev Immunol.* 2002;21(4-5):305-37.
259. Jayne D, et al. Phase II randomised trial of type I interferon inhibitor anifrolumab in patients with active lupus nephritis. *Ann Rheum Dis.* 2022;81(4):496-506.
260. Triantafyllopoulou A, et al. Proliferative lesions and metalloproteinase activity in murine lupus nephritis mediated by type I interferons and macrophages. *Proc Natl Acad Sci U S A.* 2010;107(7):3012-7.
261. Michalska A, et al. A Positive Feedback Amplifier Circuit That Regulates Interferon (IFN)-Stimulated Gene Expression and Controls Type I and Type II IFN Responses. *Front Immunol.* 2018;9:1135.
262. Cao Q, et al. Macrophages in kidney injury, inflammation, and fibrosis. *Physiology (Bethesda).* 2015;30(3):183-94.
263. Tapia C, and Bashir K. *StatPearls*. Treasure Island (FL): StatPearls Publishing Copyright © 2022, StatPearls Publishing LLC.; 2022.
264. Parodis I, et al. Prediction of prognosis and renal outcome in lupus nephritis. *Lupus Sci Med.* 2020;7(1):e000389.
265. Devasahayam J, et al. C1q Nephropathy: The Unique Underrecognized Pathological Entity. *Anal Cell Pathol (Amst).* 2015;2015:490413.

266. Casanova-Acebes M, et al. Tissue-resident macrophages provide a pro-tumorigenic niche to early NSCLC cells. *Nature*. 2021;595(7868):578-84.
267. Pinto AR, et al. An abundant tissue macrophage population in the adult murine heart with a distinct alternatively-activated macrophage profile. *PLoS One*. 2012;7(5):e36814.
268. Fonseca MI, et al. Cell-specific deletion of C1qa identifies microglia as the dominant source of C1q in mouse brain. *J Neuroinflammation*. 2017;14(1):48.
269. Fu H, et al. Complement component C3 and complement receptor type 3 contribute to the phagocytosis and clearance of fibrillar A β by microglia. *Glia*. 2012;60(6):993-1003.
270. Chu Y, et al. Enhanced synaptic connectivity and epilepsy in C1q knockout mice. *Proc Natl Acad Sci U S A*. 2010;107(17):7975-80.
271. Cong Q, et al. C1q and SRPX2 regulate microglia mediated synapse elimination during early development in the visual thalamus but not the visual cortex. *Glia*. 2022;70(3):451-65.
272. Filipello F, et al. The Microglial Innate Immune Receptor TREM2 Is Required for Synapse Elimination and Normal Brain Connectivity. *Immunity*. 2018;48(5):979-91.e8.
273. Deng T, et al. Class II major histocompatibility complex plays an essential role in obesity-induced adipose inflammation. *Cell Metab*. 2013;17(3):411-22.
274. Bessaad A, et al. M1-activated macrophages migration, a marker of aortic atheroma progression: a preclinical MRI study in mice. *Invest Radiol*. 2010;45(5):262-9.
275. Pavlou S, et al. Higher phagocytic activity of thioglycollate-elicited peritoneal macrophages is related to metabolic status of the cells. *J Inflamm (Lond)*. 2017;14:4.
276. Fujiu K, et al. Cardioprotective function of cardiac macrophages. *Cardiovasc Res*. 2014;102(2):232-9.

277. Qian J, et al. TLR2 Promotes Glioma Immune Evasion by Downregulating MHC Class II Molecules in Microglia. *Cancer Immunol Res.* 2018;6(10):1220-33.
278. Redpath S, et al. Murine cytomegalovirus infection down-regulates MHC class II expression on macrophages by induction of IL-10. *J Immunol.* 1999;162(11):6701-7.
279. Velásquez LN, et al. Brucella abortus down-regulates MHC class II by the IL-6-dependent inhibition of CIITA through the downmodulation of IFN regulatory factor-1 (IRF-1). *J Leukoc Biol.* 2017;101(3):759-73.
280. Nepom GT, and Erlich H. MHC class-II molecules and autoimmunity. *Annu Rev Immunol.* 1991;9:493-525.
281. Haldar M, and Murphy KM. Origin, development, and homeostasis of tissue-resident macrophages. *Immunol Rev.* 2014;262(1):25-35.
282. Tsurutani M, et al. Cell Properties of Lung Tissue-Resident Macrophages Propagated by Co-Culture with Lung Fibroblastic Cells from C57BL/6 and BALB/c Mice. *Biomedicines.* 2021;9(9).
283. Huen SC, and Cantley LG. Macrophages in Renal Injury and Repair. *Annu Rev Physiol.* 2017;79:449-69.

APPENDIX A

Supplementary Tables and Figures
for
Resident Macrophage Subpopulations Occupy Distinct Microenvironments
in the Kidney

Supplementary Table 1. Gene ontology analysis of KRM clusters 1 day after injury

Gene Ontology Analysis Day 1					
Cluster	Gene Set	Description	Enrichment		
			Ratio	p-Value	FDR
0	GO:0002478	antigen processing and presentation of exogenous peptide antigen	105.4	1.60E-04	0.0504
0	GO:0033077	T cell differentiation in thymus	32.7	1.00E-04	0.0504
0	GO:0019724	B cell mediated immunity	25.9	2.01E-04	0.0504
0	GO:2001233	regulation of apoptotic signaling pathway	12.1	4.35E-05	0.0504
1	GO:0043921	modulation by host of viral transcription	81.3	6.48E-06	0.0009
1	GO:0002548	monocyte chemotaxis	39.9	5.72E-05	0.0047
1	GO:0032611	interleukin-1 beta production	29.5	1.41E-04	0.0090
1	GO:0002688	regulation of leukocyte chemotaxis	24.9	1.90E-05	0.0021
1	GO:0007088	regulation of mitotic nuclear division	16.5	9.37E-05	0.0069
1	GO:0032496	response to lipopolysaccharide	16.0	2.18E-08	0.0000
1	GO:1903706	regulation of hemopoiesis	14.4	4.85E-08	0.0000
1	GO:0050727	regulation of inflammatory response	13.0	5.33E-06	0.0008
1	GO:0030099	myeloid cell differentiation	11.1	1.28E-05	0.0015
2	GO:0034368	protein-lipid complex remodeling	95.1	1.97E-04	0.0614
2	GO:0033006	regulation of mast cell activation involved in immune response	62.4	4.63E-04	0.0904
2	GO:0010039	response to iron ion	58.7	5.23E-04	0.0904
3	GO:1990869	cellular response to chemokine	23.2	1.90E-09	0.0000
3	GO:0045428	regulation of nitric oxide biosynthetic process	22.7	2.50E-07	0.0000
3	GO:0032611	interleukin-1 beta production	21.4	3.59E-07	0.0000
3	GO:0030593	neutrophil chemotaxis	18.5	9.83E-08	0.0000
3	GO:1990266	neutrophil migration	15.7	3.13E-07	0.0000
3	GO:0071222	cellular response to lipopolysaccharide	14.8	3.63E-12	0.0000
3	GO:0032640	tumor necrosis factor production	13.4	1.44E-07	0.0000
3	GO:0071248	cellular response to metal ion	12.3	4.95E-08	0.0000
3	GO:2000377	regulation of reactive oxygen species metabolic process	11.8	6.86E-08	0.0000
3	GO:0060326	cell chemotaxis	8.8	1.92E-07	0.0000
3	GO:0097193	intrinsic apoptotic signaling pathway	8.7	2.18E-07	0.0000
3	GO:0050900	leukocyte migration	8.6	5.59E-08	0.0000
3	GO:0042110	T cell activation	8.1	3.93E-10	0.0000
4	GO:1990868	response to chemokine	35.5	9.43E-10	0.0000
4	GO:0097529	myeloid leukocyte migration	20.8	3.81E-10	0.0000
4	GO:0070555	response to interleukin-1	14.7	1.54E-04	0.0223
4	GO:0050920	regulation of chemotaxis	10.7	9.85E-05	0.0156
5	GO:0097529	myeloid leukocyte migration	8.2	4.61E-10	0.0000
5	GO:0030595	leukocyte chemotaxis	8.2	1.23E-10	0.0000
5	GO:0008909	phagocytosis	8.0	9.97E-09	0.0000
5	GO:0042110	T cell activation	3.8	2.65E-06	0.0002
6	GO:0035457	cellular response to interferon-alpha	97.3	1.61E-11	0.0000
6	GO:0034340	response to type I interferon	27.0	1.09E-06	0.0001
6	GO:0009615	response to virus	20.6	0	0.0000
6	GO:0045088	regulation of innate immune response	19.7	0	0.0000
6	GO:0034341	response to interferon-gamma	18.9	1.60E-12	0.0000

Supplementary Table 1. Gene ontology analysis of KRM clusters 1 day after injury. Gene ontology analysis of terms with an FDR < 0.05, with the exceptions of clusters 0 and 2

where no gene sets met this requirement. The top four and three terms were listed, respectively.

Supplementary Table 2. Gene ontology analysis of KRM clusters 6 days after injury

Gene Ontology Analysis Day 6 ¹					
Cluster	Gene Set	Description	Enrichment		
			Ratio	p-Value	FDR
1	GO:0038086	p38MAPK cascade	55.8	7.56E-07	0.0003
1	GO:0030089	myeloid cell differentiation	11.7	1.83E-08	0.0004
1	GO:0070371	ERK1 and ERK2 cascade	10.7	1.88E-05	0.0022
1	GO:0071222	cellular response to lipopolysaccharide	14.2	2.44E-05	0.0028
1	GO:0097191	extrinsic apoptotic signaling pathway	14.1	2.49E-05	0.0028
1	GO:0042110	T cell activation	8.0	8.44E-05	0.0070
1	GO:0002685	regulation of leukocyte migration	13.1	2.33E-04	0.0145
2	GO:0030595	leukocyte chemotaxis	10.4	4.86E-06	0.0050
2	GO:0070371	ERK1 and ERK2 cascade	6.9	1.93E-05	0.0080
2	GO:0097530	granulocyte migration	10.9	9.54E-05	0.0138
2	GO:1990888	response to chemokine	14.0	1.94E-04	0.0208
2	GO:0072676	lymphocyte migration	12.6	2.88E-04	0.0254
2	GO:0043542	endothelial cell migration	8.0	4.10E-04	0.0297
2	GO:0002548	monocyte chemotaxis	17.4	6.79E-04	0.0428
3	GO:0032486	response to lipopolysaccharide	14.9	0	0.0000
3	GO:1903708	regulation of hemopoiesis	11.5	1.35E-14	0.0000
3	GO:0002685	regulation of leukocyte migration	14.1	3.20E-10	0.0000
3	GO:0034612	response to tumor necrosis factor	13.8	4.24E-10	0.0000
3	GO:1990286	neutrophil migration	19.7	7.79E-10	0.0000
3	GO:0097191	extrinsic apoptotic signaling pathway	12.2	1.55E-09	0.0000
3	GO:1990888	response to chemokine	22.6	2.33E-09	0.0000
3	GO:0097530	granulocyte migration	15.9	5.15E-09	0.0000
3	GO:0070372	regulation of ERK1 and ERK2 cascade	8.8	1.02E-08	0.0000
3	GO:0030595	leukocyte chemotaxis	12.0	1.04E-08	0.0000
3	GO:0002573	myeloid leukocyte differentiation	11.5	1.51E-08	0.0000
3	GO:0071621	granulocyte chemotaxis	16.7	2.80E-08	0.0000
3	GO:0070555	response to interleukin-1	16.4	2.97E-08	0.0000
3	GO:0002224	toll-like receptor signaling pathway	18.3	1.09E-07	0.0000
3	GO:0010574	regulation of vascular endothelial growth factor production	38.7	1.72E-07	0.0000
3	GO:0032640	tumor necrosis factor production	13.1	1.76E-07	0.0000
4	GO:0097529	myeloid leukocyte migration	19.1	9.17E-11	0.0000
4	GO:0071674	mononuclear cell migration	33.9	1.37E-09	0.0000
4	GO:1990888	response to chemokine	29.5	3.67E-09	0.0000
4	GO:0070555	response to interleukin-1	21.4	3.45E-08	0.0000
4	GO:0034612	response to tumor necrosis factor	13.1	1.01E-06	0.0003
4	GO:0046718	viral entry into host cell	27.1	1.10E-06	0.0003
4	GO:0070371	ERK1 and ERK2 cascade	8.3	4.59E-06	0.0009
4	GO:0002685	regulation of leukocyte migration	11.5	1.32E-05	0.0023
4	GO:0050920	regulation of chemotaxis	10.7	1.99E-05	0.0033
4	GO:0035455	response to interferon-alpha	44.8	4.00E-05	0.0059
5	GO:0002548	monocyte chemotaxis	81.4	2.11E-12	0.0000
5	GO:0048247	lymphocyte chemotaxis	58.1	2.19E-08	0.0000
5	GO:0048245	eosinophil chemotaxis	118.6	3.17E-08	0.0000
5	GO:0071621	granulocyte chemotaxis	30.9	3.48E-08	0.0000
5	GO:0009611	response to wounding	10.9	7.58E-08	0.0000
5	GO:0030593	neutrophil chemotaxis	31.9	4.60E-07	0.0001
5	GO:0070371	ERK1 and ERK2 cascade	12.1	1.35E-06	0.0003
5	GO:0050883	regulation of T cell activation	12.3	7.70E-06	0.0011
5	GO:0090025	regulation of monocyte chemotaxis	71.2	9.77E-06	0.0014
5	GO:0071675	regulation of mononuclear cell migration	39.5	5.89E-05	0.0080
5	GO:0046625	regulation of T-helper 1 cell differentiation	98.8	1.80E-04	0.0127
5	GO:0032717	negative regulation of interleukin-8 production	79.1	2.85E-04	0.0178
6	GO:0035456	response to interferon-beta	165.0	0	0.0000
6	GO:0009615	response to virus	34.6	1.11E-16	0.0000
6	GO:0002218	activation of innate immune response	41.8	8.53E-12	0.0000
6	GO:0035455	response to interferon-alpha	137.5	1.72E-08	0.0000
6	GO:0034340	response to type I interferon	63.5	1.38E-05	0.0072

¹ No significant results were returned for cluster 0

Supplementary Table 2. Gene ontology analysis of KRM clusters 6 days after injury.

Gene ontology analysis of terms with an FDR < 0.05.

Supplementary Table 3. Gene ontology analysis of KRM clusters 28 days after injury

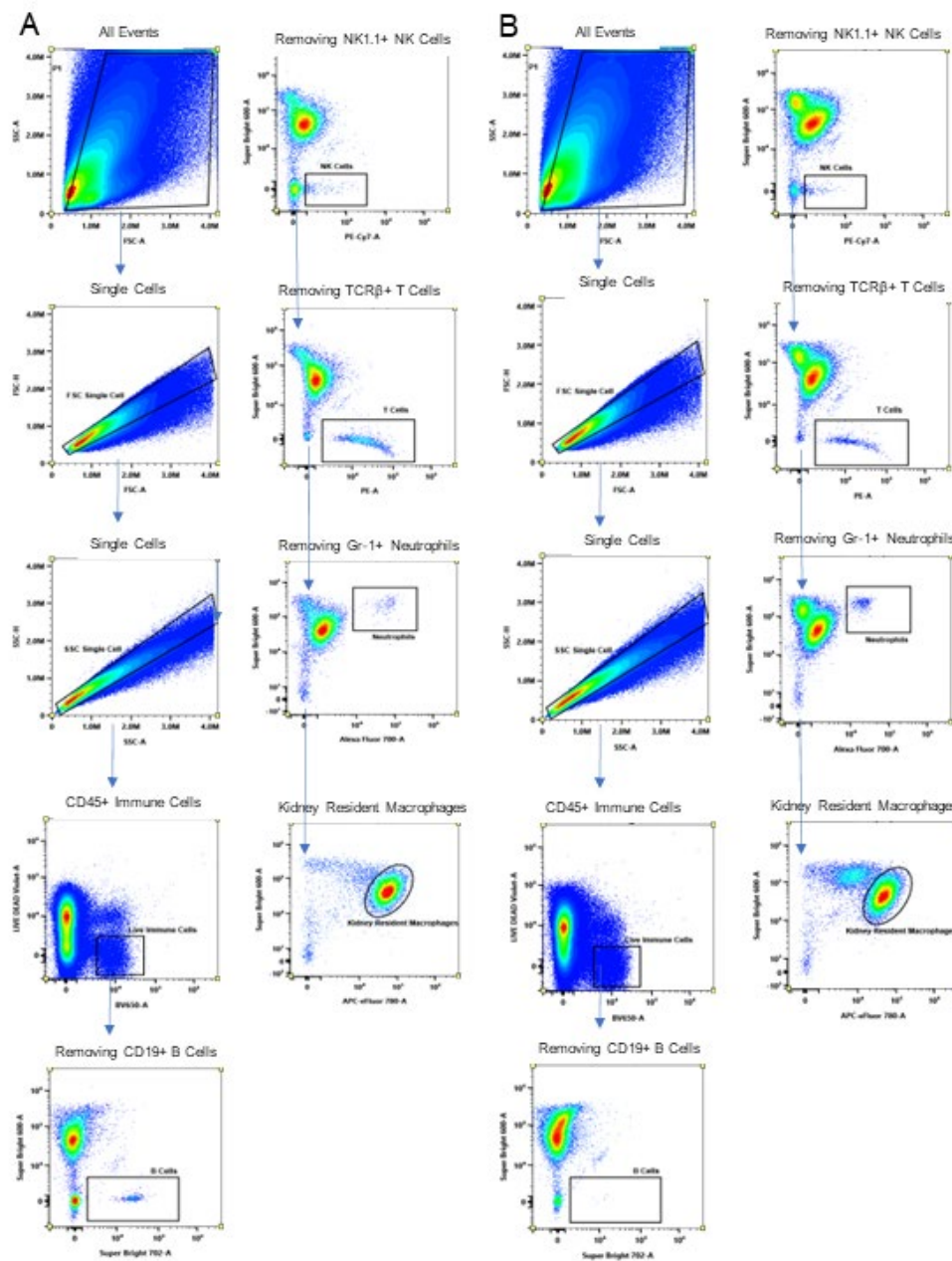
Gene Ontology Analysis Day 28¹					
Cluster	Gene Set	Description	Enrichment		
			Ratio	p-Value	FDR
1	GO:0032496	response to lipopolysaccharide	18.6	1.58E-08	0.0000
1	GO:0043921	modulation by host of viral transcription	84.3	5.79E-06	0.0008
1	GO:0070371	ERK1 and ERK2 cascade	12.3	7.17E-06	0.0008
1	GO:0051403	stress-activated MAPK cascade	14.4	2.16E-05	0.0018
1	GO:0050729	positive regulation of inflammatory response	23.2	2.47E-05	0.0020
1	GO:0002548	monocyte chemotaxis	41.3	5.11E-05	0.0038
1	GO:0051384	response to glucocorticoid	17.5	7.53E-05	0.0049
2	GO:0010631	epithelial cell migration	18.7	5.26E-06	0.0096
2	GO:0071281	cellular response to iron ion	166.4	6.23E-05	0.0248
2	GO:0034368	protein-lipid complex remodeling	95.1	1.97E-04	0.0455
2	GO:0001936	regulation of endothelial cell proliferation	25.4	2.11E-04	0.0470
3	GO:0032496	response to lipopolysaccharide	18.9	6.66E-16	0.0000
3	GO:0071219	cellular response to molecule of bacterial origin	19.3	9.01E-13	0.0000
3	GO:0051384	response to glucocorticoid	17.8	1.45E-08	0.0000
3	GO:0050729	positive regulation of inflammatory response	20.7	4.35E-08	0.0000
3	GO:0070098	chemokine-mediated signaling pathway	28.6	6.16E-08	0.0000
3	GO:0002548	monocyte chemotaxis	35.1	2.99E-07	0.0000
3	GO:0070371	ERK1 and ERK2 cascade	9.4	4.08E-07	0.0000
3	GO:0050766	positive regulation of phagocytosis	32.5	4.39E-07	0.0000
3	GO:0008630	intrinsic apoptotic signaling pathway in response to DNA damage	19.7	5.77E-07	0.0000
3	GO:0002685	regulation of leukocyte migration	13.4	8.48E-07	0.0001
3	GO:1902532	negative regulation of intracellular signal transduction	7.3	9.00E-07	0.0001
3	GO:2001233	regulation of apoptotic signaling pathway	8.2	1.22E-06	0.0001
4	GO:0070098	chemokine-mediated signaling pathway	63.2	3.95E-07	0.0014
4	GO:0034341	response to interferon-gamma	35.4	4.05E-06	0.0050
4	GO:0071219	cellular response to molecule of bacterial origin	21.3	3.03E-05	0.0235
4	GO:0034369	plasma lipoprotein particle remodeling	112.9	1.39E-04	0.0404
4	GO:0032496	response to lipopolysaccharide	14.0	1.54E-04	0.0404
4	GO:0070371	ERK1 and ERK2 cascade	13.8	1.61E-04	0.0404
4	GO:0097530	granulocyte migration	26.2	1.88E-04	0.0404
5	GO:0034341	response to interferon-gamma	13.9	1.76E-08	0.0001
5	GO:0048247	lymphocyte chemotaxis	20.2	4.73E-06	0.0045
5	GO:0070098	chemokine-mediated signaling pathway	13.7	3.17E-05	0.0164
5	GO:0006909	phagocytosis	7.4	1.62E-04	0.0481
6	GO:0045089	positive regulation of innate immune response	21.9	0	0.0000
6	GO:0045071	negative regulation of viral genome replication	43.8	4.56E-13	0.0000
6	GO:0071346	cellular response to interferon-gamma	19.2	9.55E-10	0.0000
6	GO:1900225	regulation of NLRP3 inflammasome complex assembly	56.1	1.86E-05	0.0019
6	GO:0038094	Fc-gamma receptor signaling pathway	56.1	1.86E-05	0.0019
6	GO:0001961	positive regulation of cytokine-mediated signaling pathway	24.3	2.16E-05	0.0022
6	GO:0002757	immune response-activating signal transduction	6.6	2.77E-05	0.0027
6	GO:0032680	regulation of tumor necrosis factor production	10.1	2.93E-05	0.0029
6	GO:0032481	positive regulation of type I interferon production	20.3	4.48E-05	0.0037
6	GO:0032648	regulation of interferon-beta production	19.9	4.86E-05	0.0040
6	GO:0034121	regulation of toll-like receptor signaling pathway	17.4	8.25E-05	0.0060
6	GO:0032647	regulation of interferon-alpha production	28.1	1.62E-04	0.0101

¹ No significant results were returned for cluster 0

Supplementary Table 3. Gene ontology analysis of KRM clusters 28 days after injury.

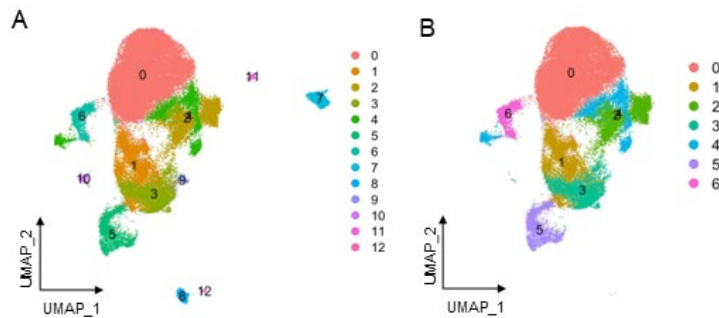
Gene ontology analysis of terms with an FDR < 0.05.

Supplementary Figure 1. Flow cytometry gating scheme to isolate kidney resident macrophages



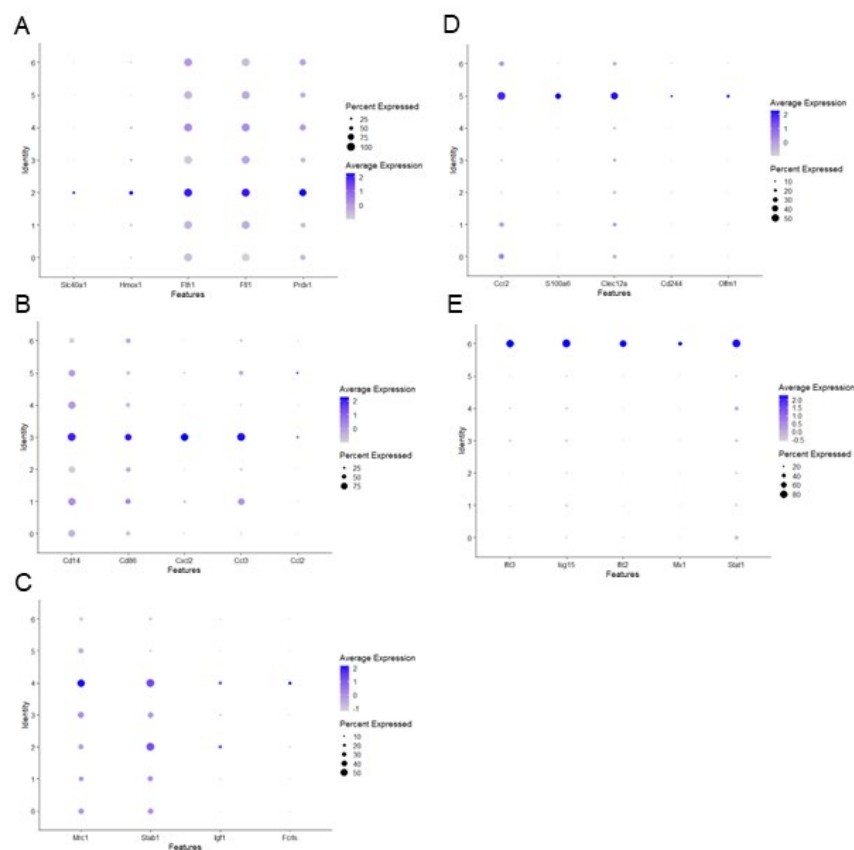
Supplemental Figure 1: Flow cytometry gating scheme to isolate kidney resident macrophages. Gating strategy from kidney single-cell suspensions using pseudocolor defaults both A) pre-injury and B) post-injury

Supplementary Figure 2. Uniform manifold approximation and projection (UMAP) plot of sequenced kidney resident macrophages (KRM) from all time points



Supplemental Figure 2: Uniform manifold approximation and projection (UMAP) plot of sequenced kidney resident macrophages (KRM) from all time points A) Uniform manifold approximation and projection (UMAP) plot of sequenced kidney resident macrophages (KRM) from all time points (quiescence, 12 hours, day 1, day 6, and day 28 postinjury) demonstrates thirteen unique clusters. Contaminating kidney parenchymal cells and clusters representing less than 1% of the population were included. B) UMAP plot of sequenced KRM from all time points (quiescence, 12 hours, day 1, day 6, and day 28 post-injury) demonstrates seven unique clusters. Contaminating kidney parenchymal cells and clusters representing less than 1% of the population were omitted from the analysis.

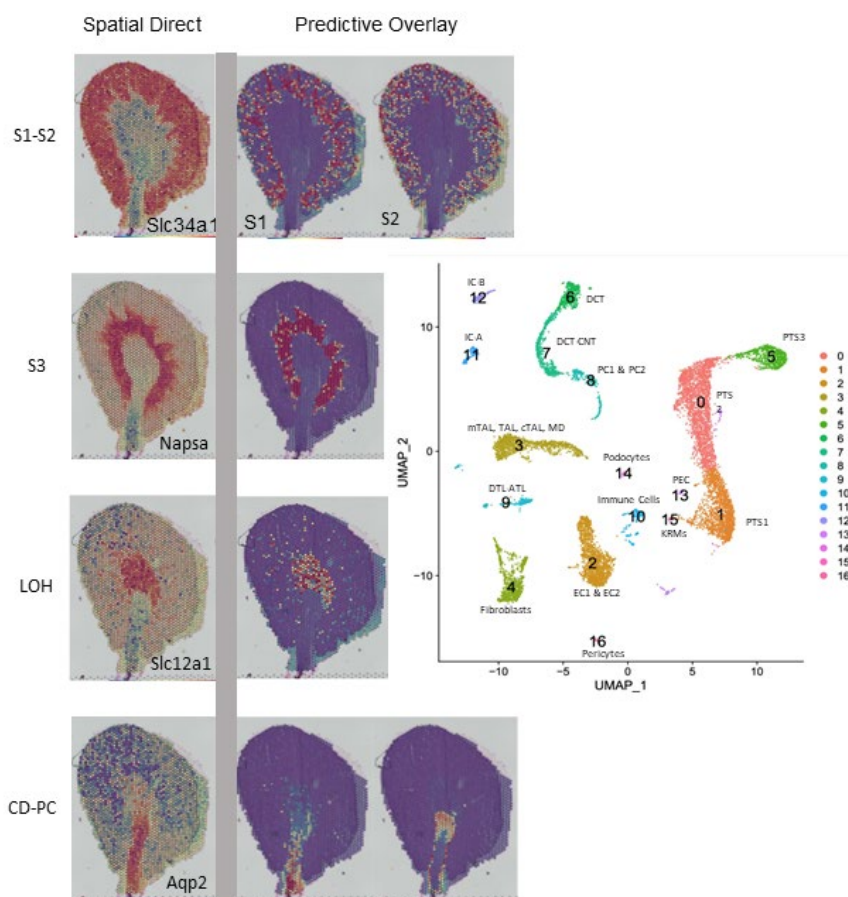
Supplementary Figure 3. Dot plots of key differentially expressed genes from each cluster



Supplemental Figure 3: Dot plots of key differentially expressed genes from each cluster

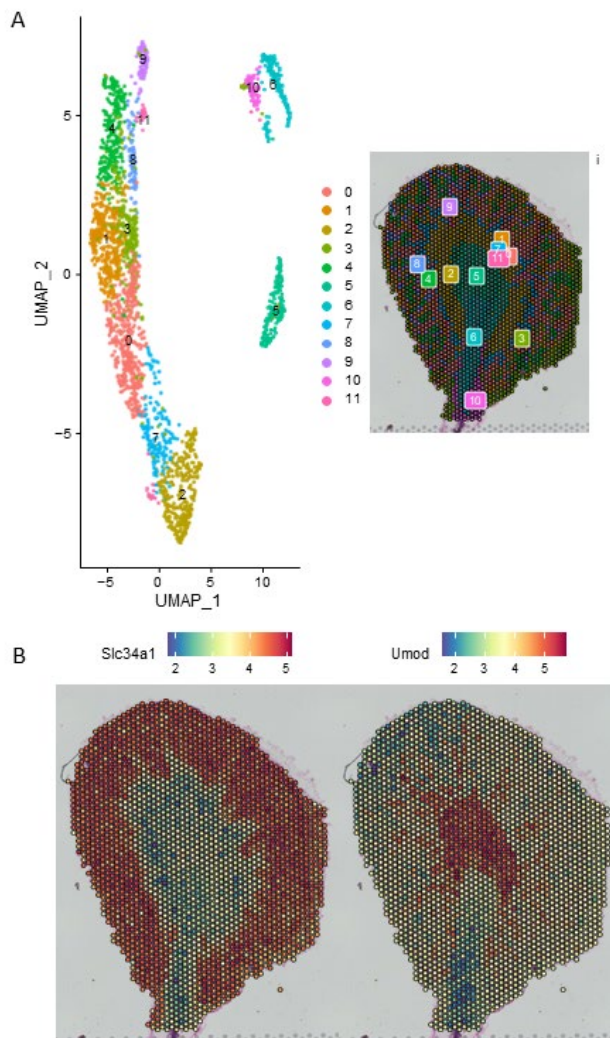
Dot plots of key differentially expressed genes from A) cluster 2, B) cluster 3, C) cluster 4, D) cluster 5 and E) cluster 6

Supplementary Figure 4. Uniform manifold approximation and projection (UMAP) and spatial plots derived from spatial sequencing data



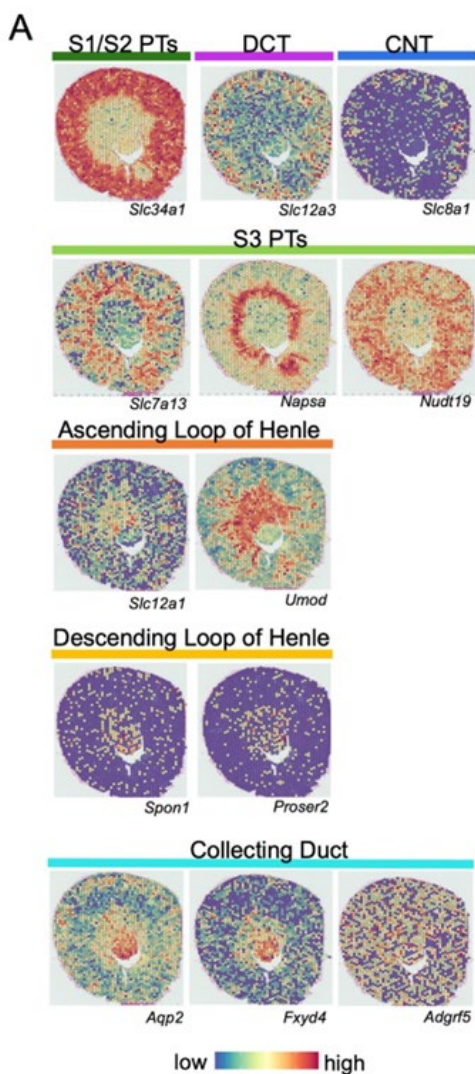
Supplemental Figure 4: Uniform manifold approximation and projection (UMAP) and spatial plots derived from spatial sequencing data. A) Uniform manifold approximation and projection (UMAP) plots derived from spatial sequencing data (left). Spatial plotting of kidney cell types onto spatial histological image (right). B) Spatial gene expression plots of *Slc34a1* (left) and *Umod* (right).

Supplementary Figure 5. Uniform manifold approximation and projection (UMAP) plots of kidney cell types derived from single nuclear RNA sequencing



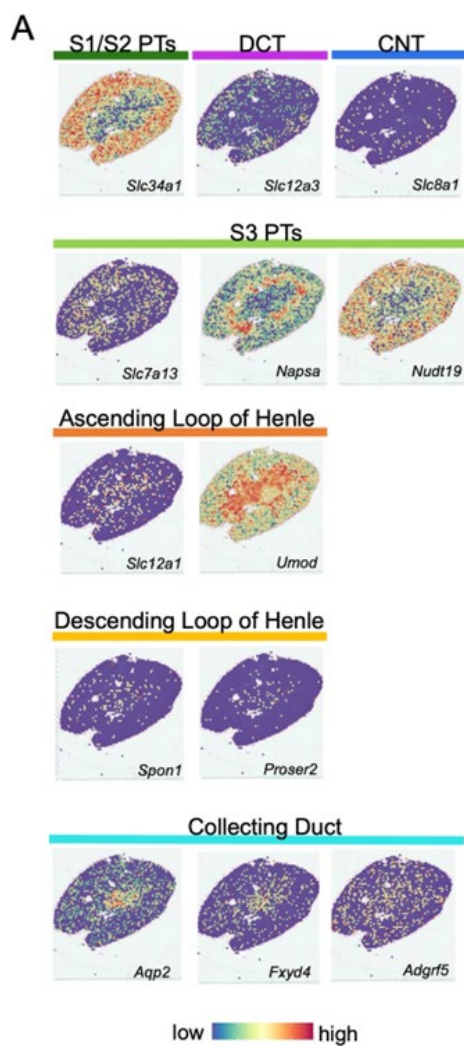
Supplemental Figure 5: Uniform manifold approximation and projection (UMAP) plots of kidney cell types derived from single nuclear RNA sequencing. Uniform manifold approximation and projection (UMAP) plots of kidney cell types derived from single nuclear RNA sequencing (right). Spatial plotting of kidney cell types from single nuclear RNA sequencing onto spatial histological image. The regions of the nephron were mapped using transcripts associated with specific cell types (e.g. *Slc34a1* for the S1/S2 region of the proximal tubule or *Umod* for the ascending loop of Henle).

Supplementary Figure 6. Zone-specific transcripts for spatial transcriptomics section 12 hours after injury



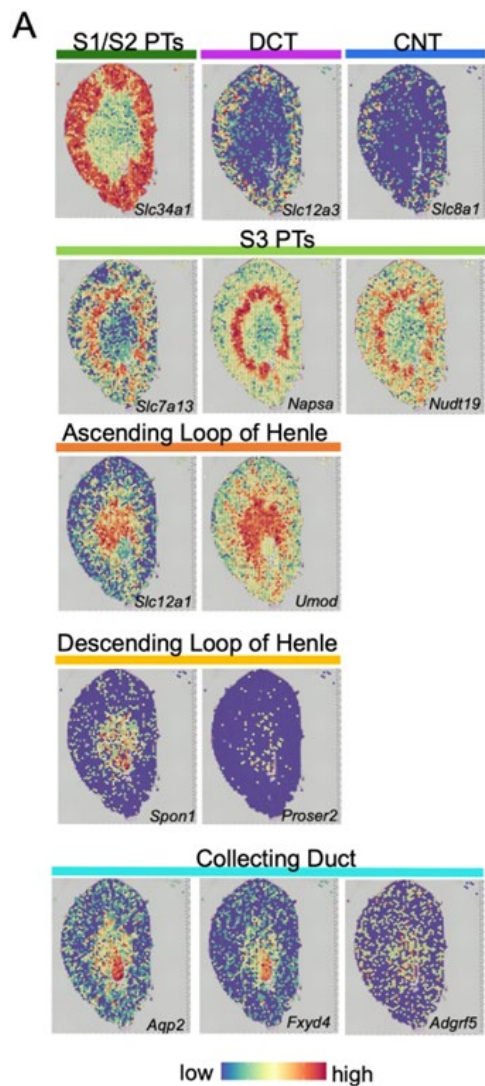
Supplemental Figure 6: Zone-specific transcripts for spatial transcriptomics section 12 hours after injury. The spatial location of the nephron segments are shown by mapping segment-specific transcripts onto the histological image. Transcript markers are listed in the bottom right-hand corner of each section. Specific nephron segments are listed above each image. Colored bars correspond to the location of the segments from the nephron in the left panel from Figure 3.

Supplementary Figure 7. Zone-specific transcripts for spatial transcriptomics section 1 day after injury.



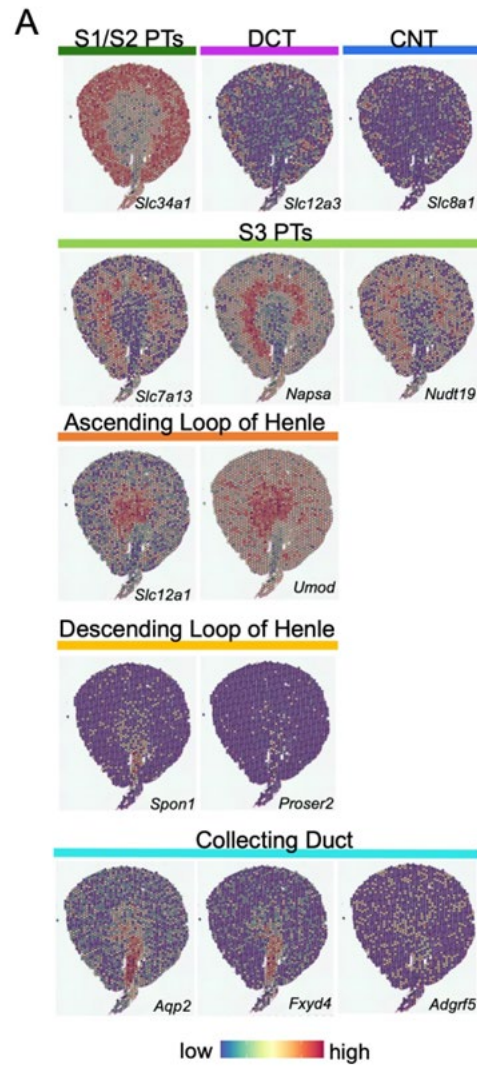
Supplemental Figure 7: Zone-specific transcripts for spatial transcriptomics section 1 day after injury. The spatial location of the nephron segments are shown by mapping segment-specific transcripts onto the histological image. Transcript markers are listed in the bottom right-hand corner of each section. Specific nephron segments are listed above each image. Colored bars correspond to the location of the segments from the nephron in the left panel Figure 3.

Supplementary Figure 8. Zone-specific transcripts for spatial transcriptomics section 6 days after injury



Supplemental Figure 8: Zone-specific transcripts for spatial transcriptomics section 6 days after injury. The spatial location of the nephron segments are shown by mapping segment-specific transcripts onto the histological image. Transcript markers are listed in the bottom right-hand corner of each section. Specific nephron segments are listed above each image. Colored bars correspond to the location of the segments from the nephron in the left panel from Figure 3.

Supplementary Figure 9. Zone-specific transcripts for spatial transcriptomics section 28 days after injury



Supplemental Figure 9: Zone-specific transcripts for spatial transcriptomics section 28 days after injury. The spatial location of the nephron segments are shown by mapping segment-specific transcripts onto the histological image. Transcript markers are listed in the bottom right-hand corner of each section. Specific nephron segments are listed above each image. Colored bars correspond to the location of the segments from the nephron in the left panel from Figure 3.

APPENDIX B

Supplementary Tables and Figures
for
Human and murine kidneys contain transcriptionally orthologous resident
macrophage subpopulations in acute kidney injury

Supplementary Table 1.

Murine KRM 4 Markers on Human

	0	1	2	3
1	<2 e-16	-	-	-
2	<2 e-16	6.0e-5	-	-
3	0.66090	1.9e-14	<2 e-16	-
4	<2 e-16	0.00075	0.66090	1.2e-14

Murine KRM 4 Markers on Qui Mouse

	0	1	2	3	4	5
1	0.10732	-	-	-	-	-
2	<2 e-16	<2 e-16	-	-	-	-
3	0.00592	0.00339	6.0e-9	-	-	-
4	<2 e-16	<2 e-16	3.4e-6	<2 e-16	-	-
5	0.82399	0.60107	1.3e-12	0.10072	<2 e-16	-
6	0.00043	0.04304	<2 e-16	1.8e-5	<2 e-16	0.04495

Murine KRM 4 Markers on Day 1 Mouse

	0	1	2	3	4	5
1	1.3e-11	-	-	-	-	-
2	<2 e-16	<2 e-16	-	-	-	-
3	<2 e-16	<2 e-16	0.00337	-	-	-
4	<2 e-16	<2 e-16	<2 e-16	<2 e-16	-	-
5	<2 e-16	<2 e-16	0.16565	0.00018	<2 e-16	-
6	0.01110	0.42359	1.1e-10	1.2e-8	<2 e-16	4.6e-9

Murine KRM 4 Qui Transcriptional Profile on Human

	0	1	2	3
1	<2 e-16	-	-	-
2	<2 e-16	0.00096	-	-
3	0.40099	<2 e-16	<2 e-16	-
4	<2 e-16	0.68202	0.01143	<2 e-16

Murine KRM 4 Day 1 Transcriptional Profile on Human

	0	1	2	3
1	1.3e-11	-	-	-
2	5.8e-5	0.25129	-	-
3	0.01422	3.6e-12	1.7e-6	-
4	3.6e-15	0.00013	5.8e-5	4.4e-15

Supplementary Table 2.

MKRM 3 Markers on Human

	0	1	2	3
1	0.0002	-	-	-
2	0.2116	2.8e-6	-	-
3	4.1e-8	<2 e-16	0.0043	-
4	0.0186	1.6e-6	0.2163	0.0754

mKRM 3 Markers on Qui Mouse

	0	1	2	3	4	5
1	<2 e-16	-	-	-	-	-
2	0.17266	<2 e-16	-	-	-	-
3	<2 e-16	<2 e-16	<2 e-16	-	-	-
4	1.3e-9	<2 e-16	0.00450	<2 e-16	-	-
5	<2 e-16	0.00018	<2 e-16	<2 e-16	<2 e-16	-
6	0.00010	<2 e-16	0.11778	<2 e-16	0.32859	3.6e-16

mKRM 3 Markers on Day 1 Mouse

	0	1	2	3	4	5
1	<2 e-16	-	-	-	-	-
2	0.05920	<2 e-16	-	-	-	-
3	<2 e-16	<2 e-16	<2 e-16	-	-	-
4	0.00054	<2 e-16	0.00032	<2 e-16	-	-
5	<2 e-16	-				
6	1.1e-11	2.0e-15	3.4e-11	<2 e-16	5.5e-6	0.00066

MKRM 3 Qui Transcriptional Profile on Human

	0	1	2	3
1	9.2E-7	-	-	-
2	0.9800	3.1e-5	-	-
3	1.9E-10	<2 e-16	2.8e-8	-
4	0.8805	0.0002	0.8805	3.9e-6

MKRM 3 Day 1 Transcriptional Profile on Human

	0	1	2	3
1	0.0211	-	-	-
2	0.0213	0.0002	-	-
3	4.3e-12	4.6e-14	0.0062	-
4	0.2599	0.0093	0.4153	9.4e-5

Supplementary Table 3.

MKRM 6 Markers on Human

	0	1	2	3
1	0.0074	-	-	-
2	<2 e-16	3.6e-15	-	-
3	0.0015	0.7460	1.4e-13	-
4	0.3384	0.2290	1.1e-14	0.1374

MKRM 6 Qui Transcriptional Profile on Human

	0	1	2	3
1	8.2e-5	-	-	-
2	1.2e-10	0.0056	-	-
3	0.0018	0.1468	0.0018	-
4	0.0077	0.9787	0.0068	0.9963

mKRM 6 Markers on Qui Mouse

	0	1	2	3	4	5
1	0.1688	-	-	-	-	-
2	0.1164	0.4485	-	-	-	-
3	0.0865	0.0211	0.181	-	-	-
4	<2 e-16	<2 e-16	2.9e-13	6.4e-8	-	-
5	0.0181	0.0058	0.0058	0.2832	0.0050	-
6	<2 e-16					

MKRM 6 Day 1 Transcriptional Profile on Human

	0	1	2	3
1	1.9e-8	-	-	-
2	1.1e-15	0.00012	-	-
3	0.00037	0.00090	8.4e-7	-
4	9.6e-9	0.01128	0.05415	0.00049

mKRM 6 Markers on Day 1 Mouse

	0	1	2	3	4	5
1	0.821	-	-	-	-	-
2	0.697	0.649	-	-	-	-
3	<2 e-16	<2 e-16	<2 e-16	-	-	-
4	<2 e-16	<2 e-16	<2 e-16	4.5e-12	-	-
5	<2 e-16	<2 e-16	<2 e-16	4.3e-10	0.075	-
6	<2 e-16	<2 e-16	<2 e-16	<2 e-16	1.4e-11	7.3e-15

Supplementary Table 4.

Microglia Profile on Human

	0	1	2	3
1	0.426	-	-	-
2	0.0064	0.1429	-	-
3	0.3867	0.1456	0.0037	-
4	< 2e-16	<2e-16	<2 e-16	< 2e-16

Microglia Markers on Human

	0	1	2	3
1	0.4295	-	-	-
2	0.02175	0.00027	-	-
3	0.08016	0.00032	0.71281	-
4	< 2e-16	<2e-16	<2 e-16	8.4e-16

Microglia Profile on Qui Mouse

	0	1	2	3	4	5
1	<2 e-16	-	-	-	-	-
2	1.8e-13	<2 e-16	-	-	-	-
3	5.6e-11	0.35000	<2 e-16	-	-	-
4	4.0e-11	<2 e-16	0.05602	< 2e-16	-	-
5	1.1e-11	0.02721	<2 e-16	0.00935	<2 e-16	-
6	8.76e-6	0.02372	<2 e-16	0.19350	<2 e-16	0.00067

Microglia Markers on Qui Mouse

	0	1	2	3	4	5
1	4.0e-16	-	-	-	-	-
2	<2 e-16	<2 e-16	-	-	-	-
3	2.9e-5	0.0857	<2 e-16	-	-	-
4	1.4e-10	<2 e-16	0.0024	6.3e-16	-	-
5	1.0e-15	2.9e-5	<2 e-16	9.6e-7	<2 e-16	-
6	6.1e-5	0.1737	<2 e-16	0.8515	2.6e-15	3.3e-6

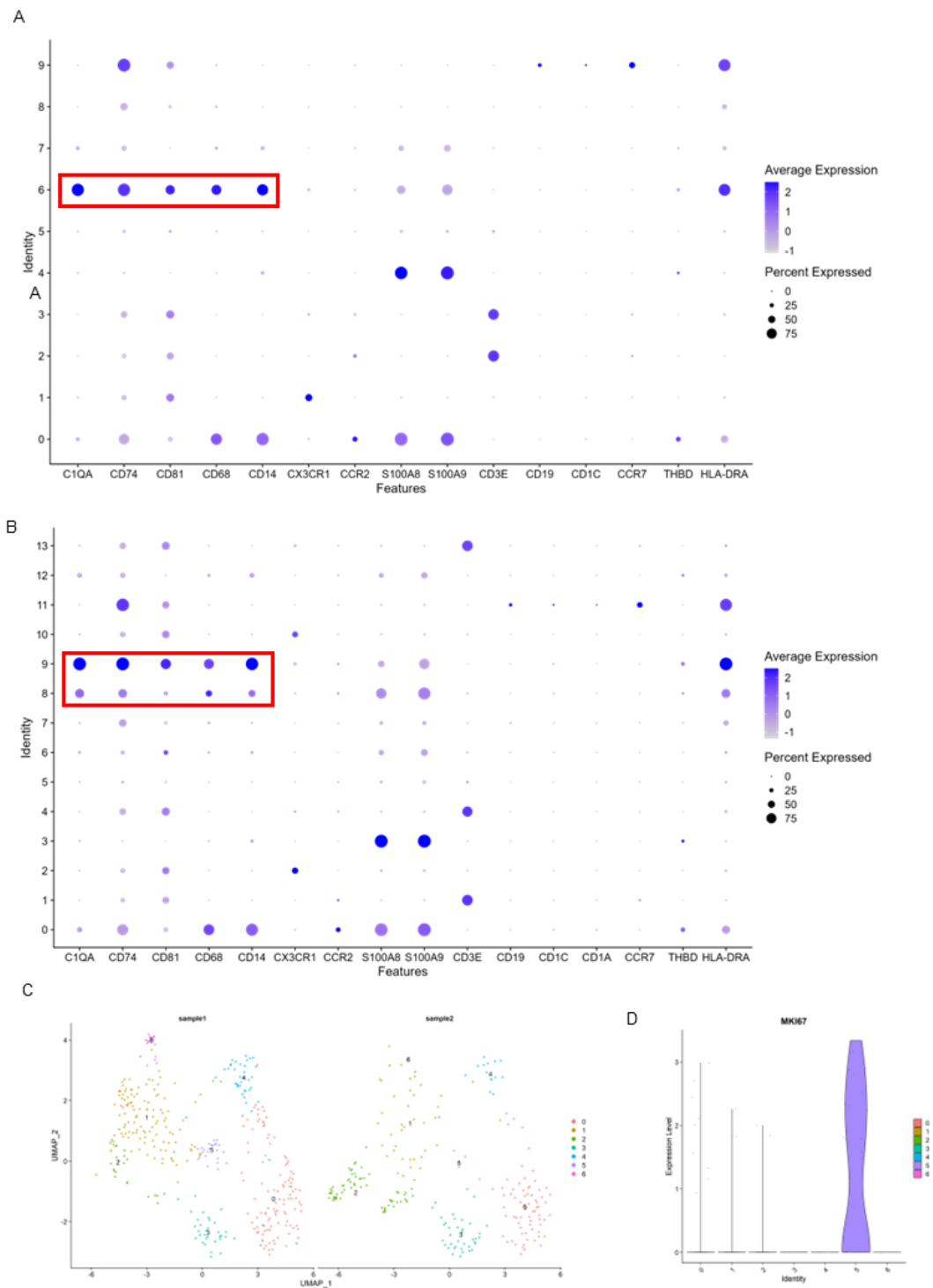
Microglia Profile on Day 1 Mouse

	0	1	2	3	4	5
1	<2 e-16	-	-	-	-	-
2	0.97332	<2 e-16	-	-	-	-
3	<2 e-16	0.31553	<2 e-16	-	-	-
4	0.87147	3.7e-11	0.87147	6.9e-15	-	-
5	0.87147	< 2e-16	0.87147	< 2e-16	0.98898	-
6	7.0e-6	0.61159	4.8e-6	0.87147	6.6e-5	0.00012

Microglia Markers on Day 1 Mouse

	0	1	2	3	4	5
1	<2 e-16	-	-	-	-	-
2	0.1281	<2 e-16	-	-	-	-
3	<2 e-16	1.5e-8	<2 e-16	-	-	-
4	4.7e-5	5.7e-7	3.5e-7	< 2e-16	-	-
5	<2 e-16	4.1e-14	<2 e-16	0.00935	<2 e-16	-
6	1.8e-5	0.8391	9.1e-7	0.0499	0.0191	0.0026

Supplementary Figure 1.

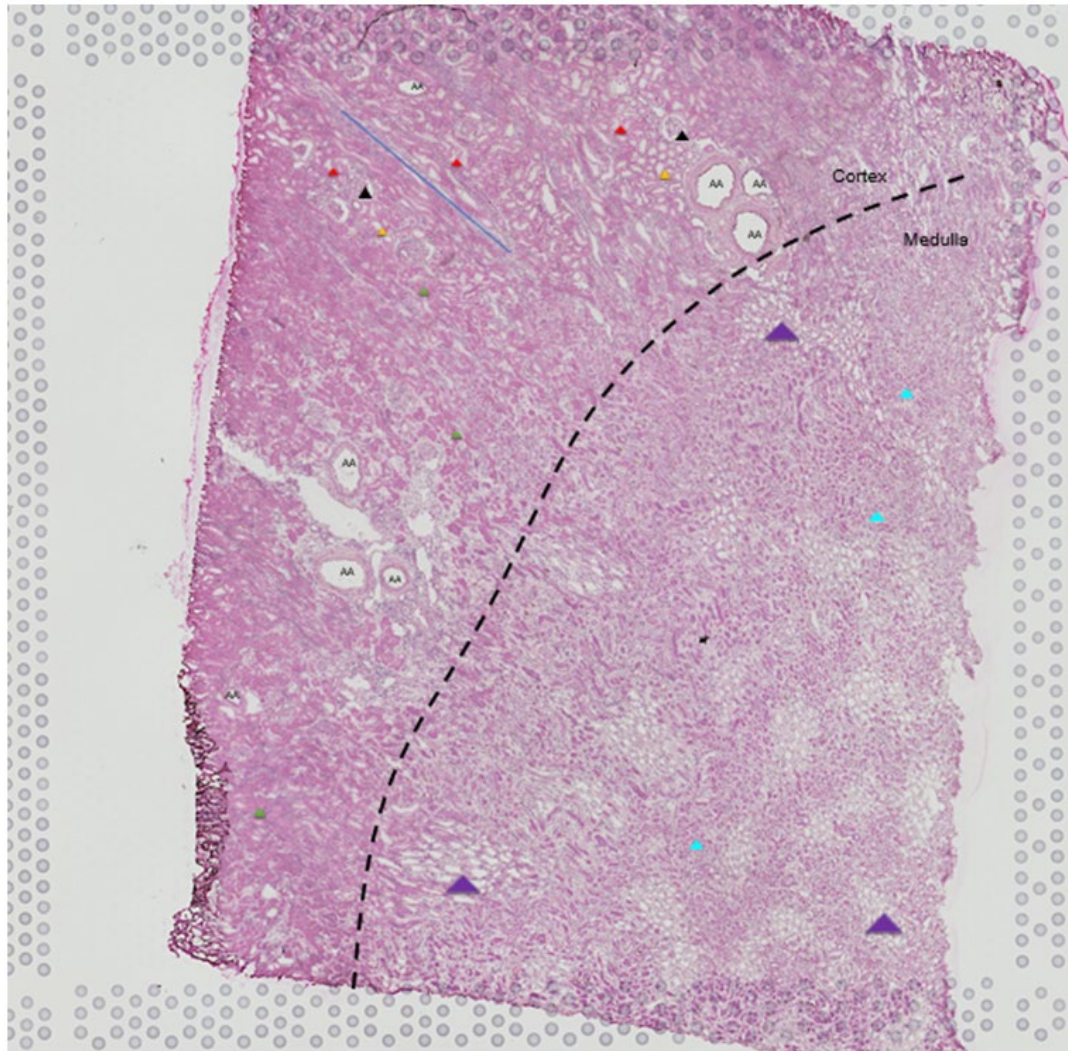


Supplementary Figure 1.

(A) DotPlot of canonical immune markers on CD45⁺ sorted cells from Donor A. Cluster 6 was identified as KRMs based on expression of *CIQA*, and the highest combined

expression of *CD74* and *CD81*. These cells are confirmed as macrophages by expression of *CD68* and *CD14*. Cluster 6 was used for all downstream analyses. Other identified populations are cluster 4 as neutrophils (highest expression of *S100A8* and *S100A9*), clusters 2 and 3 as T cells (*CD3E*) and cluster 9 as *CCR7* expressing dendritic cells (*CD1C*, *CCR7*, *HLA-DRA*). (B) DotPlot of canonical immune markers on CD45⁺ sorted cells from Donor B. Clusters 8 and 9 are identified as KRMs based on expression of *CIQA*, and the highest combined expression of *CD74* and *CD81*. These cells are confirmed as macrophages by expression of *CD68* and *CD14*. Clusters 8 and 9 were used for all downstream analyses. Other identified populations are cluster 3 as neutrophils (highest expression of *S100A8* and *S100A9*), clusters 1 and 4 as T cells (*CD3E*) and cluster 11 as *CCR7* expressing dendritic cells (*CD1C*, *CCR7*, *HLA-DRA*). (C) The resulting integration of KRMs from Donors A and B resulted in the UMAPs, split by sample. All clusters besides 6 are represented in both samples. The resulting Cluster 6 was only present in sample 1 and was therefore excluded from the following analyses. (D) Violin plot of *MKI67*, identifying Cluster 5 as cycling cells. These cells were therefore excluded from the following analyses.

Supplementary Figure 2.



Supplemental Figure 2.

Cortex,

Black arrow heads: Glomeruli

Green arrow heads: Proximal tubules

Yellow arrow heads: Distal tubules

Red arrow heads: Tubules in extensive tubulointerstitial nephritis

Blue lines: The architecture is distorted from inflammation and scarring, possible medullary rays

AA: arcuate arteries, some are dilated

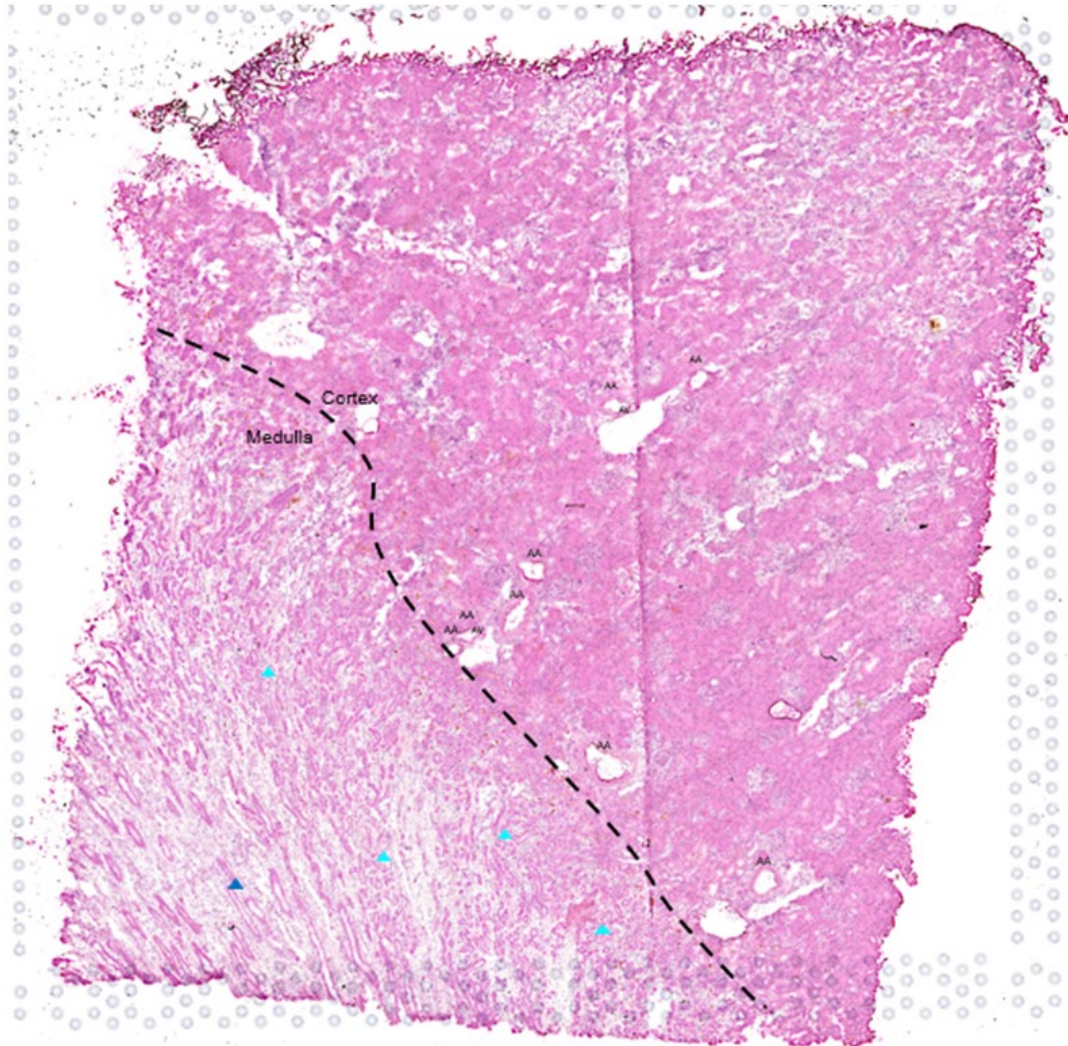
AV: arcuate veins

Medulla,

Purple triangles: vascular spaces within a background of fibrosis.

Light blue arrow heads: loop of Henle (thin or thick).

Supplementary Figure 3.



Supplemental Figure 3.

Cortex,

Interstitial fibrosis and inflammation

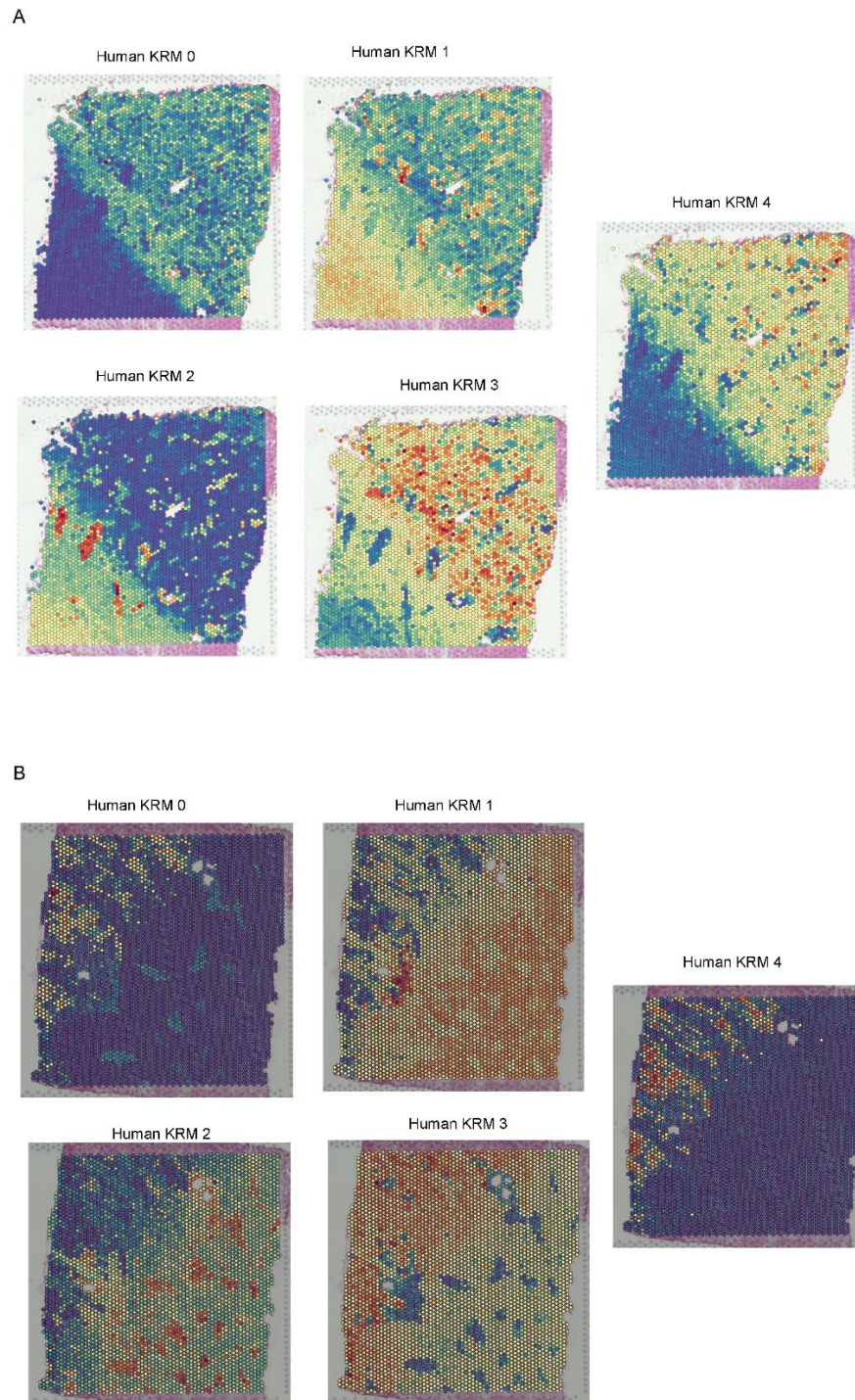
AA: arcuate arteries

AV: arcuate veins

Medulla,

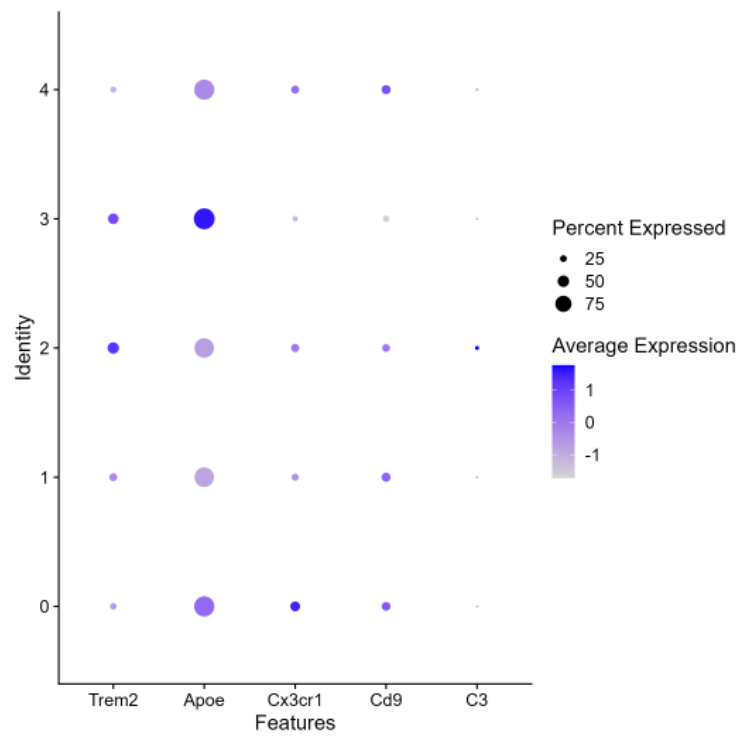
Light blue arrow heads: loop of Henle (thin or thick)

Dark blue arrow heads: collecting duct

Supplementary Figure 4.

Supplemental Figure 4. (A) Spatial locations of hKRM 0 – 4 on kidney section A (B)

Spatial locations of hKRM 0 – 4 on kidney section B

Supplementary Figure 5.

Supplemental Figure 5.

Activated microglia associated genes on unintegrated day-1 post injury murine KRM data, to ensure a potential injury specific association was not being lost in the integrated dataset.

APPENDIX C

Supplementary Tables and Figures
for
An evolutionarily conserved kidney
resident macrophage phenotype with reduced MHC II expression appears after kidney
injury

Supplementary Table 1.

	0	1	2	3	4	5	6	7
1	0.0046							
2	< 2e-16	1.8e -9						
3	< 2e-16	1.1e -9	0.12388					
4	< 2e-16	< 2e-16	1.2e -15	2.7e -8				
5	8.1e -9	2.9e -8	9.1e -8	1.3e -7	4.4e -7			
6	7.8e -5	0.60992	1.4e -6	5.4e -8	< 2e-16	3.3e -8		
7	< 2e-16	3.8e -10	3.0e -5	0.00064	0.61874	5.0e -6	8.5e -10	
8	0.64649	0.02622	< 2e-16	< 2e-16	< 2e-16	2.1e -8	0.00626	6.4e -14

	0	1	2	3	4	5	6	7
1	< 2e-16							
2	< 2e-16	0.489						
3	< 2e-16	< 2e-16	< 2e-16					
4	< 2e-16	4.7e -9	9.0e -7	< 2e-16				
5	< 2e-16	< 2e-16	< 2e-16	< 2e-16	5.9e -6			
6	< 2e-16	< 2e-16	< 2e-16	4.2e -8	3.5e -12	0.012		
7	< 2e-16	2.1e -13	1.1e -10	< 2e-16	0.016	0.076	2.8e -5	
8	1.0e -9	0.150	0.134	< 2e-16	1.0e -4	2.0e -8	1.9e -11	7.6e -6

Supplemental Table 1.

P-value from the Pairwise Wilcoxon test for nonparametric data for AKI KRM clusters, at both timepoints, for the expression of the MHC II transcriptional profile from Table 1.

Supplementary Table 2.

	0	1	2	3	4	5	6	7
1	0.07458							
2	0.00146	0.54217						
3	< 2e-16	5.1e -10	5.1e -10					
4	1.3e -8	4.5e -9	9.8e -13	< 2e-16				
5	3.4e -5	1.0e -4	0.0002	0.01699	4.6e -6			
6	0.07157	0.82005	0.82005	1.2e -7	1.2e -7	0.00016		
7	0.00641	0.00094	0.00025	4.3e -10	0.94311	1.2e -5	0.00099	
8	0.87816	0.12881	0.01887	6.5e -13	4.6e -5	4.6e -5	0.10512	0.01677

	0	1	2	3	4	5	6	7
1	0.03924							
2	<2e-16	5.6e -16						
3	<2e-16	<2e-16	2.6e -7					
4	1.1e -7	5.11e -11	<2e-16	<2e-16				
5	5.3e -6	0.00316	0.01287	3.7e -9	3.0e -14			
6	1.6e -9	6.7e -6	0.54466	0.00017	<2e-16	0.15285		
7	0.11080	0.00317	<2e-16	<2e-16	0.00759	1.6e -6	2.5e -9	
8	0.05937	0.24824	0.08314	0.00050	4.8e -5	0.69132	0.21811	0.01287

Supplemental Table 2.

P-value from the Pairwise Wilcox test for nonparametric data for AKI KRM clusters, at both timepoints, for the expression of the wound healing transcriptional profile from Table 1.

Supplementary Table 3.

	0	1	2
1	<2e-16		
2	<2e-16	<2e-16	
3	<2e-16	0.059	<2e-16

Supplemental Table 3. P-value from the Pairwise Wilcox test for nonparametric data for CKD KRM clusters for the expression of the MHC II transcriptional profile from Table 1.

Supplementary Table 4.

	0	1	2
1	3.7e -13		
2	0.4262	8.4e -10	
3	0.7888	0.0053	0.788

Supplemental Table 4.

P-value from the Pairwise Wilcox test for nonparametric data for CKD KRM clusters for the expression of the wound healing transcriptional profile from Table 1.

Supplementary Table 5.

	0	1	2	3
1	8.4e -8			
2	0.6292	0.0015		
3	0.1309	1.1e -7	0.0995	
4	< 2e- 16	< 2e- 16	< 2e- 16	3.2e - 13

Supplemental Table 5.

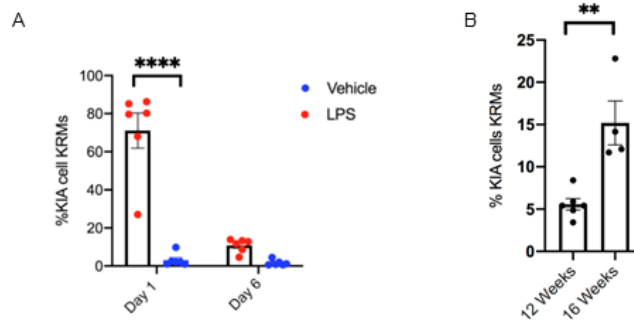
P-value from the Pairwise Wilcox test for nonparametric data for human KRM clusters for the expression of the MHC II transcriptional profile from Table 1.

Supplementary Table 6.

	0	1	2	3
1	0.01810			
2	0.37151	0.16679		
3	0.08016	0.00034	0.0174 9	
4	0.00045	1.4e -6	2.6e -5	0.02745

Supplemental Table 6.

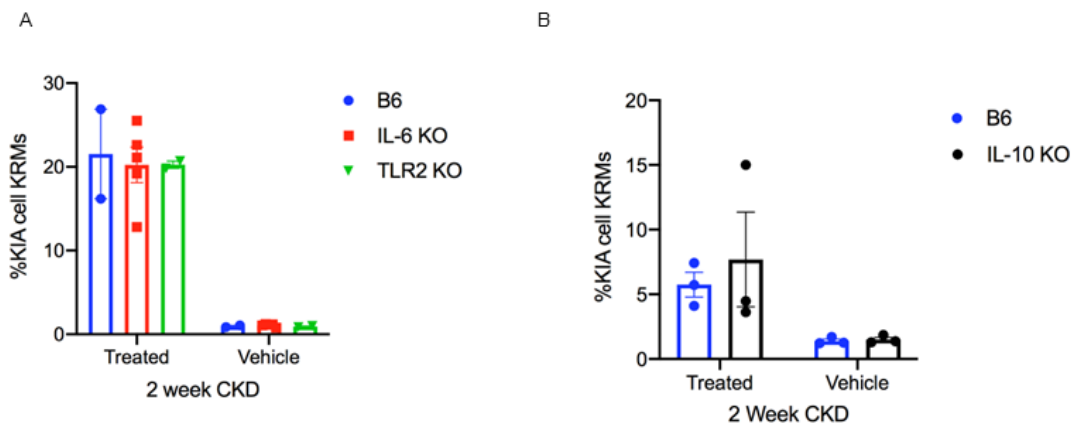
P-value from the Pairwise Wilcox test for nonparametric data for human KRM clusters for the expression of the wound healing transcriptional profile from Table 1.

Supplementary Figure 1.

Supplemental Figure 1.

(A) No difference in the percentage of KIA cells between IL-6 global KO mice or TLR2 KO mice compared to B6 controls 2 weeks post CKD induction. (B) No difference in the percentage of KIA cells between IL-10 global KO mice and B6 controls 2 weeks post CKD induction. Mice in this study received out of date aristolochic acid resulting in reduced injury. B6 controls shown here are from the same experiment and represent the appropriate controls.

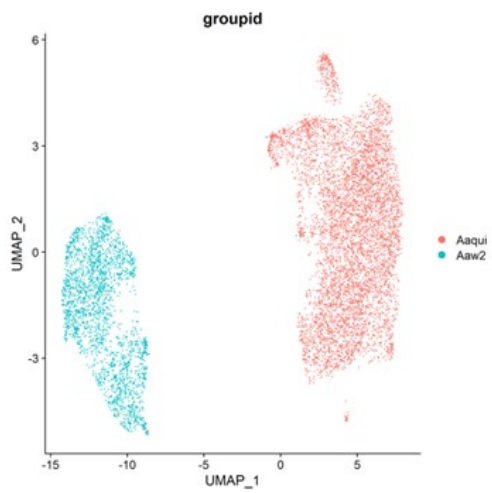
Supplementary Figure 2.



Supplemental Figure 2.

(A) No difference in the percentage of KIA cells between IL-6 global KO mice or TLR2 KO mice compared to B6 controls 2 weeks post CKD induction. (B) No difference in the percentage of KIA cells between IL-10 global KO mice and B6 controls 2 weeks post CKD induction. Mice in this study received out of date aristolochic acid resulting in reduced injury. B6 controls shown here are from the same experiment and represent the appropriate controls.

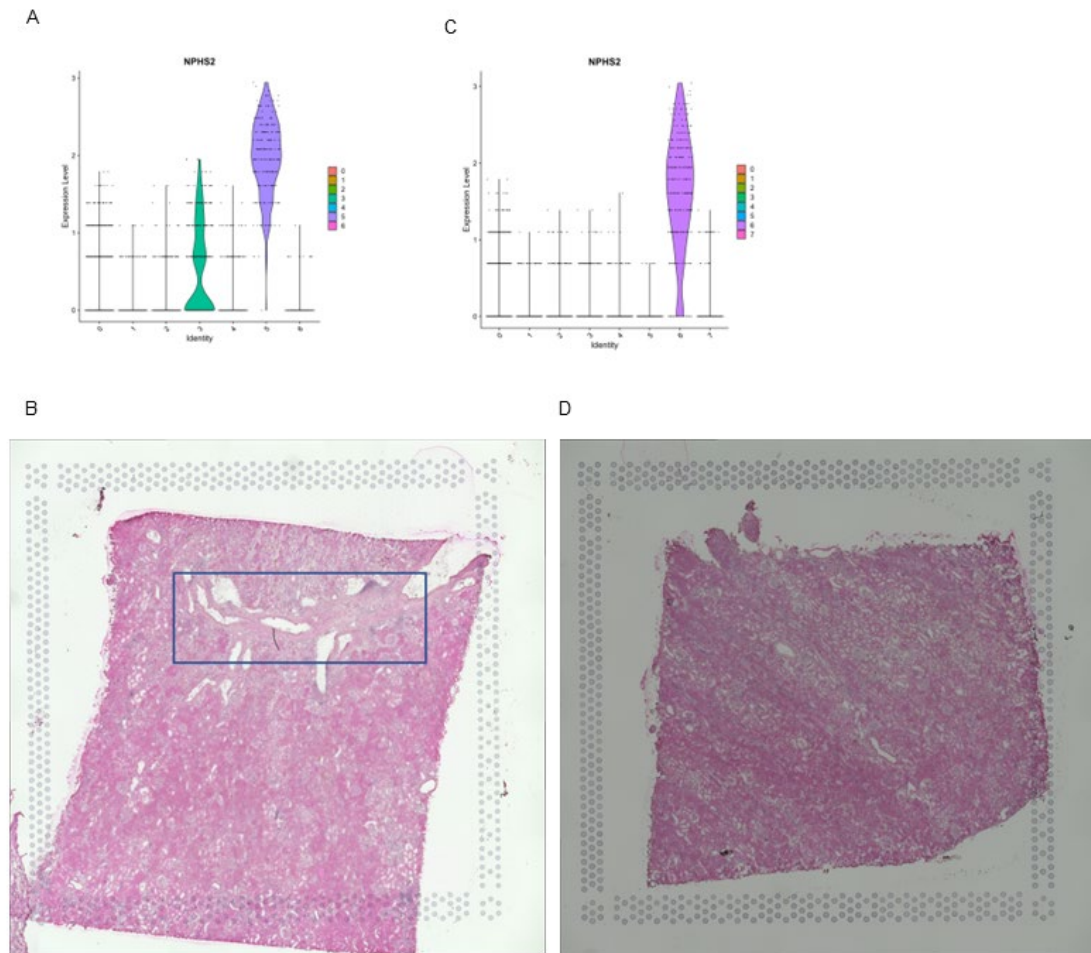
Supplementary Figure 3.



Supplemental Figure 3.

UMAP of attempted integration of quiescent and week 2 AAN-CKD showing failure of the two timepoint to integrate.

Supplementary Figure 4.



Supplemental Figure 4.

(A) Confirmation of podocin (NPHS2) expression in the spatially identified glomerular cluster for Donor A. (B) Section from Donor A presents with tubular atrophy, extensive fibrosis and interstitial inflammation. Glomeruli: reduced number of glomeruli in the section examined. At this low resolution micrograph, glomeruli show obliteration of glomerular capillaries. Boxed area: shows thickened blood vessels surrounded by fibrosis, atrophic tubules and interstitial inflammation. (C) Confirmation of podocin (NPHS2) expression in the spatially identified glomerular cluster for Donor A.

(D) The section from Donor B presents with moderately preserved renal architecture with extensive tubular atrophy and diffuse interstitial inflammation. Glomeruli: Adequate number of glomeruli, some showing atrophy and hyalinosis.

APPENDIX D

Study Approvals

IRB-300004686

GENERAL INFORMATION	
PROJECT OVERVIEW	
Project Title	Porcine Kidney Xenotransplantation into Brain-dead Human Deceased Donors
IRB Project Number	IRB-300004648
Investigator Assurance	
<ul style="list-style-type: none"> All key personnel listed on the protocol have completed initial IRB training and have or will complete continuing IRB training as required, and All personnel are qualified and licensed/credentialed for the procedures they will be performing, if applicable. 	

Name			
Erman, Elise			
Email	ermanen@uab.edu		
Department	Grad Sch - Biomed Sciences		
Principal Investigator	Start Date	End Date	Role
<input type="checkbox"/>	08-Nov-2021		Other Personnel
Certifications			
Certification	Begin	End	
Financial Conflict of Interest	25-Nov-2020	25-Nov-2024	
Degree			
Training certificates 			
Indicate the following activities in which this individual will be involved. If this individual is not involved in any of these activities, he/she should not be listed as key personnel on the IRB submission:			
<input type="checkbox"/> Involved in the design of the human subjects research			
<input type="checkbox"/> Obtaining informed consent*			
<input type="checkbox"/> Interacting/intervening with participants for research purposes			
<input checked="" type="checkbox"/> Obtaining or accessing private identifiable (or coded) data or identifiable (or coded) specimens			
<input type="checkbox"/> Administering investigational (non-FDA-approved) product (e.g., drug, device, or biologic)			
<input type="checkbox"/> Named on the FDA 1572 or device agreement*			
<input type="checkbox"/> Required to complete sponsor's conflict of interest form*			
<input type="checkbox"/> Student capstone project, thesis, or dissertation			
Yes Is the individual named above "responsible" for the design, conduct, or reporting of the research?			
No Will the individual named above be involved in explaining the study, risk-benefit, and/or alternatives to potential participants?			
No Does this individual have a financial interest in this project (see below for definition)?			
Please note: Individuals in a role of PI, Co-PI, and/or Faculty Advisor, as well as anyone who is involved in an activity marked with an asterisk, or answers yes to one of the additional questions related to responsible personnel above must file a disclosure of financial interests and complete training requirements of the UAB CIRB .			

APN 21531

GENERAL INFORMATION

USING THE ANIMAL USE REQUEST/REGISTRATION (AUR) EFORM
 If you are unfamiliar with this electronic form (eForm), please review the instructions and guidance provided by clicking on the following hyperlinks.

[INTRODUCTION](#) (Explains when submission of this eForm is required.)
[COMPLETING AND SUBMITTING THE AUR eFORM](#) (Includes links to video clips and other help.)
[GENERAL FORM FEATURES](#)
[KINDS OF QUESTIONS AND RESPONSES](#)

For help responding to specific questions throughout the AUR eForm, click on the question mark icon or the hyperlinked word or phrase beside or within the question. This will display a separate window containing additional instructions or information. In some cases, a response will result in a popup window containing a reminder or caution. If you would like assistance or if you have any questions about using or submitting the form, contact the IACUC Office at iacuc@uab.edu or (205) 934-7692.

****Your responses may generate additional questions in subsequent sections; therefore, answer all questions in the order in which they appear.****

NEW! Indicates a question or instruction that has been added since the release of the eForm in 2016. Please review your form to ensure all relevant questions have been answered.

REQUEST FOR ASSISTANCE

Yes No Do you wish to consult one of the Animal Resources Program (ARP) veterinarians or IACUC Office staff members prior to the IACUC review of this submission? (Consultation or preliminary review of the submission is not required; however, if you have questions about completing the form or about the procedures you are proposing, this is an opportunity to request assistance.)

PROJECT OVERVIEW

* PRINCIPAL INVESTIGATOR (PI) George, James F

PROJECT TITLE
 Mononuclear Phagocytes in the pathogenesis of acute kidney injury
 Animal Project Number (APN) IACUC-21531 (Reference this number on correspondence related to this application.)

Lab/Office Contact(s), if any

Name	Lab Contact?	Office Contact?	Copy on correspondence related to this submission?
George, James F	<input checked="" type="checkbox"/>	<input checked="" type="checkbox"/>	<input type="checkbox"/>
Agarwal, Anupam	<input type="checkbox"/>	<input type="checkbox"/>	<input checked="" type="checkbox"/>
LaFontaine, Jennifer R	<input checked="" type="checkbox"/>	<input checked="" type="checkbox"/>	<input checked="" type="checkbox"/>

APN 20308

GENERAL INFORMATION

USING THE ANIMAL USE REQUEST/REGISTRATION (AUR) EFORM
 If you are unfamiliar with this electronic form (eForm), please review the instructions and guidance provided by clicking on the following hyperlinks.

[INTRODUCTION](#) (Explains when submission of this eForm is required.)
[COMPLETING AND SUBMITTING THE AUR eFORM](#) (Includes links to video clips and other help.)
[GENERAL FORM FEATURES](#)
[KINDS OF QUESTIONS AND RESPONSES](#)

For help responding to specific questions throughout the AUR eForm, click on the question mark icon  or the hyperlinked word or phrase beside or within the question. This will display a separate window containing additional instructions or information. In some cases, a response will result in a popup window containing a reminder or caution. If you would like assistance or if you have any questions about using or submitting the form, contact the IACUC Office at iacuc@uab.edu or (205) 934-7692.

****Your responses may generate additional questions in subsequent sections; therefore, answer all questions in the order in which they appear.****

NEW Indicates a question or instruction that has been added since the release of the eForm in 2016. Please review your form to ensure all relevant questions have been answered.

REQUEST FOR ASSISTANCE

Yes No Do you wish to consult one of the Animal Resources Program (ARP) veterinarians or IACUC Office staff members prior to the IACUC review of this submission? (Consultation or preliminary review of the submission is not required; however, if you have questions about completing the form or about the procedures you are proposing, this is an opportunity to request assistance.) 

Which of the ARP veterinarians or IACUC Office personnel would you like to assist you? If you have no preference, answer "First Available". [First Available](#)

PROJECT OVERVIEW

* PRINCIPAL INVESTIGATOR (PI)  [Agarwal, Anupam](#)

PROJECT TITLE
 Human Heme Oxygenase-1 Gene Regulation in Renal Injury

Animal Project Number (APN) [IACUC-20380](#) (Reference this number on correspondence related to this application.)

Lab/Office Contact(s), if any

Name 	Lab Contact?	Office Contact?	Copy on correspondence related to this submission?
Traylor, Amie Mark	<input checked="" type="checkbox"/>	<input checked="" type="checkbox"/>	<input checked="" type="checkbox"/>